TONGUE AND SLOT JOINT IN COMPOSITE SANDWICH PANELS

Ghobad Rezaie Roshan

A Thesis Presented in Fulfilment of the Degree of

DOCTOR OF PHILOSOPHY

The City University

Department of Aeronautics

March, 1988

CONTENTS

		PAGE
List of Figures		iii
List of Tables		vii
ACKNOWLEDGEMENTS		ix
DECLARATION		x
ABSTRACT		1
SYMBOLS AND ABBREVIATIONS		2
1. INTRODUCTION		4
2. JOINT DESIGN		13
2.1	Definition of the Important Load Carrying Characteristics of Sandwich Panels in the Tongue and Slot Joints	14
2.2	Longitudinal Shear Loading	15
2.3	Short Transverse Shear Loading	16
2.4	Tensile Loading	16
2.5	Dimension of Reinforced Joint	17
3. FABRICATION OF JOINTS		29
3.1	Preparation and Bonding of Test Sections	30
3.2	Bonding of Reinforced Joint Specimens	32
4. JOINT TESTING		38
4.1	Design Testing of the Tongue and Slot Joint	38
4.2	Lap Shear Test	41
4.3	Longitudinal Joint Testing	43
4.4	Short Transverse Shear Test	43
4.5	Discussion	44
5. MATERIALS		60
5.1	Properties of DLS 280 G-R-7	60
5.2	Properties of the Core	61
5.3	Properties of Adhesive	62
5.4	Compression Testing of Unidirectional Composite Sandwich Panel	62
5.5	Discussion	69
6. FLEXURAL BENDING OF COMPOSITE SANDWICH BEAM		82
6.1	Three Point Bend Test of Multidirectional Composite Sandwich	82
6.2	Three Point Bend Test of Composite Sandwich Box-Beam	82

7.0 FAILURE CRITERION STUDY 92

7.1 Introduction 92
7.2 Maximum Stress Criterion 93
7.3 Maximum Strain Criterion 93
7.4 Hill Criterion or Tsai-Hill Criterion 94
7.5 Tsai-Hill/Hoffman Criterion 97
7.6 Composite Failure Criteria 97

8.0 FINITE ELEMENT ANALYSIS 99

8.1 Introduction 99
8.2 Theory 100
8.3 Two Dimensional Theory for Flat Orthotropic Sandwich Composite 102
8.4 Three Dimensional Theory for Orthotropic Sandwich Plate 117
8.5 Implementation of PAFEC 121

9. BEAM STRESS ANALYSIS AND STRENGTH PREDICTION 129

9.1 Introduction 129
9.2 Three Point Flexural Composite Sandwich Beam Stress Analysis and Strength Predictions 131
9.3 Stress Analysis and Strength Prediction of Box Beam 137

10. FINITE ELEMENT ANALYSIS OF THE JOINT 168

10.1 Introduction 168
10.2 Longitudinal Shear Joint Type '1b' 170
10.3 Longitudinal Shear Joint Type '2a' 175

11. FAILURE STRENGTH PREDICTIONS

11.1 Strength Predictions of Reinforced Joint Type '1b' 204
11.2 Strength Predictions of Joint Reinforcements Type '2a' 207

12. DISCUSSION 213

13. CONCLUSIONS 218

REFERENCES 219

NOTE TO APPENDIX 222

LIST OF FIGURES

FIGURE		PAGE
1.1	Tongue and slot joint	8
1.2	Self jigging characteristics of tongue and slot joints	9
1.3	Existing method of bonded joints	10
1.4	Definition of joint loading	11
2.1	First proposal for design of joint	19
2.2	Second proposal for design of joint	20
2.3	Third proposal for design of joint	21
2.4	Fourth proposal (internal reinforcement of the tongue)	22
2.5	Fifth proposal (external reinforcement of the tongue)	23
2.6	General description of tongue and slot joint in longitudinal shear mode	24
2.7	General description of tongue and slot joint in short transverse shear	25
2.8	General description of tongue and slot joint in tension	26
2.9	Detail drawing of tongue and slot joint	27
3.1	Tongue and slot joint with external reinforcement	33
3.2	Tongue and slot joint with internal reinforcement	34
3.3	Unsymmetrical longitudinal shear loading of the joint	35
3.4	Symmetrical longitudinal shear loading of the joint	35
3.5	Tongue and slot joint with short transverse shear specimens	36
3.6	Tongue and slot joint with tensile type of specimen	37
4.1	Core-adhesive rupture at the inner slot facing interface	48
4.2	Adhesive-adherend failure at the inner slot facing	49
4.3	Laminate failure at the root of the tongue (Type 2c)	50
4.4	Lap shear test specimen	51
4.5	Adhesive-adherend failure of lap shear test with EC2216/BA	52
4.6	Adhesive-adherend failure of lap shear test (Redux410N/A)	53
4.7	Longitudinal shear test failure of the facing at the tip of the tongue indicated by crazing of the facing	54
5.1	Failure mode of honeycomb sandwich panel	72
5.2	Short column compression testing of unidirectional sandwich specimen	73
5.3	Short column compression testing of the composite sandwich with the unidirectional facing	74

5.4	Unidirectional composite sandwich failure in short column testing	75
5.5	Intercell buckling of unidirectional composite sandwich by shear failure of the facings	76
5.6	Short column compression testing of 8-ply laminate	77
5.7	Flexural sandwich beam testing	78
6.1	Box-beam test section and method	86
6.2	Box-beam test set-up	87
6.3	Box-beam compression failure of top panel	87
6.4	S.T.B./test deflection and failure comparison	88
7.1	Cross-section of a unidirectional lamina with fibres in the 1-direction	95
8.1	Rectangular orthotropic sandwich element	124
8.2	Transverse shear stress distribution in the composite sandwich panel	125
8.3	Stress acting in the orthotropic facing laminate	126
8.4	Principal material axes and geometry of sandwich composite	127
8.5	Three dimensional orthotropic sandwich element	128
9.1	Finite element mesh for the flexural sandwich beam tests	143
9.2	Flexural bending of the standard composite sandwich mesh	144
9.3	Comparison of theory (2D) and test deflection for standard sandwich composite	145
9.4	Comparison of theory (3D) and test deflection for standard sandwich composite	146
9.5	Comparison of failure strength predictions for the standard sandwich with various core thicknesses	147
9.6	Tsai-Hill reserve factor for the cross ply high density core beam in the top facing	148
9.7	Tsai-Hill reserve factor for the multidirectional ply high density core beam in the top facing	149
9.8	Idealized 2D finite element mesh of the box beam	150
9.9	Deflected shape of the box beam at failure (test) load	151
9.10	Vital area of the mesh for the box beam (2D)	152
9.11	Tsai-Hill failure factor profile across the restrained end of the top panel for the 0 ply	153

FIGURE PAGE

9.12 Three-dimensional finite element mesh of the box beam 154
9.13 Uniform deflection of the 3D box beam facing loading 155
9.14 Local deformation due to the pressure loading at the free end 156
9.15 Vital area of the box beam at restrained end 157
9.16 Tsai-Hill factor across the width of the beam for the 0 ply of the upper facing (top panel) 158
9.17 Comparison of deflection between test and various methods of analysis 159
10.1 Two dimensional finite element mesh of tongue and slot joint 178
10.2 Deflected shape of the tongue and slot joint (2D) 179
10.3 Absolute stress concentration contour in the tongue panel 180
10.4 Maximum principal stress across the root of the tongue (top facing) 181
10.5 Maximum stress concentration in slot facing 182
10.6 Three dimensional finite element mesh of tongue and slot joint 183
10.7 Blockfill mesh of the tongue and slot joint 184
10.8 Constrained planes of symmetry of the tongue and slot joint 185
10.9 Deformation of the tongue and slot joint (type 1b) 186
10.10 Description of the important areas of stress concentration 187
10.11 Width of the composite at the root of the tongue 188
10.12 Longitudinal and transverse stress distribution of 90° ply at the root of tongue 189
10.13 Longitudinal stress distribution of 0° ply at the root of the tongue 190
10.14 Shear stress distribution for 90° ply along the root of the tongue 191
10.15 Vital area of composite at slot skin (inner) 192
10.16 Transverse stress distribution of 90° ply across the length of inner slot facing 193
10.17 Transverse stress distribution of 90° ply across the width of slot 194

FIGURE PAGE

10.18 Stress concentration at the root of the tongue (-45° ply) 195

10.19 Stress concentration at the root of the tongue (-45° ply) 196

10.20 Vital area of the far end slot composite facing (inner) 197

11.1 Failure distribution of 0°/90° ply at the root of the tongue 210

11.2 Failure distribution of 90° inner slot facing 211

11.3 Prediction of failure strength in the tensile region of the tongue composite 212

LIST OF TABLES

TABLE		PAGE
1.1	Design loads for tongue and slot joint	12
2.1	Contribution of sandwich elements to the joint strength	28
4.1	Longitudinal shear test (EC2216 B/A) unsymmetrical joint specimens	55
4.2	Tensile test on the tongue and slot joint (EC2216 B/A)	55
4.3	Longitudinal shear test (EC2216 B/A) symmetrical specimens	56
4.4	Longitudinal shear test (Redux 410 N/A) symmetrical specimens	56
4.5	Lap shear test results	57
4.6	Longitudinal shear test of reinforcement type 2.0	58
4.7	Short transverse shear test	59
5.7	Summary of different tests (see Tables 5.1 to 5.6) carried out on to find compressive strength of unidirectional composite sandwich facings.	70
5.1	Longitudinal short column compression of unidirectional sandwich	79
5.2	Longitudinal short column test of 8-ply laminate	79
5.3	Transverse short column compression of 8-ply laminate	79
5.4	Four point flexural bend test	80
5.5	Three point flexural bend test	80
5.6	Flexural three point cross ply - sandwich beam testing	81
6.1	(a) and (b) Flexural cross ply sandwich beam testing	89
6.1	(c) Flexural cross ply sandwich beam testing	89
6.2	Flexural multidirectional sandwich beam testing	90
6.3	Comparison of box beam failure deflecton δ_f	91
9.1	Comparison of deflections in tests and F.E.A. (2D)	160
9.2	Strength prediction of (0°/90°-C0°) Beam $=h_c/h_f=33.2$	161
9.3	Strength predictions of multidirectional sandwich beams	162
9.4	Comparison of deflections in tests and F.E.A. (3D)	163
9.5	Strength predictions of various sandwich beams (3D)	164
9.6	Comparison of beam strength predictions between tests and theory	165

TABLE		PAGE
9.7	Predicted strength of box-beam using 2-D element	166
9.8	Predicted strength of box-beam using 3-D element	167
10.1	Stress concentration in the composite at the root of the tongue	198
10.2	Position just below the root of the tongue	199
10.3	Stress concentration of slot inner composite skin (S_{M1})	200
10.4	Stress concentration in the composite at the root of the tongue	201
10.5	Stress concentration in the composite at the root of the tongue	202
10.6	Stress concentration in the composite at the inner slot facing	203

ACKNOWLEDGEMENTS

I would like to express my deepest gratitude to [redacted] for the invaluable guidance and encouragement he has given me during the course of the research.

Thanks must also go to the following people for their support:

[redacted], Secretary to the Department of Aeronautics for typing the thesis.

[redacted], The Department Laboratory Technician for his help in preparation and testing of material specimens.

C.F. Taylor (Metal Workers) Ltd., Wokingham for their support and use of facilities.

[redacted], The Laboratory Supervisor at C.F. Taylor Ltd. for his constructive advice and help.

[redacted], The Test Engineer at C.F. Taylor for his help in testing of various specimens.

[redacted], The Computer System Supervisor at C.F. Taylor for his help and patience during many computer runs.

Finally, but not least, I would like to thank [redacted] for being tolerant and morally supportive during the whole time that I was engrossed in the research work and also to [redacted] for keeping me company during the writing-up.

DECLARATION.

I grant powers of discretion to The University Librarian to allow this thesis to be copied in whole or in part without further reference to me. This permission covers only single copies to be made for study purposes, subject to normal conditions of acknowledgements.

ABSTRACT

Methods of joining composite sandwich panels together using adhesive bonding were reviewed. The tongue and slot joint was chosen for the basis of this investigation associated with the box structures used in aircraft galleys. The important load carrying characteristics of sandwich panel were defined and the problems involved in transfering load from one panel to another were identified. Joint designs to alleviate these problems were obtained initially by experimental work and an evolving process of reinforcing the joints locally to eliminate failures up to the design loads required for current galley structures.

These joints were then investigated by finite element stress analysis with the object of predicting their static strength for the purpose of including this analysis in future design methods so reducing the experimental requirement. Material static testing was carried out to obtain strength and stiffness to insert in this analysis.

The predictions were largely successful when compared to the test results indicating that the analysis could be used in the design of such joints. The joint designs represented a useful weight and cost savings over previous methods of joining the panels together.

SYMBOLS AND ABBREVIATIONS

p_o - Load

t - Thickness (Plate, Laminate)

h,H - Sandwich Panel Thickness

h_f - Facing Thickness

h_c - Core Thickness

b - Breadth or Width

L - Length

$1,2$ - Maximum and Minimum Principal Material Direction

ν_{12} - Major Poisson's Ratio

ν_{21} - Minor Poisson's Ratio

E_{11} - Young's Modulus in Fibre Direction

E_{22} - Young's Modulus Transverse to Fibre Direction

G - Shear Modulus

σ_o - Applied Tensile Strength

σ_{UT} - Ultimate Tensile Strength

σ_{UC} - Ultimate Compressive Strength

τ_U - Ultimate Interlaminate Shear Strength

θ - Angle of Principal Plane or Ply Angle

Cθ°(ie C90°)-Standard Core Transverse to Core Ribbon Direction

H.D.Cθ°(ieH.D.C90°)-High Density Core Transverse to Core Ribbon Direction

I_o - Section Second Moment of Area

δ - Deflection

S.T.B. - Simple Theory of Bending

R.F.- Tsai-Hill Failure Criterion Parameter

PE - Potential Energy

WD - Work Done Under External Load

SE - Strain Energy

U_x, U_y, U_z - Cartesian Displacement

n - Number of Element

ϕ_x, ϕ_y, ϕ_z - Angle of Rotation in x,y,z Axes

$\epsilon, \epsilon_{xx}, \epsilon_{yy}, \epsilon_{zz}$ - Strain and Strain Component in x,y and z Direction

$K, K_{xx}, K_{yy}, K_{xy}$ - Curvature, Curvature Components

$\gamma, \gamma_{xz}, \gamma_{yz}, \gamma_{xy}$ - Shear Strain, Shear Strain Components

Q_{sx}, Q_{sy} - Shear Force per Unit Width in xz and yz Plane

$M, M_{xx}, M_{yy}, M_{x,y}$ - Bending Moment, Bending Moment Components

$F, F_{xx}, F_{yy}, F_{xy}$ - Flexural Rigidity and its Components

[B] - Element Strain/Displacement Matrix

[A] - Matrix Relating Constants to Node

[D] - Stress/Strain Matrix

$[S_{ij}]$ - Compliance Matrix

[QO] - Ply Stiffness Matrix in the Matrial Axis

[QO] - Ply Stiffness Matrix in the Element Axis

[T] - Transformation Matrix

Z_U, Z_L - Position of Plies Relative to Mid-Plane

[K] - System Stiffness Matrix

D.C.A.- Direction Cosine Array

h/L - Element Aspect Ratio

1. INTRODUCTION

As the design of aircraft has progressed it has always been the intent of the aircraft industry to utilize the latest development in materials. This has encouraged the aircraft interior industries to design structures such as galleys to be more weight efficient.

In the early stages these structures were made of metal stringers and angles riveted to thin metal skins. Later aluminium alloy sandwich panels were used joined by extrusions, the two assemblies mechanically fastened together.

It is only recently that composites have become widely used in this type of structure, mostly in the form of glass fibre laminated sandwich panel. These have far better bending stiffness/weight ratio than previous materials. Other advantages of glass fibre sandwich panels are their resistance to corrosion and the reduction of the number of detail parts required for a given structure (i.e. no stringers).

Little emphasis has been placed on suitable methods of joining glass fibre reinforced panels for the galley type of structure. The program of work reported here was initiated to investigate improvements in the various means by which panels might be joined together to form a structural unit. Conventional means of attachment such as bolts, rivets, etc. were deliberately avoided because of the concentrated stress build up at the holes. Structural adhesive bonding has been practised since the beginning of technology. One of the earliest military applications was the fabrication of laminated bows by the Egyptians 4000 years ago and Genghis Khan's remarkable success was partially due to his archers' use of small, powerful bows made by laminating different materials with animal and vegetable derivatives used as gluing agents [Refs. 1,2]. Exposure to moisture severely weakened these bows and caused them to fail after some use. The loss of strength due to moisture strictly

limited the structural importance of such adhesives until the development of synthetic adhesives.

With the development of synthetic resin adhesives came the possibility of new applications. Adhesive bonds have been used on every aircraft and missile ever made. Their extent, and structural significance, has increased steadily as their advantages were realised. There are a number of reasons why the replacement of mechanical fasteners and welded joints by adhesives is attractive. There is a more uniform distribution of stress over the joint area than with mechanical fasteners, therefore providing longer fatigue life [Refs. 3,4]. Dissimilar materials can be effectively joined with adhesive where an alternative joining procedure would have been non-existent or prohibitively difficult before. A good example is the metal-paper honeycomb sandwich. Structural applications such as honeycomb sandwich and fibrous composites have been made possible with strong adhesives. Yet another important advantage is an economic one. Adhesive joining eliminates a number of production costs associated with setting up and assembling joints with rivets and bolts. The tongue and slot joint (Fig. 1.1) is particularly favourable in this respect because it is already in use for its self-jigging characteristics thus eliminating expensive jigging equipment (see Fig. 1.2). The principal strength is provided by bonding G.R.P. angle sections along each corner of the whole length of the panel (Fig. 1.3).

The object of this investigation is to see whether the tongue and slot joint alone could be used for strength thus eliminating the angle section saving weight and cost. The need was to avoid local failures around the joint by using suitable reinforcement. A definite effort was made to utilize the special characteristics of unidirectional reinforced glass fibre laminates, such as the ability to arrange the fibres in the

direction of the greatest load. The type of loading on these joints is principally longitudinal shear with secondary loadings in short-tranverse shear and tension (Fig. 1.4). The joints were compared for strength to the design loads for a current typical galley. If a joint strength exceeded this level then it was considered satisfactory and not developed further. This gave a target joint strength which could not be defined easily otherwise (see Table 1.1). Major consideration was also given to the practicality of fabrication techniques and the cost of materials in respect to overall cost-effectiveness of the joint design considered here in this work.

The difficulties met by a stress analyst or designer in determining whether or not he has correctly analyzed the stress distribution in an actual adhesive joint is the most formidable disadvantage to the use of this joining procedure. There are several reasons why this is so. A realistic adhesive joint is influenced by factors that most analytical methods neglect. Evaluation of experimental static test results is required to predict accurately the regions in which failure will occur. Other factors are air bubbles or voids, residual stresses due to improper curing, and variation of the adhesive layer thickness, all significantly influence the stress concentration and stress distributions within an adhesive joint. This means that the care taken in the fabrication of an adhesive joint is a determining factor of its strength - a factor which, unfortunately, cannot be accounted for in a deterministic fashion.

Experimental research and widespread engineering use of adhesive is hampered by the lack of a fully reliable nondestructive test. Where experimental research is held back, analytical work is also hindered. As Sherlock Holmes [Ref. 5] said, "I have no data yet it is a capital mistake to theorize before one has data. Insensibly one begins to twist

facts to suit theories, instead of theories to suit facts." Theory without the experimental confirmation cannot be completely relied upon.

No literature on the analysis of sandwich panel joints (i.e. tongue and slot joint or similar joint configuration) has been found. This is a complete three-dimensional adhesive joint problem which is difficult to analyze.

These three facts - the statistical nature of adhesive joints, uncertainty in reliable nondestructive testing techniques, and the lack of available theories - have limited the use of adhesives and plagued joint designers. Nevertheless, empirical results currently must be used as the best available means of estimating joint characteristics for design purposes. After manufacturing has commenced, destructive tests on a sampling basis are normally conducted to ensure joint reliability.

The present thesis is concerned with establishing a method of analysis of this type of joint by finite element techniques where all the important parameters which can influence joint strength can be represented as well as establishing the practicality of the joint itself.

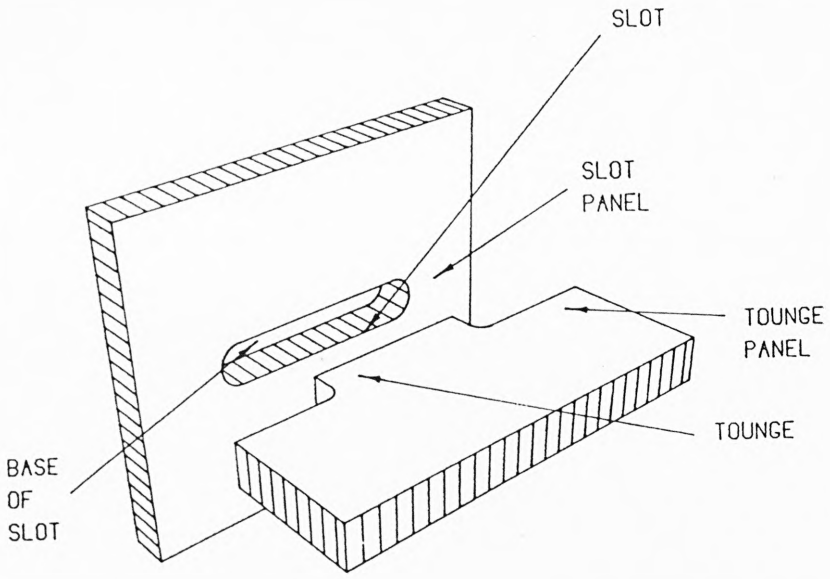

FIG 1.1
TONGUE AND SLOT JOINT

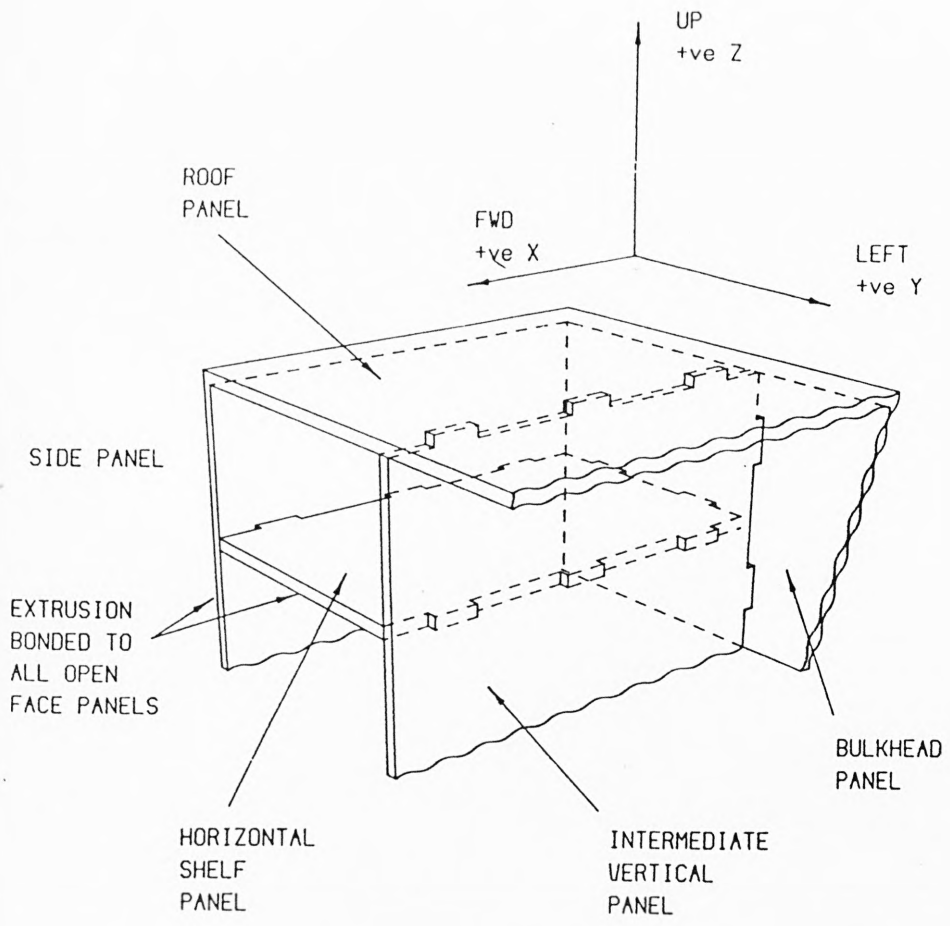

FIG 1.2
SELF JIGGING CHARACTERISTICS OF
TONGUE AND SLOT JOINTS

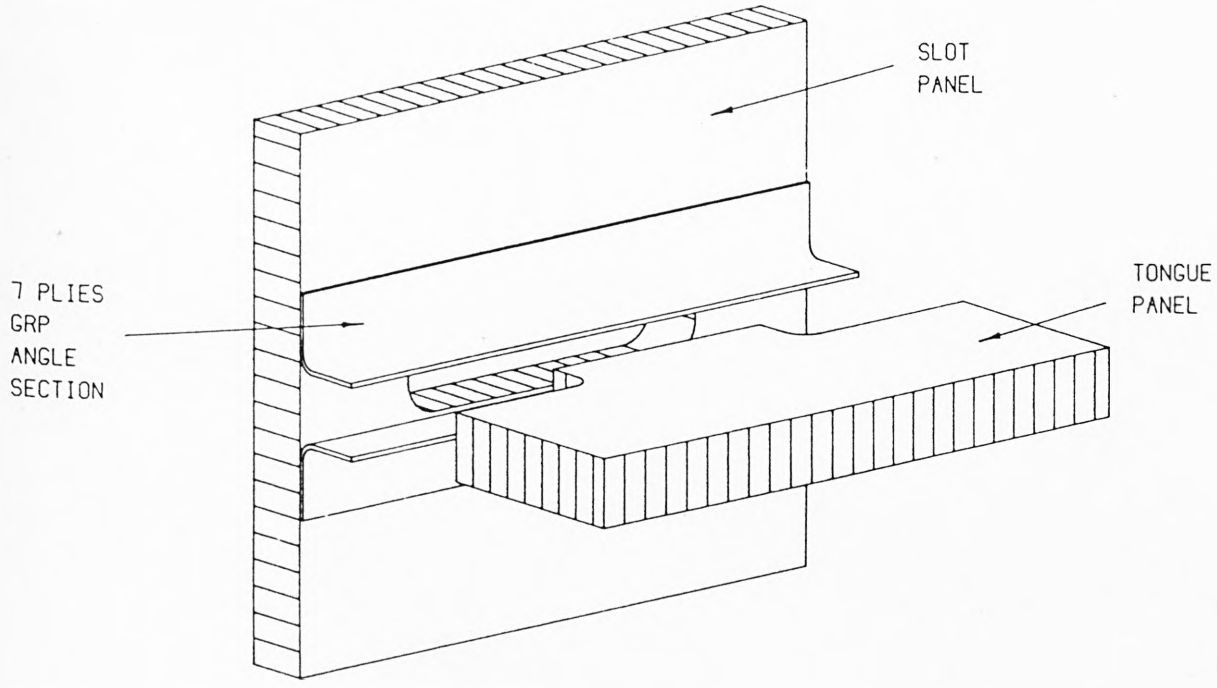

FIG 1.3
EXISTING METHOD OF BONDED JOINT

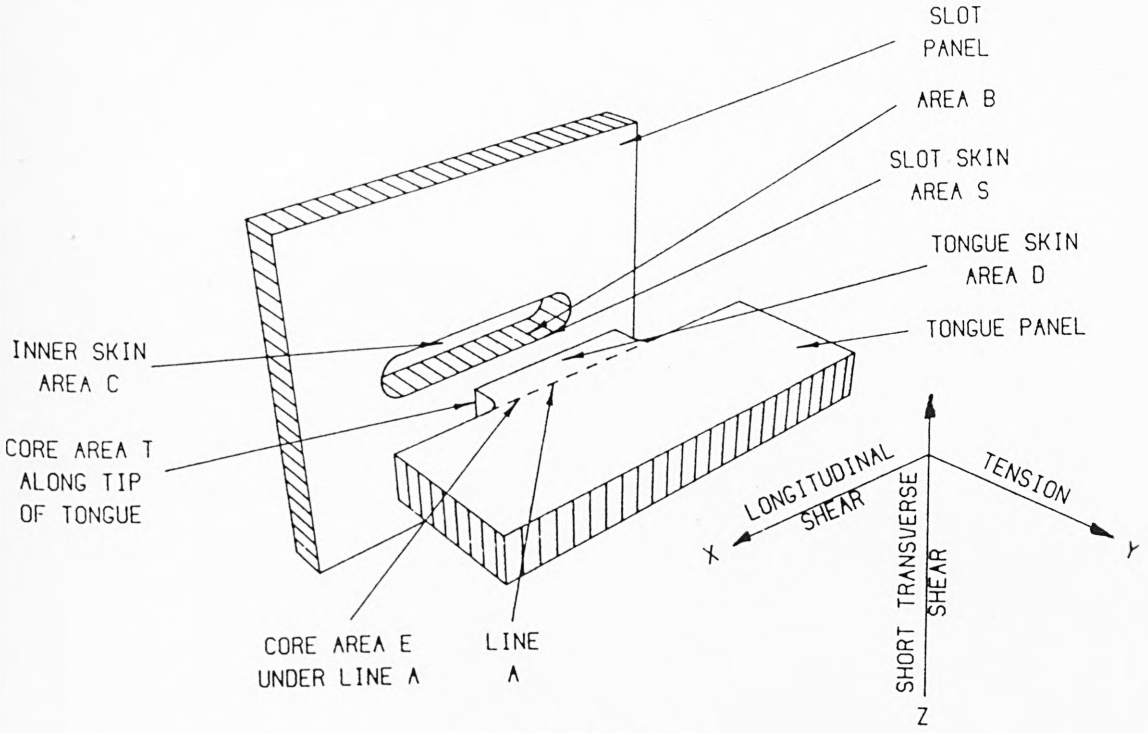

FIG 1.4
DEFINITION OF JOINT LOADING

LOADING MAGNITUDE	MINIMUM DESIGN LOAD PER JOINT (N)		
	LONGITUDINAL SHEAR LOADING	SHORT TRANSVERSE SHEAR LOADING	TENSION
LIGHTLY LOADED PANEL	6000	1700	2500
SEVERELY LOADED PANEL	9500	3000	2500

TABLE 1.1

DESIGN LOADS FOR TONGUE AND SLOT JOINT

2. JOINT DESIGN

The primary considerations in the design of structures using composite materials are the stiffness and strength (particularly with respect to weight) of these materials in the various forms in which they are available. Therefore, an equally important requirement for the complete design of practical structures is the development of attachment methods, joint design, and the problem of load introduction in composite structures. Without proper joints, it is not possible to take full advantage of the high stiffness and strength of the composite sandwich panel.

The design phase of the program was initiated by an effort to join the sandwich panels together by every possible means using adhesive bond. Many sketches depicting different joining methods were prepared and some of these preliminary sketches are shown in Figs. 2.1, 2.2, 2.3, 2.4 and 2.5.

Through the process of elimination these early designs were narrowed to the basic essentials. The screening process was based on:-

(a) Ability of the joint to transmit longitudinal shear, tension and short transverse shear load.

(b) Practicality of fabrication - unless the particular design lent itself to a reasonable production method it was eliminated as a consideration.

(c) Cost of fabrication - an attempt was made to hold the production cost to a minimum.

Figs. 2.4 and 2.5 show the designs which were selected for the program of tests carried out and reported here.

2.1 DEFINITION OF THE IMPORTANT LOAD CARRYING CHARACTERISTICS OF SANDWICH PANELS IN THE TONGUE AND SLOT JOINTS

The structural sandwich element consists of:

(a) the core

(b) the two facings

(c) the core to facings adhesive.

Table 2.1 shows qualitatively how these elements contribute to the strength of the joint (Fig. 1.4).

The primary function of an adhesively bonded joint is to transfer load from one structural member to another. In most bonded joints i.e. lap joints, the load transfer takes place through interfacial shear. The interfacial shear gives rise to high interlaminar stresses in the adhesive layer. The magnitude of the stresses depends on many geometric and material property parameters, such as the thickness and length of the adhesive layer compared to the corresponding values for the adherend materials flexibility of adhesive and type of load to be transferred. In the tongue and slot joint additional parameters can effect the load bearing capacity in all three different modes of loading mainly because of the heterogeneous and anisotropic nature of the composite sandwich panel as well as the complexity of the joint geometry itself. The following section of this chapter are a preliminary discussion on the problems involved with this type of joint. The "best" joints are selected on their merits in achieving the design loads of Table 1.1 in Chapter 1.

2.2 LONGITUDINAL SHEAR LOADING

2.2.1 Due to the low stiffness and strength of the core in both the tongue and slot panel, see Fig. 1.4, Areas 'T' and 'B' respectively, the adhesive forms a large fillet, a major bridging connection between the two panels by bonding the tongue and slot facing together at the inner facing of the slot and at the tip of the tongue (see Fig. 2.6 Section 'AA'). It was found that the adhesive bond layer at this interface needed to be thick enough to avoid any adhesive/core rupture at the tip of the tongue. Also the bulk use of adhesive in the slot panel formed a major load path for the transfer of shear and bearing stresses from the tongue to the outer facing of the slot, see Fig. 2.6 Area 'S'. The adhesive layer at Area 'B' Fig. 1.4 contributed little to the longitudinal shear strength of the joint, due to the low strength of the core in the slot panel in this direction. It did reduce the peel stress effect in the adhesive (caused by the inplane rotation of the tongue) by providing a connection to the slot panel through its thickness. The inplane rotation occurred because of the separation of the lines of the applied loads, giving rise to an inplane bending of the tongue panel. This effect was more pronounced in the small test specimens than it would be in a large panel.

2.2.2 The longitudinal shear strength of the tongue root along the line 'A' of Fig. 2.6 proved to be very low without special reinforcement such as that shown in Fig. 2.5. A laminate was used to reinforce the skins locally in this area to avoid this local failure.

2.2.3 The slot facing can fail on the inner face (Area 'C' Fig. 1.4) due to normal and shear stresses from the tongue. This was found to be the

ultimate failure mode of the joint, after the skin of the tongue was reinforced (Section 2.2.2 above).

2.3 SHORT TRANSVERSE SHEAR LOADING

2.3.1 The core shear stiffness and strength in the 'Z' direction are the main functions of the core in a sandwich panel, therefore the short transverse strength of the joint is limited by the shear strength of the core in the root of the tongue (see Area 'E', Fig. 2.7). It was found to be necessary to increase the core strength in this area by inserting a denser core (Fig. 2.4).

2.3.2 The facings of the tongue add very little shear strength in this direction, due to the very thin facings in the panels used here, except when reinforced by additional material, such as in Figs. 1.3 and 2.3. Often this additional material is added for other purposes such as increasing the tensile or longitudinal shear strength of the tongue.

2.4 TENSILE LOADING

2.4.1 Local bending of the facing sheets of the slot panel, Fig. 2.8(a), causes change in the distribution of the shear stresses in the adhesive on the slot core (Area 'B') and of the tensile stresses on the slot inner face (Area 'C').

The stress concentration in these areas is increased thus reducing the joint strength. These bending deformations can be reduced by

reinforcing the facing sheets of the slot panel around the slot, Fig.2.8(c).

Inserting a high density core in the slot panel around the slot could also help, but this is difficult and therefore expensive and does not help in any other load case. It should only be investigated if it proves necessary to meet the design requirements in a particularly severe case. It will not form part of this investigation. Some form of resin injection by puncturing the cells might be feasible but heavy. This is also useful for other load cases and the weight penalty involved may be acceptable in such circumstances.

2.4.2 The load is transferred primarily by shear from the tongue facings (Area 'D') to the slot core (Area 'B'), Fig.2.8(b). This is the primary failure mode in tests showing that this is the major load transfer area, see Table 2.1. The failure is in the slot core and again a high density core around the slot would help, but would be expensive and heavy.

2.4.3 The local bending deformation in the Area 'C', Fig. 2.8(a), is so severe that it probably triggers the failure. It does not seem to need further investigation, because the joint strength is adequate with the final design obtained using an improved bond on Area 'C'.

2.5 DIMENSION OF REINFORCED JOINT

2.5.1 The length of the joint is based on the present tongue and slot dimensions which is used mainly for ease of location during assembly of

the unit. This eliminates the need for manufacturing of further tool parts (Fig. 2.9).

2.5.2 Due to the nature of the joint, a larger slot will reduce the bending effectiveness of the slot sandwich panel local to the joint.

2.5.3 The critical section of the joint is the root of the tongue (Ref. Fig. 2.6 Line 'A') both for longitudinal and short transverse shear loading. Therefore the core insert was made adequately enough to spread the load so as to reduce the stress concentration. There are also production difficulties in removing the core and inserting the denser core thus limiting the size of the insert. This did not prevent an adequate strength being achieved.

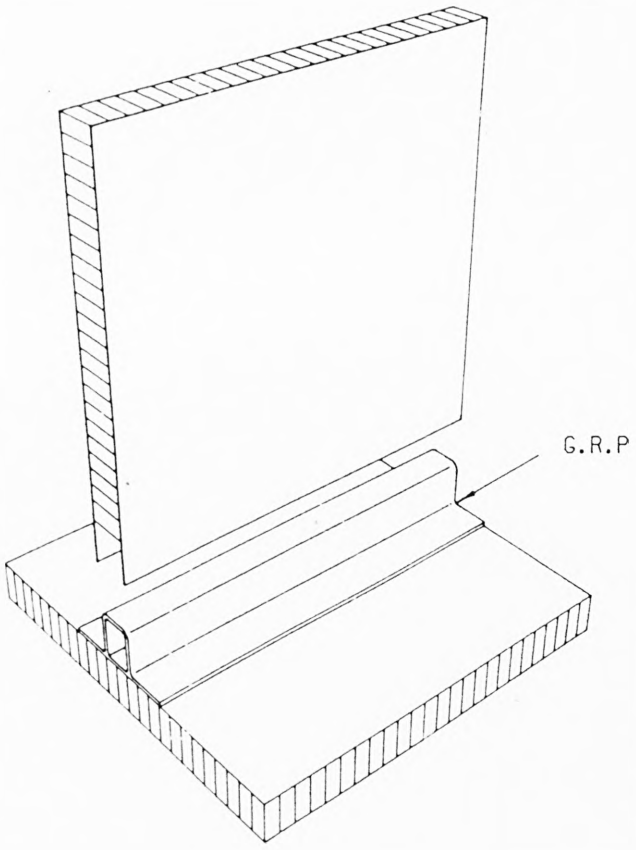

FIG 2.1
FIRST PROPOSAL FOR DESIGN OF JOINT

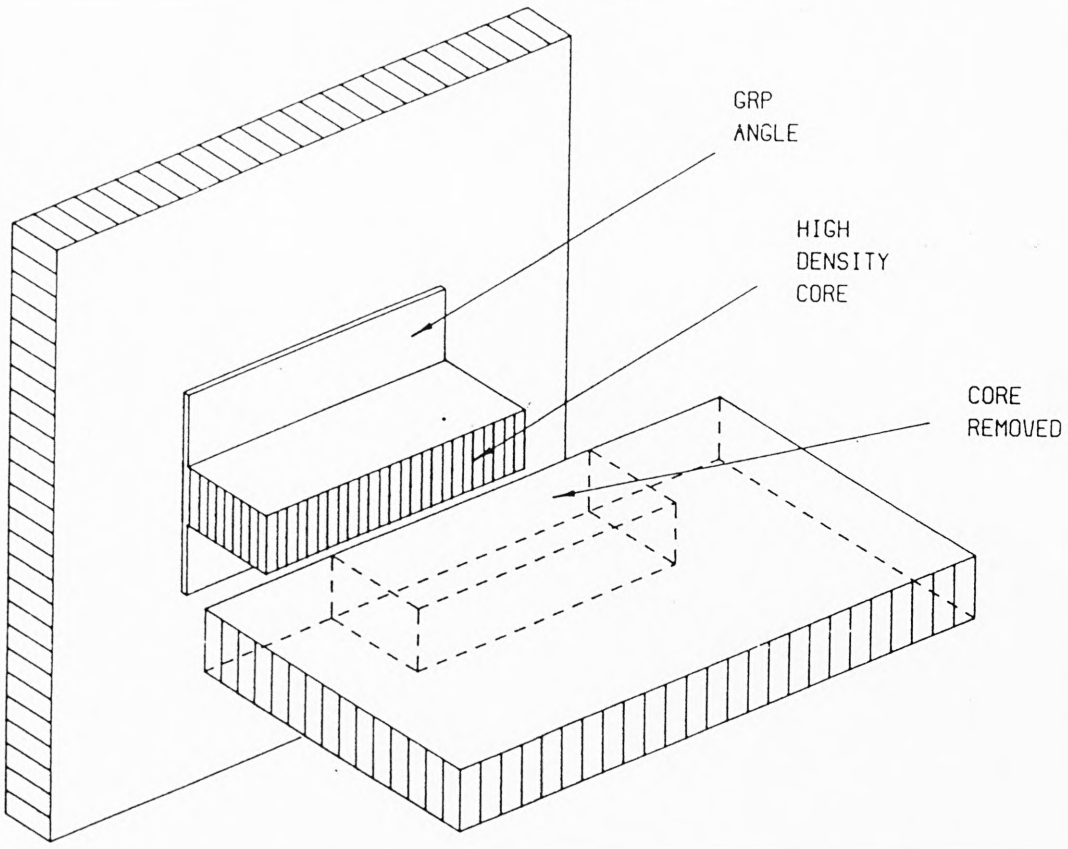

FIG 2.2
SECOND PROPOSAL FOR DESIGN OF JOINT

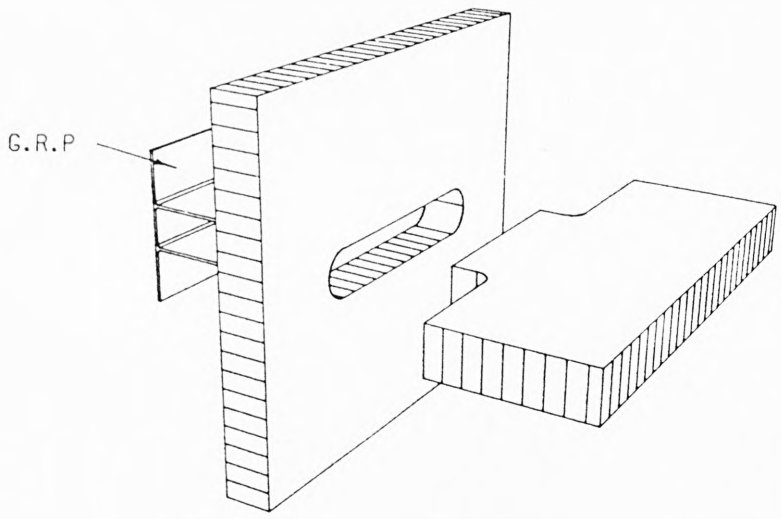

FIG 2.3
THIRD PROPOSAL FOR DESIGN OF JOINT

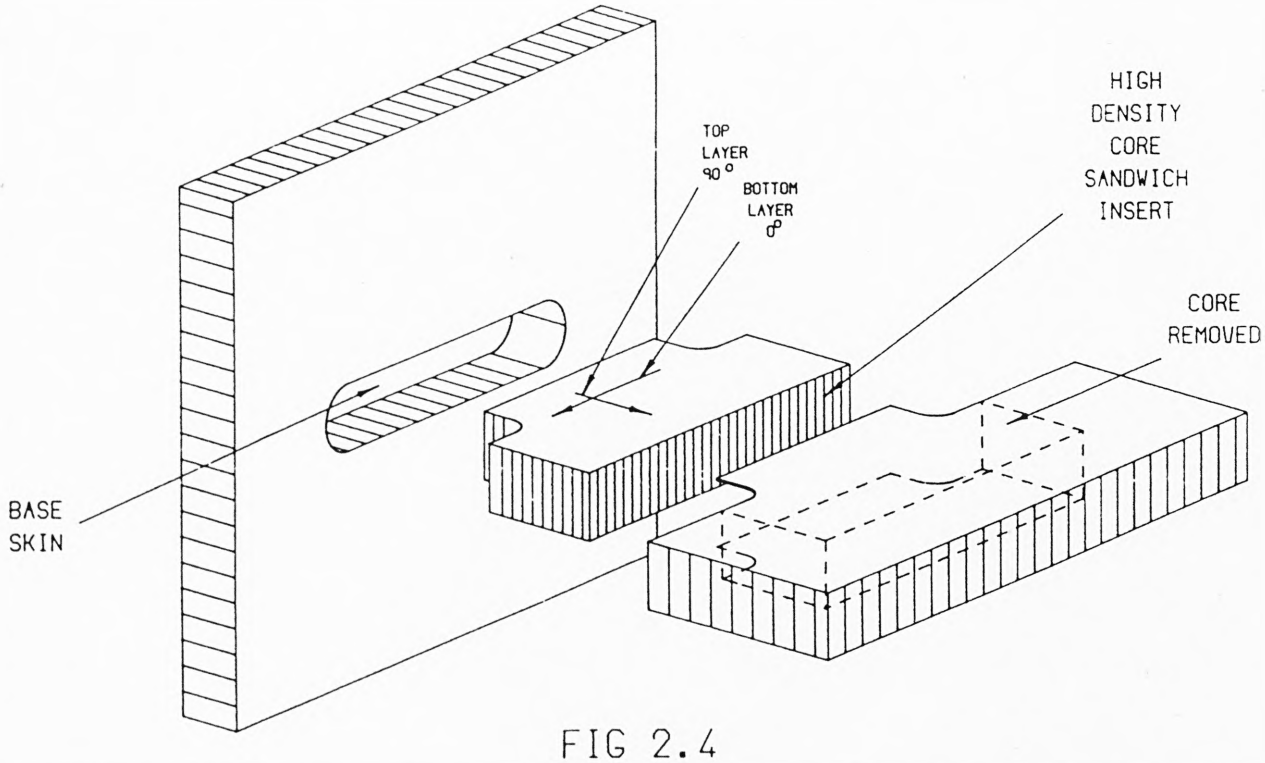

FIG 2.4

FOURTH PROPOSAL (INTERNAL REINFORCEMENT OF THE TONGUE)

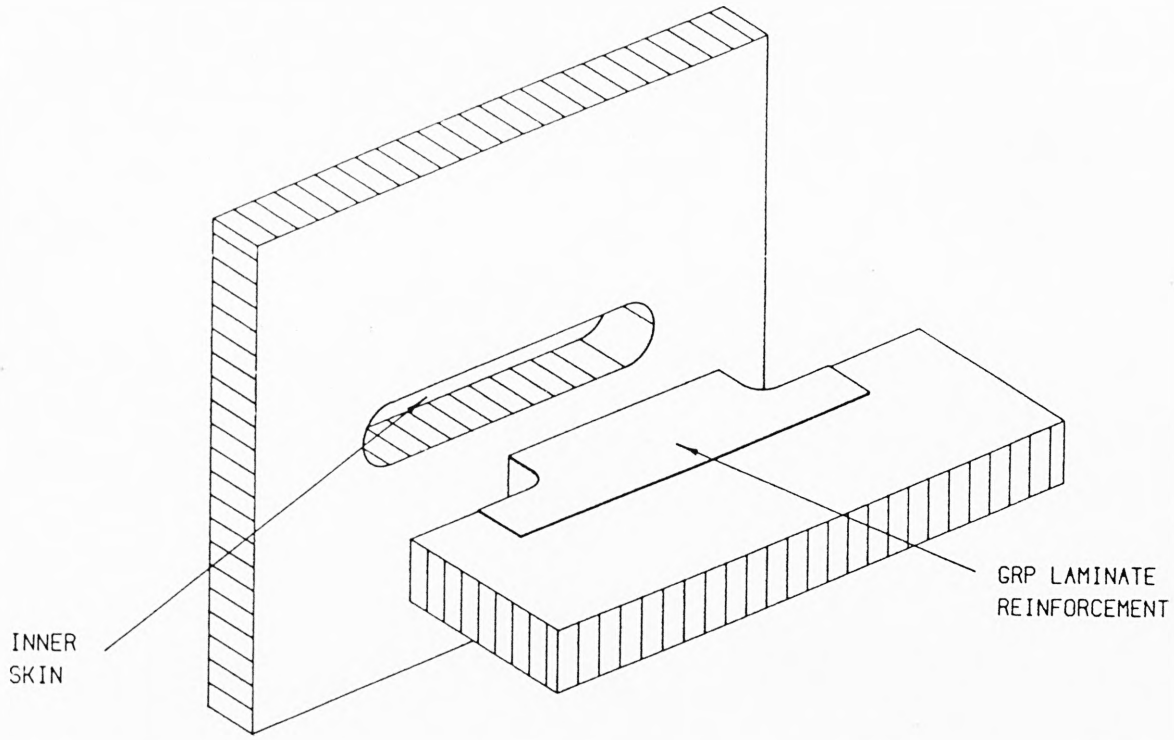

FIG 2.5
FIFTH PROPOSAL (EXTERNAL REINFORCEMENT OF THE TONGUE)

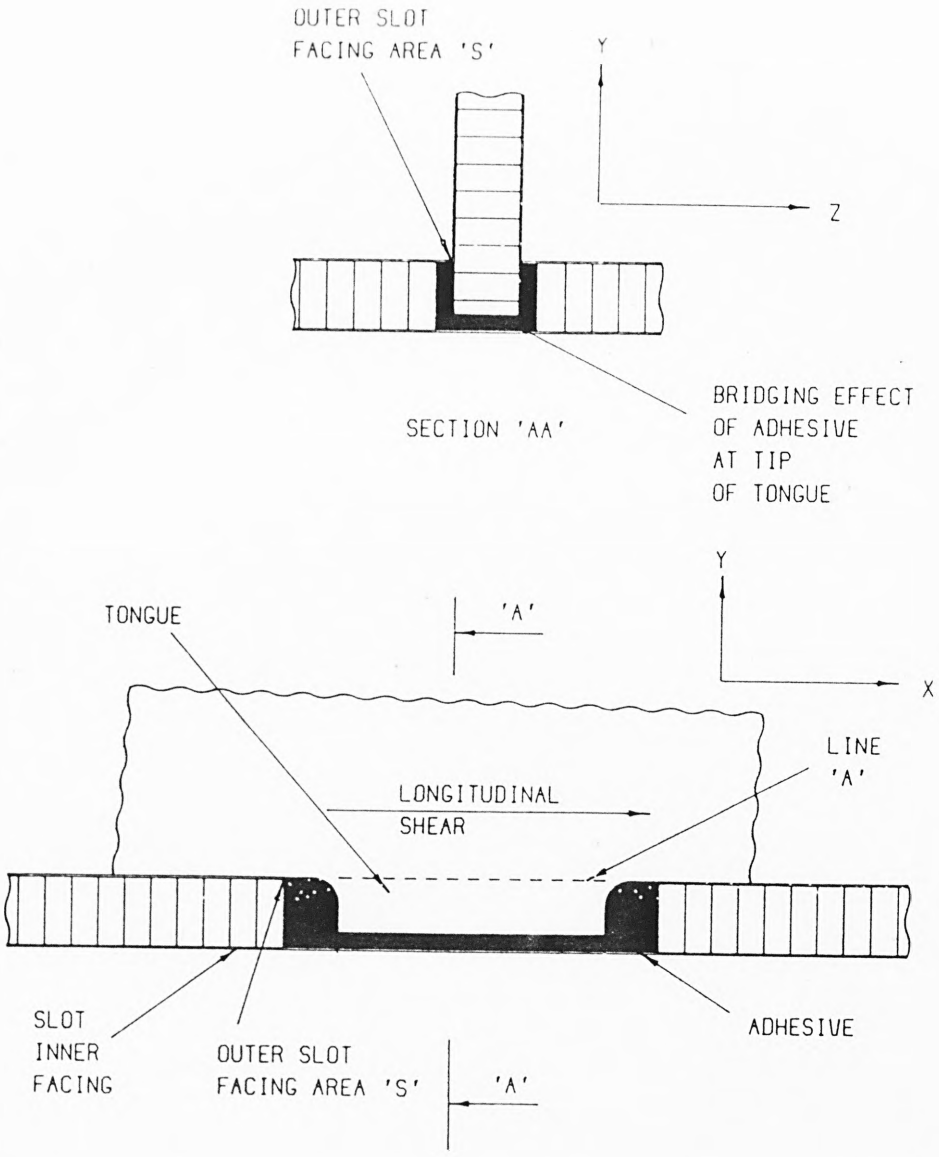

FIG 2.6
GENERAL DESCRIPTION OF TONGUE & SLOT JOINT
IN LONGITUDINAL SHEAR MODE

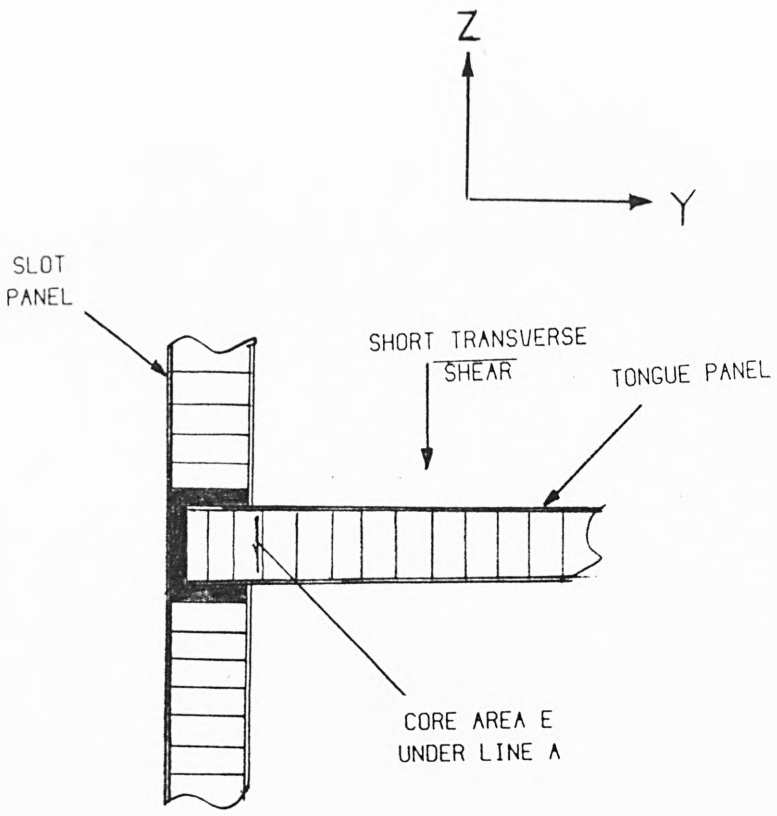

FIG 2.7

GENERAL DESCRIPTION OF
TONGUE AND SLOT JOINT IN SHORT TRANSVERSE SHEAR.

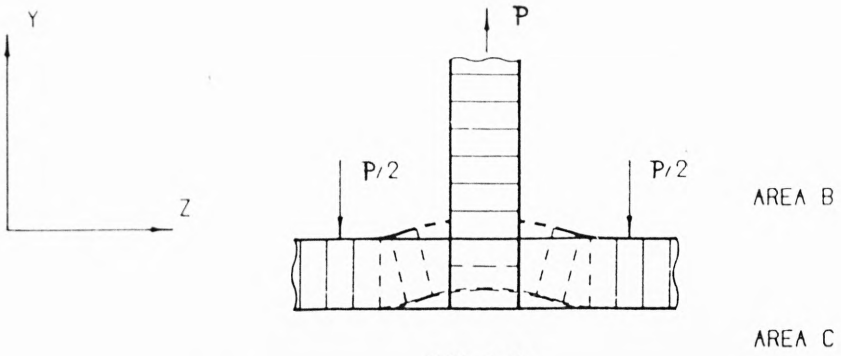

FIG 2.8a
LOCAL BENDING DEFORMATION UNDER TENSILE LOAD

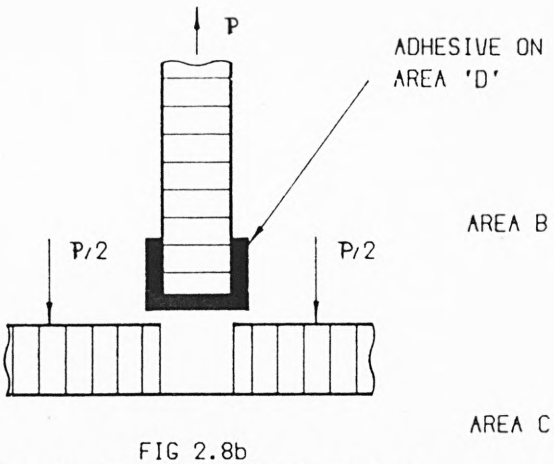

FIG 2.8b
SHEAR OUT IN CORE OF THE SLOT PANEL

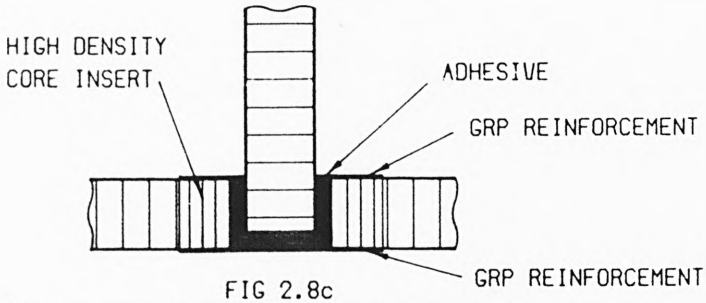

FIG 2.8c
POSSIBLE REINFORCEMENTS TO PREVENT THE FAILURE
MODE SHOWN IN FIGS 10a & 10b

FIG 2.8
GENERAL DESCRIPTION OF TONGUE AND SLOT JOINT IN TENSION

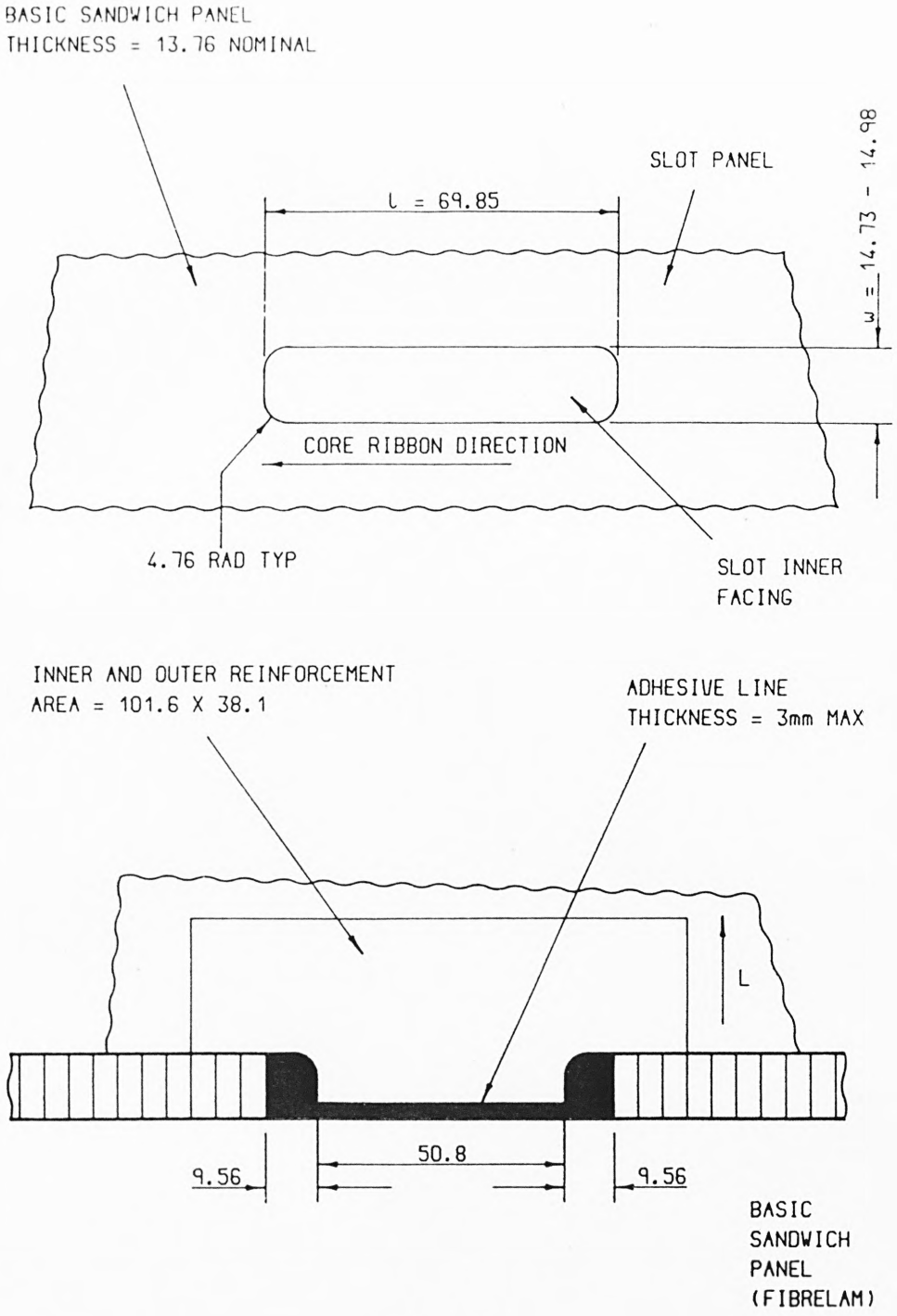

FIG 2.9

DETAIL DRAWING OF TONGUE AND SLOT JOINT

LOADING	CORE	FACING	CORE/FACING ADHESIVE
LONGITUDINAL SHEAR	LITTLE AREA B,S	MAJOR AREA C AND LINE A	MAJOR
SHORT TRANSVERSE SHEAR	MAJOR AREA E	LITTLE AREA C,D	MEDIUM
TENSION	MAJOR AREA B	MEDIUM AREA C,D	MEDIUM

TABLE 2.1

CONTRIBUTION OF SANDWICH ELEMENTS TO THE JOINT STRENGTH

3. FABRICATION OF JOINTS

The second phase of the work required that the best joint designs be actually fabricated and subsequently adhesive bonded together. The basic sandwich panel chosen for fabrication of the joints was "Fibrelam" which has facings of two unidirectinal plies of glass fibre reinforced plastic at right angles (DLS 280/280 G-R-7) and Nomex core type A1-64-5 with a density of 410 lb/ft^3 (64 kg/m^3) and cell size of 3/16" (4.76mm) bonded together with BSL-377 film adhesive forming the sandwich type construction.

The reinforcing laminated sheet was two unidirectional plies of glass fibre reinforced plastic (DLS 280/280 G-R-7). The high density core sandwich insert was constructed with Nomex core type A1-123-3 which has a density of 8.7 lb/ft^3 (123kg/m^3) with cell size of 3mm and a two-or four-ply facings of the same specification as above. All of these materials were obtained from CIBA-GEIGY Plastics, Bonded Structures Division, Duxford, Cambridge.

The adhesives used for bonding of the test sections were Redux 410 N/A which is a two part epoxy paste, room temperature curing, adhesive system, also obtained from CIBA-GEIGY, and EC 2216.B/A adhesive used currently at C.F. Taylor (Metal Workers) Ltd which is a two part paste room temperature curing, modified epoxy resin purchased from Scotchweld 3M United Kingdom Limited, Bracknell, Berkshire.

A preliminary study was initiated to look at the use of EC 2216.B/A adhesive system and its compatibility with the joint configuration designed in this work. This was essential because of the cost involved in introducing a new adhesive for manufacturing of the structures for which this joint is to be used. A detailed study is reported in Chapter 4.

3.1 PREPARATION AND BONDING OF TEST SECTIONS

The sections were cut using a diamond grit circular saw. One facing and the local core were internally routed to form the slot panel. The edge of the other panel was profile routed to form the tongue panel, see Fig. 2.9.

3.1.1 Bonding of Re-inforcements

Reinforcement Type 1 = Fig. 3.1

3.1.1.1 The G.R.P. reinforcing laminate was shaped prior to bonding, according to relevant part of Fig. 2.9.

3.1.1.2 The section faces, sides of the tongue and faces of reinforcement were lightly abraded with Scotchbrite No. F4/1.

3.1.1.3 Areas to be bonded were thoroughly wiped clean using lint free cloth dampened with chlorinated hydro carbon (CH_3CCl_3).

3.1.1.4 A uniform coating of adhesive was applied to the surfaces of the tongue and reinforcement with a spatula.

3.1.1.5 After the application of adhesive, the surfaces were brought together and were held by the application of 2 p.s.i. of dead weight to ensure an adequate contact.

3.1.1.6 The surplus adhesive was cleaned off with solvent and the section was allowed to partly cure for 24 hours before handling.

3.1.2 Reinforcement Type 2 = Fig. 3.2

3.1.2.1 The high density core sandwich panel was shaped according to

relevant part of Fig. 2.9.

3.1.2.2 The equivalent core area of the tongue panel was removed. Fig. 2.4.

3.1.2.3 The inner faces of the tongue skin and the surfaces of reinforcement were lightly abraded and cleaned according to Para. 3.1.1.2 and 3.1.1.3.

3.1.2.4 A sufficient amount of adhesive was applied to the open core and to the inner surface of the skin.

3.1.2.5 A uniform coating of adhesive was applied to each surface of the sandwich insert.

3.1.2.6 After the application of adhesive the surfaces were brought together and held by application of 2 p.s.i. of dead weight. Excess adhesive was squeezed out along the edges and cleaned off with solvent.

3.1.2.7 The section was allowed to cure partly for 24 hours before handling.

For ease of production the rectangular reinforcements (101.6 x 38.1mm) can be bonded to the trimmed panel edge prior to the shaping of the tongue. Trimming can be achieved using an automatic router machine controlled by computer aided manufacturing technique.

Room temperature bonding and curing of the reinforcements can be speeded up by using a hot press technique, i.e. applying heat (2 hours at 60°C) and pressure (2 p.s.i.) simultaneously, thus making the whole process more cost effective.

3.2 BONDING OF REINFORCED JOINT SPECIMENS

3.2.1 All test sections were bonded according to Figs. 3.3 to 3.6.

3.2.2 The areas to be bonded were thoroughly wiped clean using a lint free cloth dampened with a chlorinated hydro carbon.

3.2.3 A uniform coating of adhesive was applied to each surface of the tongue with a spatula. Area D Fig. 1.4.

3.2.4 A wedge of adhesive was worked into the open core of the honeycomb along the tip and edges of the tongue with a spatula. Area T Fig. 1.4.

3.2.5 A wedge of adhesive was worked into the open core of the honeycomb along the sides and base of the slot with a spatula. Areas B and C Fig.1.4.

3.2.6 Immediately after the application of adhesive the surfaces were brought together with the tongue panel vertical. To maintain joint integrity a 4lb weight was placed on the upper horizontal panel and the surplus adhesive was cleaned off with chlorinated hydro carbon.

3.2.7 The joint was allowed to partly cure for 24 hours at room temperature.

3.2.8 Partial cure was accelerated by heating the test sample to 140°F (60°C) for two hours in the case of EC 2216, and to 120°C for one hour in the case of Redux 410 M/A.

3.2.9 Test sample was allowed to cool to room temperature before loading.

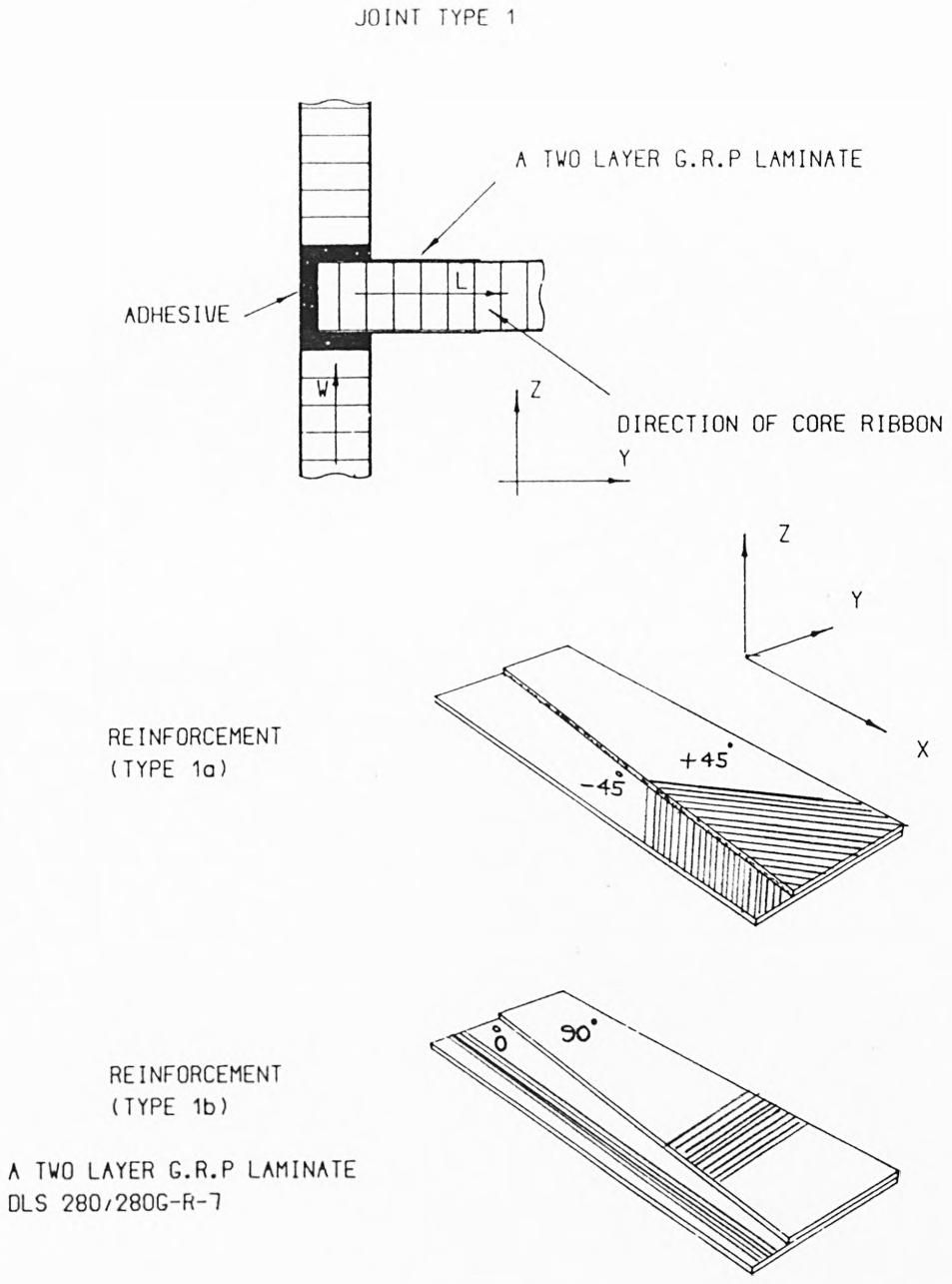

FIG 3.1
TONGUE AND SLOT JOINT
WITH EXTERNAL REINFORCEMENT

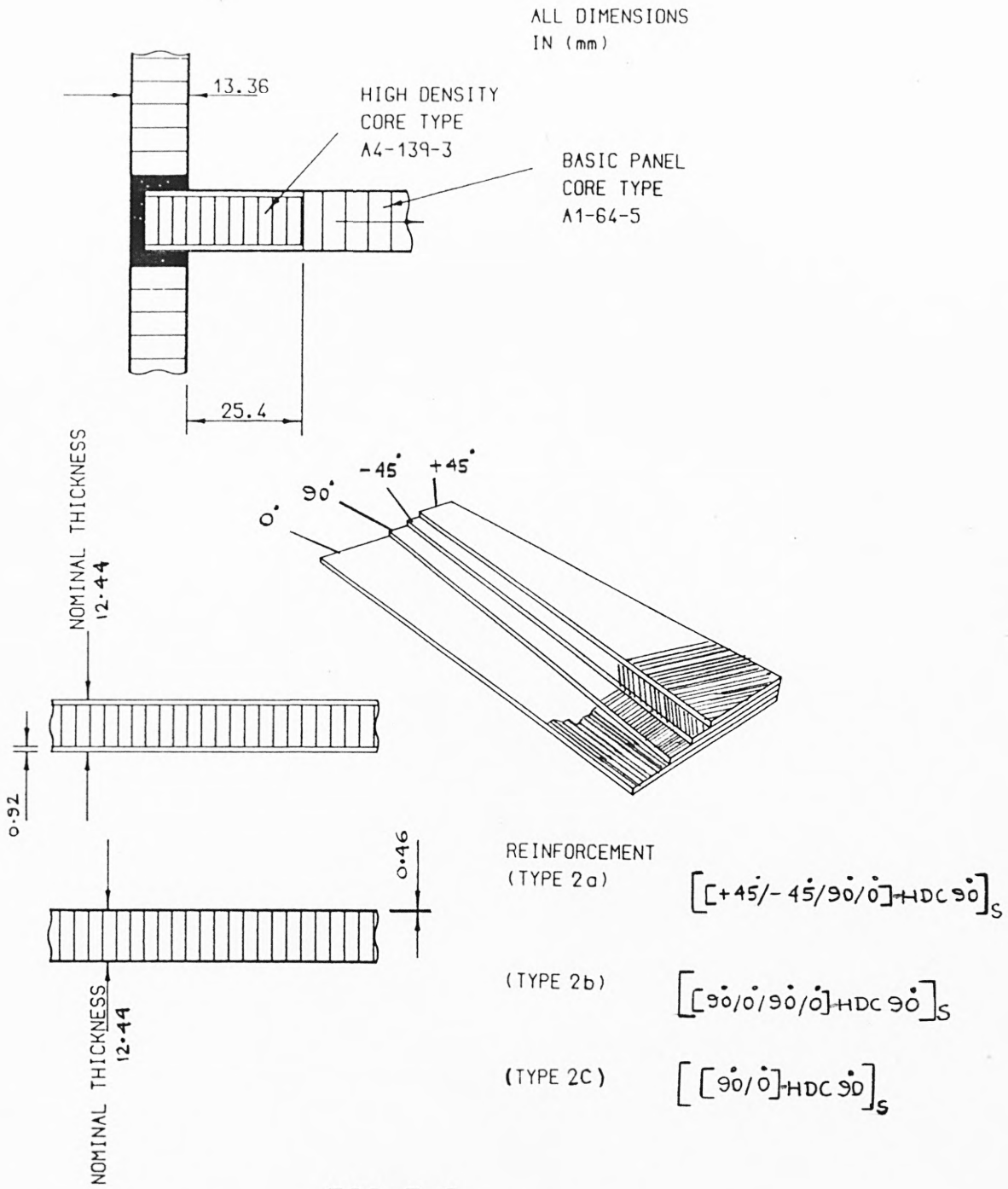

FIG 3.2
TONGUE AND SLOT JOINT WITH
INTERNAL REINFORCEMENT

D = 76.2 OR 101.6

ALL DIMENSIONS
IN (mm)

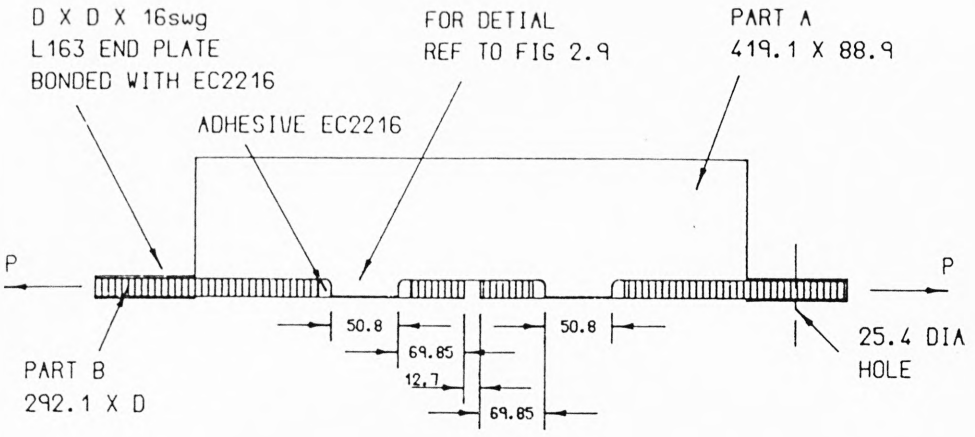

FIG 3.3
UNSYMETRICAL LONGITUDINAL SHEAR
LOADING OF THE JOINT

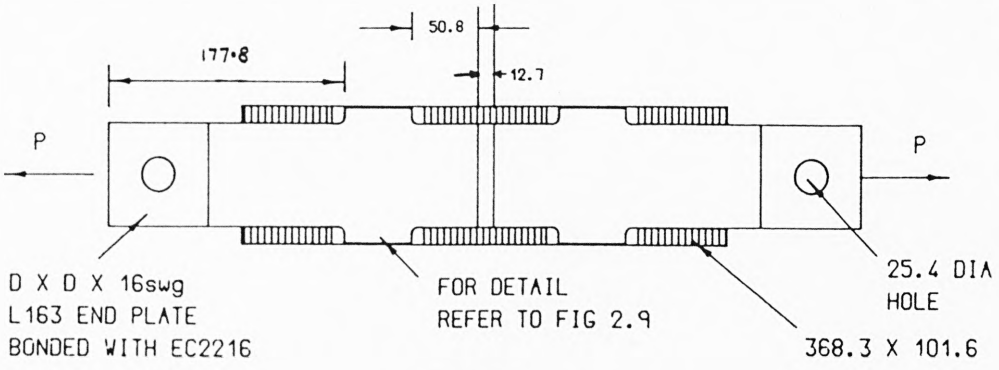

FIG 3.4
SYMETRICAL LONGITUDINAL SHEAR
LOADING OF THE JOINT

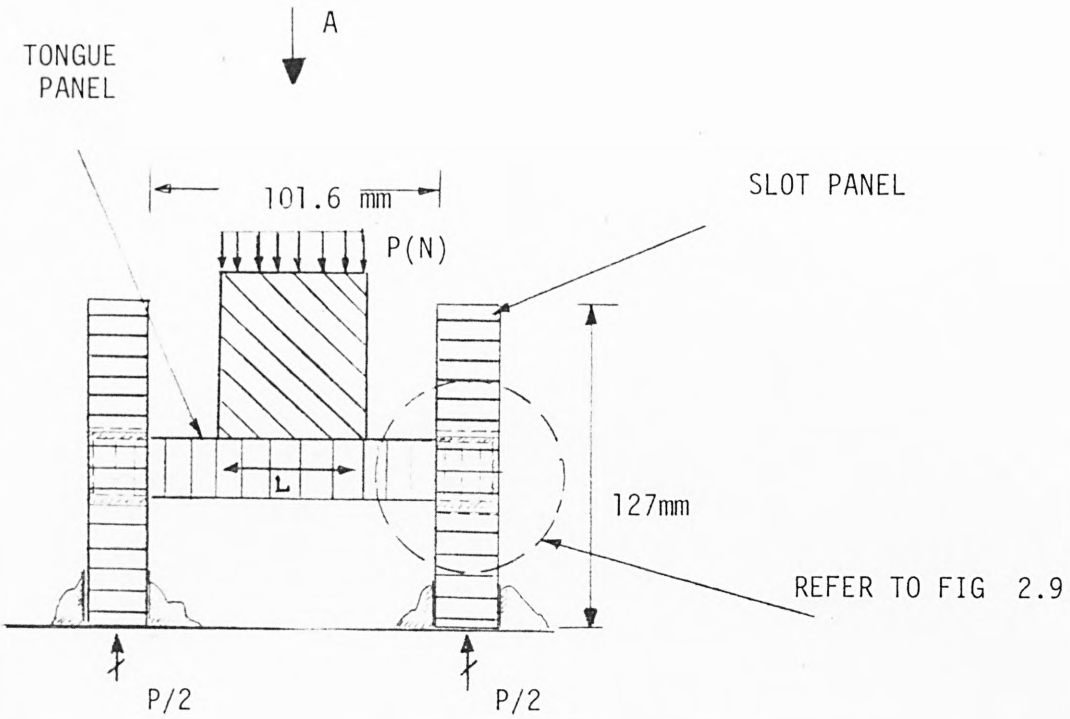

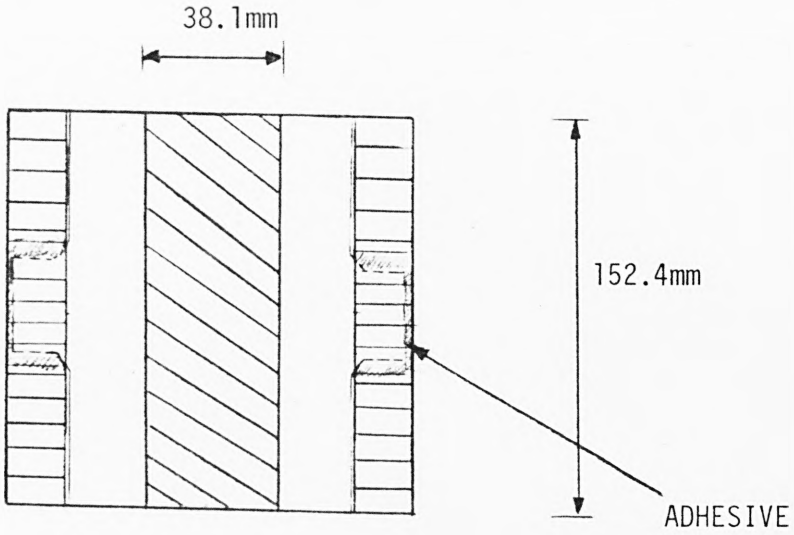

VIEW ON ARROW A

FIG 3.5

TONGUE AND SLOT JOINT WITH SHORT TRANSVERSE SHEAR SPECIMENS.

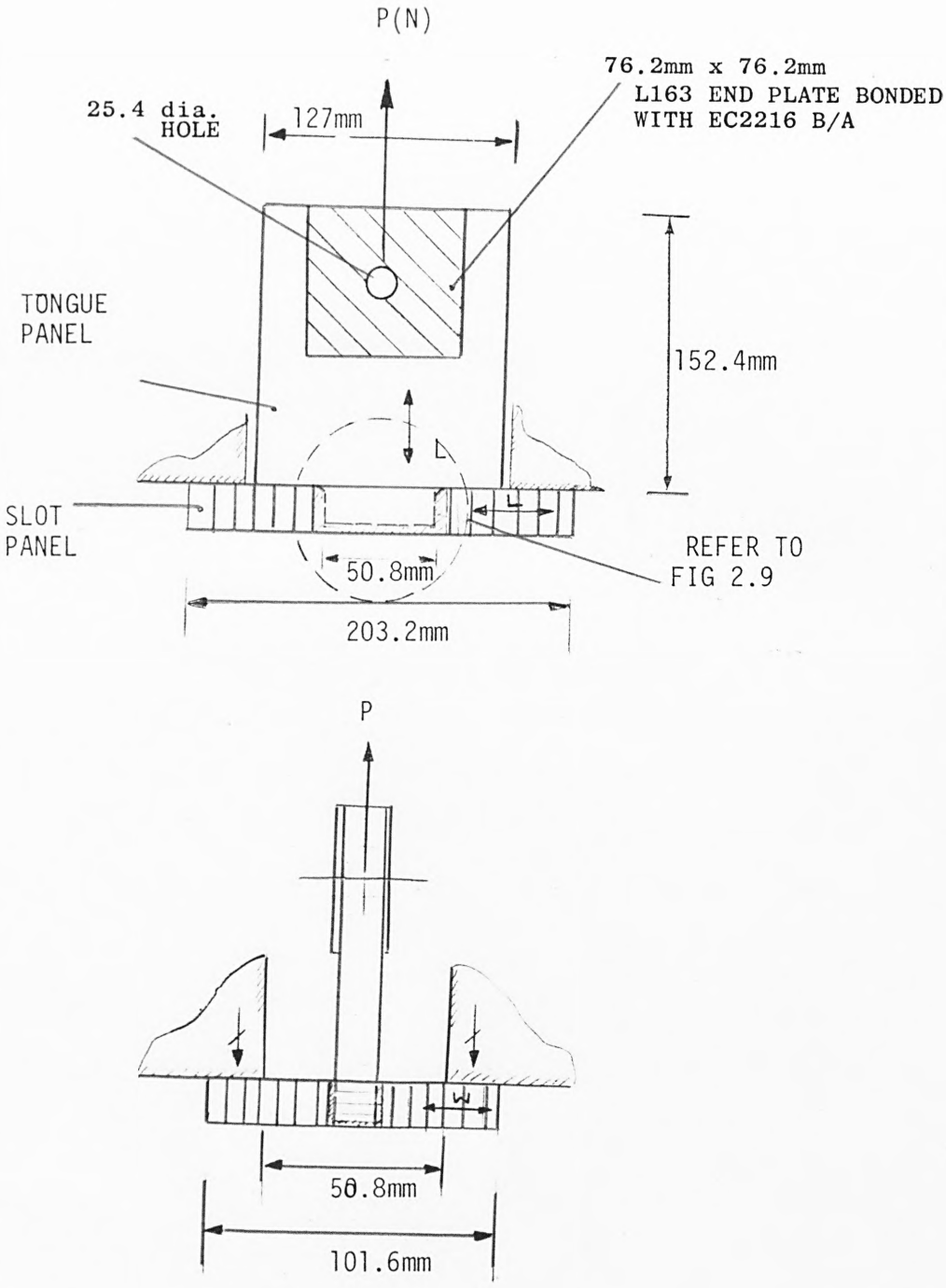

FIG 3.6

TONGUE AND SLOT JOINT WITH TENSILE TYPE OF SPECIMEN

4. JOINT TESTING

4.1 DESIGN TESTING OF THE TONGUE AND SLOT JOINT

Following the preliminary design study of the tongue and slot joint in Chapter 2, most of the problems identified were eliminated by bonding suitable reinforcements which were adequate in achieving the set design loads. Much emphasis was placed on the adhesive bonding since the integrity of the joint relies wholly on the continuity between the adhesion and adherend.

Another parameter which influences the strength of the joint is the degree of adhesive flexibility. The EC 2216 (from 3M) adhesive system was not compatible with the inner surface of the slot facing where a film adhesive (from CIBA-GEIGY) is used for fabrication of the basic sandwich panel. Hence a new epoxy adhesive system, Redux 410 M/A (from CIBA-GEIGY), was introduced and was found to be satisfactory in tests for the primary and secondary load cases, namely longitudinal shear loading and the tensile loading of the joint.

These were considered to be appropriate since the adhesive stresses are significantly greater than for the short tranverse shear loading.

4.1.1 Definition of Adhesive Bonds

The strength of an adhesive bond is governed by two fundamental factors, adhesion and cohesion. The former is the degree to which the adhesive is attached to the adherend, the latter is the strength of the adhesive itself. In a good bond the adhesive strength will always be higher than the cohesive strength, that is to say that when a

satisfactory bonded lap joint is pulled apart the adhesive will remain attached to the skins; no adherend surface will be visible.

Adhesion

No single theory explainig the mechanism of adhesion has been formulated, and few non-destructive test methods are able to characterise the adherend surface prior to bonding to ensure that the pre-treatment has been successful and the optimum adhesive strength can be attained.

The pre-treatment has three principal functions:-

(a) To remove the contamination.

(b) To generate the correct oxide layer.

(c) To produce the correct topography.

Cohesion

The principal parameters affecting cohesive strength are the adhesive thickness, modulus and density. Variations in these properties are caused by deviations from the optimum manufacturing procedure. Time, temperature and pressure must be strictly controlled during the cure. The adhesive is volatile and thickness cannot be controlled entirely due to joint configuration. However, modern epoxy paste adhesives are tolerant to large variations in thickness and are suitable for thick glue lines (i.e. 3mm).

4.1.2 Joint Design Test

Test specimens were fabricated according to Figs. 3.3, 3.6 and to the instructions of Chapter 3 by bonding the tongue and slot panel together using the two part adhsive EC 2216 B/A. They were tested to

ultimate failure on a 50,000lbs Macklow-Smith Universal testing machine on the 10,000lb range certified accuracy to within 1% of the actual force applied. For the longitudinal shear test of Fig. 3.3, the core of the adhesive ruptured at the tip of the tongue followed by de-bonding of the tongue from the inner facing of the slot at a slightly higher load, see Table 4.1, Fig. 4.1. This was the primary mode of failure. The tensile test specimens did not have the local reinforcement in the tongue area since the external reinforcement, type 1.0 does not make any difference to the joint tensile strength, see Chapter 2, Section 2.4.1. The failure mode of core-adhesive rupture was present again, if the high density core was inserted in the tongue panel locally, i.e. reinforcement type 2.0, this might have increased the strength by delaying the core-adhesive rupture. This was not done because the joint strength in this mode of loading was adequate for the design load of Tables 1.1 and 4.2. However, in the case of longitudinal shear test specimens, the two types of failure described above indicated that the joint in fact failed prematurely for which the possible reasons were thought to be:

(a) The unsymmetrical loading of test section which caused bending deformation in part A of the specimen, thus inducing peel stresses in the adhesive at the slot inner face.

(b) The extreme flexibility of the adhesive EC 2216 B/A which caused shear failure at the tip of the tongue. Fig. 2.6 Section AA. Due to low stiffness and strength of the core in the tongue panel, the adhesive forms a bridge connection between the two facings of the tongue panel. This bridge connection is more effective when the adhesive is less flexible.

(c) The existence of incorrect topography between the pre-cured film adhesive at the inner surface of the inner slot facing and the

paste adhesive used.

The first possibility was investigated further by a symmetrical test section, Fig. 3.4, (D = 76.2mm) to eliminate this unsymmetrical loading.

The second and third possibilities are investigated by introducing a different and less flexible epoxy paste adhesive, Redux 410 B/A, made by CIBA-GEIGY and hence are likely to be compatible with the core/facing film adhesive.

The mode of failure in the joints using EC 2216 B/A adhesive remained unchanged, while with the Redux 410 B/A the strength of the joint increased by about 16% on average. The failure mode of the tests with Redux 410 was still debonding of the adhesive from the inner surface of the slot facing, see Fig. 4.2, together with shear failure at the root of the tongue, see Fig. 4.3, Table 4.3 and 4.4.

The debonding of the adhesive was thought to be due to the glossy surface finish of the cured film adhesive between the core and the facings of the sandwich panel. This was investigated further by applying a vigorous abrasion to this surface prior to bonding the joint.

4.2 LAP SHEAR TEST

Fig. 4.4 shows the lap shear test specimen used to test method of treatment of the core/facing adhesive surface as in the tongue and slot joint. The facings of the basic sandwich panel were separated by cutting through the core and the inner surface was abraded with Scotchbrite F400 or with a rotary stainless thin steel wire brush until the glossy surface was removed. The surface was then treated according to Para. 3.1.1.3 of Section 3. Test samples for both adhesives (EC 2216

B/A and R410 M/A) were fabricated by bonding sheets of the facing between two L163 aluminium alloy sheets which were etch treated prior to bonding. These sheets were then cured in accordance with Para. 3.1.1.5, 8 and 9. They were then cut into four smaller specimens. Saw cuts are then made such that all the load transfer occurred across the core/

adhesive surface joining the two L163 sheets at the centre of the specimen. All the lap shear tests were carried out on a 5,000lbs Hounsfield Tensometer. Neglecting the peaking effect of the adhesive shear stresses across the edges, parallel to the notch where a sudden change of section occurs, the shear strength was calculated by dividing the failure load by the surface area between the saw cuts. Table 4.5 shows the very different bond strength obtained from the two adhesives.

The failure of the test sections was due to the debonding of the adhesive from the abraded core cell area at the inner surface of the facings. The surface abrasion, using a rotary thin stainless steel wire brush, was most effective on the Redux 410 M/A specimens. This doubled the bond strength on average. These specimens failed cohesively in the 410 M/A adhesive. The strength of specimens using the EC 2216 B/A did not increase significantly. The predominant mode of failure was adhesive failure unlike the Redux 410 M/A specimens, where the failure was cohesive, see Figs. 4.5 and 4.6. Without the surface treatment other than the solvent wipe, the only effective bond area where cohesive failure had not taken place was the removed cell core circumference in the inner surface of the facing. Therefore the adhesion strength of the actual joint test could be increased by removing the glossy surface using suitable mechanical means.

4.3 LONGITUDINAL JOINT TESTING

The longitudinal shear tests of the joint were now repeated with the reinforcement type 2.0 a, b, c, see Fig. 3.2. The width of the tongue panel in the geometry of the test specimen (Fig. 3.4) was increased by 25.0mm (D = 101.6mm). This was done so as to reduce the large deformation of the composite facings which occured in the tongue panel. With this type of reinforcement the joint was strongest and failure occurred primarily in the composite facing at the root of the tongue and finally on the inner slot facing.

Fig. 4.7 shows the latter failure. This was delamination of the 0°/90° laminated facing at the tip of the tongue. Interlaminar stresses caused a transverse tensile failure in the 90° ply being the first adherend layer in the inner flot facing. Therefore the strength of the joint could be increased by switching over the ply position, allowing the 0° layer to take the strain in the fibre direction. This was not tested since the set design load was achieved with this ply orientation. Table 4.6 gives the results of tests carried out in which failure of the joint was limited to the composite only.

4.4 SHORT TRANVERSE SHEAR TEST

Test sections were bonded according to Fig. 3.5 and to the instruction of Chapter 3 using the Redux 410 N/A adhesive system. They were tested to ultimate failure on the Macklow Smith Universal testing machine by applying a distributed load via a metal block. As expected from the initial design studies of the joint the core shear strength and stiffness has proved to be the deciding mode of joint failure in this

type of loading. Inserting a high density core of reinforcement, type 2.0, limited the failure to the boundary of the insert in the basic tongue panel thus avoiding local joint failure at the root of the tongue, see Table 4.7. The facings laminate contributes little to the joint strength in this direction because they were so thin, increasing still further the shear stiffness and strength of the core locally by using an even denser core would not give rise to a significant increase in strength without a significant increase in weight. This was not necessary since the design requirement was achieved with the present reinforcement.

4.5 DISCUSSION

In the last few sections the problems associated with the tongue and slot method of joining composite sandwich panels were outlined and, through a process of elimination by experimental studies, the design requirements of Table 1.1 were achieved for the three loading cases. As emphasized in the preceeding chapters the primary loading of the joint is in the longitudinal direction for which the major load transfer occurs. The tensile loadig of the joint arises not because of direct tension as in the test specimen, see Fig. 3.6, but rather from the large inplane deformation of individual panels of a large structure such as a galley due to the fwd. 'g' case, see Fig. 1.2. The short transverse shear loading is directly related to the out of plane bending of the composite sandwich panel working as beam which normally arises from the up and down 'g' inertia case. Providing such out of plane stiffness and strength is after all the main characteristics of composite sandwich

panels and so it was not surprising that these were the least harmful loadings.

It is concluded from the results of the tests described in this chapter that the adhesive system EC 2216 B/A, which is a two part modified epoxy paste, is not compatible with the joint configuration considered in this work partly because of its flexibility and partly due to the lack of adhesion to the core/facing adhesive (inner surface of slot facing laminate). However the flexible characteristics of this adhesive enables it to be used effectively in other applications, e.g. external bonding of aluminium alloy sections to a sandwich panel. A less ductile but more compatible epoxy adhesive such as Redux 410 M/A was found to be effective in eliminating the bond interface failure with the inner slot facing as well as providing a major bridge connection at the tip of tongue between the two tongue facing laminate, hence avoiding the possibility of the adhesive-core rupture, see Fig. 4.1. Generally it is desirable for the tongue and slot joint not to fail at the bond interface because adhesively bonded joints can suffer from environmental degradation which causes debonding, this is particularly important for structures such as galleys where heat from ovens and moisture from beverages are some of the main features. It is normal to use polymeric matrix composite materials because many matrix resins are also good adhesives. For example, epoxies are used as adhesives for fibre reinforced epoxy laminates as well as for many other materials. When the matrix material of the laminates is also used as the adhesive in the joint, excellent adhesion can result, i.e. Redux 410 M/A and BSL-377. However, even with this excellent adhesion, there is a problem when the sandwich panel facing consists of several layers. The joint represents a discontinuity in the material resulting in high delamination stresses which can initiate joint failure.

The allowable loads on the tongue and slot joint are the loads at which micromechanical damage first occurs that will eventually lead to macromechanical damage. Thus the micromechanical damage can be the basis for the selection of ultimate-load prediction techniques and the prediction of failure modes of the joints. The micromechanical damage may initiate in the adhesive layer, at the interface, or in the adherends forming the joint. The modes of micromechanical damage in the joint may be summarized as follows:

(1) Cohesive failure within the adhesive layer

(2) Adhesive-adherend interface failure

(3) Interlaminate failure in the adherend laminate

(4) Transverse lamina failure caused by failure of resin

(5) Transverse lamina failure resulting from interface failure

(6) Longitudinal lamina failure.

The cohesive failure within the adhesive layer may occur by brittle fracture or by a rubbery tearing, depending on the type of adhesive used. The adhesive-adherend interface failure occurs on a macroscale when incorrect topography exists at the interface. Interlaminar failure in the laminate may be caused by poor processing, voids, delaminations, or thermal stresses. The last three types of failure are lamina failures which also occur in the longitudinal shear loading of the joint and are the subject of investigation in Chapter 10.

To obtain the optimum joint strength in the primary load case, it is necessary to arrange the fibre in the direction of greatest load. The optimization of joint strength could be investigated experimentally by trying different arrangements evolving the best one for each type of reinforcement. This is obviously very costly and time consuming and should there be a change of material or of thickness of sandwich panel, or of joint configuration such as curved or angled, the whole process

would have to be repeated again. It was for these reasons that it was decided to investigate the joint failure analytically. The finite element method was chosen for the purpose of joint stress analysis and strength prediction because it could deal with the complex geometry of the joint. It could be used for future development of such joints. Nothing was found in the literature on the analysis of such joints in composite sandwich panels. The following chapters give step by step procedures in developing a method from which the composite sandwich panel and the tongue and slot joint could be analysed and its strength predicted for different ply orientation.

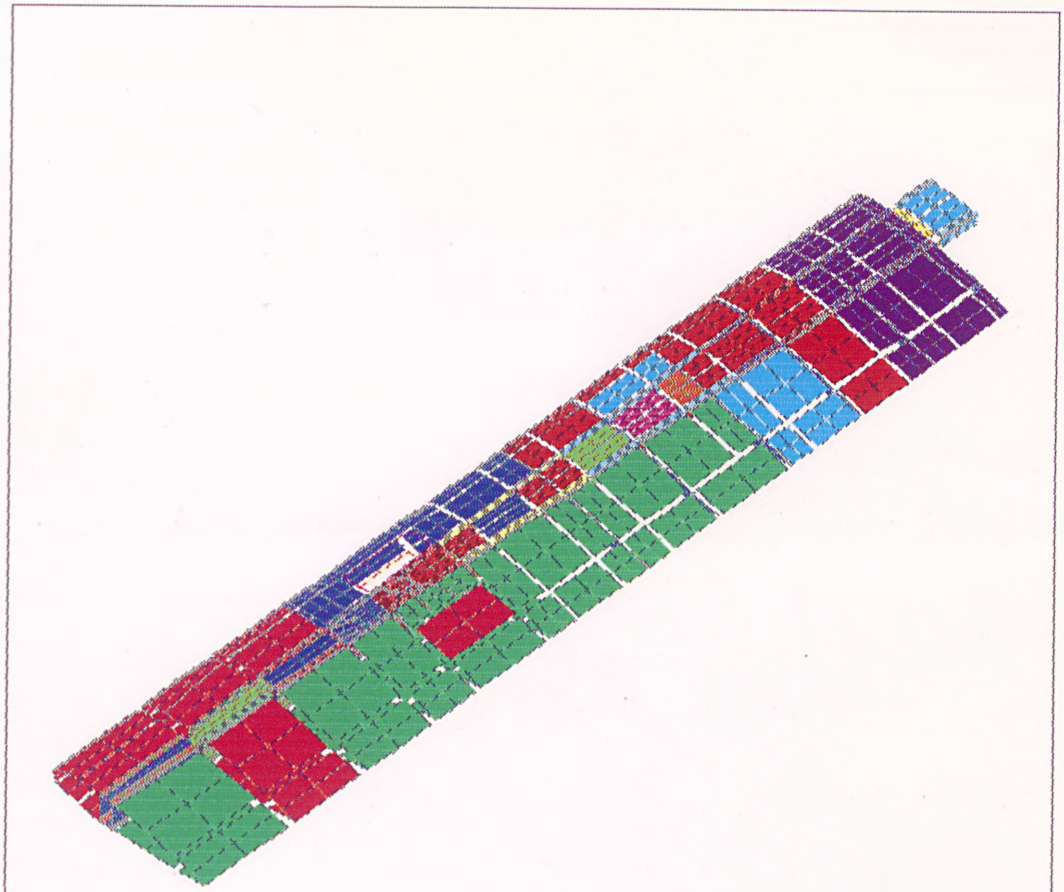

APLOT

PLOT AREAS FROM 1 TO 579 BY 1

PREP7 -INP=

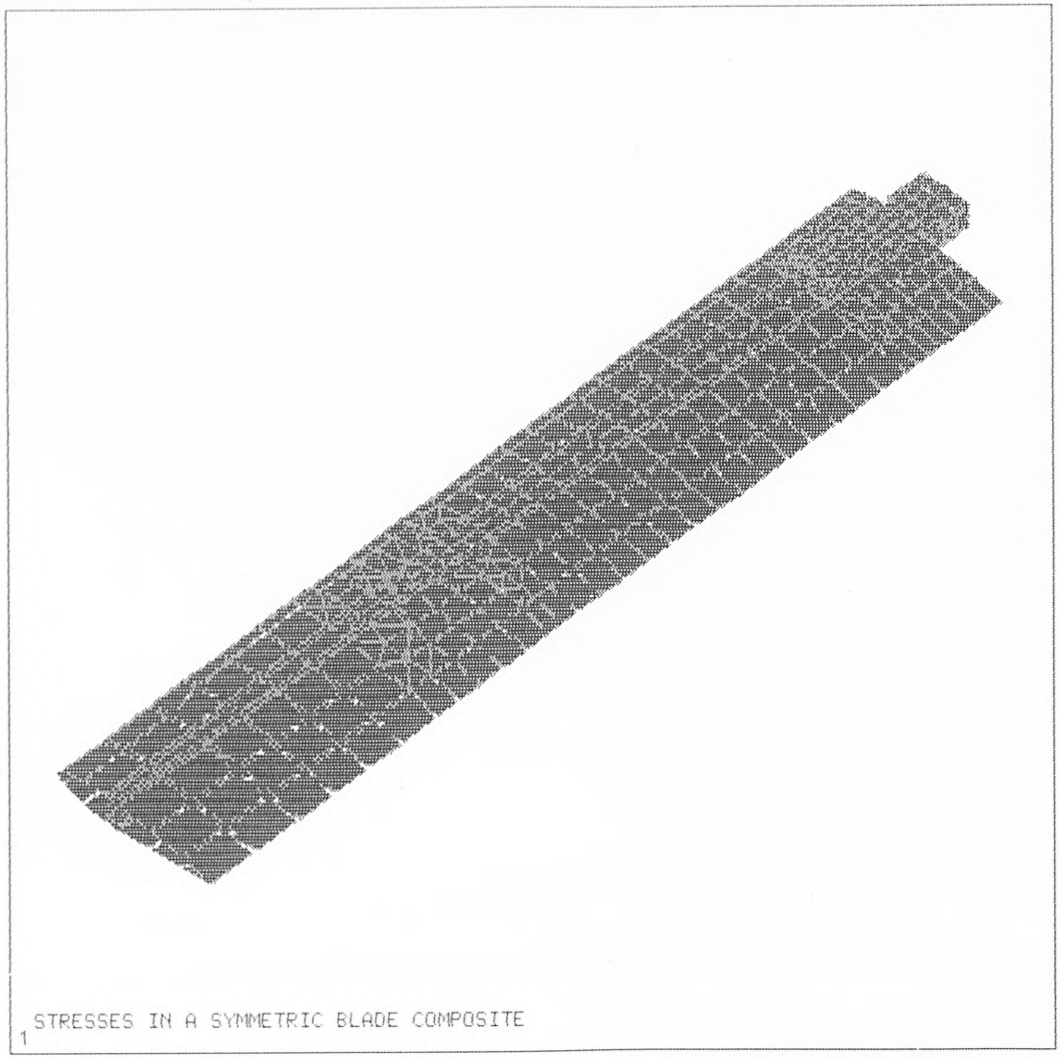

***WARNING *** CP= 544.8100 TIME= 15.

ELEMENT NO. 1451. NOT PLOTTED BECAUSE CORNER NODE(S) NOT DEFINED

PREP7 -INP=

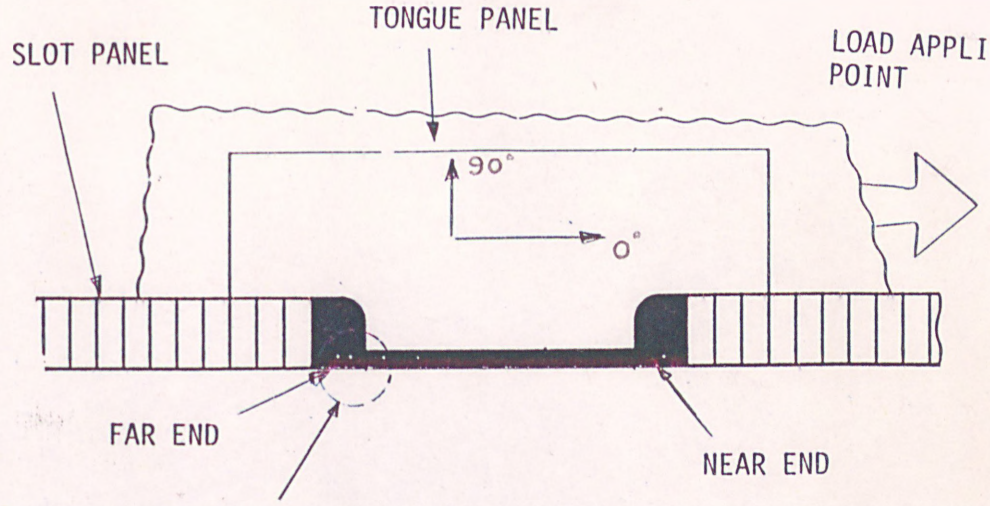

RUPTURED CORE/ADHESIVE AREA AT THE TIP OF THE TONGUE

DEBONDED AREA OF THE TONGUE

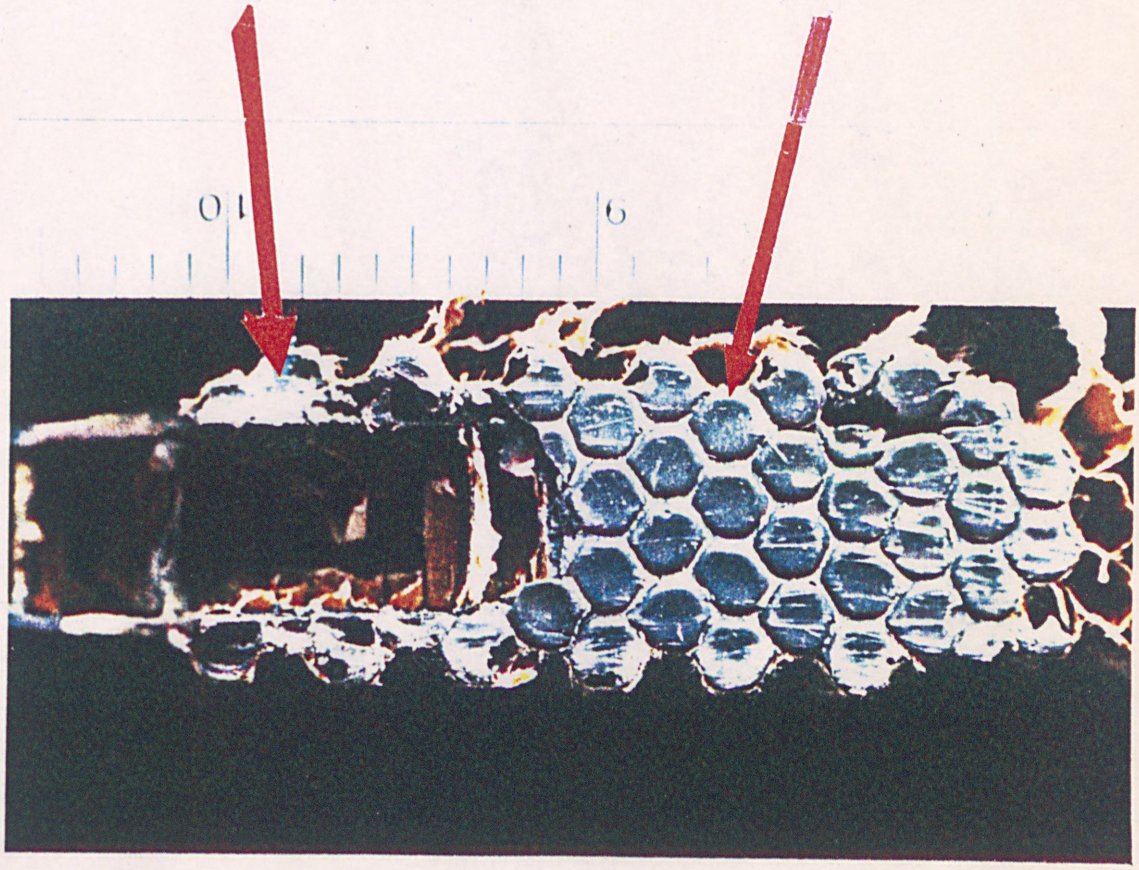

FIG 4.1

CORE-ADHESIVE RUPTURE AT THE INNER SLOT FACING INTERFACE

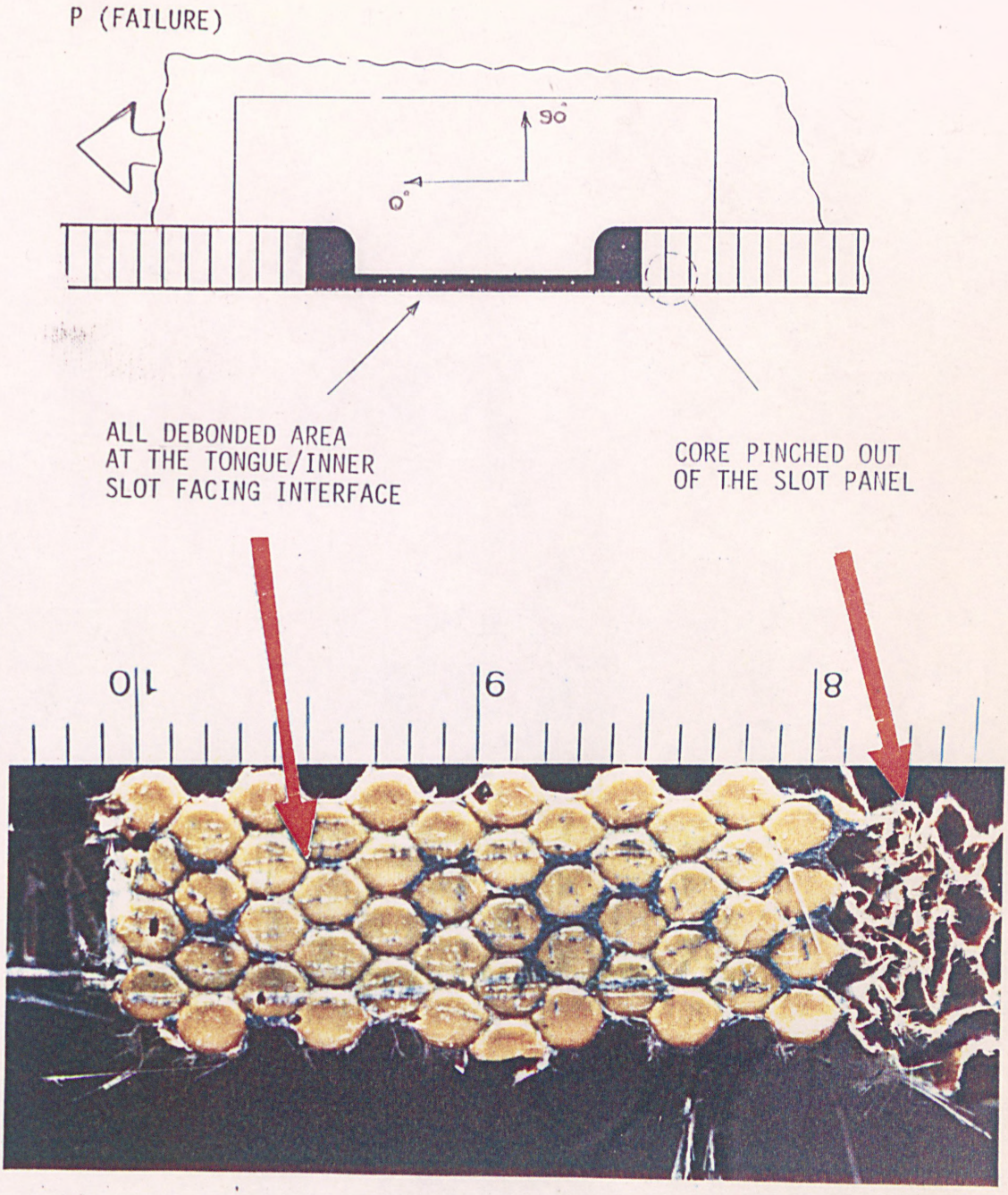

FIG 4.2

ADHESIVE-ADHEREND FAILURE AT THE INNER SLOT FACING

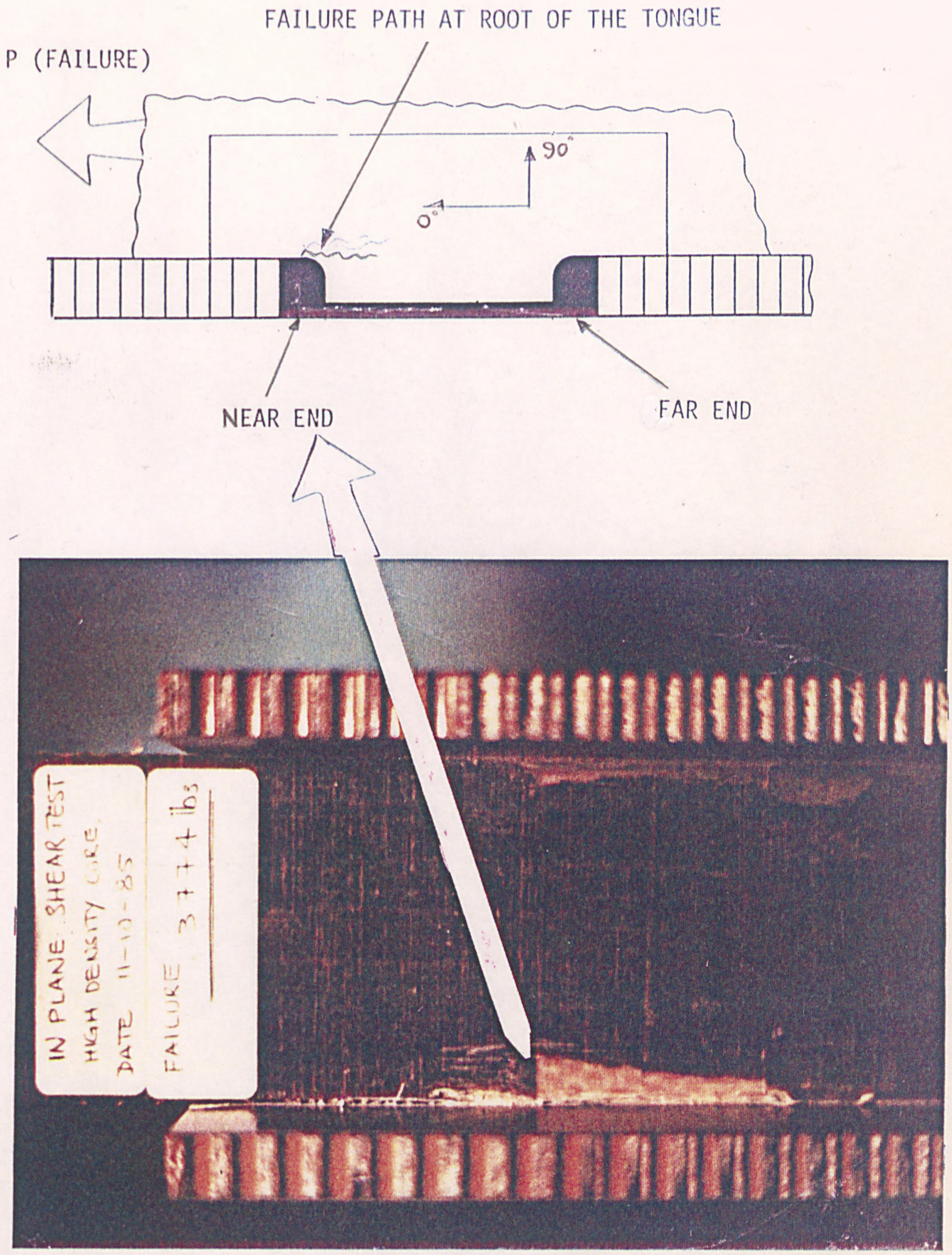

FIG 4.3

LAMINATE FAILURE AT THE ROOT OF THE TONGUE
(TYPE 2C TABLE 4.3)

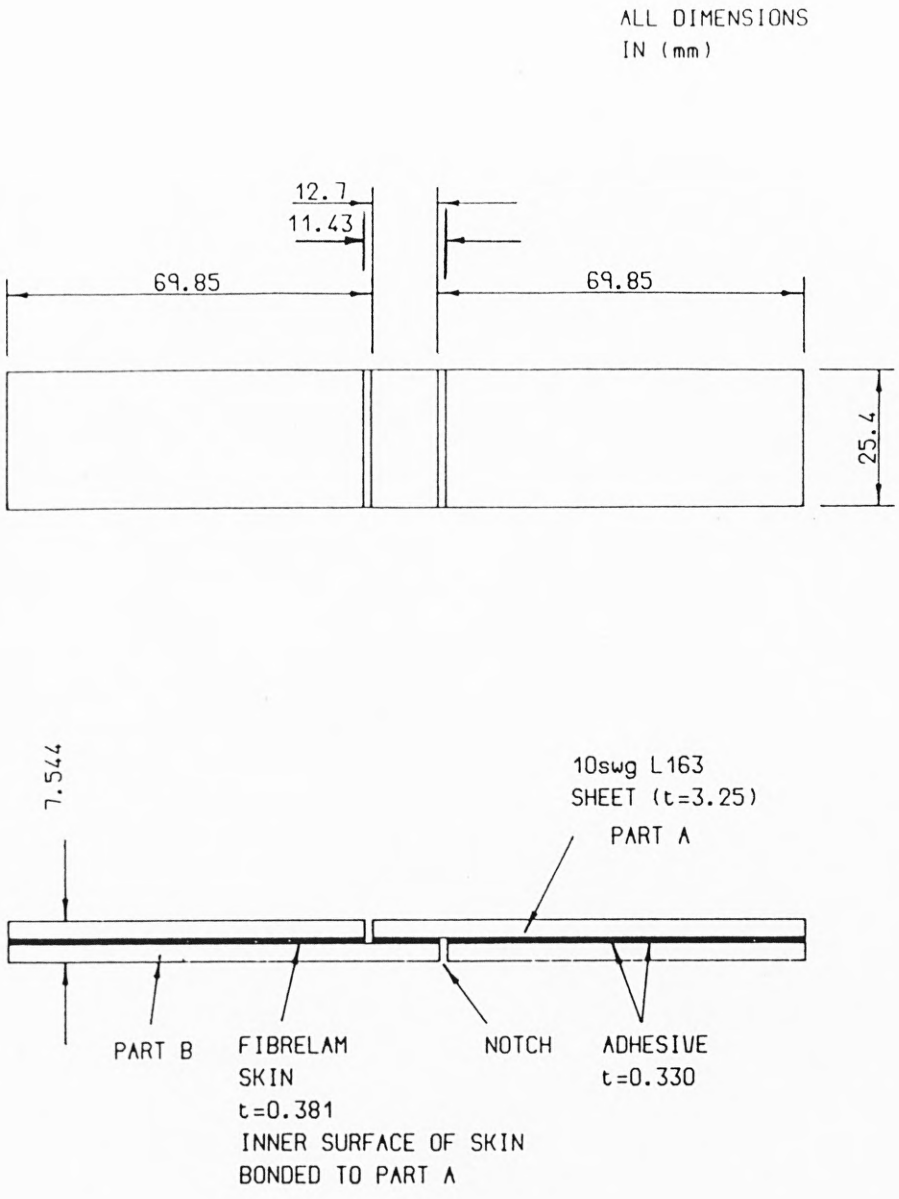

FIG 4.4
LAP SHEAR TEST SPECIMEN

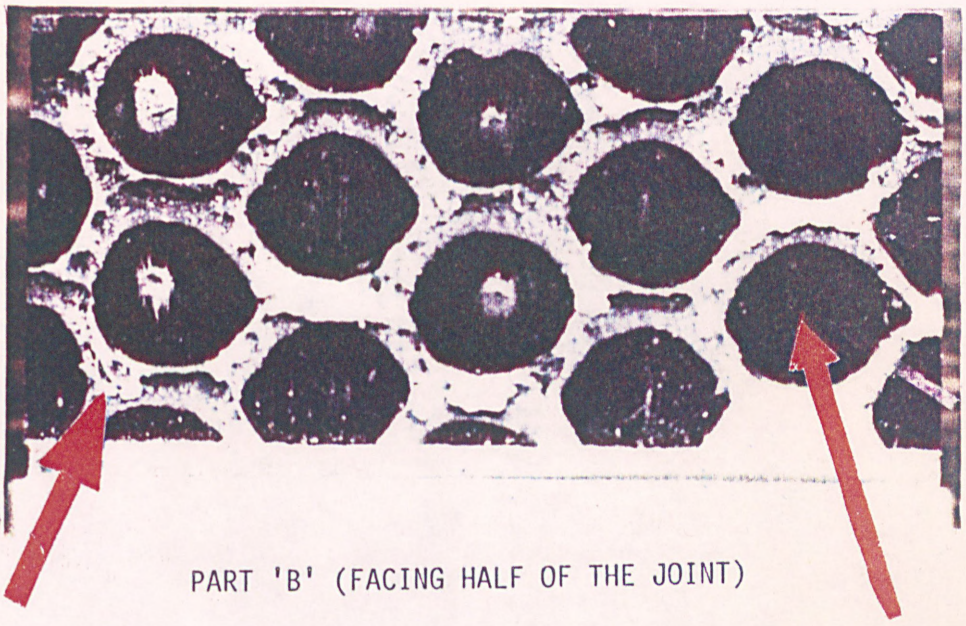

PART 'B' (FACING HALF OF THE JOINT)

ADHESIVE STILL BONDED TO INNER SURFACE OF FACING (ABOVE) AND METAL (BELOW). (COHESIVE FAILURE)

DEBONDED AREA OF INNER SURFACE OF THE SKIN (CORE CELL SITE ABOVE) FROM THE ADHESIVE (EC2216, BELOW).

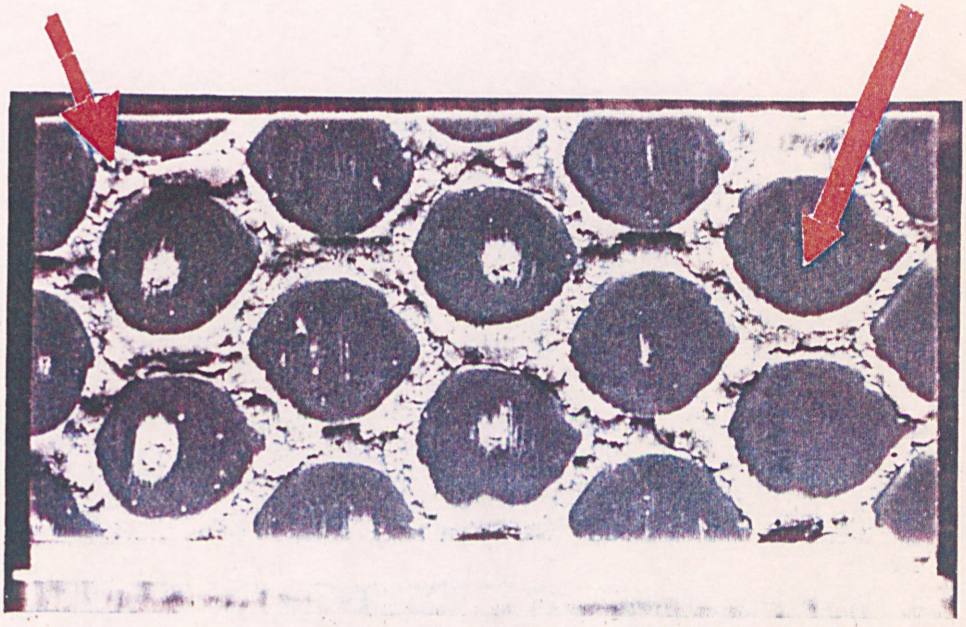

PART 'A' (METAL HALF OF THE JOINT)

FIG 4.5

ADHESIVE-ADHEREND FAILURE OF LAP SHEAR TEST WITH EC2216/BA

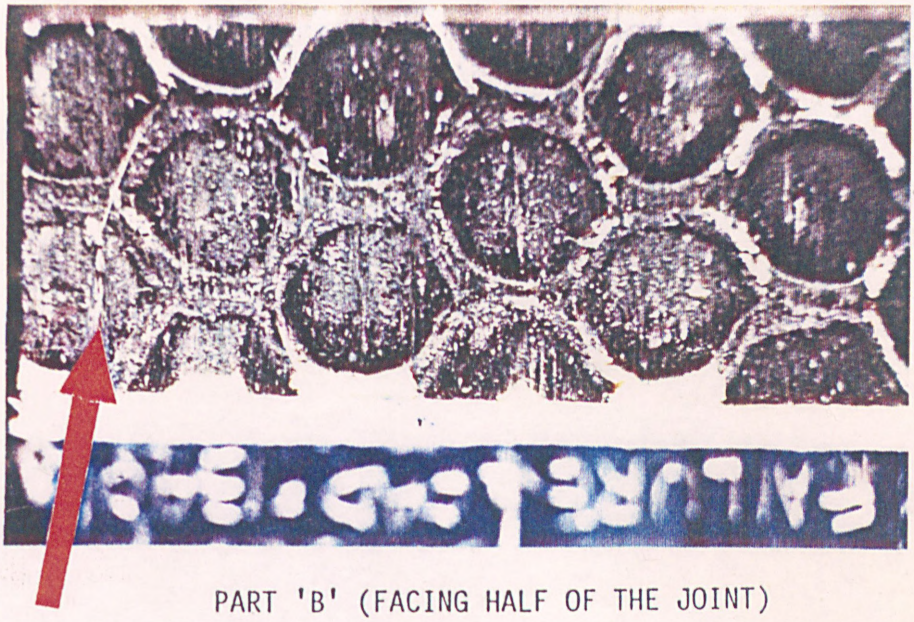

PART 'B' (FACING HALF OF THE JOINT)

IMPROVED BOND AREA

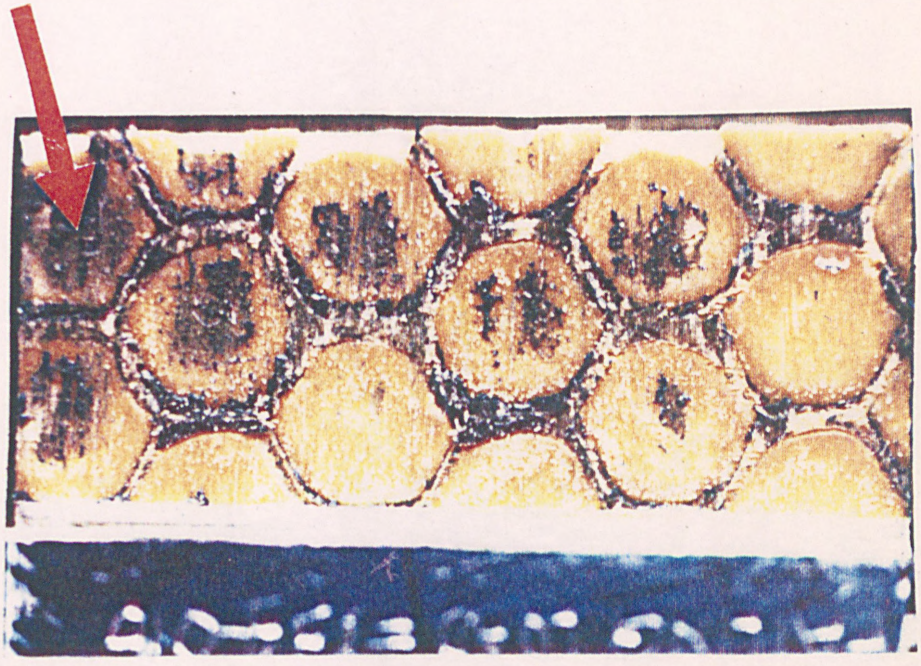

PART 'A' (METAL HALF OF THE JOINT)

FIG 4.6

ADHESIVE-ADHEREND FAILURE OF LAP SHEAR TEST (REDUX410N/A)

P (FAILURE)

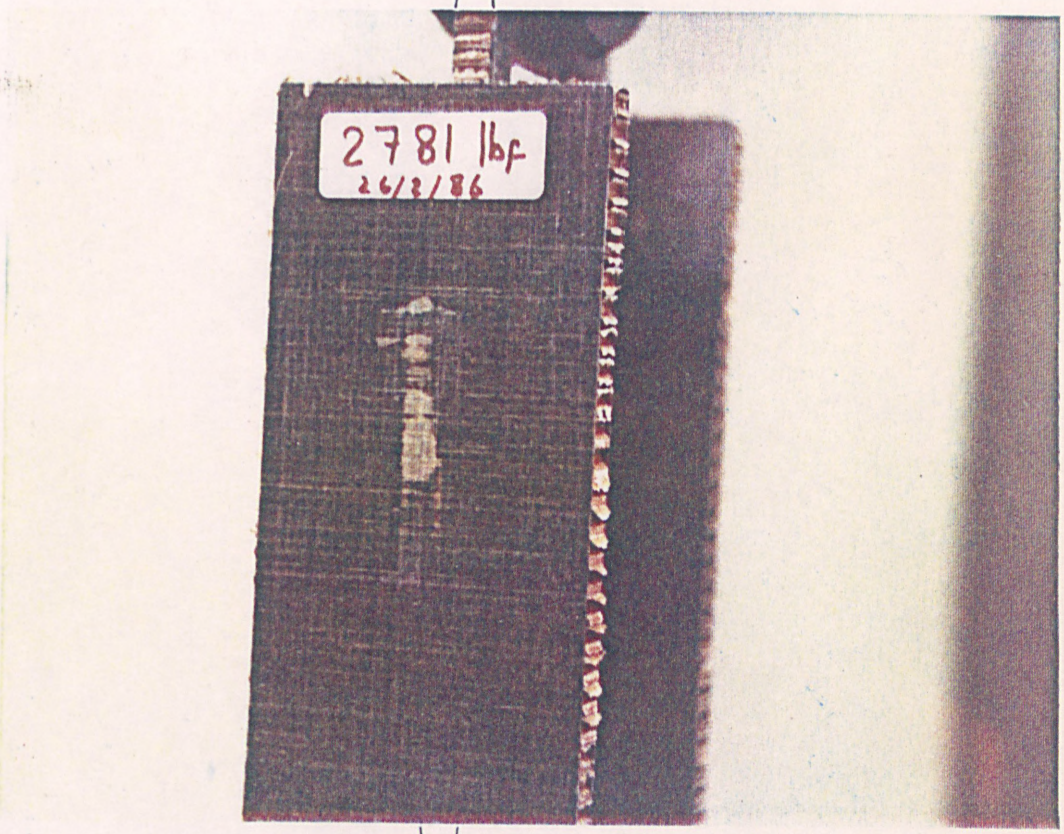

P (FAILURE)

FIG 4.7

LONGITUDINAL SHEAR TEST FAILURE OF THE FACING AT THE TIP OF THE TONGUE INDICATED BY CRAZING OF THE FACING

TEST No.	TYPE OF REINFORCEMENT	FIBRE ORIENTATION	FAILING LOAD PER JOINT (N)	MODE OF FAILURE
1	1a	$(+45^{\circ}/-45^{\circ})_s$	6023	R*
2	1a	$(+45^{\circ}/-45^{\circ})_s$	6485	T*
3	1b	$(90^{\circ}/0^{\circ})_s$	6094	R*

TABLE 4.1

LONGITUDINAL SHEAR TEST (EC 2216 B/A) UNSYMMETRICAL JOINT SPECIMENS

NOTATION

R - SHEAR RUPTURE OF THE CORE AND ADHESIVE AT THE TIP OF THE TONGUE.
T - ADHESIVE AT THE TIP OF THE TONGUE DEBONDED FROM THE INNER SURFACE OF SLOT.
s - SYMMETRIC LAMINATE REINFORCEMENT.

TEST No.	TYPE OF RINFORCEMENT	FAILURE LOAD (N)	FAILURE MODE
1	NONE	3372	R*
2		3362	R*
3		3541	R*

TABLE 4.2

TENSILE TEST ON THE TONGUE AND SLOT JOINT (EC 2216 B/A)

TEST No.	TYPE OF REINFORCEMENT	FIBRE ORIENTATION	FAILING LOAD PER JOINT (N)	MODE OF FAILURE
1	1a	$(+45^{\circ}/-45^{\circ})_s$	5827	R
2	1a	$(+45^{\circ}/-45^{\circ})_s$	6316	T
3	1a	$(+45^{\circ}/-45^{\circ})_s$	6005	R

TABLE 4.3

LONGITUDINAL SHEAR TEST (EC 2216 B/A) SYMMETRICAL SPECIMENS

NOTATION

R - SHEAR RUPTURE OF THE CORE AND ADHESIVE AT THE TIP OF THE TONGUE.

T - ADHESIVE AT THE TIP OF THE TONGUE DEBONDED FROM THE INNER SURFACE OF THE SLOT.

s - SYMMETRIC LAMINATE FACINGS.

TEST No.	TYPE OF REINFORCEMENT	FIBRE ORIENTATION	FAILING LOAD PER JOINT (kN)	MODE OF FAILURE
1	1b	$(90^{\circ}/0^{\circ})_s$	7.833	S
2	1a	$(+45^{\circ}/-45^{\circ})_s$	7.206	T
3	2c	$(90^{\circ}/0^{\circ})_s$ and high density core insert	7.71	T

TABLE 4.4

LONGITUDINAL SHEAR TEST (REDUX 410 N/A) SYMMETRICAL SPECIMENS

NOTATION

S - SHEAR FAILURE AT THE ROOT OF THE TONGUE.

T - ADHESIVE AT THE TIP OF THE TONGUE DEBONDED FROM THE INNER SURFACE OF THE SLOT.

s - SYMMETRICAL LAMINATE FACINGS.

TEST No.	ADHESIVE	SURFACE ABRASION METHOD	FAILURE LOAD P (kN)	BOND STRENGTH (MPa)
1	REDUX 410 N/A	ABRADED WITH SCOTCHBRITE F/400	2.49	9.6
2			3.336	11.24
3			3.25	11.4
4			3.0	10.05
1	REDUX 410 N/A	ABRADED WITH ROTARY THIN GAUGE STAIN-LESS STEEL WIRE BRUSH	5.25	20.34
2			5.96	22.70
3			4.94	19.45
4			5.38	21.38
1	EC 2216 B/A	ABRADED WITH SCOTCHBRITE F/400	2.05	6.85
2			2.89	10.5
3			2.58	10.52
4			2.56	8.47
1	EC 2216 B/A	ABRADED WITH ROTARY THIN GAUGE STAIN-LESS STEEL BRUSH	3.4	11.38
2			2.82	10.5
3			3.26	12.8
4			3.09	12.14

TABLE 4.5

LAP SHEAR TEST RESULTS

PHASE III

TEST No.	TYPE OF REINFORCEMENT	FIBRE ORIENTATION	FAILING LOAD PER JOINT (kN)	MODE OF FAILURE
1	$2b_D = 101.6$	$(90^\circ/0^\circ/90^\circ/0^\circ)_s$ and high density core	11.9	d
2	$2a_D = 101.6$	$(45^\circ/-45^\circ/90^\circ/0^\circ)_s$ and high density core	12.37	d
3	$2c_D = 75.04$	$(90^\circ/0^\circ)_s$ and high density core	8.394	S

TABLE 4.6

LONGITUDINAL SHEAR TEST OF REINFORCEMENT TYPE 2.0

NOTATION

S - SHEAR FAILURE AT THE ROOT OF THE TONGUE.

d - DELAMINATION OF THE INNER FACING OF THE SLOT.

s - SYMMETRIC LAMINATE FACINGS.

TEST No.	TYPE OF REINFORCEMENT	FIBRE ORIENTATION	FAILING LOAD PER JOINT (N)	MODE OF FAILURE
1	1a	$(+45^{\circ}/-45^{\circ})_s$	2055	f
2	2c	$(90^{\circ}/0^{\circ})_s$ and high density core insert	3247	e
3	1b	$(90^{\circ}/0^{\circ})_s$	2224	f

TABLE 4.7

SHORT TRANSVERSE SHEAR TEST

NOTATION

f - CORE SHEAR FAILURE LOCAL TO THE JOINT (See Area E, Fig. 1b).

e - CORE SHEAR FAILURE IN THE BASIC SANDWICH PANEL AWAY FROM THE REINFORCEMENT.

s - SYMMETRIC LAMINATE FACINGS.

The properties of all the materials (facing laminate, honeycomb core, adhesive) used in the fabrication of the joints and test specimens were obtained experimentally on the Avery-Denison (6156) 20kN range Universal Servo-controlled testing machine certified to BS 1610 Grade 1, unless otherwise stated. In addition to the materials described in Chapter 3, an 8-ply unidirectional laminate (DLS 280 G-R-7) with a nominal thickness of 1.65mm, also provided by CIBA-GEIGY, was used for determining the elastic properties of the sandwich facings. The resin and the fibre content of the composites were determined by gravimetric analysis using a high temperature furnace to burn off the carbon content of the samples. The ratio of resin to fibre content were 36.7% by weight and % by volume with ± 2% variation. It was found that the strengths were within the acceptable scatter expected for batch differences.

5.1 PROPERTIES OF DLS 280 G-R-7

For orthotropic materials with equal properties in tension and compression, certain basic experiments can be performed to obtain the properties in the principal material directions. However, difficulties encountered in analysis of materials with different strengths in tension and compression which will be described later in the section (5.4). The data obtained from the standard material tests are given below:

5.1.1 Tensile test at 0° and 90° on unidirectional specimens:

E_{11} = 48.8 GN/m² E_{22} = 12.9 GN/m²

Major Poisson's Ratio = ν_{12} = .28

Minor Poisson's Ratio = ν_{21} = .078

5.1.2 Rail shear test:

G_{12} = 3.74 GN/m^2

5.1.3 Three point flexural tests on 0° and 90° unidirectional beams.

For specimens with fibres aligned along the beam axis, it was found that a 50mm span was the most suitable.

σ_{1UT} = 1700 MN/m^2 σ_{2UT} = 111.4 MN/m^2

E_{11} = 50.2 GN/m^2 E_{22} = 12.996 GN/m^2

5.1.4 Interlaminar shear strength

τ_{12U} = 76.56 MN/m^2

5.2 PROPERTIES OF THE CORE

Nomex core type A1-64-5 with density of 64 kg/m^3

cell size = 4.76mm

G_{1z} = 53.5 MPa G_{2z} = 29.0 MPa

Nomex core type A1-123-3 with density of 123 kg/m^3

cell size = 3mm

G_{1z} = 100 MPa $\qquad$ G_{2z} = 50 MPa

5.3 PROPERTIES OF ADHESIVE

The adhesive used for this work was Redux 410 N/A, a two part paste epoxy adhesive obtained from CIBA-GEIGY Plastics, Cambs. The following data were obtained from basic experimental tests:

E = 1.8 GPa

ν (Poisson's Ratio) = 0.46

G = 0.4 GPa

Tensile Strength σ_{UT} = 41.0 MPa

τ_U = 35 MPa .

5.4 COMPRESSION TESTING OF UNIDIRECTIONAL COMPOSITE SANDWICH PANEL

Honey-comb sandwich structures in compression can fail in a number of characteristic modes which depend upon the relative size and materials properties of the component parts of the sandwich. In order that the sandwich construction be lightweight, the core is usually a thick layer of low-density honeycomb (Nomex) and the facings are made from thin layers of composite (G.R.P.). As a consequence of employing a lightweight core and thin laminate facings, the design method in compression has to account for the core shear deformation resulting

from its low effective shear modulus and from the low transverse modulus of unidirectional composite facings. The main difference in design procedures for composite sandwich structural elements as compared to that of non-sandwich composites is the inclusion of the effects of core shear properties on deflection, buckling, and stress as well as the effect of low buckling stiffness of the thin composite. The modes of failure that may occur in a sandwich panel under edge-wise compression loading are shown in Fig. 5.1.

a) Euler Buckling (Fig. 5.1(a)

Fig. 5.1(a) shows the general buckling. This is an overall Euler type instability and is caused by insufficient panel thickness or low core shear rigidity.

b) Shear Buckling (Fig. 5.1(b)

Shear buckling occurs as a result of low core shear rigidity or shear strength in which the wave length of the buckles is very small and usually follows as a consequence of general Euler type buckling. The shear buckling can occur suddenly and may cause shear failure in the bond between the facing and core.

c) Face Wrinkling (Fig. 5.1(c)

This is a rather involved mode of failure and depends upon the core elastic tensile and compressive properties and the initial waviness of the facing material. The mode of failure is characterised by the local buckling of one or both facings into or away from the core. The direction of failure (into or away from the core) depends upon the relative tensile strength of the skin-to-core adhesive and the compression strength of the core.

d) Intercell Buckling (face dimpling) (Fig. 5.1(d)

The faces of a honeycomb sandwich panel when loaded in bending or column compression may show a pattern of dimple of the same size as the honeycomb cells. This dimpling is essentially the buckling of the facing material over the area of each honeycomb cell, acting as simply supported hexagonal plate under compression. The amplitude of the dimples may be large enough to cause the dimples to grow across the core cell walls and result in a wrinkling of the facings.

e) Local Crushing of Core (Fig. 5.1(e)

This takes place when an excessive local load is concentrated on the sandwich. Failure is caused by low core compressive strength. This can be avoided by placing high density core, either locally or throughout the panel, depending upon circumstances.

f) Facing Failure and Transverse Shear Failure in Flexural Bending (Fig. 5.1(f)

In order to predict the compressive failure by the finite element analysis it is necessary to have the failure strength in the appropriate modes. The tests described in this section were carried out in a search to find the most appropriate test for compressive strength of the facings. Tests in some of these modes, e.g. Euler buckling, were not necessary because the basic structural criteria can be easily checked in the initial design under the most common loading conditions, so as to ensure that the deflection, stresses in the facings and the core shear stresses do not exceed the acceptable levels. A good review of design methods are given in Ref.6. A more detailed theoretical approach to the behaviour of sandwich columns in general instability and face wrinkling

of sandwich panels with isotropic facings and honeycomb orthotropic core is reported in Ref.7.

It was found that the mode of failures in compression most needed for strength prediction were the compressive strength of the laminate facings in flexural bending and of a thick laminate in short column compression. The object was to find the ply compressive strength for use in the finite element analysis.

The tests carried out are described below and the results show the very different results that can occur by different test methods.

5.4.1 Short Column Compression Testing

5.4.1.1 Longitudinal compression testing of unidirectional composite sandwich.

The unidirectional composite sandwich panel was obtained from CIBA-GEIGY. The core was of Nomex type A1-64-5 and the facings were made from two unidirectional DLS/280/280 G-R-7 plies with fibres orientated along the axis and transverse to the core ribbon direction. Figs. 5.2 and 5.3 show the test set up for the compression testing.

The specimens were cut and prepared by bonding a thick fillet of adhesive (EC 2216 B/A) in the removed core area along the width at the load application edge according to the instructions of Chapter 3. This was done so as to avoid the local crushing of the thin unidirectional facings. A width to length ratio of not less than 1.425 was used which was adequate to avoid the buckling modes of Fig. 5.1(a)(b)(c). There were physical difficulties in the preparation of smaller samples. Fig. 5.4 shows the failure mode of this test which indicated that it was intercell buckling across the width. This led to failure only when the

amplitude of the dimples arising from the facings buckling into or out of the spaces between the core walls became large enough to cause the dimples to grow across the core cell walls on the facing failed in shear, one part sliding over the other. See Fig. 5.5. One way of improving the compressive strength of composite facing with respect to intercell buckling is to reduce the core cell size thus reducing the amplitude of the dimples or by increasing the facing thickness. None of these were done because the cell size represented that of standard panel. A compressive strength in the fibre direction of σ_{1uc} = 279 MPa was obtained, see Table 5.1.

5.4.1.2 Longitudinal Compression Testing of an 8-Ply Laminate

The difficulties outlined in the previous test in short column mode, for obtaining the compressive strength of the laminated facings of the sandwich, were overcome by using an 8-ply laminate which was thick enough to reduce the buckle amplitude as well as limiting the failure to that of plies buckling in the fibre dirction. The test rig of Fig. 5.2 was modified by adding additional support blocks with the saw cuts at the centre thick enough to cater for the 8-ply laminate thickness, see Fig. 5.6.

The depth of the support end of the specimens were set to be 4.9mm average leaving an unsupported length of 4.5mm average. This was thought to be appropriate in representing the average cell-size of the two different core densities used in the sandwich panel and the joint. The compressive failure occurred in the support end of the specimens by crushing the fibres longitudinally. A compression strength of 641.0 MPa was achieved which is only about 38% of the tensile strength, see

Table 5.2. The low value of compressive strength shows the complexity of fibre composite failure in compression which are notoriously difficult to obtain and define. There are several factors which can influence the buckling strength of the laminate including the fibre and resin properties, the interface bond strength and void contant and, particularly, the volume fraction.

In addition to compressive failure due to buckling, the shear stresses arising from the compression loading in the laminate may be sufficient to cause a shear mode of failure particularly if the shear strength of the laminate is less than its buckling strength. The magnitude of the shear stresses is a maximum on all surfaces at 45° to the compressive axis. The detailed study of compressive failure in fibre composite is beyond the scope of this thesis. A number of failure modes have been proposed by various authors. A good review is given in Ref. 8.

5.4.1.3 The Transverse Compression Testing of 8-ply laminate

The main difference between this test and that of the preceeding longitudinal test was the fibre orientation. Failure of the specimens occurred at the middle in the unsupported length where considerable lateral buckling deflection was observed during the test. This gave rise to the shear stresses which ultimately caused the failure at 45° to the compressive axis across the width of the specimens. An average transverse compressive strength of σ_{2uc} = 161 MPa was obtained from the test results of Table 5.3.

5.4.2 Flexural Sandwich Beam Testing

5.4.2.1 Longitudinal Flexural Testing of Unidirectional Sandwich Beam

The unidirectional composite sandwich panel used for the flexural beam tests was the same as that used in the short-column compression testing (Section 5.4.1.1). Both three and four point bend tests were carried out for which the test arrangement is shown in Fig. 5.7. The results are given in Tables 5.4 and 5.5. Longitudinal compressive fracture occurred in both tests at the top facing the middle of the beam under the edge of the thin load spreader sheet used to avoid local core crushing. There was a small difference in the compressive strength between these two tests as calculated from the failure load by the simple theory of bending with the four point bend tests giving the smallest value. The three point bend test, although giving a higher longitudinal compressive strength, fell short of the strength obtained from the cross ply facing (0°/90°). The low strength was probably associated with the inter cell buckling of the unidirectional laminae where the matrix provides the only support to the surrounding fibres within the core cell-area.

Failure of this connection due to the rising shear stresses in the matrix will cause buckling of the fibres hence the low longitudinal compressive strength (σ_{1uc} = 367.0 N/mm^2).

5.4.2.2 Flexural Cross-Ply Sandwich Beam Testing

Three point bend tests were carried out on standard cross ply sandwich panels with two types of ply stacking sequence (see Fig. 5.7(b)). Using the procedure explained in Section 8.3.2.6 and 7, the ply

strength (stresses) were calculated for the failure load along and transverse to the fibre direction at the top compression facing of the sandwich, see Table 5.6(a)(b). The longitudinal compressive strength obtained from tests of Table 5.6(b) was about 12% higher to that of the previous unidirectional tests given in Table 5.5. The main difference between the two tests was that the two facing plies were at right angles to each other, This suggests that the 90° ply provides stability for the 0° ply in buckling. Furthermore, by rotating the loading through 90° (Table 5.6(a)), even higher compressive strength was obtained because of the higher shear stiffness of the core in 0° orientation (along the ribbon) and the 0° ply being the top ply therefore taking most of the strain. Because of the varying compressive strength arising from the two different load directions, an average of longitudinal and transverse strengths values was thought to be appropriate. See Table 5.6(c).

σ_{1uc} = 440 MPa

σ_{2uc} = 116.0 MPa

5.5 DISCUSSION

In the last few sections, different tests were carried out to obtain the compressive strength of unidirectional composite sandwich facings, a summary comparing these results with different methods of testing are listed in Table 5.7 below.

TABLE	METHOD OF TEST	FAILURE COMPRESSIVE STRENGTH	
		LONGITUDINAL MPa	TRANSVERSE MPa
5.1	SHORT COLUMN UNIDIRECTIONAL SANDWICH COMPRESSION	279.0	-
5.2 5.3	SHORT COLUMN UNIDIRECTIONAL 8-PLY LAMINATE	641.0	161.0
5.4	FOUR POINT FLEXURAL BEND $(0^\circ/0^\circ - C90^\circ)_s$	348.0	-
5.5	THREE POINT FLEXURAL BEND TEST $(0^\circ/0^\circ - C90^\circ)_s$	367.0	-
5.6	THREE POINT FLEXURAL BEND TEST $(0^\circ/90^\circ - C0^\circ)_s$ and $(90^\circ/0^\circ - C90^\circ)_s$	440.0	116.0

The low compressive strength of facing laminate from Table 5.1 could be due to the fact that the facings are very thin and of very low stiffness material in the transverse direciton so that intercell buckling can develop early. This caused the shear stress in the facings to rise as their angle to the load increased and final failure was by shear across the facing thickness. This can be seen in the specimen Fig. 5.5, where the facing shears into the cell for one cell and out of the cell in the next cell alternately across the width of specimen. It was concluded that the value obtained under this loading condition is not representative of the compressive strength of a unidirectional laminate considered for the purpose of this work, i.e. locally within the tongue and slot joint where the complex geometry supports the facings, preventing such a buckling.

In predicting the strength of the box beam, it was found that the average results from the 3-point bend test in the cross ply panels,

Table 5.6(c), gave the closest prediction (using F.E. analysis) to the box beam result in the [90°/0°-C90°]s case (Section 9.2). The [0°/90°-C0°]s case was not tested.

In predicting the strength of single panels by F.E. analysis in Section 9.1 these results also gave the closest prediction to experiments for all the ply orientations and sandwich thicknesses.

The reason for this particular material test (Table 5.6(c)) being appropriate for use in the F.E. analysis is thought to be that, the conditions of the material test must really represent the conditions in the structural tests. Of course the standard single panel structural test of [0°/90°-C0°]s is the same as the material test, the only difference being the F.E. analysis. However the close strength prediction of other sandwich configuration does show that the analysis works in this case. The box beam was more of a structure and more closely demonstrated that this material test and F.E. analysis can be combined to give accurate strength predictions.

For the tests where the stability effect of the cross-ply was absent, a variety of local buckling effects caused large differences in the compressive strength recorded. Only the 8-ply laminate was thick enough to overcome these effects, but being so thick it was obviously not representative of the sandwich panel structure of the box beam, away from the stress concentration. However in the joints one is looking at very small localised areas in which these instabilities do not occur and hence the 8-ply laminate strength was representative as is shown in the comparison of theory with experiments in Section 10.4.

This whole section of the work showed the need for very careful selection of failure strength in the compressive mode in such panels, more than one mode needing to be considered depending on the circumstances.

a)
EULER BUCKLING.

b)
SHEAR BUCKLING.

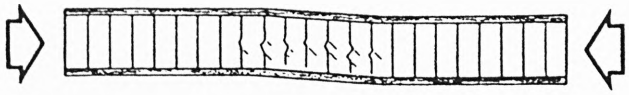

c)
FACE WRINKLING.

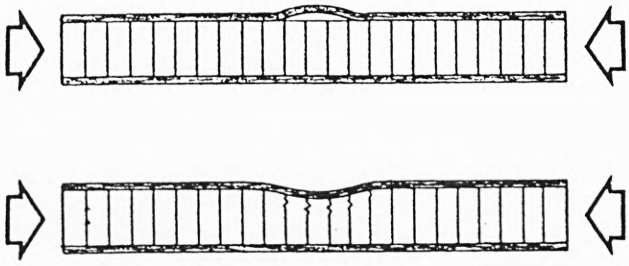

d)
INTERCELL BUCKLING.
(FACE DIMPLING)

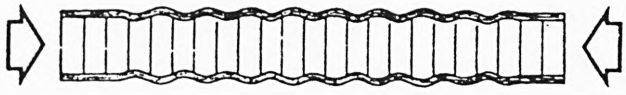

e)
CORE LOCAL CRUSHING.

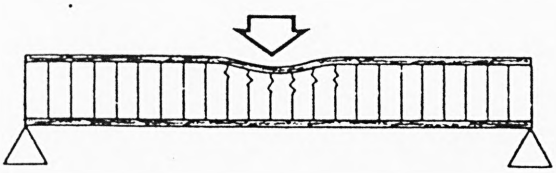

f)
FACING FAILURE IN
COMPRESSION.

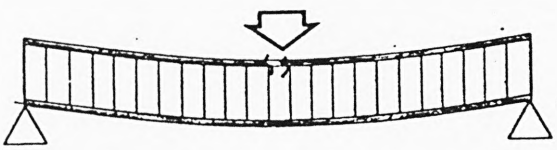

g)
CORE TRANSVERSE SHEAR
FAILURE.

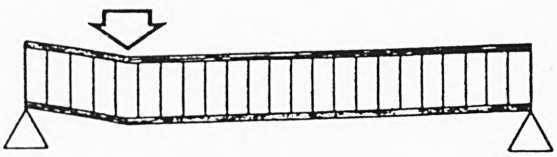

FIG 5.1
FAILURE MODE OF HONEY-COMB SANDWICH PANEL.

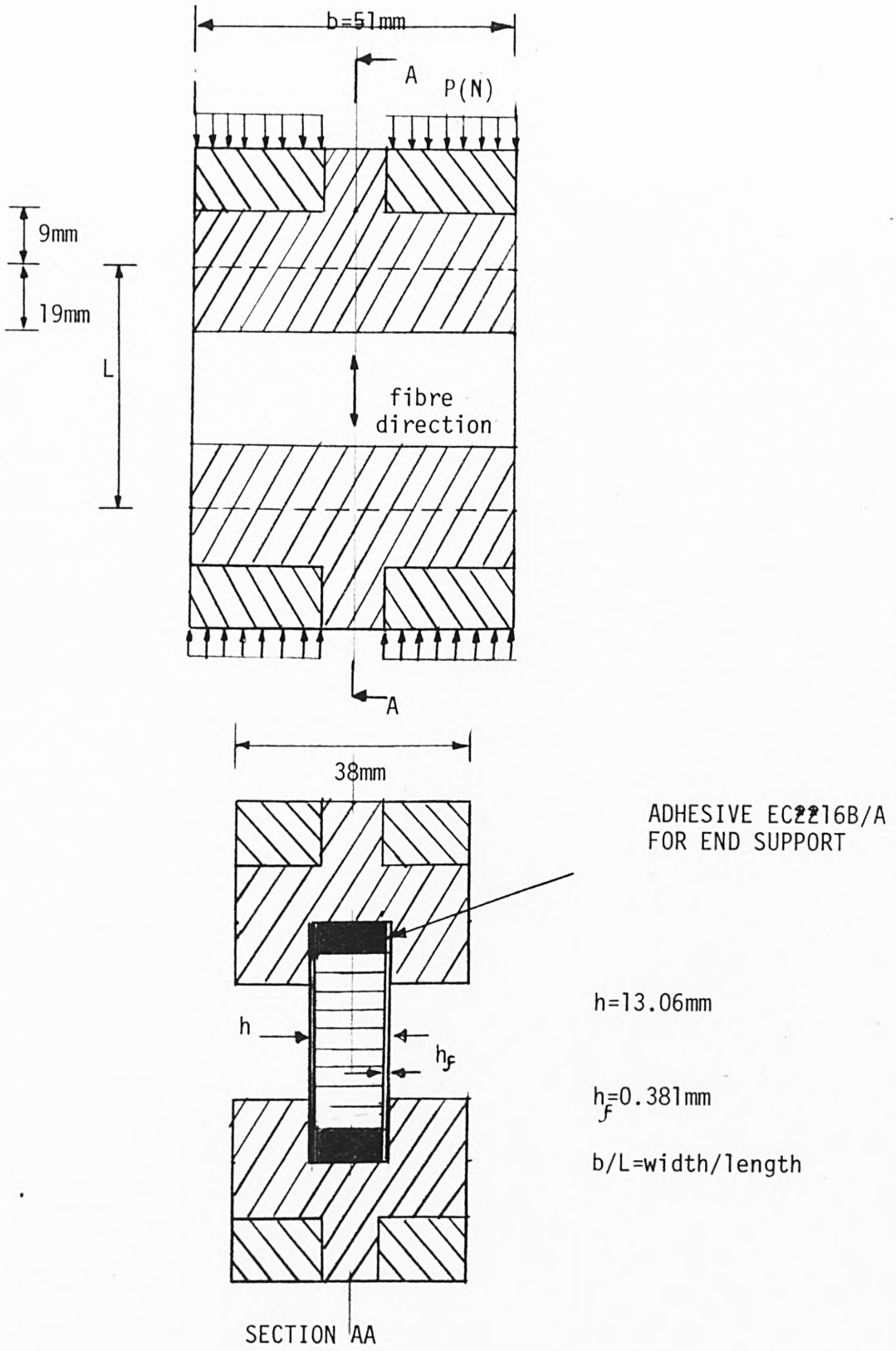

FIG 5.2

SHORT COLUMN COMPRESSION TESTING OF UNIDIRECTIONAL SANDWICH SPECIMEN

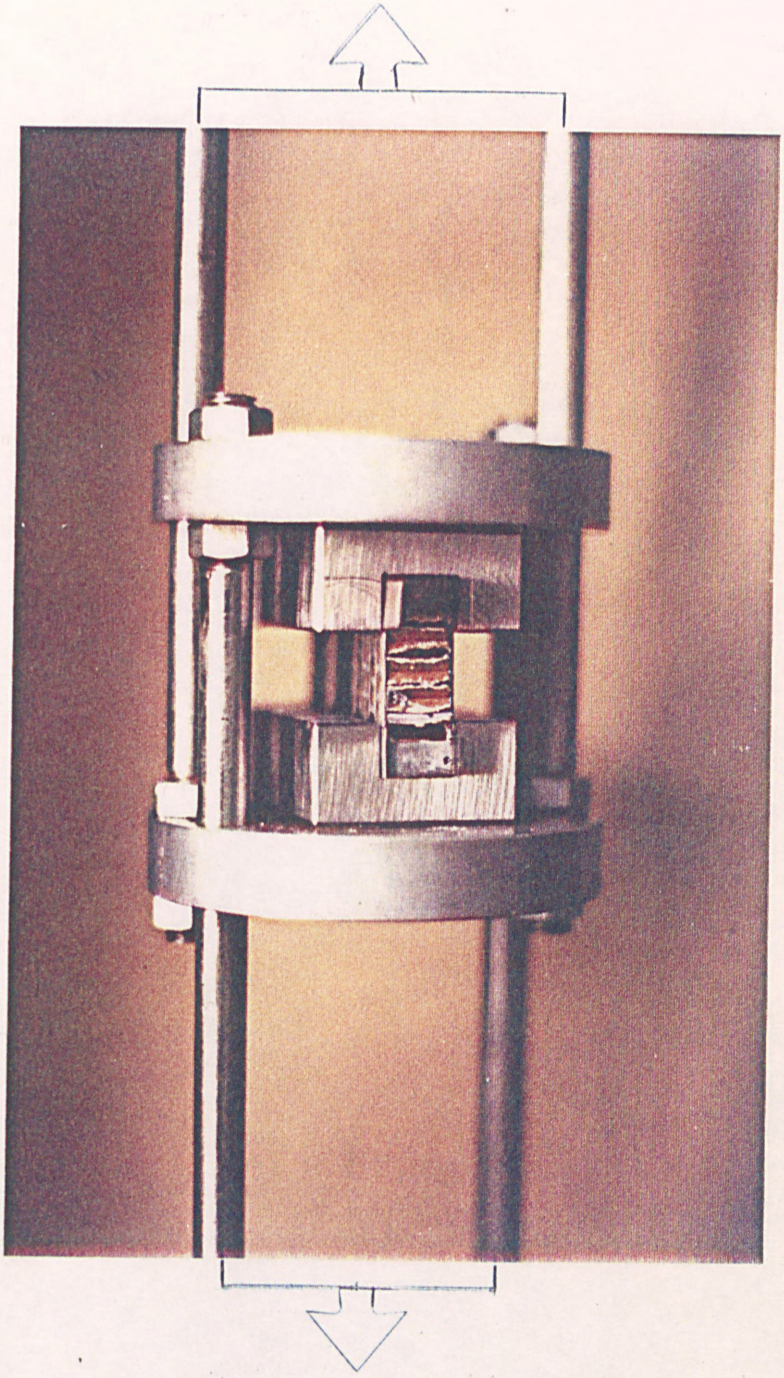

FIG 5.3

SHORT COLUMN COMPRESSION TESTING OF THE
COMPOSITE SANDWICH WITH THE UNIDIRECTIONAL FACING

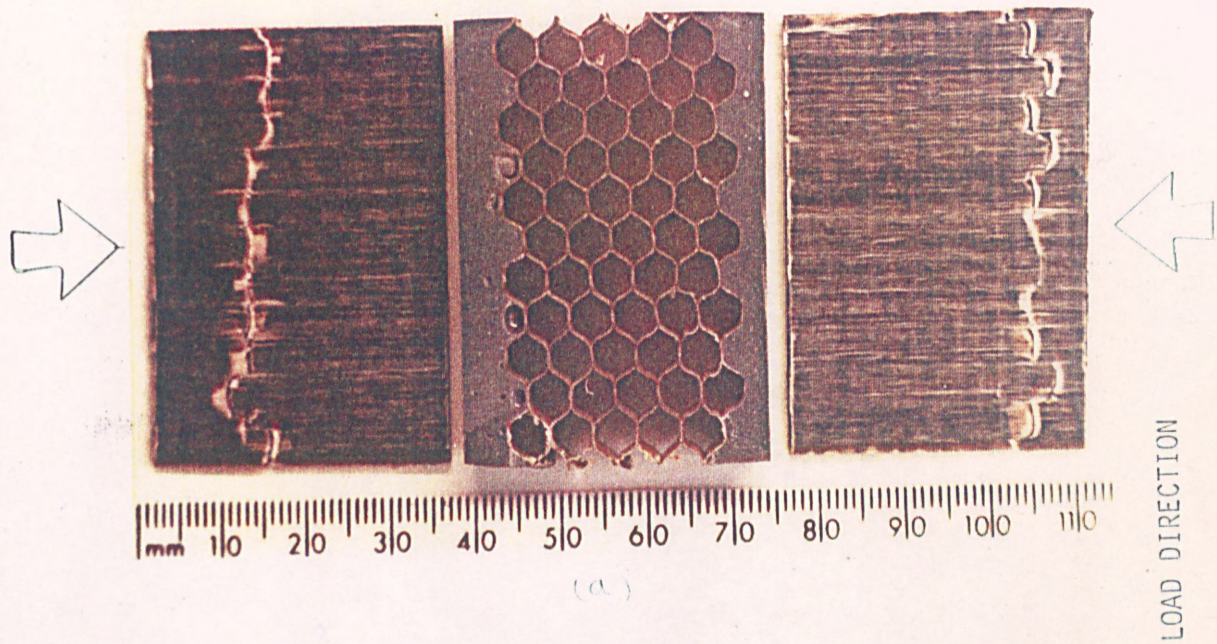

FIG 5.4

UNIDIRECTIONAL COMPOSITE SANDWICH FAILURE IN SHORT COLUMN TESTING

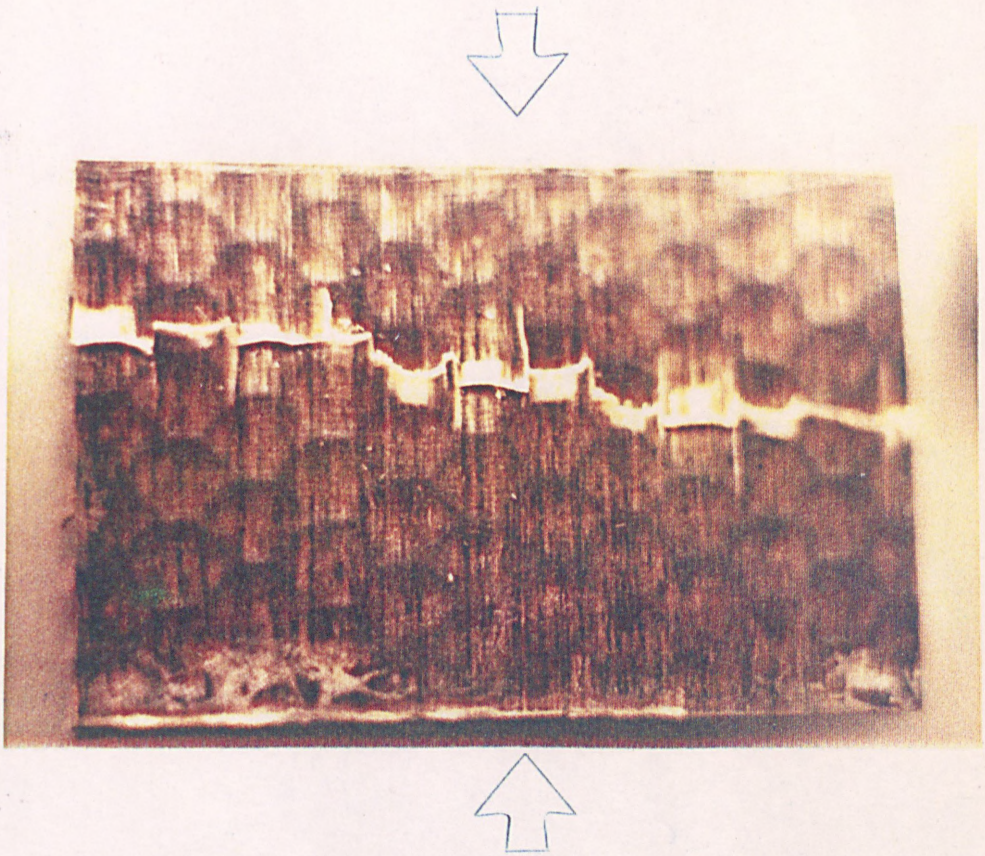

LOAD DIRECTION

FIG 5.5

INTERCELL BUKCLING OF UNIDIRECTIONAL COMPOSITE SANDWICH BY SHEAR FAILURE OF THE FACINGS

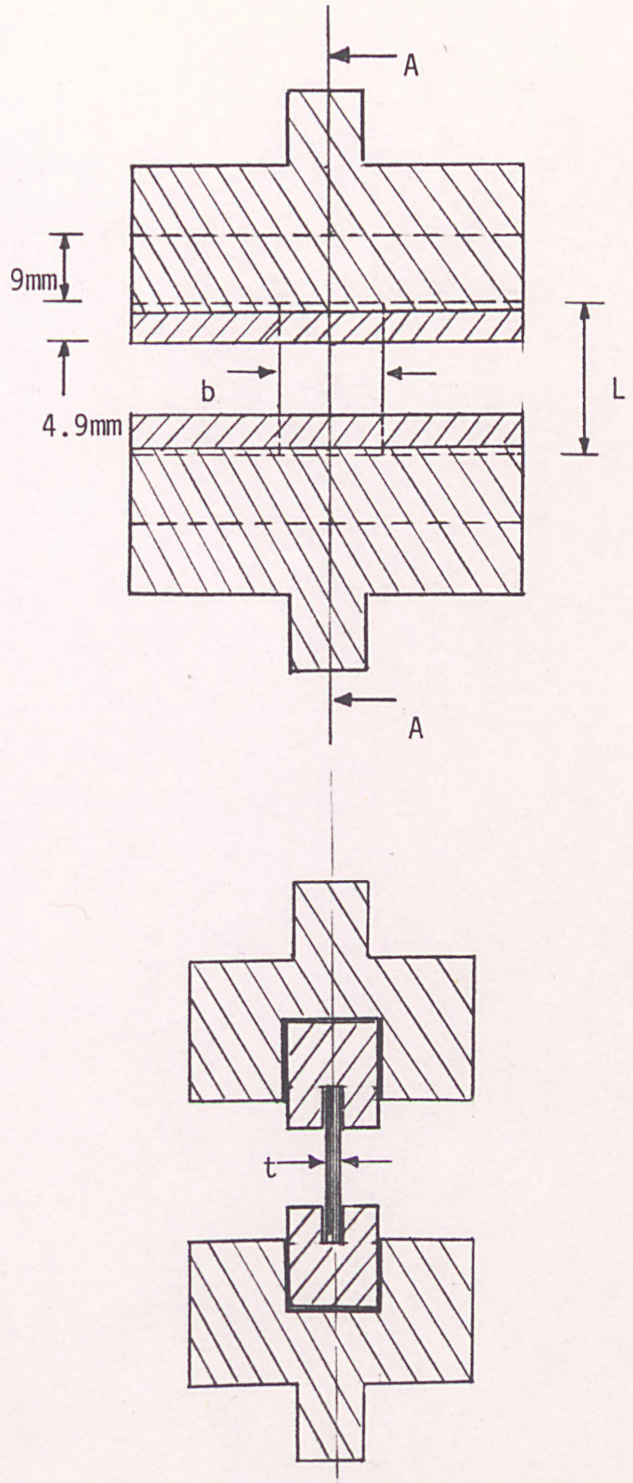

FIG 5.6

SHORT COLUMN COMPRESSION TESTING OF 8-PLY LAMINATE

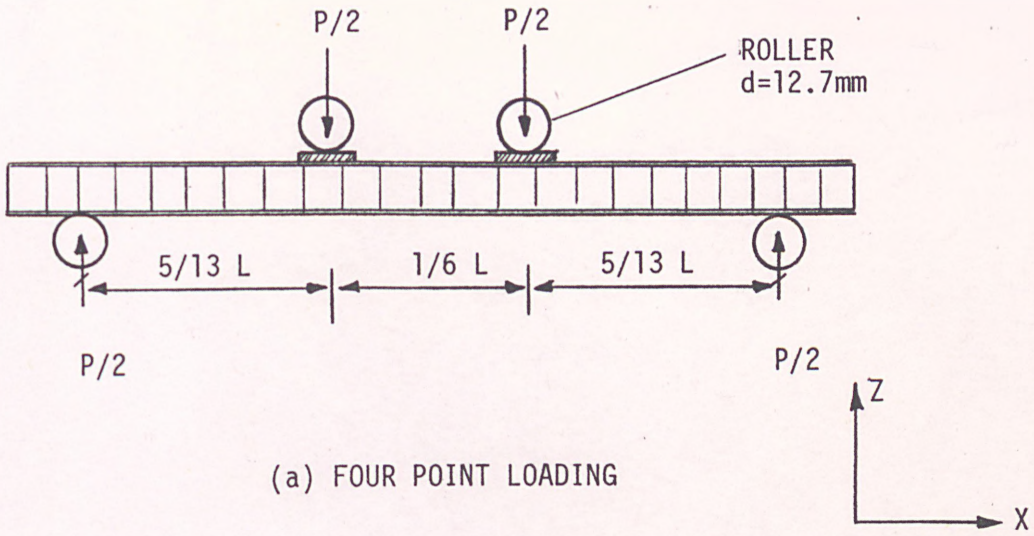

(a) FOUR POINT LOADING

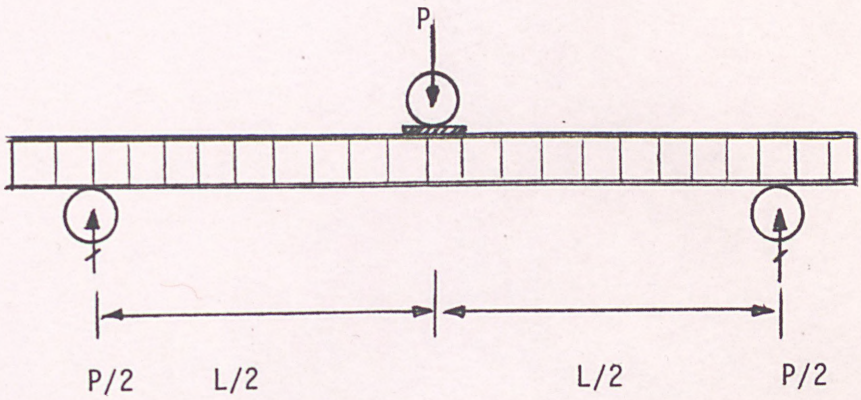

(b) THREE POINT LOADING

FIG 5.7

FLEXURAL SANDWICH BEAM TESTING

SPECIMEN NUMBER	b/ℓ WIDTH/LENGTH	FAILURE LOAD P_F N	σ_{1UC} N/mm^2
1	1.45	10402	267
2	1.425	10476	278
3	1.45	11384	293
		AVERAGE =	279

TABLE 5.1 LONGITUDINAL SHORT COLUMN COMPRESSION OF UNIDIRECTIONAL SANDWICH

SPECIMEN NUMBER	b (mm)	t (mm)	$\frac{b}{\ell}$	FAILURE LOAD P_F N	σ_{1UC} N/mm^2
1	12.5	1.61	.893	12788	635.4
2	12.76	1.63	.873	13456	647.0
				AVERAGE =	641.0

TABLE 5.2 LONGITUDINAL SHORT COLUMN TEST OF 8-PLY LAMINATE

SPECIMEN NUMBER	b (mm)	t (mm)	$\frac{b}{\ell}$	FAILURE LOAD P_F N	σ_{1UC} N/mm^2
1	14.68	1.55	1.05	3703.7	163
2	11.57	1.52	.839	2800	159.2
				AVERAGE =	161.0

TABLE 5.3 TRANSVERSE SHORT COLUMN COMPRESSION OF 8-PLY LAMINATE

SPECIMEN NUMBER	SPAN (mm)	PANEL THICKNESS (mm)	WIDTH (mm)	P_F (N)	σ_{1UC} N/mm^2
1	457.2	13.06	75	1302.4	345
2	457.2	13.06	74.9	1323.4	351
3	457.2	13.06	76	1325	348

t_{ply} = .1905 mm

STACKING SEQUENCE $(0^\circ/0^\circ - C90^\circ)_s$

$\frac{348}{}$ = σ_{1UC} AVERAGE

TABLE 5.4 FOUR POINT FLEXURAL BEND TEST

SPECIMEN NUMBER	SPAN (mm)	PANEL THICKNESS (mm)	WIDTH (mm)	P_F (N)	σ_{1UC} N/mm^2
1	457.2	13.06	75	1166.8	376.5
2	457.2	13.06	77.5	1170	366
3	457.2	13.06	77.59	1176	366.7
3	508	13.06	74.0	988.0	359
4	508	13.06	75.06	1009.6	361.6
5	508	13.06	75.06	1034.4	370.5

$\frac{370.0}{}$ = σ_{1UC} AVERAGE

367.0 N/mm^2

t_{ply} = .1905 mm

STACKING SEQUENCE $(0^\circ/0^\circ - C90^\circ)_s$

364.0 = σ_{1UC} AVERAGE

TABLE 5.5 THREE POINT FLEXURAL BEND TEST

SPECIMEN NUMBER	OVERALL SANDWICH THICKNESS	BEAM BREADTH b (mm)	FAILURE LOAD P_F N	UPPER SURFACE OF TOP PLY. AVERAGE STRESSES N/mm^2
1	13.40	78	907	FROM 0° LAYER $\sigma_{1UC} = -469.0$
2	13.45	77.45	832	FROM 90° LAYER $\sigma_{2UC} = -120$
3	13.38	77.45	921.4	
AVERAGE RESULT	13.41	77.63	886.8	

(a) STACKING SEQUENCE $(0^\circ/90^\circ - C0^\circ)_s$ BEAM SPAN = 508mm

t_{ply} = .1905mm

SPECIMEN NUMBER	OVERALL SANDWICH THICKNESS	BEAM BREADTH b (mm)	FAILURE LOAD P_F	UPPER SURFACE OF TOP PLY. AVERAGE STRESSES N/mm^2
1	13.45	75.5	746.4	FROM 90° LAYER $\sigma_{2UC} = -112.0$
2	13.45	76.1	781.8	
3	13.4	76.1	755.2	FROM 0° LAYER $\sigma_{1UC} = -412$
AVERAGE RESULT	13.43	75.9	761.13	

(b) STACKING SEQUENCE $(90^\circ/0^\circ - C90^\circ)_s$ BEAM SPAN = 508mm

t_{ply} = .1905mm

LONGITUDINAL STRENGTH σ_{1UC} MPa	TRANSVERSE STRENGTH σ_{2UC} MPa
440.0	116.0

(c)

TABLE 5.6 FLEXURAL THREE POINT CROSS PLY - SANDWICH BEAM TESTING

6.0 FLEXURAL BENDING OF COMPOSITE SANDWICH BEAM

6.1 THREE POINT BEND TEST OF MULTIDIRECTIONAL COMPOSITE SANDWICH

The program of tests reported in this section were carried out to ensure that the material properties and the strengths data obtained in the preceding chapter represented those of the composite sandwich panel. Different sandwich thicknesses with the standard panel orientation, i.e. [0°/90°-C0°]s were tested according to Fig. 5.7(b) over the span of 50.8mm for their deflections in both the elastic range and at the ultimate failure load, the results of which are given in Table 6.1(a)(b)(c). Note that the results of Table 6.1(c) are the same as the material tests of Table 5.6(a). Table 6.2 shows the result of the flexural bending tests carried out over the span of 254mm for the high density core sandwiches with the facings having multidirectional ply orientation which are used for the joint reinforcement type 2.0. See Fig. 3.2. The failure mode common to all these tests was ply compression failure at the top facing. The failure load as well as the deflection was predicted closely by the finite element analysis in Section 9.2.

6.2 THREE POINT BEND TEST OF COMPOSITE SANDWICH BOX-BEAM

The box-beam was made from the standard size composite panel with nominal sandwich thickness of 13.36mm, see Fig. 6.1(a) for beam cross-section and 6.1(b) for test method. The beam was bonded together with Redux 410 adhesive using the bonding procedure described in Chapter 3. The use of L shaped adhesive filleting was thought to be appropriate in constructing a fully symmetrical section without the use of additional

reinforcement such as angle section at each corner. The L shaped adhesive joint was adequate in providing continuity between the top and side panels as well as giving additional bearing strength on the thin facing under the loading point. A thick steel plate, 51mm span, was placed under the loading roller in order to spread the load thus avoiding the local crushing of the side sandwich panels. A magnetic dial gauge was clamped to the rig to directly measure the cross-head deflection, see Fig. 6.2. Due to the possible twist and lack of flatness in the specimen, deflections at very small loads were unreliable therefore the test was started from a small pre-load sufficient to straighten out the twist and hold the specimen flat over the length of the supports. It was also necessary to carry out a complete cycle of loading and unloading prior to taking measurements in order to ensure that all bearings were firmly and properly seated.

The box beam was tested to ultimate failure on the 50,000 lb Macklow-Smith Universal testing machine on the 10,000 lb range. The compression failure was initiated at the top corner of the box-section where the thin facing of the top panel was adhesively bonded to the thickness of the side panels, see Fig. 6.3. The load/deflection results are shown in Fig. 6.4. The object of the test was to provide experimental results on composite sandwich panel in a simple structure where the top and side panels provide the stiffnesses and strengths in bending and shear deformation respectively. This was then applied as a test to the finite element analysis using both the 2-D and 3-D orthotropic sandwich elements where full strength predictions are given in Chapter 9. However the simple theory of bending was used to check the value of the compressive strength of the 0° ply along the fibre direction given in Table 5.6(c).

It was thought to be reasonable to assume for the purpose of strength prediction that only 0° plies were effective for carrying the load and that the 90° plies prevented the buckling of the type discussed in Section 5.4.2.1. Hence half of the section modulus, $I_o = 5.3386 \times 10^5 mm^4$. As for prediction of the maximum deflection at the centre, the stiffnesses of both plies (90°/0°) were taken into account, i.e. $I_{90°/0°} = 10.677 \times 10^5 mm^4$. For this an effective E value of 24115 MPa was used, which was obtained by experiment and is not reported in this work. Table 6.3 gives the comparison between the simple theory of bending and the test results.

The close prediction of failure load (4.5% underestimate comparing to the test) by inserting the longitudinal compressive strength (σ_{1uc} = 440 MPa) in the simple theory of bending, showed that this value was in fact a reasonably close estimate, bearing in mind the material variability and therefore could be used for the strength prediction in the finite element analysis in the flexural mode of bending. The large difference in the failure deflection (29.8%) was accounted for mainly by shear deformation of the side panels, which was neglected in the simple theory of bending. Also there was some non-linear deformation as shown in Fig. 6.4. The deflection due to the shear deformation was calculated using the shear modulus of a single unidirection ply (τ_{12} = 3.74 GPa) and a factor of 0.9 for the non-uniform distribution of the shear stress. This gave a shear deflection of 3.4mm thus giving a total deflection of 12.27mm which was over-estimated by 6.1%. Furthermore the shear deformation was about 38% of the bending deformation which was also an overestimate. The shear deflection could be reduced by replacing the 90°/0° facings side panels with ones at +45°/-45° which would be stiffer in shear. This was not done as the emphasis was on the joint strength prediction and work was

conducted on monitoring the behaviour of both 2-D and 3-D element on this test. This will be discussed fully in Chapter 9. where predictions of strength and deflection are compared with experiment.

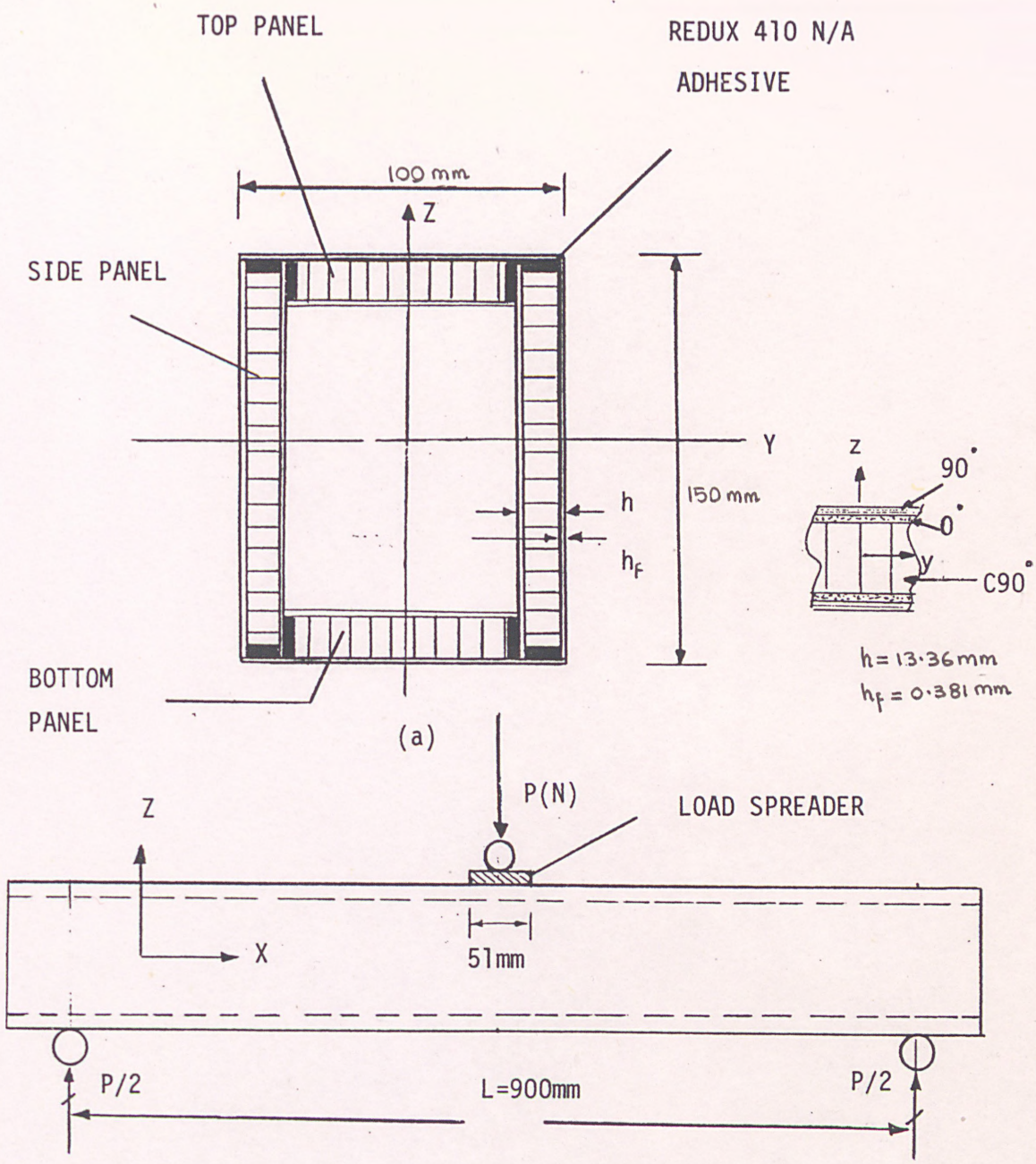

FIG 6.1
BOX-BEAM TEST SECTION AND METHOD

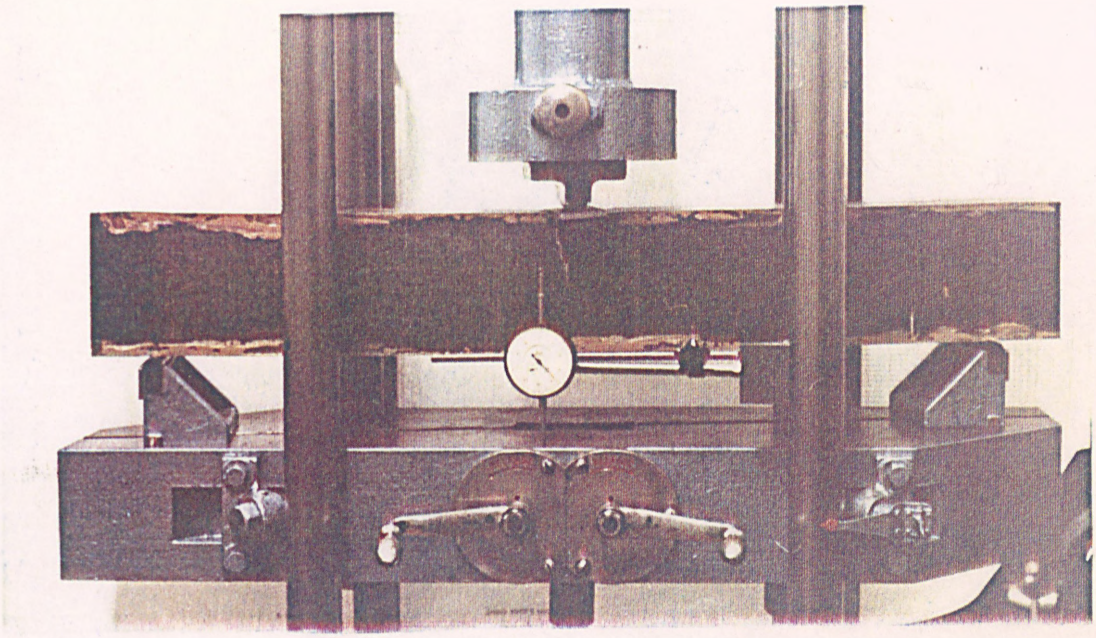

FIG 6.2

BOX-BEAM TEST SET-UP

FIG 6.3

BOX-BEAM COMPRESSION FAILURE OF TOP PANEL

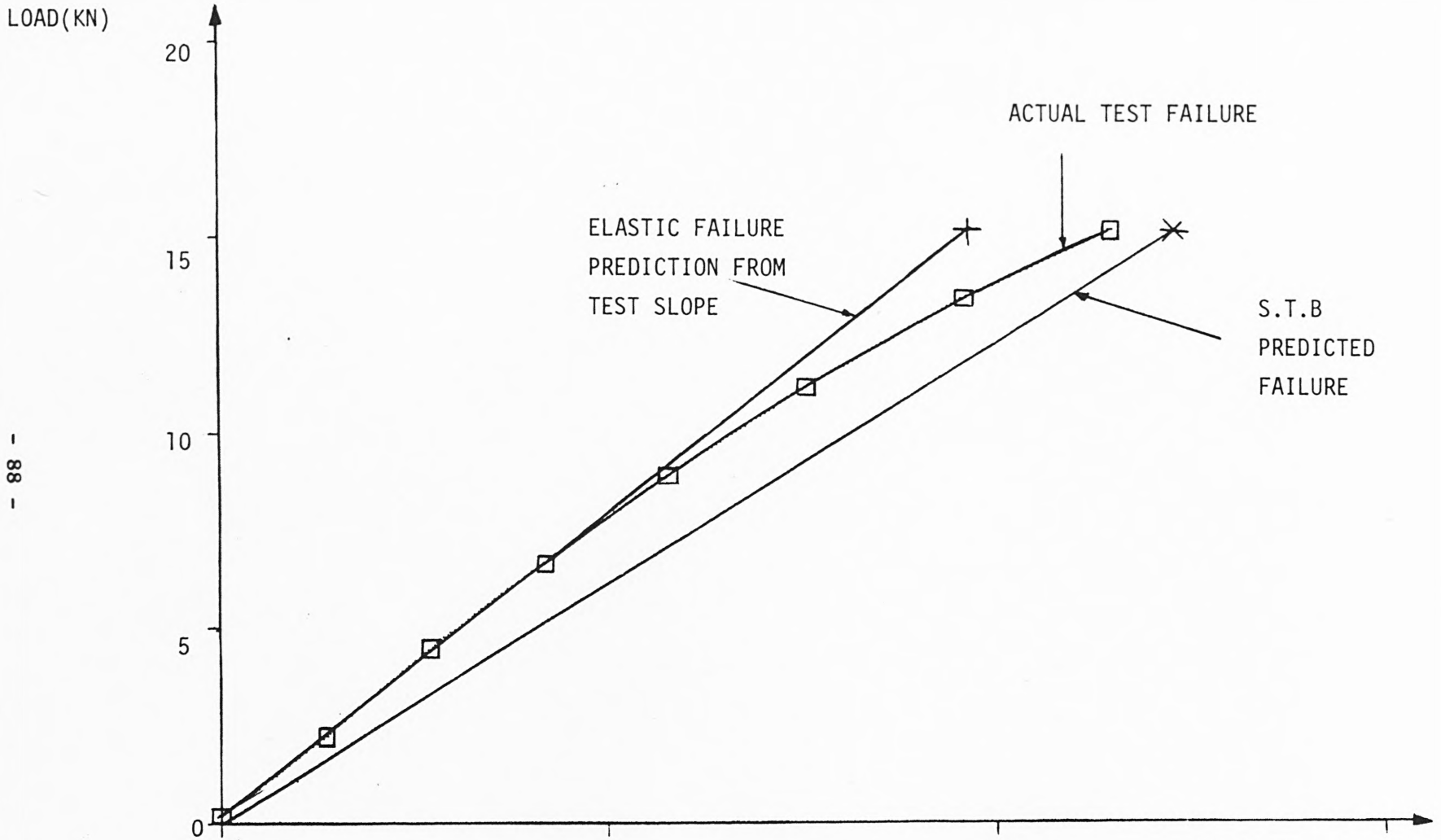

FIG 6.4

S.T.B/TEST DEFLECTION AND FAILURE COMPARISON

SPECIMEN NUMBER	h_c+2h_f (mm)	b (mm)	δ_E(mm) AT 600N	δ_F (mm)	P_f (N)	0° σ_{1UC} (N/mm^2)	90° σ_{2UC} (N/mm^2)
1	26.28	76.9	6.43	18.93	1762.8		
2	26.28	77.1	6.36	18.7	1726.6	σ_{1UC} =471	σ_{2UC} =123
3	26.28	76.8	6.57	20.1	1819.8		
AVERAGE	h_{av}=26.28	76.933	6.45	19.24	1769.73		

STACKING SEQUENCE $(0/90 - C0)_s$

SPAN (ℓ) = 508mm $\quad \frac{h_c}{h_f} = 67 \quad$ t_{ply} = .1905mm

TABLE 6.1(a)

SPECIMEN NUMBER	h_c+2h_f (mm)	b (mm)	δ_E(mm) AT 150N	δ_F (mm)	P_f (N)	0° σ_{1UC} (N/mm^2)	90° σ_{2UC} (N/mm^2)
1	6.96	76.5	20.28	70.85	442		
2	6.96	77.1	20.57	69.7	443	σ_{1UC} =468	σ_{2UC} =117
3	6.98	77.2	20.28	68	434		
AVERAGE	h_{av}=6.96	76.933	20.37	69.5	439.6		

STACKING SEQUENCE $(0^\circ/90^\circ - C0^\circ)_s$

SPAN(ℓ) = 508mm $\quad \frac{h_c}{h_f} = 16.27 \quad$ t_{ply} = .1905mm

TABLE 6.1(b)

TABLE 6.1 FLEXURAL CROSS PLY SANDWICH BEAM TESTING

SPECIMEN NUMBER	h_c+2h_f (mm)	b (mm)	δ(150) (mm)	δ_F (mm)	P_f (N)	0° σ_{1UC} (N/mm^2)	90° σ_{2UC} (N/mm^2)
1	13.4	78	5.86	37.86	907		
2	13.45	77.45	6.06	35.14	832	469	120
3	13.38	77.45	5.6	36	921.4		
AVERAGE	13.41	77.63	5.84	36.33	886.8		

STACKING SEQUENCE $(0^\circ/90^\circ-C0^\circ)_s$

SPAN(ℓ) = 508mm $\quad \frac{h_c}{h_f} = 33.2$ $\quad t_{ply} = .1905$

TABLE 6.1(c)

STACKING SEQUENCE	h_c+2h_f (mm)	b (mm)	$\frac{h_c}{h_f}$	δ(600N) (mm)	δ_f (mm)	P_f (N)	$\frac{h_f}{4xt_{ply}}$
$(90^\circ/0^\circ/90^\circ/0^\circ$ $-HDC90^\circ)_s$	10.1	38.5	11.25	6.2	12.9	1195.6	t_{ply}= .1905mm
$(+45^\circ/-45^\circ/0^\circ$ $/90^\circ=HDC90^\circ)_s$	11.07	38.3	10.03	4.43	15.64	1536.8	t_{ply}= .23mm

SPAN(ℓ) = 254mm

TABLE 6.2 FLEXURAL MULTIDIRECTIONAL SANDWICH BEAM TESTING

PLY STACKING SEQUENCE	S.T.B. VALUE (N)	EXPERIMENTAL VALUE (N) P_f	PERCENTAGE DIFFERENCE (%) $\frac{S-E}{S} \times 100$
$(90\dot{}/0\dot{}^{\circ}\text{-}C90\dot{})$	143.81	15034	-4.5

$\sigma_{1UC} = 440$ MPa

COMPARISON OF BOX BEAM FAILURE LOAD (P_f)

S.T.B. δ_s (mm) SHEAR	S.T.B. δ_b (mm) BENDING	EXPERIMENTAL VALUE (mm)	$\frac{S.T.B.-EXP}{S.T.B.} \times 100$ (%)
3.4	8.87	11.52	BENDING ONLY -29.8
$\delta_{TOTAL} = \delta_s + \delta_b$ 12.27		11.52	OVERALL 6.1

COMPARISON OF BOX BEAM FAILURE DEFLECTION δ_f

TABLE 6.3

7. FAILURE CRITERION STUDY

7.1 INTRODUCTION

The problem considered here is broadly that of predicting the ultimate strength of an orthotropic lamina subjected to a biaxial stress field, given the relevant strength data obtained experimentally in previous chapter.

i.e. σ_{1UT} (longitudinal tensile strength)

σ_{2UT} (transverse tensile strength)

τ_{12U} (interlaminar shear strength)

σ_{1UC} (longitudinal compressive strength)

σ_{2UC} (transverse compressive strength)

For predicting the strength of an orthotropic laminated facing of a sandwich panel subjected to loads that produce complex stress states, the actual stress field must be referred to the principal material axes and then compared with the preceding strengths. The initial failure of orthotropic materials can be predicted with the help of a suitable failure criterion. There are a number of theories available for prediction of the failure of orthotropic lamina subjected to a plane stress state. In this chapter, four of the strength theories (criteria) for composite materials based on maximum stress, maximum strain, Tsai-Hill (maximum work) and Tsai-Hill/Hoffman are briefly discussed. A more detailed review can be found in Refs. 10 and 11.

7.2 MAXIMUM STRESS CRITERION

In the maximum stress theory, the stresses in the principal material axes must be less than the respective strengths otherwise fracture is said to have occurred, that is for tensile stresses:

$$\sigma_1 < \sigma_{1UT}$$

$$\sigma_2 < \sigma_{2UT}$$

$$\tau_{12} < \tau_{12U}$$

For compressive stresses:

$$\sigma_1 < \sigma_{1UC}$$

$$\sigma_2 < \sigma_{2UC}$$

$$\tau_{12} < \tau_{12U}$$

This is the simplest criterion which assumes that failure occurs when any of the above conditions are violated. Note that there is no interaction between the modes of failure in this criterion which is actually not one criterion but five subcriteria. Thus this does not adequately represent the experimental strength situation.

7.3 MAXIMUM STRAIN CRITERION

The maximum strain theory is quite similar to the maximum stress theory. It is possible to obtain the ultimate strains for a single ply (rather than ultimate stress) and then set up a strain criterion similar

to that of stress criterion. However this also does not adequately represent the experimental strain situation.

7.4 HILL CRITERION OR TSAI-HILL CRITERION

The criterion much used for static failure prediction of composite laminates is known as the Hill Criterion. In fact the Hill Criterion as such, Hill (12), was adapted as a generalisation of the Von Mises Criterion for anisotropic materials. It was then further developed by Tsai to a failure criterion for laminated composites the derivation of which is given below.

Writing the Von Mises criterion in principal material directions.

$$I(\sigma_2 - \sigma_3)^2 + G(\sigma_3 - \sigma_1)^2 + H(\sigma_1 - \sigma_2)^2 + 2L\tau_{23}^2 + 2M\tau_{31}^2 + 2N\tau_{12}^2 = 1$$

for failure, where I-N are constants.

Let X,Y,Z be tensile yield stresses and R,T,S be shear yield stresses. If σ_1, σ_2, σ_3 acts on the body we have:

$$\frac{1}{X^2} = G + H \quad , \quad \frac{1}{Y^2} = I + H \quad , \quad \frac{1}{Z^2} = I + G \ .$$

If τ_{12}, τ_{23}, τ_{13} acts on the body, then

$$2N = \frac{1}{S^2} \quad , \quad 2L = \frac{1}{R^2} \quad , \quad 2M = \frac{1}{T^2} \quad .$$

Hence

$$2I = \frac{1}{Y^2} + \frac{1}{Z^2} - \frac{1}{X^2}$$

$$2G = \frac{1}{Z^2} + \frac{1}{X^2} - \frac{1}{Y^2}$$

$$2H = \frac{1}{X^2} + \frac{1}{Y^2} + \frac{1}{Z^2}$$

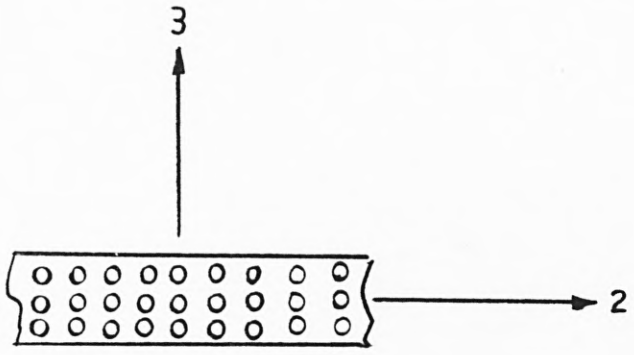

Fig. 7.1 Cross-section of a unidirectional lamina with fibres in the 1-direction.

For plane stress in the 1-2 plane of a unidirectional lamina with the fibres in the 1-direction $\sigma_3 = \tau_{13} = \tau_{23} = 0$.

Thus the criterion simplies to:

$$I\,\sigma_2^2 + G\,\sigma_1^2 + H(\sigma_1 - \sigma_2)^2 + 2N\,\tau_{12}^2 = 1$$

for failure from Fig. 7.1 for a transversely isotropic composite Y = Z then

$$2I = \frac{2}{Y^2} - \frac{1}{X^2} \;:\; 2G = \frac{1}{X^2} \quad : \quad 2H = \frac{1}{X^2} \quad .$$

therefore

$$\frac{\sigma_1^2}{X^2} + \frac{\sigma_2^2}{Y^2} - \frac{\sigma_1 \sigma_2}{X^2} + \frac{\tau_{12}}{S^2} = J^2,$$

for failure = 1.

Using a safety factor F = $\frac{\text{ULTIMATE STRENGTH}}{\text{APPLIED STRESS}}$

$$X^2 J^2 = X^2 \quad \text{or} \quad F^2 = \frac{X^2}{X^2 J^2} \quad \text{or} \quad F = \frac{X}{\sqrt{X^2 J^2}}$$

or written in its usual form

$$F = \frac{X}{\sqrt{\sigma_1^2 - \sigma_1\sigma_2 + \left(\frac{X}{Y}\right)^2 \sigma_2^2 + \left(\frac{X}{S}\right)^2 \tau_{12}^2}}$$

as the governing failure criterion in terms of three of the six principal strength constants (X, Y and S), thus limiting the use to specially orthotropic materials with plastic incompressibility, and with equal strength in tension and compression.

Jones, Ref.13, compared the results for this criterion against the experimental data for E glass/epoxy laminae at various orientation in biaxial stress fields and has shown that the assessment between theory and experiment is quite good. Considerable interaction exists between the failure strengths X, Y, S in the Tsai-Hill Criterion, but none exists in the other criteria discussed previously where axial, transverse and shear failures are presumed to occur independently.

7.5 TSAI-HILL/HOFFMAN CRITERION

Hoffman (14) extended the Tsai-Hill Criterion to account for differing strengths in tension and compression (which is the usual situation) by adding linear terms to the theory. The resulting criterion is shown below with the usual notation:

$$F_1 \sigma_1 + F_2 \sigma_2 + F_{12} \sigma_1 \sigma_2 + F_{11} \sigma_1^2 + F_{22} \sigma_2^2 + F_{66} \tau_{12}^2 = 1$$

where

$$F_1 = \frac{1}{\sigma_{1UT}} + \frac{1}{\sigma_{1UC}} \quad , \quad F_2 = \frac{1}{\sigma_{2UT}} + \frac{1}{\sigma_{2UC}} \quad , \quad F_{11} = \frac{-1}{\sigma_{1UT}\,\sigma_{1UC}} \quad ,$$

$$F_{22} = \frac{-1}{\sigma_{2UT}\,\sigma_{2UC}} \quad , \quad F_{66} = \frac{1}{\tau_{12U}^2} \quad , \quad F_{12} = F_{11} \, .$$

Increasing the number of terms in the prediction theory will improve the correlation between theory and experiment. However there are some theoretical objections to the above criterion on the grounds of lack of "tensor invariance". A more refined criterion, often known as the Tsai-Wu Criterion, which does not suffer that objection has been developed in Ref.15, but it contains another material constant that is difficult to determine as the material used has to be tested where σ_1 and σ_2 are not zero. This obviously presents difficulties and therefore has not been followed in this work.

7.6 COMPOSITE FAILURE CRITERIA

Tsai-Hill and Tsai-Hill/Hoffman Failure Criteria have been found to be suitable for the strength prediction of orthotropic laminae under plain-stress conditions where the state of stress is uniaxial off-axis. In the Tsai-Hill Failure Criteria, the difference in the compressive and

tensile strength is not taken into account. However, a close prediction can be made be replacing the relevant tensile strength by compressive strengths in the criteria when σ_1 and σ_2 are negative, see Chapter 9, for beam stress analysis. The comparison of the failure criteria is made in the strength prediciton of the joint in the longitudinal shear loading where considerable interaction occurs between σ^1, σ_2 and τ_{12} in both tension and compression, see Chapter 10. This was thought to be appropriate for the very reason that no single stress is dominant in the joint as they are in the case of beam bending.

8.0 FINITE ELEMENT ANALYSIS

8.1 INTRODUCTION

The Finite Element Method (FEM) has been established as a standard tool for dynamic and static analysis of engineering structures and components for which exact mathematical solutions can be obtained. Such solutions are usually only possible for simplified problems, e.g. the deformation of a thin, elastic, simply-supported, uniformly loaded plate. When confronted with complex engineering problems, engineers resort to numerical methods. Such methods yield approximate but acceptable solutions at a finite number of points in a structure.

With the FEM a structure is represented as an assemblage of subdivision (elements) which are interconnected at their junctions (nodal points). With the FEM the amount of data to be handled is dependent on the number of elements into which a structure is subdivided. The volume of this data can be considerable depending on the complexity of the problem and the accuracy desired. There are several packages available to industry which provide numerical solutions to many complex engineering problems. However these packages are written for general purpose and researchers often need to modify or write additional routines to cater for their own specific problems.

The package available for the stress analysis of the joints designed in this work was PAFEC (Program for Automatic Finite Element Calculation) which is written in FORTRAN 77 and intended to be machine independent.

The routines in PAFEC are very general, and this facilitates their use in research work in various fields. The system is quite flexible and facilities exist to enable users to develop their own routines

within the system. A full description of modification needed to analyse the orthotropic sandwich composite for this work will be given in later sections. Other facilities include automatic data generation and plotting of deformed shapes of a structure.

8.2 THEORY

This section describes briefly the formulation of matrices used in PAFEC (Ref.16). The package uses the displacement method, a full description of which is given by Zienkiewicz (Ref.17). The finite element analysis of a problem commences with the geometrical discretization of the structure into elements. An assumption is first made about the deformed shape of the structure. From this assumption a stiffness matrix is derived for each element. These are then merged together to form a stiffness matrix for the whole structure.

The solution method used is based on minimisation procedure. The unknown displacements at the nodes are used to build an expression for the potential energy (PE) of the structure. In order to evaluate PE the strain energy (SE) is needed, and is obtained from the assumed displacement functions for each element. The finite element solution is given by those displacements which cause a minimum potential energy value for the structure.

In static problems the minimum potential energy is written as

$$PE = SE - WD \qquad \ldots\ldots\ldots (1)$$

where SE, the strain energy, is a quadratic function of the displacements $\{U\}$

$$SE = \{U\}^T[K]\{U\} \qquad \ldots\ldots\ldots (2)$$

[K] is a square symmetric matrix known as the stiffness matrix. WD is the work done by the known externally applied forces or loads {P} and hence

$$WD = \{U\}^T\{P\} \qquad \ldots\ldots\ldots (3)$$

Minimising the PE with respect to the unknown displacements involves setting the appropriate derivatives of PE to zero giving

$$\{P\} = [K]\{U\} \qquad \ldots\ldots\ldots (4)$$

The expressions for SE can be formed from a sum of the strain energies of the different elements SE_i

$$SE = \sum_{i=1}^{n} SE_i \qquad \ldots\ldots (5)$$

$$SE_i = \frac{1}{2} \{u_e\}^T [K_e]_i \{u_e\}_i$$

where there are n elements in the structure and the subscript e shows that the quantity refers to an element.

From (4) we see that

$$\text{(EXTERNAL FORCES)} = \text{SUM OF PRODUCTS } [K_e]_i\{U_e\}_i \qquad \ldots\ldots (6)$$

A static problem is solved by merging K_e matrices to give the system matrix [K] and then solving the set of linear simultaneous equations (4).

8.3 TWO DIMENSIONAL THEORY FOR FLAT ORTHOTROPIC SANDWICH COMPOSITE

8.3.1 Introduction

Increasingly the finite element method is being used for stress analysis of composite laminated plates in a large structure, however, little emphasis has been given to the analysis of structures with sandwich type composite. An increasing number of structural designs especially in the aerospace industry are utilizing composite sandwich panels in the fabrication of major structural components. Design methods and concepts have been evolving which will enable engineers and designers to make efficient use of these new materials by sizing the precise reinforcement needed to maintain the structural integrity.

The inherent low stiffness characteristics of glass reinforced plastics often limits their effective use in sandwich construction. However, with the development of high strength and low density materials such as carbon, boron, graphite and metal fibres, the sandwich type construction can be used effectively to form a strong lightweight structure. The simplest type of composite sandwich consists of two thin laminated facings and a thick core of low density material which is usually much less stiffer and weaker than the faces. The bending theory of sandwich panels grows naturally from the ordinary theory of bending. The relatively weak core of sandwich construction means that shear deformation cannot be neglected. This fact brings the analysis of such a construction into the same area as thick plate theory.

The more complicated types of composite sandwich construction consist of thick laminated facings where shear deformation of the facings cannot be neglected. Ref.18 deals with the bending of orthotropic flat sandwich plates of constant thickness, and assumes the

shear stresses to be parabolic through the thickness of the faces and the core. Schmit, J.R. and Monforton, G.R. (Ref.19) deal with the geometrically nonlinear behaviour of sandwich plates and cylindrical shell structures with unbalanced laminated facings. The orthotropic sandwich plate used in this work was that of thin laminated facings with honeycomb core, and so the existing PAFEC thin facings isotropic sandwich plate was extended to take into account the orthotropic effect of the facings and the core as well as including the bending effectiveness of each ply of the facing by adding an extra strain energy term due to bending of the facing plies. A full theoretical background in the displacement assumptions, generation of stress/strain matrix and the implementation of the modified element will be given in the following sections.

8.3.2 Theory

The displacement method is used for generating the elements for composite sandwich panel analysis. Expressions for the displacement are first set up. This enables the derivation of expressions for the strains and stresses. Finally expressions for the strain energy of the sandwich are set up to enable the generation of matrices for the solution of the sandwich problem.

8.3.2.1 Displacements

The elements are designed so that the facings cater for membrane and bending deformation while the core provides shear stiffness (Fig.8.1(a)). The membrane deformations are represented by two quantities U_x, U_y, which respectively are the linear displacements of any points in the plate in the X, Y directions, while the bending deformation is represented by a set of three independent quantities U_z, ϕ_x, ϕ_y. U_z represents the transverse displacement, ϕ_x and ϕ_y represents the rotations of a "normal" to the plate surface about the X and Y axes respectively. Therefore the displacements at each node are represented by five quantities U_x, U_y, U_z. ϕ_x, ϕ_y. Fig. 8.1(b) shows a cross-section of an orthotropic sandwich element in the XZ plane. Let U, V represent the displacement due to shear deformation in the X, Y direction at a point in the core such as C, a distance Z above the middle surface of the sandwich core. The normal has rotated through an angle $\frac{\partial U_z}{\partial x}$ to the line OB but OC has rotated through a similar angle $-\phi_y$ to OC.

The displacement in the X direction is therefore given by

$$U = -(-Z\ \phi_y) = Z\ \phi_y$$

Similarly considering the YZ plane we have

$$V = -\ Z\ \phi_x \qquad \ldots\ldots\ldots (7)$$

Similarly the displacements at any point in the orthotropic facing are given by

$$U = -\left[-\frac{h_c}{2}\phi_y + \left(Z - \frac{h_c}{2}\right)\frac{\partial U_z}{\partial x}\right]$$

$$V = -\left[\frac{h_c}{2}\phi_x + \left(Z - \frac{h_c}{2}\right)\frac{\partial U_z}{\partial y}\right] \qquad \ldots\ldots\ldots (8)$$

Assumptions:

1. In the X-Y plane the honeycomb core is much less stiff than the facings, therefore the contribution of the core to the flexural rigidity of the sandwich is negligible.

2. The facings are multidirectional specially orthotropic and thin in comparison to the core thickness.

3. The deflection of the sandwich are small. The classical laminated theory is valid, and there is no stretching of the middle plane of the laminate when transverse displacements occur.

4. Stresses in the faces and core in the Z direction are negligible and therefore ignored.

5. The core transverse shear stresses τ_{xz}, τ_{yz} are constants through the core thickness. The assumed theoretical shear stress distribution in the composite sandwich is compared with the theoretical and actual distribution in Fig. 8.2. A shear stress correction factor K which will be described later in this section is used to correct this approximation.

8.3.2.2 Strains

The expression for strains in an orthotropic sandwich are obtained in terms of differentials of displacements. The membrane strains are denoted by ϵ_{xx}, ϵ_{yy} and γ_{xy}. The first two represent the direct membrane strains in the x, y directions and the last is a shear strain in the X-Y plane. The expressions for these strains can be obtained from the following

$$\epsilon_{xx} = \frac{\partial u_x}{\partial x}$$

$$\epsilon_{yy} = \frac{\partial u_y}{\partial y}$$

$$\nu_{xy} = \frac{\partial u_x}{\partial y} + \frac{\partial u_y}{\partial x}$$

(a)

$$\text{or } \{\epsilon_m\} = \begin{Bmatrix} \epsilon_{xx} \\ \epsilon_{yy} \\ \gamma_{xy} \end{Bmatrix} \quad \ldots\ldots\ldots (9)$$

(b)

For bending the curvatures of the deflection surface in planes parallel to the coordinate planes XZ, YZ and XY are represented by K_{xx}, K_{yy}, K_{xy} where

$$K_{xx} = -\frac{\partial \phi_y}{\partial x}$$

$$K_{yy} = \frac{\partial \phi_x}{\partial y}$$

$$K_{xy} = \frac{\partial \phi_x}{\partial x} - \frac{\partial \phi_y}{\partial y} \qquad \text{(a)}$$

$$\{\varepsilon_b\} = \begin{Bmatrix} K_{xx} \\ K_{yy} \\ K_{xy} \end{Bmatrix} \qquad \text{(b)} \qquad \ldots\ldots (10)$$

In addition to the direct strains (10) transverse shear strains γ_{xz} and γ_{yz} are set up in the XZ and YZ planes. These strains are given by the following

$$\gamma_{xz} = \frac{\partial u_z}{\partial x} - \phi_x$$

$$\gamma_{yz} = \frac{\partial u_z}{\partial x} + \phi_y \qquad \text{(a)}$$

$$\{\gamma_s\} = \begin{Bmatrix} \gamma_{xz} \\ \gamma_{yz} \end{Bmatrix} \qquad \text{(b)} \qquad \ldots\ldots (11)$$

Combining expressions (9), (10), (11) we can obtain the listing of generalised strains in the orthotropic sandwich element for membrane and bending deformation. These strains together with the listings of generalised nodal displacement of various kinds are shown in Ref.16 equation 184.

8.3.2.3. Stresses

Stresses set up in a two dimensional orthotropic sandwich element can be obtained from strains using the usual elasticity relations. The membrane stress resultants can be obtained from the expressions for membrane strains thus:

$$\{\sigma_m\} = \begin{Bmatrix} \sigma_x \\ \sigma_y \\ \tau_{xy} \end{Bmatrix} = \frac{1}{1-\nu_{xy}\nu_{yx}} \begin{bmatrix} E_{xx} & \nu_{yx}E_{xx} & 0 \\ E_{yy} & \nu_{xy}E_{yy} & 0 \\ 0 & 0 & (1-\nu_{xy}\nu_{yx})G_{xy} \end{bmatrix} \begin{Bmatrix} \varepsilon_{xx} \\ \varepsilon_{yy} \\ \gamma_{xy} \end{Bmatrix} \ldots\ldots (12)$$

Similarly the bending moments and transverse shear stress resultants due to bending can be obtained from the expressions for bending curvatures (10) and transverse shear strains (11). It is assumed in Section 8.3.2.1 that the flexural rigidity of the core is negligible and hence is ignored. The flexural rigidity of each facing is given by:

Let F_{xx} be the flexural rigidity of facings in X direction.

$$F_{xx} = \frac{E_{xx}}{(1-\nu_{xy}\nu_{yx})} \left[\frac{h_f^3}{12} + \frac{h_f d^2}{4} \right]$$

Similarly

$$F_{yy} = \frac{E_{yy}}{(1-\nu_{xy}\nu_{yx})} \left[\frac{h_f^3}{12} + \frac{h_f d^2}{4} \right] \qquad \ldots\ldots\ldots (13)$$

Similarly

$$F_{xy} = \frac{G_{xy}}{(1-\nu_{xy}\nu_{yx})} \left[\frac{h_f^3}{12} + \frac{h_f d^2}{4} \right]$$

where the total sandwich thickness $h = 2h_f + h_c$ and $d = h_f + h_c$. see Fig. 8.1(a). The first part of equation (13) is the flexural rigidity about its own axis and the second part is about the middle surface of the sandwich core. Hence the equations for bending moment resultants can be written as:

$$\{\sigma_b\} = \begin{Bmatrix} M_{xx} \\ M_{yy} \\ M_{xy} \end{Bmatrix} = 2 \begin{bmatrix} F_{xx} & \nu_{yx}F_{xx} & 0 \\ F_{yy} & \nu_{xy}F_{yy} & 0 \\ 0 & 0 & F_{xy} \end{bmatrix} \begin{Bmatrix} K_{xx} \\ K_{yy} \\ K_{xy} \end{Bmatrix} \qquad \ldots\ldots\ldots\ldots (14)$$

We can define the shear forces per unit length in the XZ and YZ planes by Q_{sx} and Q_{sy} respectively. The shear stresses in the XZ and YZ planes are denoted as τ_{xz} and τ_{yz}. Q_{sx} and Q_{sy} are the shear stress resultants and can be obtained from the following expressions;

$$Q_{sx} = \int_{-h_c/2}^{+h_c/2} \tau_{xz}\, d_z = G_{xz} \int_{-h_c/2}^{+h_c/2} \gamma_{xz}\, d_z = \frac{G_{xz}\, h_c\, \gamma_{xz}}{K}$$

Similarly

$$Q_{sy} = \frac{G_{yz}\, h_c\, \gamma_{yz}}{K} \qquad \text{(a)} \qquad \ldots\ldots\ldots (15)$$

A shear stress vector can be defined as

$$\{\tau_s\} = \begin{Bmatrix} Q_{sx} \\ Q_{sy} \end{Bmatrix} \qquad \text{(b)} \qquad \ldots\ldots\ldots (15)$$

where K is the shear stress correction factor that accounts for the fact that the transverse shear stresses are not constant across the sandwich thickness. Various values have been suggested by various authors for K. Determination of K factor is fully explained in Ref.20 which uses different values of K in XZ and YZ planes. Also in Ref.21 a K value of 6/5 is used for the analysis of laminated plates including transverse shear effect. Reissner, Ref.22, uses a K value of $12/\pi^2$. However, in the PAFEC scheme the value used is 6/5 and this is the value used in this work.

8.3.2.4 Strain Energy

To obtain solutions to problems with finite elements an expression for the strian energy of the deformed structure has to be set up. The general expression for the strain energy of an element of area dx dy, after integrating with respect to the thickness coordinate Z, is

$$\text{S.E.} = \frac{h}{2} \{\varepsilon\}^T \{\sigma\}\, dx\, dy \qquad \ldots\ldots\ldots (16)$$

Stresses and strains can be expressed in terms of each other using standard elasticity relations. Assuming general elastic behaviour the relationship between stresses and strains are linear and are of the form

$$\{\sigma\} = [D^*]\{\varepsilon\} \qquad \ldots\ldots\ldots (17)$$

The stress strain relations in (12),(14),(15) can be rewritten as

$$\{\sigma_m\} = [D_m^*]\{\varepsilon_m\} \quad ....(a)$$

$$\{\sigma_b\} = [D_b]\{\varepsilon_b\} \quad ....(b) \qquad ..... (18)$$

$$\{\tau_s\} = [D_s]\{\gamma_s\} \quad ....(c)$$

where [D*] is an elasticity matrix and can be obtained from orthotropic stress strain relationships. The thickness of the facings can be incorporated in the [D*] matrix to give the modified elasticity matrix [D].

Therefore $[D_m] = h\,[D_m^*]$ ..... (19)

where $h = 2h_f + h_c$ but $h_c = 0$ since the core has no strength in the X-Y plane.

Substituting (19) into (18)(a) and finally into (16) to obtain expressions for strain energy in terms of strains only

$$S.E_m = \tfrac{1}{2}\{\varepsilon_m\}^T[D_m]\{\varepsilon_m\}\,dx\,dy$$

$$S.E_b = \tfrac{1}{2}\{\varepsilon_b\}^T[D_b]\{\varepsilon_b\}\,dx\,dy \qquad ..... (20)$$

$$S.E_s = \tfrac{1}{2}\{\gamma_s\}^T[D_s]\{\varepsilon_s\}\,dx\,dy$$

Substituting from (11)(b) for the membrane strain vector and from (12) for the membrane stresses, we have

$$S.E_m = \frac{h_f}{(1-\nu_{xy}\,\nu_{yx})} \int_{dA} [E_{xx}\varepsilon_{xx}^2 + E_{yy}\varepsilon_{yy}^2 + 2\nu_{yx}E_{xx}\varepsilon_{xx}\varepsilon_{yy} + (1-\nu_{xy}\nu_{yx}) G_{xy}\gamma_{xy}^2]\,dx\,dy \quad ....(21a)$$

Similarly for bending

$$S.E_b = \frac{1}{(1-\nu_{xy}\nu_{yx})} \frac{h_f^3}{12} + \frac{h_f d^2}{4} \int_{dA} [E_{xx}K_{xx}^2 + E_{yy}K_{yy}^2 + 2\nu_{yx}K_{xx}K_{yy} + (1-\nu_{xy}\nu_{yx}) G_{xy}K_{xy}^2] \, dx \, dy \quad \ldots\ldots\ldots (21b)$$

Similarly for transverse shear

$$S.E_s = \frac{h_c}{2K} \int_{dA} (G_{xz}\tau_{xz}^2 + G_{yz}\tau_{yz}^2) \, dx \, dy \quad \ldots\ldots\ldots (21c)$$

Expressions (21(a)(b)(c) are combined to give the strain energy of the orthotropic sandwich plate element for membrane and bending deformation.

$$S.E. = S.E_m + S.E_b + S.E_s \quad \ldots\ldots\ldots (22)$$

In the case of an orthotropic sandwich plate with a core material having sufficient stiffness in the X-Y plane so that the contribution of the core to the strain energy due to membrane and bending deformation cannot be neglected, equations (21(a)) and (21(b)) are added to the overall strain energy of equation (22). This can be done simply by including the compliance matrix of the core derived from its elastic properties since the facing plies and the core are treated as individual layers capable of being orientated at different angles to the principal material axis which is explained further in the implementation on the PAFEC system at the end of this chapter.

8.3.2.5 Isoparametric Facet Shell Element for Orthotropic Sandwich Plate

It is evident that the reliability of finite element solutions does depend on the accuracy with which the idealised elements can represent the true geometry of the structure. A family of simple elements that have been found to model complex shape accurately are the isoparametric facet shell elements. With these elements suitable coordinate

transformations are used to map curvilinear elements with curved boundaries into simple geometric shapes. The functions used to describe the geometry and the displacement variations are identical hence the term isoparametric. The procedure for generating the stiffness matrix in terms of displacements for orthotropic sandwich elements with membrane, bending and transverse shear capabilities in two dimensional analysis remains the same as that for isotropic sandwich elements, a full description of this is given in Ref.16, Section 2.6.3, and will not be repeated in this work. The resulting stiffness matrix for the element in terms of element displacements is

$$\text{S.E.} = [A^*]^{-T} \iint_{\text{AREA}} [B]^T [D][B] \, dx \, dy \, [A^*] \qquad \ldots\ldots\ldots (23)$$

where [B] = ELEMENT STRAIN - DISPLACEMENT MATRIX

and [A] = MATRIX RELATING CONSTANTS TO NODAL VALUES

[D] = STRESS/STRAIN MATRIX.

8.3.2.6 Formulation of Stress-Strain Matrix [D] for Orthotropic Sandwich Element

An orthotropic material has 3 planes of symmetry of its material properties, see Fig. 8.3(a). These planes are mutually perpendicular to each other - hence the 'ortho' part of the name. Because of material symmetries in an orthotropic material, with the stress/strain coordinate axes referred to the principal material directions, the shear strains are independent of direct stresses and the direct strains are independent of shear stresses. Also by application of Maxwell's Reciprocal Theorem, the numbers of elastic constants in a general three-dimensional state of stress reduces from 36 to 9. Hence Hooke's Law can be written in matrix notation, in terms of the compliance matrix S_{ij} as

$$\begin{Bmatrix} \varepsilon_{11} \\ \varepsilon_{22} \\ \varepsilon_{33} \\ \gamma_{23} \\ \gamma_{31} \\ \gamma_{12} \end{Bmatrix} = \begin{bmatrix} s_{11} & s_{12} & s_{13} & 0 & 0 & 0 \\ & s_{22} & s_{23} & 0 & 0 & 0 \\ & & s_{33} & 0 & 0 & 0 \\ & & & s_{44} & 0 & 0 \\ & & & & s_{55} & 0 \\ & & & & & s_{66} \end{bmatrix} \begin{Bmatrix} \sigma_{11} \\ \sigma_{22} \\ \sigma_{33} \\ \tau_{23} \\ \tau_{31} \\ \tau_{12} \end{Bmatrix} \quad \ldots\ldots (24)$$

For the orthotropic sandwich element considered in this section, it has been assumed that the orthotropic facings are in a two dimensional state of stress, see Fig. 8.3(b, which contributes to the strain energy in membrane and bending deformation of the sandwich plate, while the thick orthotropic core contributes to strain energy due to its transverse shear deformation, thus the stress-strain matrix in terms of compliance matrix for the facing laminates can be written as

$$\begin{Bmatrix} \varepsilon_{11} \\ \varepsilon_{22} \\ \gamma_{12} \end{Bmatrix} = \begin{bmatrix} s_{11} & s_{12} & 0 \\ s_{21} & s_{22} & 0 \\ 0 & 0 & s_{66} \end{bmatrix} \begin{Bmatrix} \sigma_{11} \\ \sigma_{22} \\ \tau_{12} \end{Bmatrix} \quad \ldots\ldots\ldots (25)$$

The [S] matrix reduces to 4 elastic constants where

$$S_{11} = \frac{1}{E_{11}} \quad , \quad S_{22} = \frac{1}{E_{22}} \quad , \quad S_{12} = \frac{-\nu_{21}}{E_{22}} \quad , \quad S_{21} = \frac{-\nu_{12}}{E_{11}}$$

and $S_{66} = \frac{1}{G_{12}}$.

For the orthotropic core the equation (24) reduces to

$$\begin{Bmatrix} \gamma_{23} \\ \gamma_{31} \end{Bmatrix} = \begin{bmatrix} S_{44} & 0 \\ 0 & S_{55} \end{bmatrix} \begin{Bmatrix} \tau_{23} \\ \tau_{31} \end{Bmatrix} \quad \ldots\ldots\ldots (26)$$

where $S_{44} = \frac{1}{G_{23}}$, $S_{55} = \frac{1}{G_{31}}$.

The stress-strain matrix [D] used in the expression for the element stiffness matrix (Equation 23) is related to the stresses and strains in

the element axes (X_e,Y_e,Z_e). When the material symmetry axes coincide with the element axes, the strain-stress equations of (25) and (26) can be written:

$$\begin{Bmatrix} \varepsilon^e_{xx} \\ \varepsilon^e_{yy} \\ \gamma^e_{xy} \end{Bmatrix} = \begin{bmatrix} s_{11} & s_{12} & 0 \\ s_{21} & s_{22} & 0 \\ 0 & 0 & s_{66} \end{bmatrix} \begin{Bmatrix} \sigma^e_{xx} \\ \sigma^e_{yy} \\ \tau^e_{xy} \end{Bmatrix} \quad \ldots\ldots\ldots \quad (27)$$

and

$$\begin{Bmatrix} \gamma^e_{yz} \\ \gamma^e_{xz} \end{Bmatrix} = \begin{bmatrix} s_{44} & 0 \\ 0 & s_{55} \end{bmatrix} \begin{Bmatrix} \tau^e_{yz} \\ \tau^e_{xz} \end{Bmatrix} \quad \ldots\ldots\ldots \quad (28)$$

The facings of the sandwich plate considered here consist of several orthotropic layers that have principal material directions aligned with the laminate axes. Since the thicknesses locations and material properties of the laminae are symmetric about the middle surface of the sandwich, there is no coupling between bending and extension. Fig. 8.4(b) shows the material symmetry axes orientated at angle θ to the element axes. For this the strain-stress matrix of equations (27), (28) is inverted to give the stiffness matrix in the material direction and then transformed to give the stiffness matrix in the element axis.

$$[QO] = [S]^{-1} \quad \ldots\ldots\ldots \quad (29)$$

$$[\overline{QO}] = [T]^{-1}[QO][T]^{-T} \quad \ldots\ldots\ldots \quad (30)$$

where $[QO]$ = stiffness matrix in material direction

$[\overline{QO}]$ = stiffness matrix in element axis

$[T]$ = transformation matrix

$$[T] = \begin{bmatrix} m^2 & n^2 & 2mn \\ n^2 & m^2 & -2mn \\ -mn & mn & (m^2-n^2) \end{bmatrix} \qquad \text{where } m = \cos\theta, \quad n = \sin\theta$$

The stress-strain matrix [D] can now be obtained by using $[\overline{QO}]$.

For membrane deformation, see Fig. 8.4(c)

$$[D_m] = \sum_{K=1}^{n} C_1 \begin{bmatrix} \overline{QO}_{11} & \overline{QO}_{12} & \overline{QO}_{16} \\ \overline{QO}_{21} & \overline{QO}_{22} & \overline{QO}_{26} \\ \overline{QO}_{61} & \overline{QO}_{62} & \overline{QO}_{66} \end{bmatrix} \text{ N/mm} \qquad \ldots\ldots(31)$$

For bending deformation

$$[D_b] = \sum_{K=1}^{n} C_3 \begin{bmatrix} \overline{QO}_{11} & \overline{QO}_{12} & \overline{QO}_{16} \\ \overline{QO}_{21} & \overline{QO}_{22} & \overline{QO}_{26} \\ \overline{QO}_{61} & \overline{QO}_{62} & \overline{QO}_{66} \end{bmatrix} \text{ N/mm} \qquad \ldots\ldots(32)$$

For shear deformation

$$[D_s] = 2C_1 \begin{bmatrix} \overline{QO}_{44} & 0 \\ 0 & \overline{QO}_{55} \end{bmatrix} \text{ N/mm} \qquad \ldots\ldots(33)$$

where

$$C_1 = Z_u - Z_L$$

$$C_2 = Z_u + Z_L$$

$$C_3 = \frac{C_1^3}{12} + \frac{C_1 C_2^2}{4}$$

for 0° or 90° layers $\overline{QO}_{16} = \overline{QO}_{26} = 0$.

Therefore the [D] matrix for an orthotropic sandwich plate can be obtained by combining equations (31),(32),(33).

$$D = \begin{bmatrix} D_{11} & D_{12} & D_{13} & 0 & 0 & 0 & 0 & 0 \\ D_{21} & D_{22} & D_{23} & 0 & 0 & 0 & 0 & 0 \\ D_{31} & D_{32} & D_{33} & 0 & 0 & 0 & 0 & 0 \\ 0 & 0 & 0 & D_{44} & D_{45} & D_{46} & 0 & 0 \\ 0 & 0 & 0 & D_{54} & D_{55} & D_{56} & 0 & 0 \\ 0 & 0 & 0 & D_{64} & D_{65} & D_{66} & 0 & 0 \\ 0 & 0 & 0 & 0 & 0 & 0 & D_{77} & 0 \\ 0 & 0 & 0 & 0 & 0 & 0 & 0 & D_{88} \end{bmatrix} \quad \ldots\ldots(34)$$

Substituting the [D] matrix into the equation (23) and integrating over the area will give the element stiffness matrix [K_e], see equation (6). System matrix [K] is obtained by merging the element stiffness matrices. Hence equation (4) is solved for element displacement.

8.3.2.7 Determination of Ply Stresses

The aim of the analysis of the composite sandwich plate is to determine the stresses and strains in each of the plies forming the facing laminates and in the thick honeycomb core in their principal material directions. These stresses and strains can then be used to predict the load at which failure initiates. The failure of the laminates can be related to the strength of the ply where the complete failure of the facing is usually preceded by the fracture of an individual ply. The main failure processes are assumed to be the same as that of the laminate plate which are:

1) Fibre fracture

2) Transverse tensile cracking parallel to the fibres

3) Shear fracture parallel to the fibres

σ_1 is the critical stress parallel to the fibres associated with fibre fracture, σ_2 and τ_{12} are the corresponding stresses for transverse and shear cracking respectively. For the honeycomb core the transverse shear stresses through the thickness τ_{13} and τ_{23} are the only stresses significant enough to cause core shear failure. The method of determining these stresses and strains for the known displacements in the element axes for a given stacking sequence is given below.

The strains in a lamina caused by external loading are functions of the laminate midplane strains, plate curvatures and distance from the geometrical midplane of the laminate, see Fig. 8.4(c). Note that the honeycomb core is treated as an individual layer providing only transverse shear stiffnesses.

The relation between these quantities can be written as

$$\begin{Bmatrix} \varepsilon^e_{xx} \\ \varepsilon^e_{yy} \\ \gamma^e_{xy} \end{Bmatrix} = \begin{Bmatrix} \varepsilon^m_{xx} \\ \varepsilon^m_{yy} \\ \gamma^m_{xy} \end{Bmatrix} + Z \begin{Bmatrix} K_{xx} \\ K_{yy} \\ K_{xy} \end{Bmatrix} \qquad \ldots\ldots (35)$$

where suffix 'm' denotes the membrane definition.

Hence the stresses in the facing laminae can be obtained by transforming the strains to the material directions and multiplying by the stiffnesses of the laminae, thus:

$$\begin{Bmatrix} \sigma_1 \\ \sigma_2 \\ \tau_{12} \end{Bmatrix} = \begin{bmatrix} QO_{11} & QO_{12} & QO_{13} \\ QO_{21} & QO_{22} & QO_{23} \\ QO_{31} & QO_{32} & QO_{33} \end{bmatrix} \begin{bmatrix} m^2 & n^2 & 2mn \\ n^2 & m^2 & -2mn \\ -mn & mn & (m^2-n^2) \end{bmatrix}^{-T} \begin{Bmatrix} \varepsilon^e_{xx} \\ \varepsilon^e_{yy} \\ \gamma^e_{xy} \end{Bmatrix} \quad \ldots.(36)$$

For the transverse shear stresses in the core

$$\begin{Bmatrix} \tau_{23} \\ \tau_{13} \end{Bmatrix} = \frac{1}{K} * \begin{bmatrix} QO_{44} & 0 \\ 0 & QO_{55} \end{bmatrix} \begin{bmatrix} m^2 & n^2 & 2mn \\ n^2 & m^2 & -2mn \\ -mn & mn & (m^2-n^2) \end{bmatrix}^{-T} \begin{Bmatrix} \gamma^e_{yz} \\ \gamma^e_{xz} \end{Bmatrix} \quad \ldots\ldots(37)$$

where the K value accounts for the discrepancy between the assumed shear stress distribution (Fig. 8.2(b)) and the actual shear stress distribution (Fig.8.2(a)).

8.4 THREE DIMENSIONAL THEORY FOR ORTHOTROPIC SANDWICH PLATE

8.4.1 Introduction

In the preceding section of this chapter the problem of two dimensional analysis of orthotropic sandwich was discussed, with which the stress analysis of large sandwich structure could be performed, i.e. box-beam, where one is looking for approximate but acceptable solutions at a finite number of points in the structure. However with the joint analysis, accurate strength prediction depends largely on the geometrical representation by including all the important parameters which can influence the state of stress concentration. The interaction of these parameters can only be represented with three dimensional orthotropic sandwich elements. A three dimensional elasticity solution has been developed for a sandwich plate by Yen et al (Ref.23).

Furthemore N.J. Pagano (Ref.24) applied the elasticity solution to thin facing bidirectional composite sandwich plate and compared the

results with that of C.P.T. (Classical laminated Plate Theory). He concluded that the convergence of elasticity solution to C.P.T. is more rapid for the stress components than plate deflection, therefore emphasizing that particular care must be taken in selecting the form of a plate theory required in the solution of a specific problem. The approach undergone for the stress analysis of the problem reported in this thesis is a combination of 2-D and 3-D elasticity solution, where the former can be represented for the facing laminate and the later for the thick honeycomb core. The existance of 2-D and 3-D orthotropic laminated plate elements in the PAFEC package meant that no changes were required to the routines in calculating the stiffness matrix for the displacements. Therefore eight and six noded orthotropic isoparametric plain stress elements (facing laminate) could be added to the top and bottom faces of twenty and fifteen noded orthotropic isoparametric brick and wedge type elements (core) respectively, which would take the same form as the sandwich plate geometrically, see Fig. 8.5. The overall stiffnesses of the sandwich is obtained by merging the two independent stiffness matrices (2D, 3D). A bief description of the assumptions for displacements, strains and stresses are given in the following.

8.4.2 Displacements

The sandwich elements are constructed so that the deformations at any point in the plate are represented by three sets of linear displacements U_x, U_y and U_z in the X,Y,Z directions respectively. The inplane displacements U_x and U_y cater for the membrane deformation of the laminated facings, since the honeycomb core has little stiffness in the

X-Y plane. The transverse displacement U_z represents the shear deformation of the core in the Z-direction. The shear stress distribution through the thickness of the core is no longer constant, see Fig. 8.2(a), for true shear stress distribution. Finally the stresses in the faces and the core in the Z-direction are small and therefore can be ignored.

8.4.3 Strains and Stresses

The expressions for strains for the orthotropic sandwich are obtained in terms of differentials of displacement which is based on the small deflection theory. The strain-displacement relationship can be written as

$$\varepsilon_{xx} = \frac{\partial u_x}{\partial x}, \qquad \gamma_{yz} = \frac{\partial u_z}{\partial y} + \frac{\partial u_y}{\partial z}$$

$$\varepsilon_{yy} = \frac{\partial u_y}{\partial y}, \qquad \gamma_{zx} = \frac{\partial u_z}{\partial x} + \frac{\partial u_x}{\partial z} \qquad \ldots\ldots\ldots (38)$$

$$\varepsilon_{zz} = \frac{\partial u_z}{\partial z} \qquad \gamma_{xy} = \frac{\partial u_x}{\partial y} + \frac{\partial u_y}{\partial x}$$

where ϵ_{xx}, ϵ_{yy}, γ_{xy} are the only common terms between the core and the facing laminate. These strains are set up using the polynomials and their derivatives with respect to X,Y and Z. A full description of which is given in Ref.16.

The expression for the stresses can be related to the elastic strains by means of Hooke's Law for a three dimensional state of stress. The stress vector $\{\sigma\}$ is therefore connected to the strain vector $\{\epsilon\}$ by the relation

$$\{\sigma\} = [D]\{\epsilon\} \qquad \ldots\ldots\ldots (39)$$

where [D] is the stress-strain matrix.

8.4.4 Derivation of [D] Matrix

The formulation of the expression for the element stiffness matrix of both 2-D and 3-D elements are similar to that of equation (23) and are given in Ref.16, Section 2.4 and the stress-strain matrix [D], is the only matrix affected by material orthotropy. The Hooke's Law in matrix notation in terms of the compliances matrix of equations (27) and (28) can be rewritten for the orthotropic sandwich plate as:

$$\begin{Bmatrix} \varepsilon^e_{xx} \\ \varepsilon^e_{yy} \\ \varepsilon^e_{zz} \\ \gamma^e_{yz} \\ \gamma^e_{xz} \\ \gamma^e_{xy} \end{Bmatrix} = \begin{bmatrix} s_{11} & s_{12} & s_{13} & 0 & 0 & 0 \\ & s_{22} & s_{23} & 0 & 0 & 0 \\ & & s_{33} & 0 & 0 & 0 \\ & & & s_{44} & 0 & 0 \\ & \text{SYMMETRIC} & & & s_{55} & 0 \\ & & & & & s_{66} \end{bmatrix} \begin{Bmatrix} \sigma^e_{xx} \\ \sigma^e_{yy} \\ \sigma^e_{zz} \\ \tau^e_{yz} \\ \tau^e_{xz} \\ \tau^e_{xy} \end{Bmatrix} \qquad \ldots\ldots (40)$$

$[S^m]$ is then inverted to give the stress-strain matrix $[D^m]$ corresponding to [D] matrix of equation (39). Thus the merged stress-strain matrix is given by:

$$[D] = \begin{bmatrix} D^{FC}_{11} & D^{FC}_{12} & D^{C}_{13} & 0 & 0 & D^{F}_{16} \\ & D^{FC}_{22} & D^{C}_{23} & 0 & 0 & D^{F}_{26} \\ & & D^{C}_{33} & 0 & 0 & 0 \\ & & & D^{C}_{44} & 0 & 0 \\ & \text{SYMMETRIC} & & & D^{C}_{55} & 0 \\ & & & & & D^{FC}_{66} \end{bmatrix} \qquad \ldots\ldots (41)$$

where FC denotes the contribution of the facing and core to the stress-strain matrix

C denotes the contribution of the core to the stress-strain matrix.

8.5 IMPLEMENTATION OF PAFEC

8.5.1 2-D Isoparametric Thick Shell Orthotropic Sandwich Element

The approach undertaken for the implementation of orthotropic sandwich element was to contain the modification of the existing isotropic sandwich element (45210) in the routines supplying the stiffness matrix without changing the general organisation of the main controlling routines, such as R45010 which solves the problem for displacements and R95010 which determines the stresses from the calculated displacements since most of the calculation carried out or controlled by these routines concern other families of elements within the PAFEC system. For the displacement a flow diagram for the routine R45010 is given in Ref.25 which describes most of what is happening. The routines concerned with finding the material properties and setting up the [D] matrix for the isotropic case were R45009, R09960 and R12270. The modification to these routines were carried out within the R45009. The modified version of the elements allows each element to have any number of layers each having different properties and material orientations. The calculation of mass, pressure and distributing loading matrices exactly follows the isotropic element. The required modifications are as follows:-

1. Call routine to retrieve orthotropic material properties.
2. Call routine to find the angle which the material direction makes with the respective axis.
3. Call routines to set up stiffnes matrix by inverting the compliance matrix in the material directions (DCA).
4. Call routine to relate the stiffness matrix from one set axis (material direction) to another (i.e. global) so that the Z axis remains the thickness of the layers.
5. Finally the contribution of each layer to the stress-strain matrix [D] of equation (34) is obtained for a multi-layered element.

Familiarity with the FORTRAN codings of the PAFEC routines was found to be essential for the inclusion of the orthotropic element. This is a particular problem in a general purpose F.E.M. package, which researchers always have to overcome.

Note that a common block has to be set up for the direction cosines in the main controlling routine R45010 for the displacement which is used in the main controlling routine R95010 for stressing purpose. The routine concerned with the stressing of the element is R95004, which is called by the controlling routine (R95010), and again all the modifications were contained in these routines where the output is given for the stresses in the material directions, together with the position of the layers defined by variables ALOW and AUPP, as well as the angle of orientation with the respective axes. These modifications can be kept in two separate FORTRAN files which then can be supplied in the appropriate phases of a given data file containing a combination of other elements by using the PAFEC facility such as 'USE.FILENAME' option. These routines were put to a number of vigorous tests, in plane and out of plane bending, box beam bending, some of which are given in Chapter

9. Appendix (1) gives the complete version of the modified routines needed for the analysis of 2-D orthotropic sandwich plate.

8.5.2 3-D Isoparametric Orthotropic Sandwich Element (36215 + 37115, 36115 + 37215)

No changes were required for setting up the stress-strain [D] matrix of equation (41). Nevertheless the related routines needed to be checked for the correct set of matrices. The routines giving these matrices for the core were R37905 and R37955 representing the isoparametric brick and wedge type elements respectively and R36020 representing the isoparametric quadralateral triangular plain stress elements for the facing laminate. For stressing purposes minor modifications were carried out in routines R86022 and R86023 which relate to the facing elements mainly by including the laminae failure criteria and the stressing output similar to that of thick shell elements. Appendix (2) gives the modified versions of these routines.

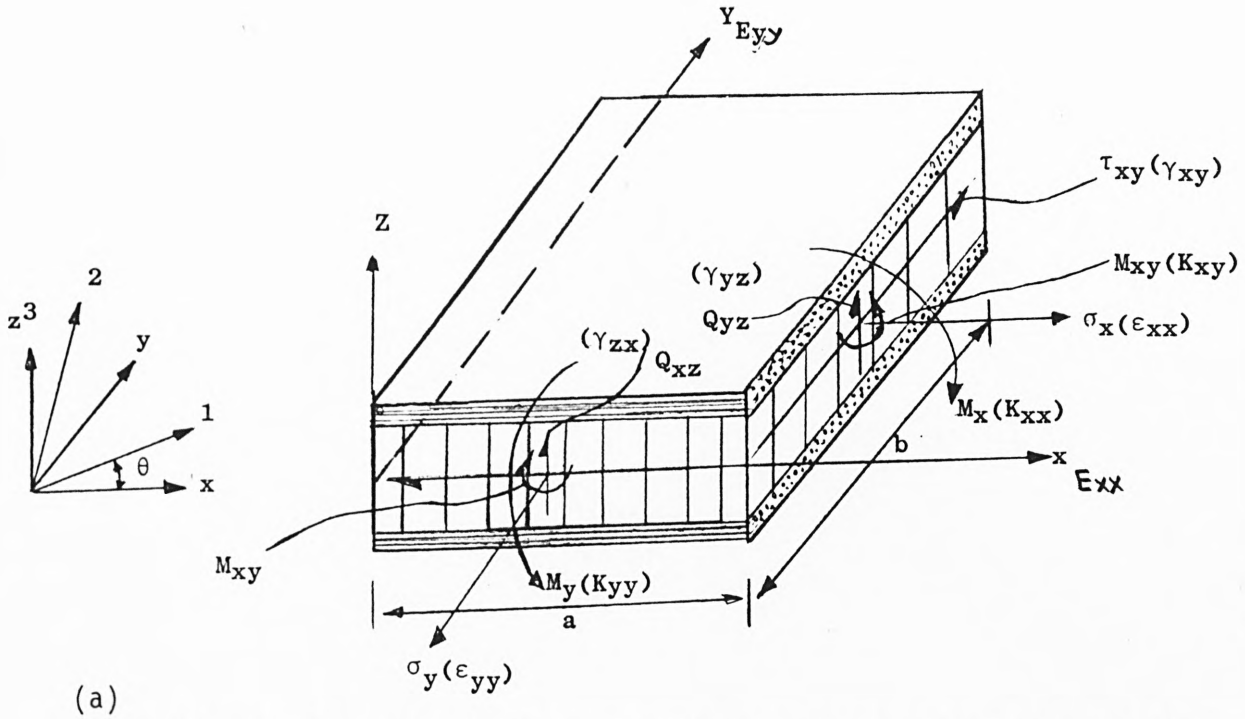

(a)

dimensions, orthotropic elastic constants, membrane stresses (strains), bending moments (curvatures) and transverse shear stresses (strains) of an orthotropic sandwich element.

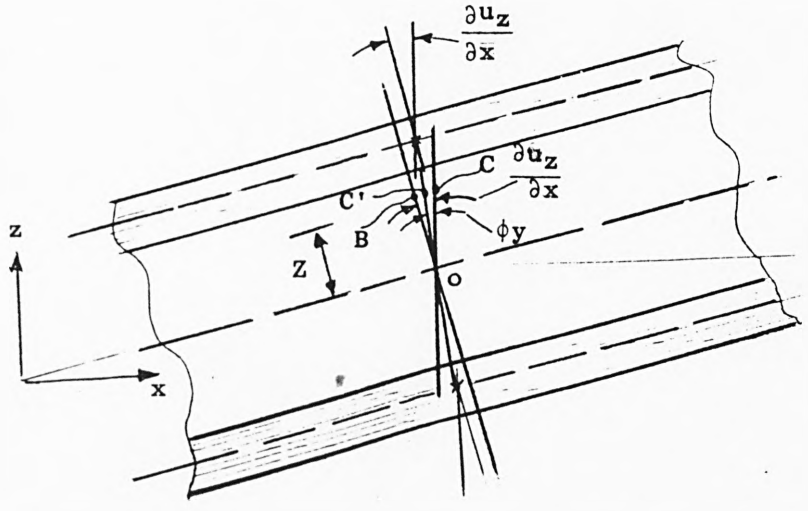

(b)
Section in xz plane of composite sandwich element

Fig. 8.1 RECTANGULAR ORTHOTROPIC SANDWICH ELEMENT

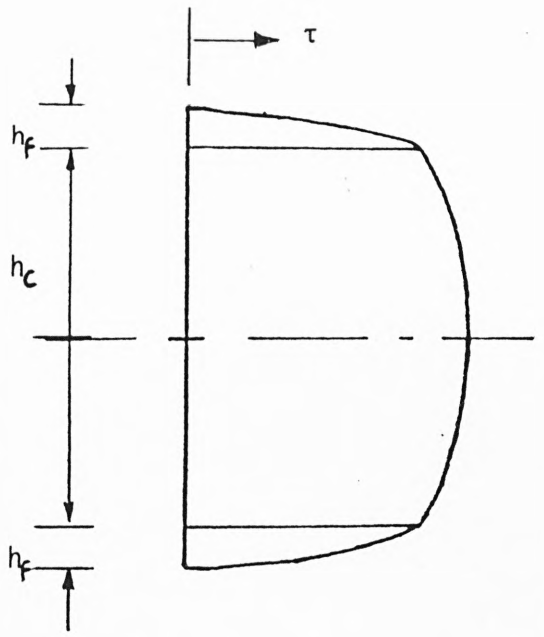

(a) TRUE SHEAR STRESS DISTRIBUTION.

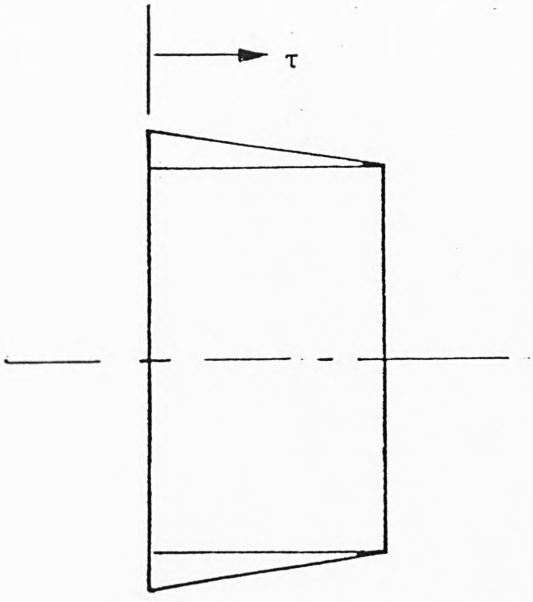

(b) ASSUMED SHEAR STRESS DISTRIBUTION.

FIG 8.2

TRANSVERSE SHEAR STRESS DISTRIBUTION IN THE COMPOSITE SANDWICH PANEL.

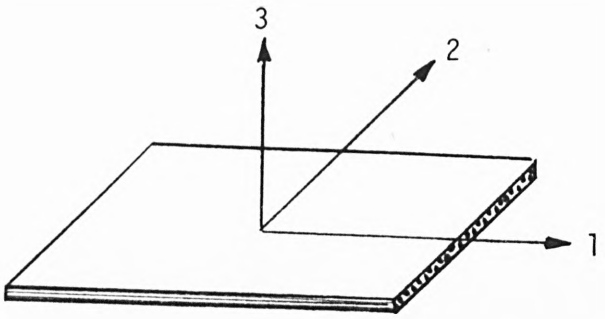

(a) PRINCIPAL PLANES.

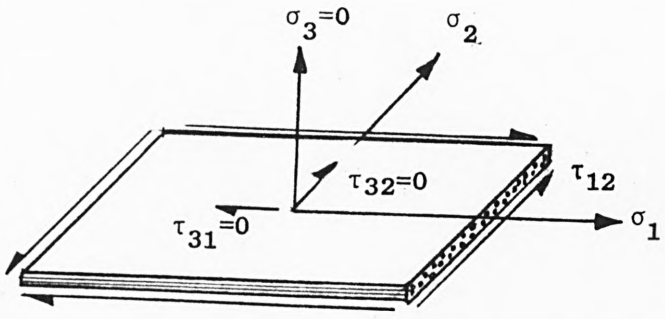

(b) TWO-DIMENSIONAL STRESS SYSTEM.

FIG 8.3

STRESS ACTING IN THE ORTHOTROPIC FACING LAMINATE.

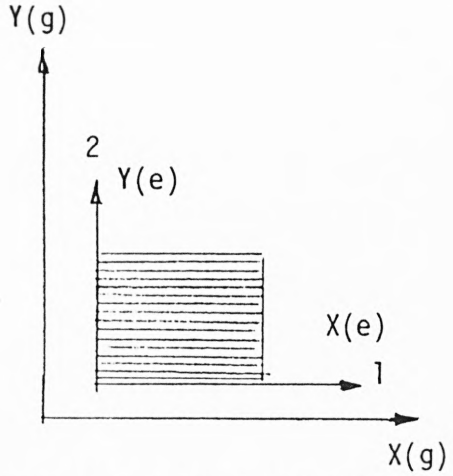

(a) MATERIAL AXIS PARALLEL TO GLOBAL AXIS.

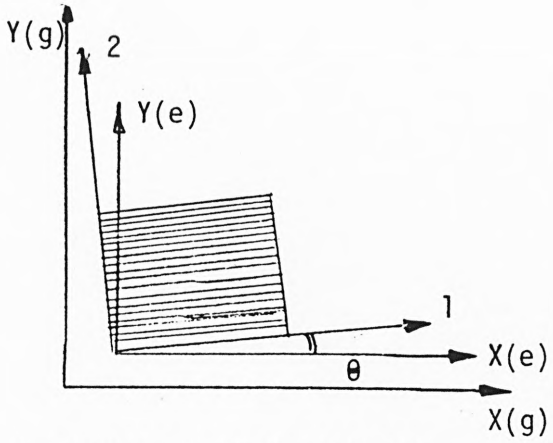

(b) MATERIAL AXIS DISPLACED BY ANGLE θ.

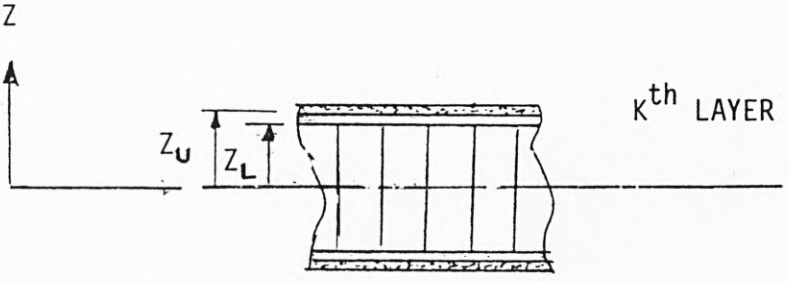

(C) POSITION OF LAYERS.

FIG 8.4

PRINCIPAL MATERIAL AXES AND GEOMETRY OF SANDWICH COMPOSITE.

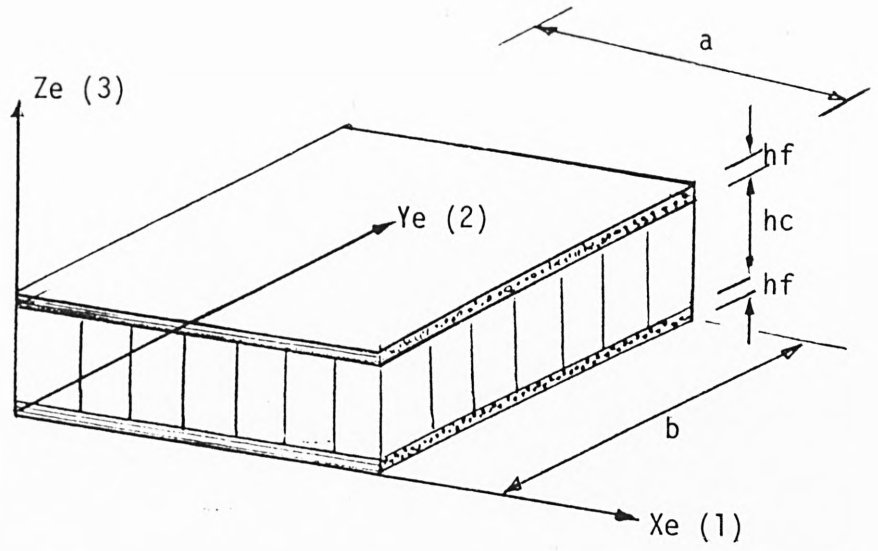

(a) 3D SANDWICH ELEMENT

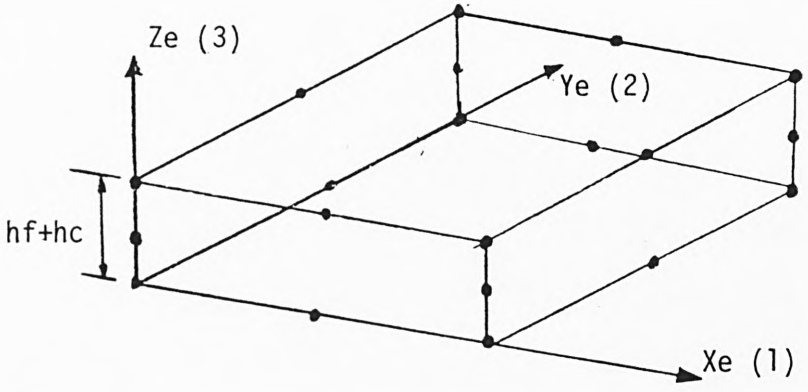

(b) IDEALIZED 3D SANDWICH ELEMENT

FIG 8.5

THREE DIMENSIONAL ORTHOTROPIC SANDWICH ELEMENT

9. BEAM STRESS ANALYSIS AND STRENGTH PREDICTION

9.1 INTRODUCTION

The program of work reported in this chapter is an attempt at proving that the analysis can be used for designing structures made of composite sandwich panels. It uses the two dimensional orthotropic thick shell element for deformation of a large structure. Also, for analysing the complex stress interactions of these panels when joined together by the tongue and slot joints, it uses the three dimensional orthotropic element described previously. Both of these elements are used in the stress analysis and strength prediction of tests reported in Section 6. This was found to be necessary in order to check the working of the elements, as well as to gain experience on a preliminary analysis before tackling the complex three dimensional stress interaction involved in the tongue and slot joint. All the strength predictions in this chapter were done on the nodal position of the element at the high stressed area, which proved to be satisfactory. However in predicting the joint strength the nodal points give rise to stress concentrations which are not representative and so the Gauss-points were used for the joint stress analysis. This is discussed further in Chapter 10.

The comparison between the Tsai-Hill and Hill/Hoffman Criterion was thought not to be appropriate since the failure strength of tests reported in this chapter were dependent only on the compressive strength of the facing laminate. Thus the Tsai-Hill Criterion was used throughout this chapter and the comparison between the two criteria are given in Chapter 10 for joint strength prediction.

When using the Tsai-Hill Failure Criterion the difference between the failure strengths in uniaxial tension and compression was taken into account simply by replacing the tensile strength with the appropriate compressive strength. The criterion can be re-written:-

$$\text{RESERVE FACTOR R.F.} = \frac{X}{\sqrt{\sigma_1^2 - \sigma_1\sigma_2 + \left(\frac{X}{Y}\right)^2 \sigma_2^2 + \left(\frac{X}{S}\right)^2 \tau_{12}^2}}$$

where failure occurs when R.F. $\leq$ 1.0.

Four conditions arise,

a) when σ_1, σ_2 are positive, $X = \sigma_{1UT}$

$Y = \sigma_{2UT}$

b) when σ_1, σ_2 are negative, $X = \sigma_{1UC}$

$Y = \sigma_{2UC}$

c) when $\sigma_1 = +ue$, $\sigma_2 = -ue$, $X = \sigma_{1UT}$

$Y = \sigma_{2UC}$

d) when $\sigma_2 = +ue$, $\sigma_1 = -ue$ $X = \sigma_{1UC}$

$Y = \sigma_{2UT}$

Note that the sign convention used is that the strength is written positively in the algebra and the numerical values of stress inserted as positive in tension and negative in compression. This can cause a negative value of reserve factor R.F. If this happened it was simply converted to a positive value by changing the sign.

Negative shear stress does not affect the R.F. because it is squared. The compressive failure strengths used for predictions are the average ply strengths obtained from Table 5.6(c). This was found to be appropriate because the stiffness of the sandwich honeycomb core in the transverse direction (90°) is nearly half that of longitudinal direction

(0°) which gives rise to larger deflections and hence a lower failure strength.

9.2 THREE POINT FLEXURAL COMPOSITE SANDWICH BEAM STRESS ANALYSIS AND STRENGTH PREDICTIONS

9.2.1 Beam Stress Analysis with the 2-D Orthotropic Sandwich Element

The average flexural sandwich beam test results of Tables 5.6(a)(b) and 6.1(a)(b)(c) were analysed using the 2-D orthotropic element described in Section 8.3. The full length of these single panel beams were meshed for simplicity since the total number of elements needed for the analysis was small. The vital area of the meshes (beam centre) are given in Fig. 9.1 where the letters indicate the positions of high stress at the nodal points. This was necessary in order not to confuse the reader with different finite element meshes which were needed for the different sandwich thicknesses for the reason that as h/L (h = sandwich thickness, L = plate length) decrease shear deformation becomes more important. A general element aspect ratio of .25 ≤ h/L ≤ .5 was used throughout. The finite element meshes were restrained in the vertical direction at the ends of the span and the test failure loads were applied at the beam centre as a uniformly distributed load across the beam width. Fig. 9.2 shows the finite mesh for the standard panel (h_c/h_f = 33.2) which was also appropriate for the high density core sandwich beams with multidirectional laminate facings, i.e. h_c/h_f = 11/25, 11.07. Note that the beam span and width were virtually half that of the standard beam (L = 50.8, b = 38.5, 38.3).

Fig. 9.3 shows the comparison of deflection between theory (F.E.A.) and test for the standard beam with h_c/h_f = 33.2. The analysis predicted a small variation of deflection across the width of the beam. This was due to the application of point loads at the nodal positions as the equivalent to the distributed load, hence an average deflection value was used. Table 9.1 gives the comparison between tests and theory. In both elastic and failure deflections for different sandwich thicknesses, the scatter of the predictions are within the acceptable batch differences in the material properties.

The strength predictions of the single panel beams were also based on the average ply stresses across the width of the beam. The compression strengths used for the predictions were dependent on the number of facing plies, that is to say for the two ply facing sandwich beams the postulated average compressive strengths of Table 5.6(c) were used. For beams with more than two plies in each facing the strength of the 8-ply laminate was thought to be appropriate in representing the failure mode of the facings. A typical strength prediction for the standard beam is given in Table 9.2 with the ply angles and position letters from Fig. 9.1 inserted to show the plies in which the maxima occurred.

Note that although the 90° ply in the bottom facing fails first it does so due to the transverse tensile cracking, which does not constitute complete beam failure because the 0° ply takes up the additional tensile stresses and prevents complete failure. Thus the failure strength prediction can be based on the strengths of the compressive facings as was observed in the tests. Moreover the difference in predicted strength between the upper and lower surface of the two ply facing sandwich beams was small enough to be neglected and hence and average value was taken. However for the high density core beams, with four plies in each facing, the predictions were made at both

the compressive and tensile facings at the lower and upper position of the ply with the lower having the most negative value. Table 9.3 gives the strength predictions of various sandwich thicknesses. The failure of the high density core beams were one of progressive ply failures initiated in the tensile facing which is particularly severe in the multidirectional case, nevertheless the 0° ply provides adequate strength so that the overall failure of the beam is dependent to the compressive facing strength. The predictions and the comparison between the theory and tests are discussed later in Section 9.2.3.

9.2.2 Beam Stress Analysis with the 3-D Orthotropic Sandwich Element

The single panel beams were re-analysed using the 3-D orthotropic sandwich element with general aspect ratio of $0.52 \leq h/L \leq 2.0$. Two cases were analysed: first the load was uniformly distributed widthwise along the centreline to represent a roller and secondly a pressure load was applied to the finite element mesh over two element lengths to represent the flat L163 plate load spreader (50.8mm length) used in the actual flexural tests. The results are given in Table 9.4. The predicted deflections for both cases were larger than the test values particularly for the central loading case because the point loads gave rise to a larger local deformation. This is because of the core being represented by 3-D elements which provide stiffness in the 'Z' direction whereas the facing is represented by 2-D plane stress elements which have no stiffness through the thickness. Therefore the use of the pressure loading was more suitable in order to spread the load over more core area so avoiding the local effect on the deflection. Generally the results of this table show that the analysis works. This is also

illustrated graphically in Fig. 9.4, the comparison of deflection and test for the standard sandwich beam.

The strength predictions were made similar to the 2-D analysis at the compressive facing by averaging the ply stresses widthwise and using the Tsai-Hill Failure Criterion. The results are given in Table 9.5 where different ply compressive strengths were used depending on the number of facing plies. The predictions for the bottom facing which undergoes tensile deformation remains the same as in the 2-D analysis by initiating the failure first in the 90° plies but not the 0° plies. Therefore they are not repeated here.

Table 9.5 shows that the 0° and 90° plies fail at loads which are very close to each other in all the beams. This is accounted for by the fact that the strains are the same throughout the facing thickness (i.e. no local bending of the facings) and so there is the same ratio between the stresses as the elastic moduli which happens to be very nearly the same as the ratio of the compressive strengths for this material. Hence the stresses in the two plies are very different, but so are the strengths in the same ratio. This means that both plies fail at nearly the same load on the beams.

9.2.3 Strength Predictions and Comparison Between Tests and Theory

it has been shown from the predicted deflections for the various sandwich beams that the finite element analysis works with reasonable accuracy for these simple bending cases, the accuracy of which depends on the element aspect ratio and the material properties. The 3-D predicted deflections for the standard cross-ply facing beams with various core thickness were closer to the test results (Table 9.4) than the 2-D predicted ones (Table 9.1) and the opposite occurred for the

four ply facing high density core but with larger difference. This was due to the fact that as the number of facing plies increases, the contribution of the facing to the local bending deformation increases and the 2-D element takes this deformation into account, whereas in the 3-D case the facings are represented by plane-stress elements and hence any local bending deformations are ignored.

In predicting the strengths of the standard facing (0°/90°) sandwich beams, the 3-D analysis gave better reserve factor than the 2-D analysis, the comparison of which are given in Table 9.6 for various core thicknesses. The lowest reserve factor for these beams at the top facing occurs in the 0° ply which shows that the final collapse of the beams is in fact due to the 0° ply failure in the compressive mode. Although compressive failure occurred in the actual tests, the initial ply failures were impossible to detect by the naked eye during the tests. Therefore the prediciton is better at indicating which ply is more likely to fail first. Fig. 9.5 shows graphically the comparison of strength predictions between test results and theory (2-D and 3-D) for beams with standard cross-ply facings and various honeycomb core thicknesses.

For the high density core beams with four-ply facings, the 2-D analysis predicted a progressive ply failure with the uppermost and lowermost plies taking most of the strain, see Table 9.3. The lowest reserve factors were in the tensile facings (bottom facings) in the lowermost and uppermost 90° ply for the cross-ply and multi-directional ply facings at R.F. values of 0.878 and 0.76 giving a strength prediction of 1049.7 N and 1167.9 N respectively. These underestimate the final failure by about 13.9% in the cross-ply facings beam and 31.6% in the multidirectional facings beam due to the 0° plies continuing to carry the tensile loads as previously described. The next lowest reserve

factors highly stressed plies are the uppermost 90° ply in the compressive facing at R.F. of 0.922 and the lowermost 45° ply in the tensile facing at R.F. of 0.895 for the cross-ply and multidirectional ply facings beams, giving a strength prediction of 1102.3 N and 1375.4 N respectively. These values indicate that the ply failures in the tensile facings are particularly severe in the multidirectional case where all but one ply, namely the 0° ply, fails due to the tensile cracking. This is because the angle plies (±45°) are not as effective in bending as they are in shear and furthermore the 90° plies are particularly vulnerable to tensile loading in the transverse direction. These initial failures do not however constitute the overall beam failure, the presence of 0° plies in both beams were more than adequate for the final failure to be shifted to the compressive facings. Figs. 9.6 and 9.7 give the comparison of failure factor (R.F.) for the 2-D and 3-D analysis in the compressive facings (top facings).

These figures clearly show the effect of bending deformation of the facing laminates (unlike the 3-D analysis where the facings midplane strains are also the strains for individual plies) and therefore give closer reserve factors for the individual layers. It can be argued that the compressive collapse of the cross-ply beam (high density core) ultimately depends on the uppermost 0° ply failure. The predicted strength for this ply by 2-D and 3-D analysis were 1131.0 N and 1279.3 N which are under and over estimated by 5.7% and 6.5% respectively. For the multidirectional case, in the compressive facing, the uppermost +45° ply is expected to fail first in the 2-D analysis at 1472.2 N followed by -45° ply at 1530.6 N. These underestimate actual failure by about 4.4% and 0.4% respectively which seems reasonably accurate. However, from the 3-D analysis (Table 9.5), initial failure was shown to be in the 0° ply followed by the angle plies at 1613.6 N and 1629.9 N which

overestimate the test failure by about 4.7% and 5.6% respectively. As a general conclusion to the last two paragraphs, it can be stated that the 3-D analysis gives generally a higher predicted strength than the 2-D analysis for the simple bending case.

9.3 STRESS ANALYSIS AND STRENGTH PREDICTION OF BOX BEAM

9.3.1 Analysis and Strength Prediction of the Box Beam with 2-D Orthotropic Sandwich Element

The sandwich box beam test of Section 6.2 was used as a further test of the 2-D orthotropic element since it was more of a structure than the single panel beam tests thus providing a further check of the analysis. Some necessary geometrical idealizations had to be made in representing a 3-D structure by 2-D finite element mesh. The width of the box beam was taken from the centre of the side panels (Fig. 6.1(a)) and the height from the centroid of the top and bottom panels. Only one half of the test beam was meshed with half of the test failure load applied as a uniformly distributed load to the side panels over a 25.4mm length which was appropriate in representing the load spreader (L163 plate) as used in the test (Fig. 6.1(b)). Furthermore, it was also assumed that the 'L' shaped adhesive filleting provided continuity between the top and bottom and side panels therefore giving all the nodes in the mesh the same number of degrees of freedom (i.e. 5 D.O.F.). Fig. 9.8 shows the self-equilibrating loads and the constrained mesh for the plane of symmetry where an element aspect-ratio of $.3 \leq h/L \leq .5$ was used throughout. The deflected shape of the beam under these conditions is given in Fig. 9.9 from which the maximum deflection (at the tip) was

calculated as 11.0mm compared to the test failure deflection of 11.52mm. The vital area of the mesh (constrained-end) is given in Fig. 9.10 where the position letters (A-G) denote the high-stressed area of the beam for both top and bottom panels. The stresses at these positions are given by the Hill Criterion Factors (R.F.) from which the strength predicitons are made. These values for the upper and lower facings of the top and bottom panels together with the ply angle are shown in Table 9.7. Note that the longitudinal stresses in the 0° plies and the transverse stresses in the 90° plies dominate the values of R.F. factor.

In predicting the strength of the box beam, Table 9.7, the R.F.values for the upper facing (0°/90° plies) were plotted against the width of the beam at the top panel, see Fig. 9.11. Although the failure is symmetrical about the mid-plane of the beam, a lower strength (R.F.) is predicted at positions 'A' and 'G'. This is because stress averaging does not take place at positions (nodes) of the plate bending elements meeting at an angle. Therefore the stresses at positions A, B, F and G were not representative. Consequently the prediction in each ply was based on average strength across the beam width. It is interesting to note that the 90° ply in the lower facing of the bottom panel fails first in the transverse tensile mode at 1413 N which is typical of the unidirectional plies. This underestimates the test failure by 6.4% which seems reasonably accurate. However the effect of this ply failure in the test was not visually evident from the macroscopic examination of the beam. As the load increases, the loss of beam stiffness becomes evident and the overall response of the beam deviates from its original straight-line behaviour, see Fig. 6.4. However, the beam is still able to carry additional loads, mainly due to the stiffness of the 0° ply, although the additional loads produce larger deflections than those which would have been produced by the same loads without the first ply

failure. The next highly stressed plies are in the upper facing (90°,0°) of the top panel failing at 1479 N which is an underestimation of 1.6% to that of test failure and this was the most evident final mode in the tests. The simultaneous failure of both 90° and 0° plies shows again the behaviour of thin facing cross ply sandwich plate in compression noted in the single panel beam tests.

9.3.2 Analysis and Strength Prediction with 3-D Orthotropic Element

In the analysis of the box beam using the 3-D element there was no difficulty in accurately representing the beam, unlike the 2-D analysis where idealization had to be made. Due to the symmetry, only half of the beam section and length was meshed. The elements had a general aspect ratio of $.35 \leq h/L \leq .86$ with smaller aspect ratios in the area of detail interest, i.e. the restrained end for the stressing purpose and the free end for checking the failure deflection. Moreover the 'L' shaped adhesive joint at each corner of the box were ignored and the connections were provided simply by joining the nodal points along the length of the beam, see Fig. 9.12. The failure load was applied to the facing laminate of the side panel as a uniformly distributed load over 25.4mm length which was appropriate since the stiffness of the side panel was considerably greater than that of the top panel, see Fig. 9.13 for failure deflection. Furthermore it might be argued that the load spreader (steel plate) used in the actual test exerts the distributed load to the facings of the side panel mainly because of the negligible core stiffnesses in the X-Y plane. This was demonstrated by the application of the pressure load to the side panel (core and facings) over 25.4mm length. This gave rise to the deflection locally (see Fig.

9.14) causing buckling of the facings in an outward mode. This did not cause failure and hence was ignored.

The vital area of the mesh (i.e. the constrained end) is given in Fig. 9.15 where the position letters show the high stressed area of the beam for both top and bottom panels. Note that although these letters are the same as that of the 2-D analysis of previous section, they are different in terms of geometry. The values of the Tsai-Hill Factor (R.F.) together with the predicted strengths are given in Table 9.8. The values of R.F. were then plotted against the width of the beam at the given positions for the 0° ply in the upper facing of the top panel, see Fig. 9.16. It is important to note that the failure distributions both in 2-D and 3-D meshes are quite similar. The irregularity which occurs at the corner joint between the top and side panels was due to the fact that the facing elements were joined physically at an angle (right angle) in positions 'E' and 'G', where stress averaging does not take place hence the larger stress concentrations which are not representative. Therefore the prediction was based on the average strength (R.F.) across the width of the beam. The 90° ply of the bottom panel in the lower facing fails first by about 3% overestimation, this does not constitute the overall beam failure for the same reason given in the 2-D analysis. The next highly stressed ply is the 0° ply of the top panel in the upper facing failing at 16128 N which is an overestimation of 6.8%. This is followed by the failure of the 90° ply at 16282 N (overestimation by 7.6%). The failure of the top panel (and hence the beam) differs to that of the 2-D analysis where both plies fail simultaneously, by only 0.8% which is a small difference allowing for all the possible errors.

9.3.3 Comparison of Test and Theory (Box Beam)

In the last few sections of this chapter, methods of predicting beam failure strengths were attempted. The predictions for the single panel bending with various core thicknesses and facing ply orientations were largely successful when compared to the actual tests values. The accuracy of the methods in these simple cases were thought to hinge mainly on the material data (especially compressive strength) and the tolerance to which these panels were manufactured. Nevertheless it did show that the analysis predicts similar behaviour to that of the tests. In the analysis of the box beam which was more of a structure than the single panel both the out of plane and the in plane deformation were investigated by the two proposed methods of analysis. Fig. 9.17 shows the comparison of deflection between test and various methods of analysis with the simple theory of bending giving the largest difference in the load/deflection slope when compared to the elastic test slope. Although the 2-D analysis gave the closest predicted failure deflection, it has done so by geometrical idealization of the structure which was necessary in creating a 2-D mesh of a 3-D structure. The 3-D analysis gave the most representative prediction of the deflection within the linear elastic range as expected.

In predicting the strength of the box beam, the postulated compressive strength values of Fig. 5.6(c) gave the closest predictions by all the methods considered, the comparisons of which are given in the following table.

EXPERIMENTAL FAILURE LOAD P_f(N)	S.T.B. PREDICTED FAILURE LOAD (N)	% DIFF	2D F.E.A. PREDICTED FAILURE LOAD (N)	% DIFF	3D F.E.A. PREDICTED FAILURE LOAD (N)	% DIFF
15034	14381	-4.5	14798	1.6	16128	6.8

The close prediction of failure deflection and the strength by the 2-D analysis was thought to be because of the idealization of the structure as explained previously and therefore indicating that the method can be used for the deformation of a large structure for the interface loads as well as the strength prediction of the plies which are most likely to fail first. This will provide adequate information for the stress analyst to tailor the precise reinforcement needed in order to maintain the integrity of the structure and therefore utilizing to the full the special characteristics of the fibre composites. In so far as the analysis of the joint system is concerned, the 3-D method predicts the behaviour of the composite sandwich panel close enough within the linear elastic theory so that it can be used effectively in order to predict the static failure strength of the joint system provided that the facing elements of the sandwich are not joined together directly, and provided that very large plastic deformations do not occur, which they did not.

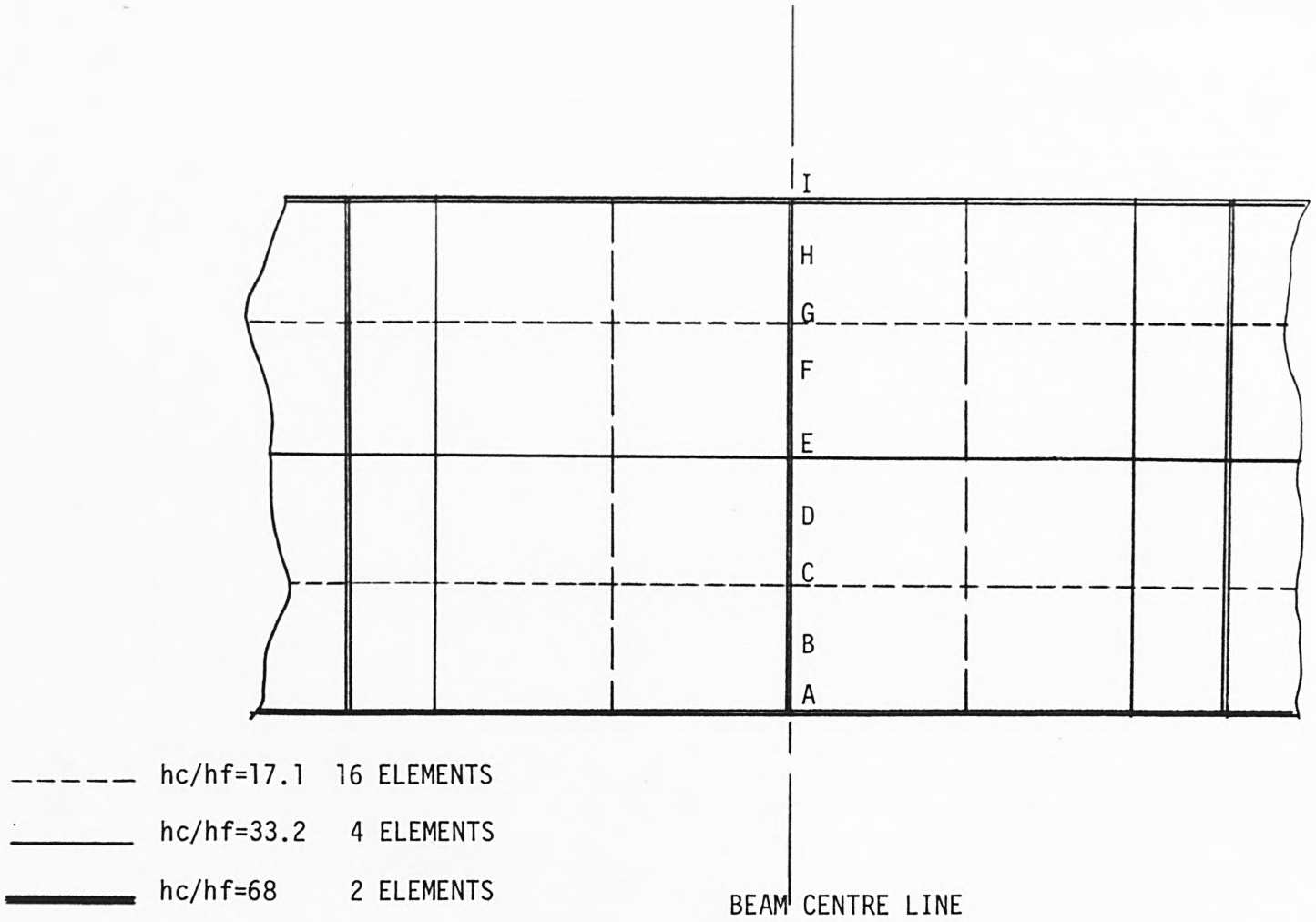

FIG 9.1

FINITE ELEMENT MESH FOR THE FLEXURAL SANDWICH BEAM TESTS.

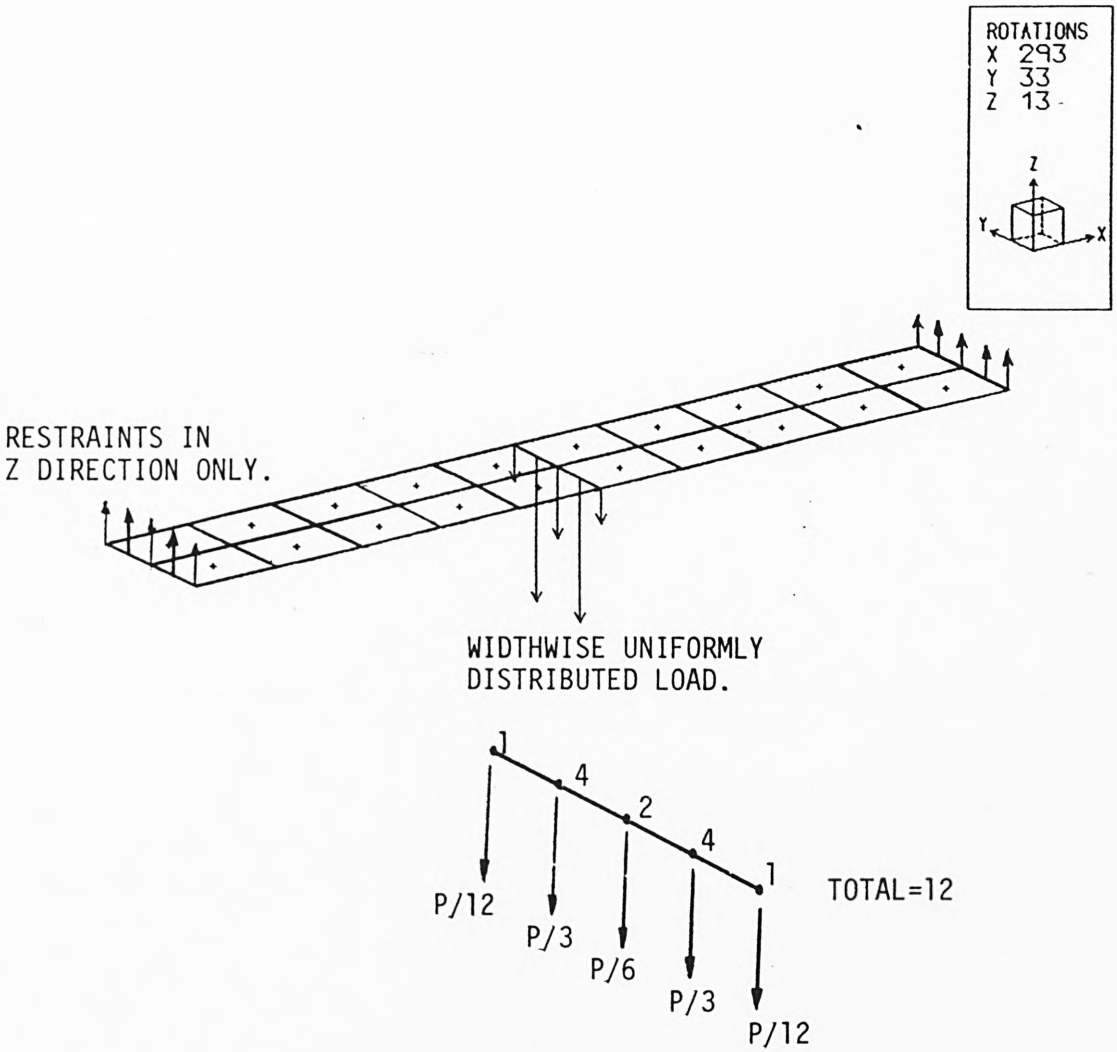

EQUIVALENT DISTRIBUTED LOAD IN PAFEC.

FIG 9.2

FLEXURAL BENDING OF THE STANDARD COMPOSITE SANDWICH MESH.

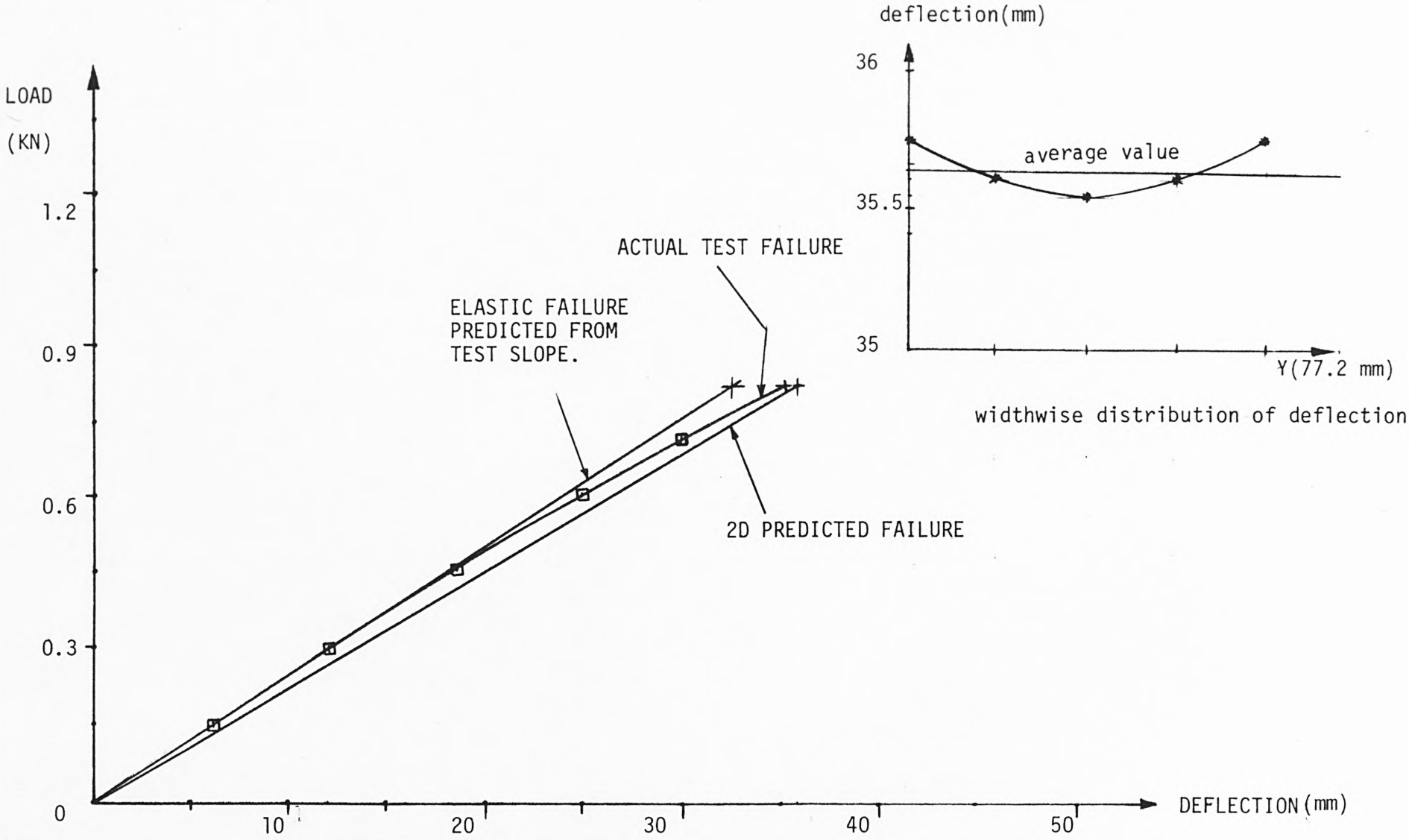

FIG 9.3 COMPARISON OF THEORY (2D) AND TEST DEFLECTION FOR STANDARD SANDWICH COMPOSITE.

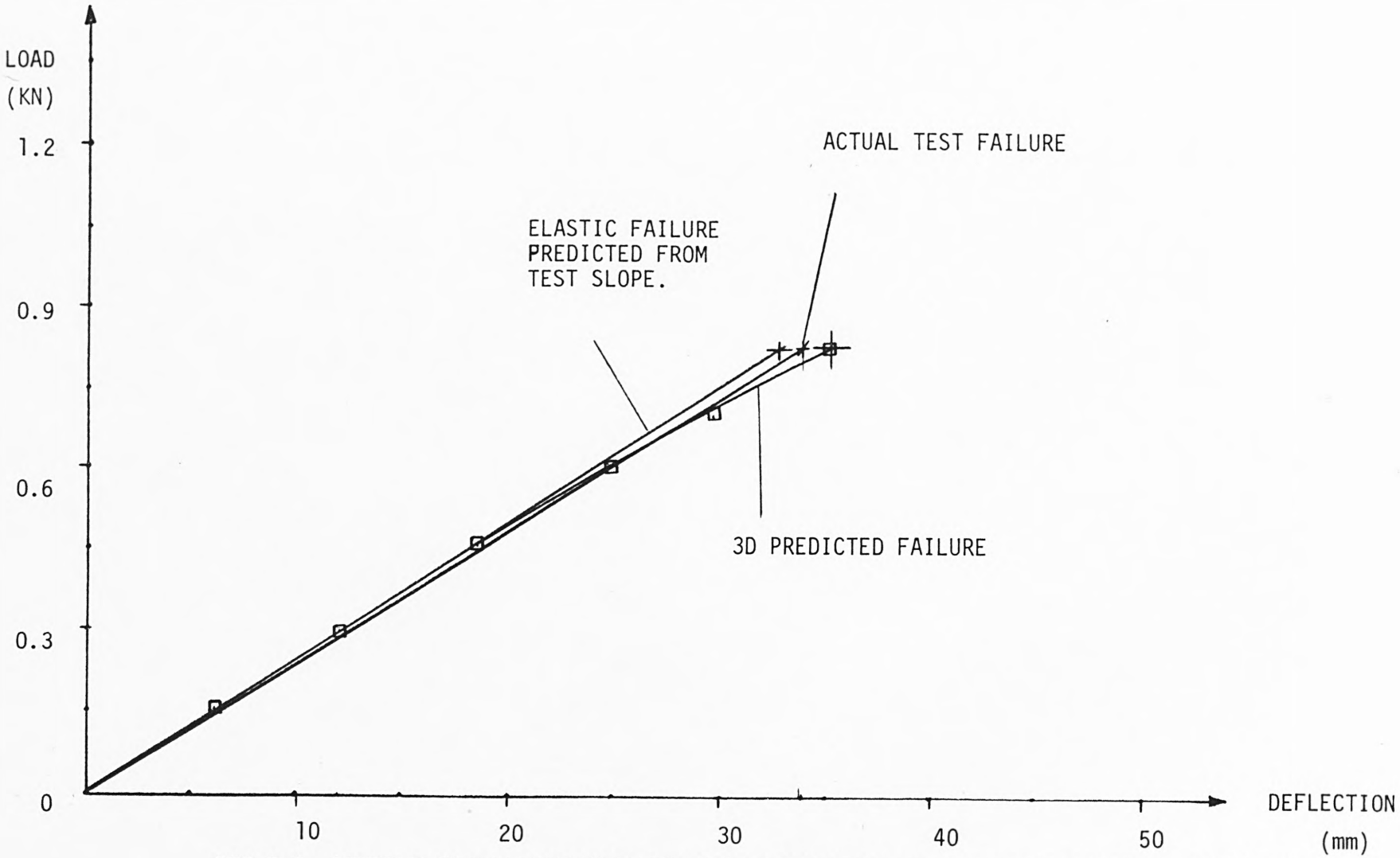

FIG 9.4 COMPARISON OF THEORY(3D) AND TEST DEFLECTION FOR STANDARD SANDWICH COMPOSITE.

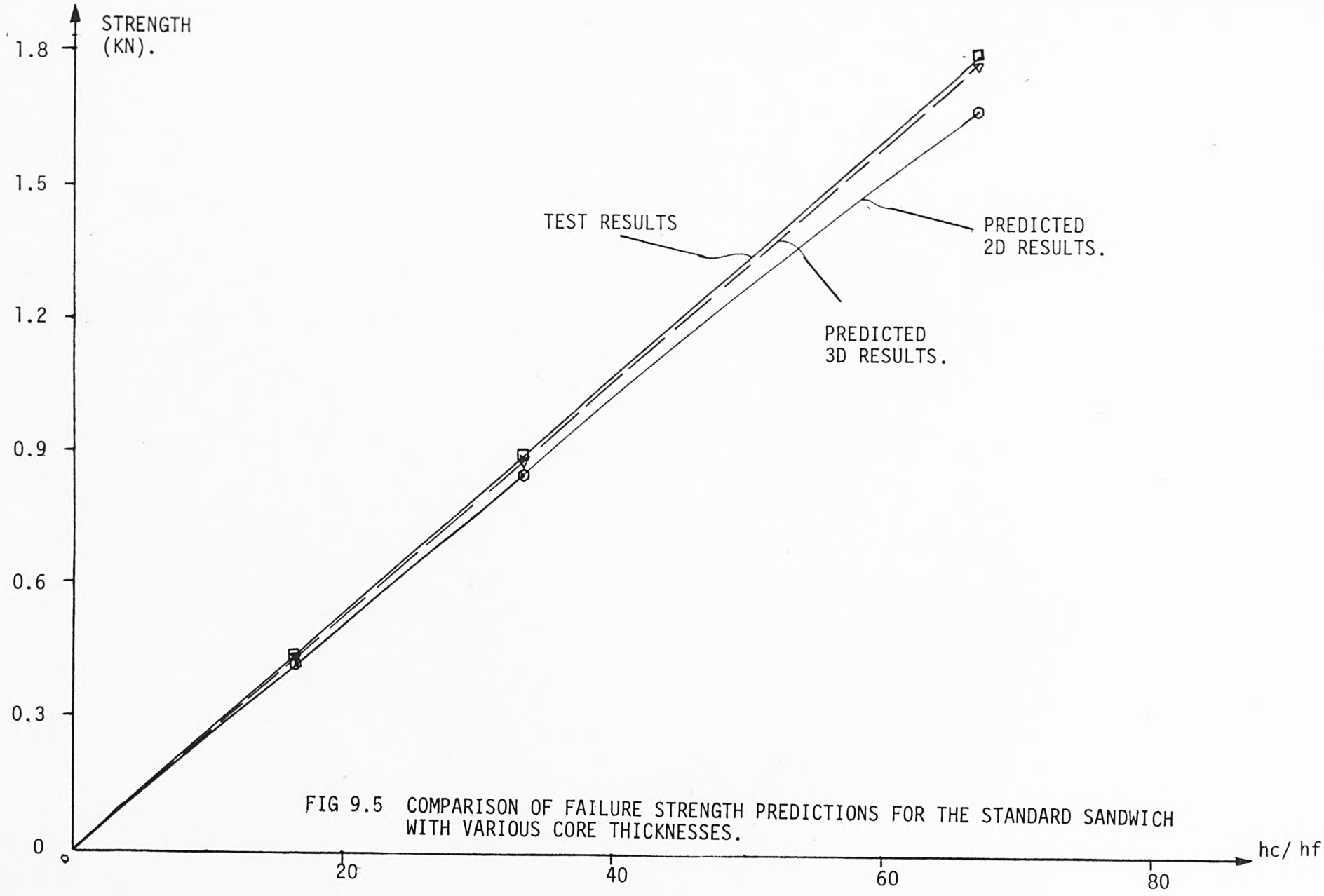

FIG 9.5 COMPARISON OF FAILURE STRENGTH PREDICTIONS FOR THE STANDARD SANDWICH WITH VARIOUS CORE THICKNESSES.

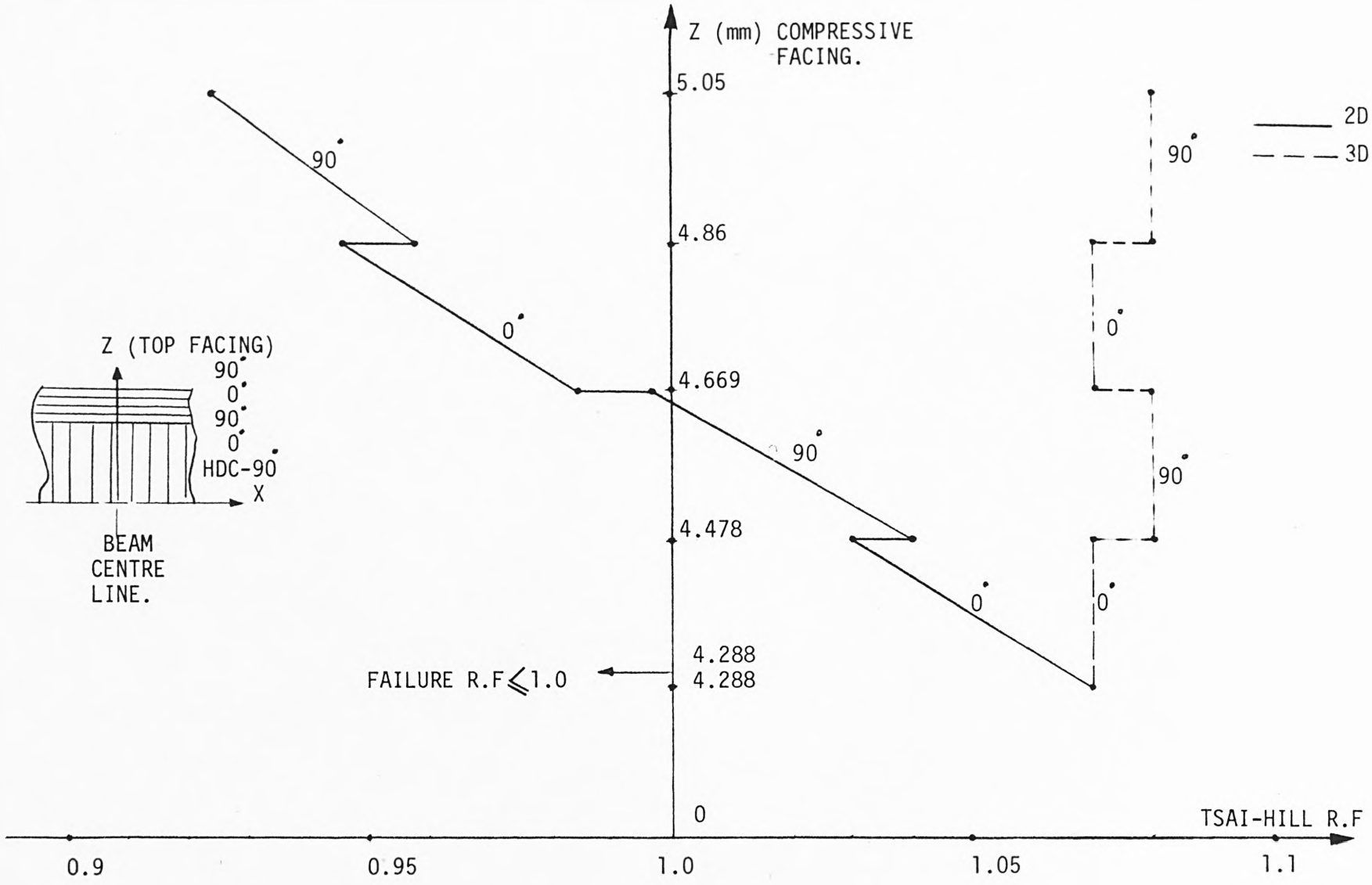

FIG 9.6 TSAI-HILL RESERVE FACTOR FOR THE CROSS PLY HIGH DENSITY CORE BEAM IN THE TOP FACING.

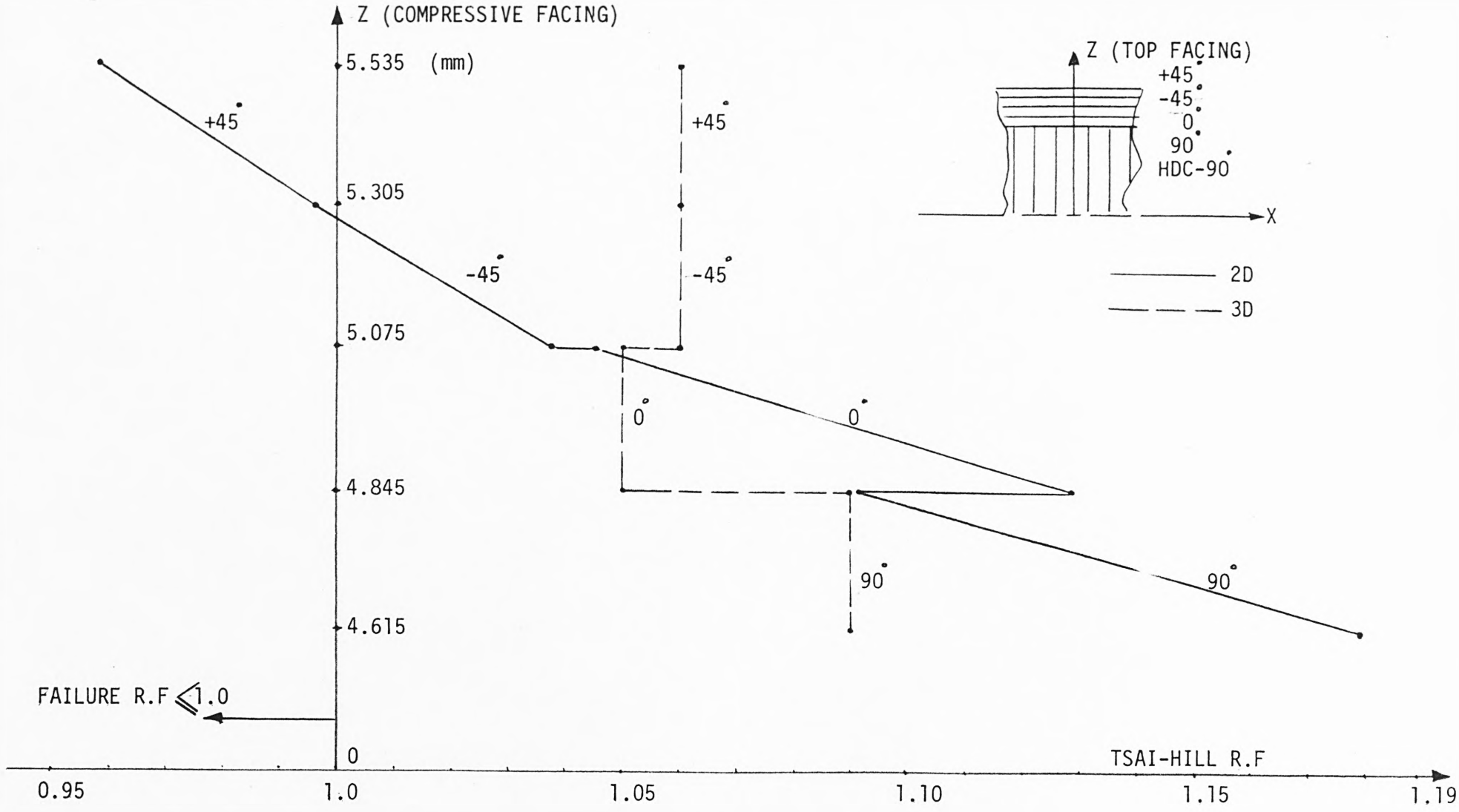

FIG 9.7 TSAI-HILL RESERVE FACTOR FOR THE MULTIDIRECTIONAL PLY HIGH DENSITY CORE BEAM IN THE TOP FACING.

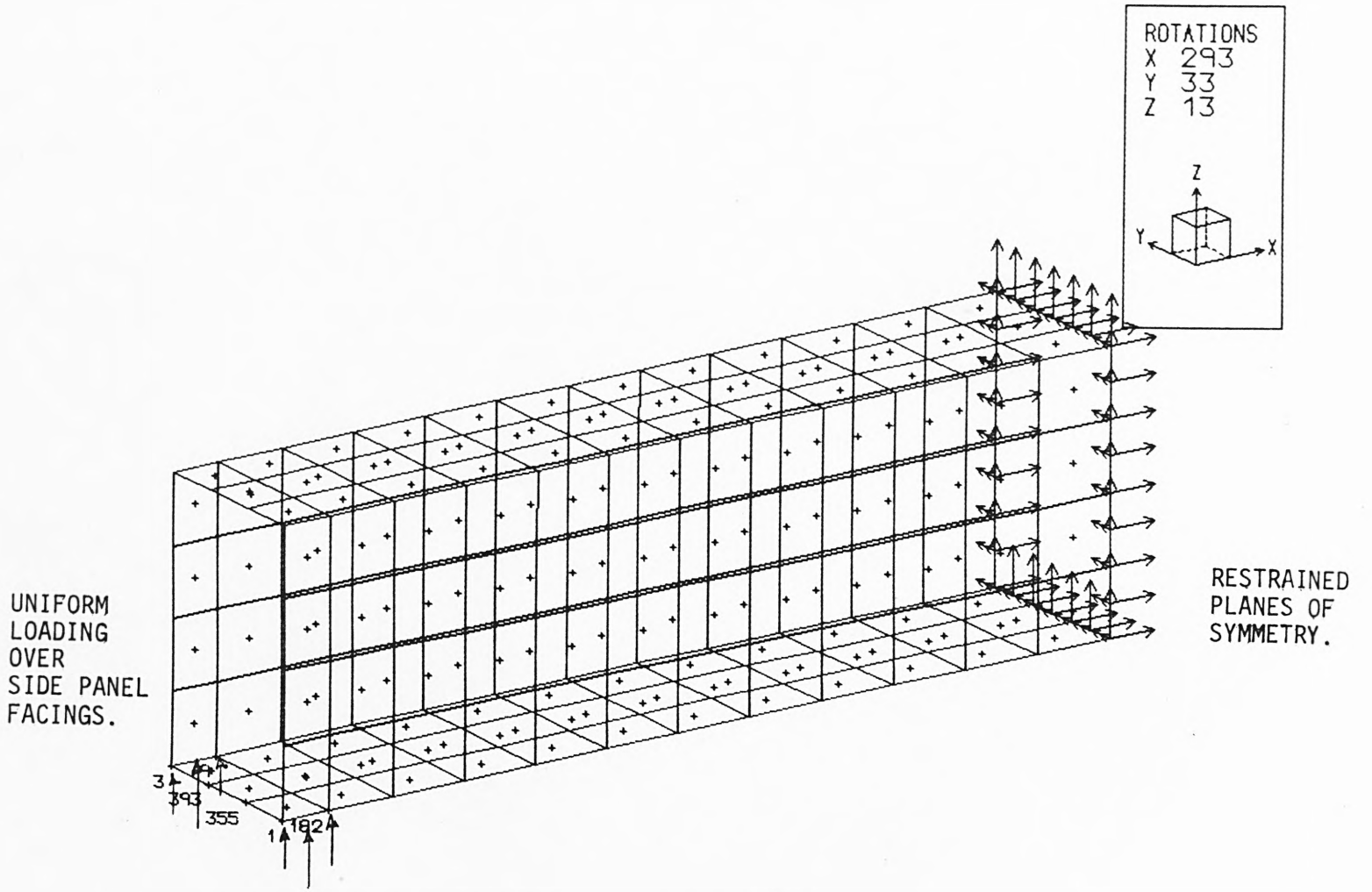

FIG 9.8 IDEALIZED 2D FINITE ELEMENT MESH OF THE BOX BEAM.

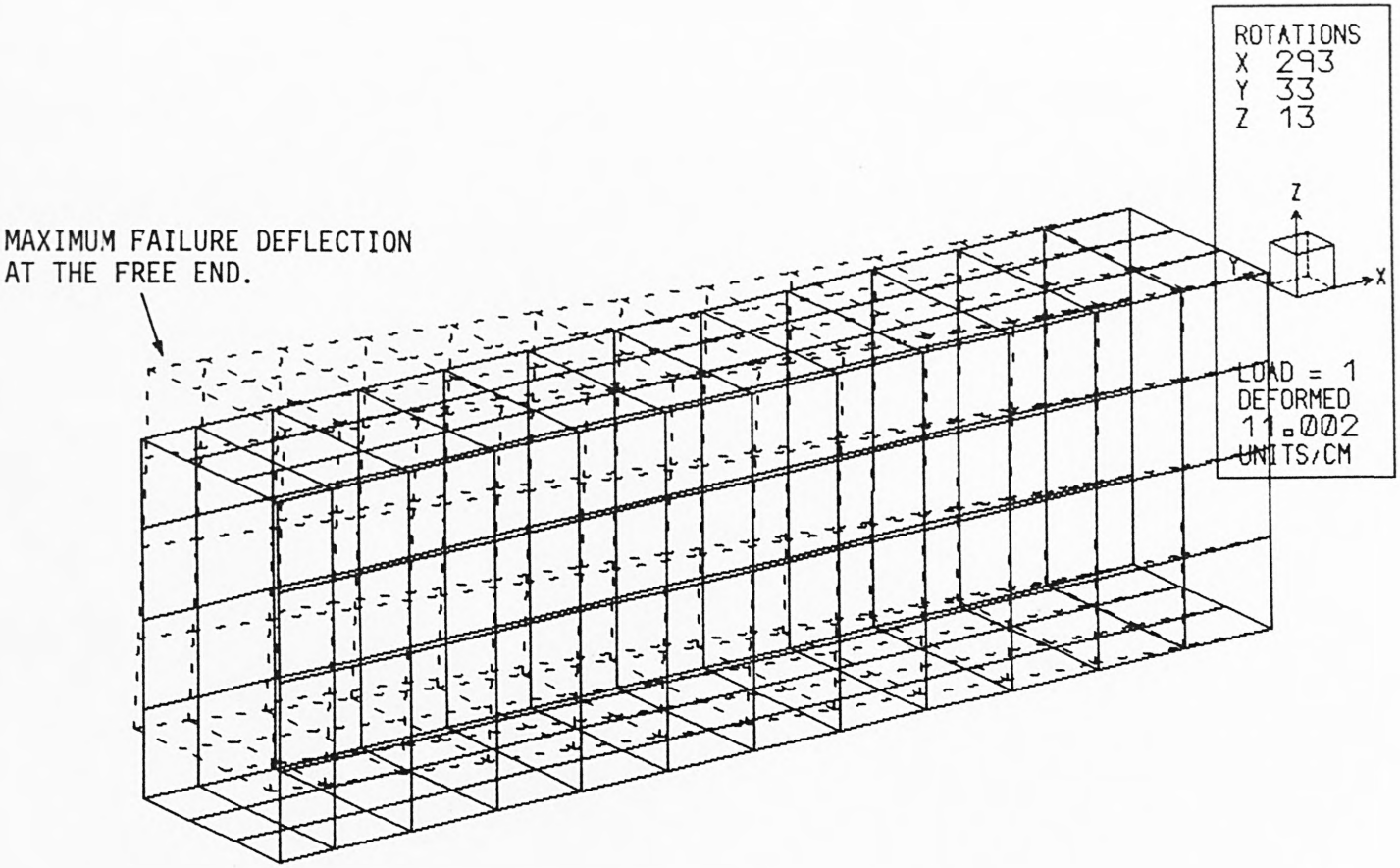

FIG 9.9 DEFLECTED SHAPE OF THE BOX BEAM AT FAILURE (TEST) LOAD.

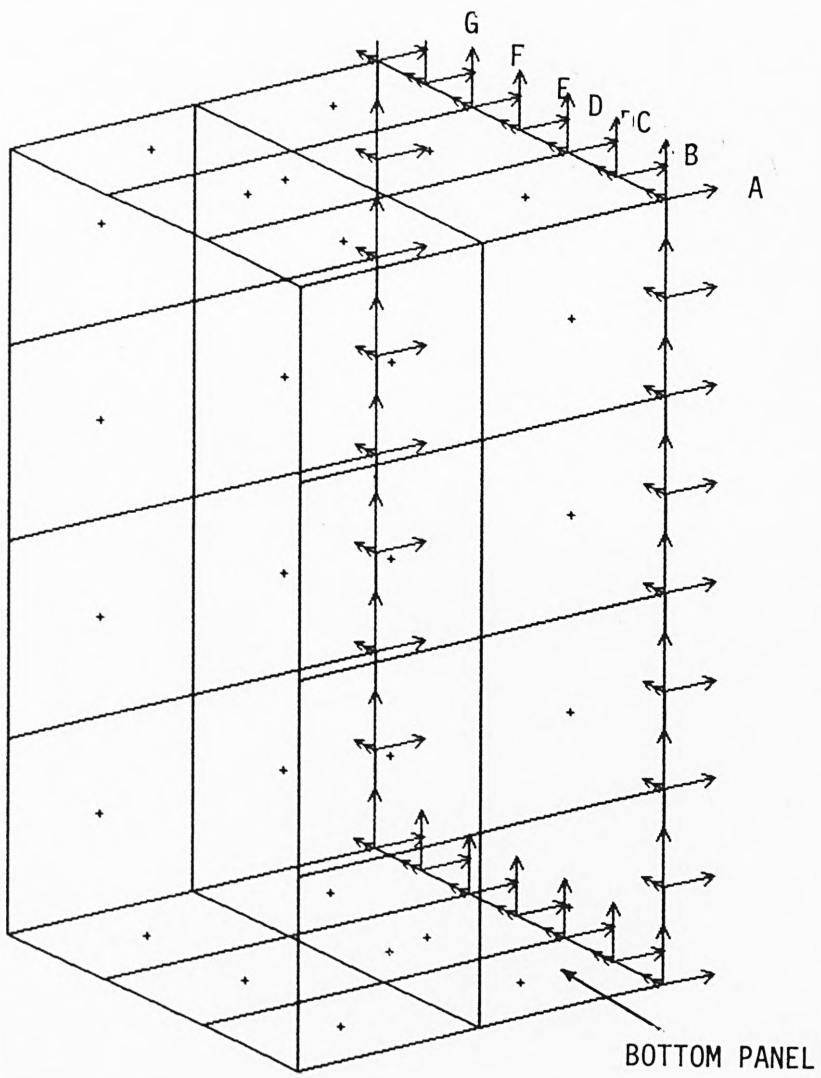

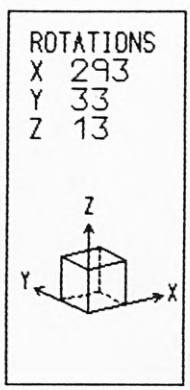

FIG 9.10 VITAL AREA OF THE MESH FOR THE BOX BEAM (2D)

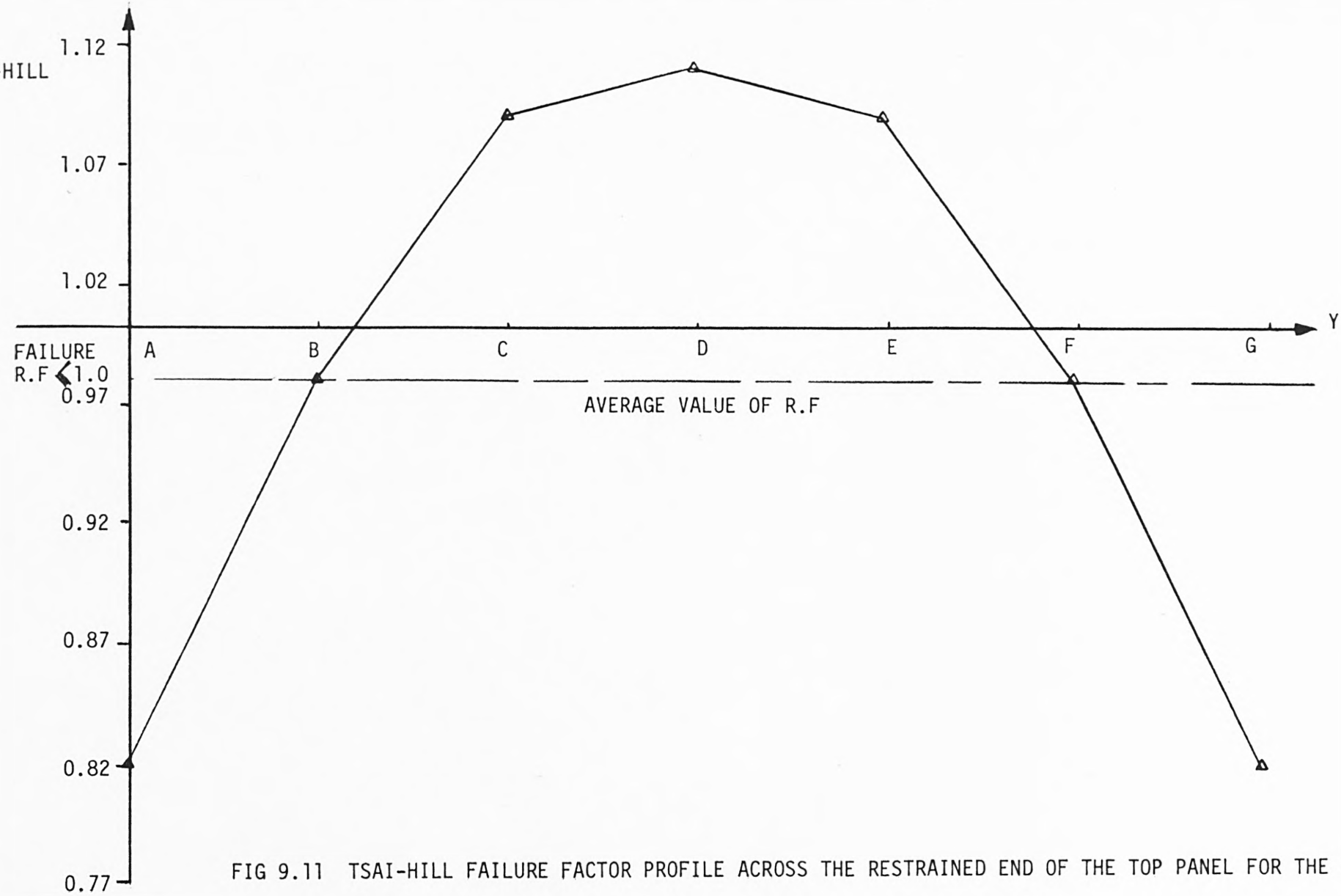

FIG 9.11 TSAI-HILL FAILURE FACTOR PROFILE ACROSS THE RESTRAINED END OF THE TOP PANEL FOR THE 0 PLY.

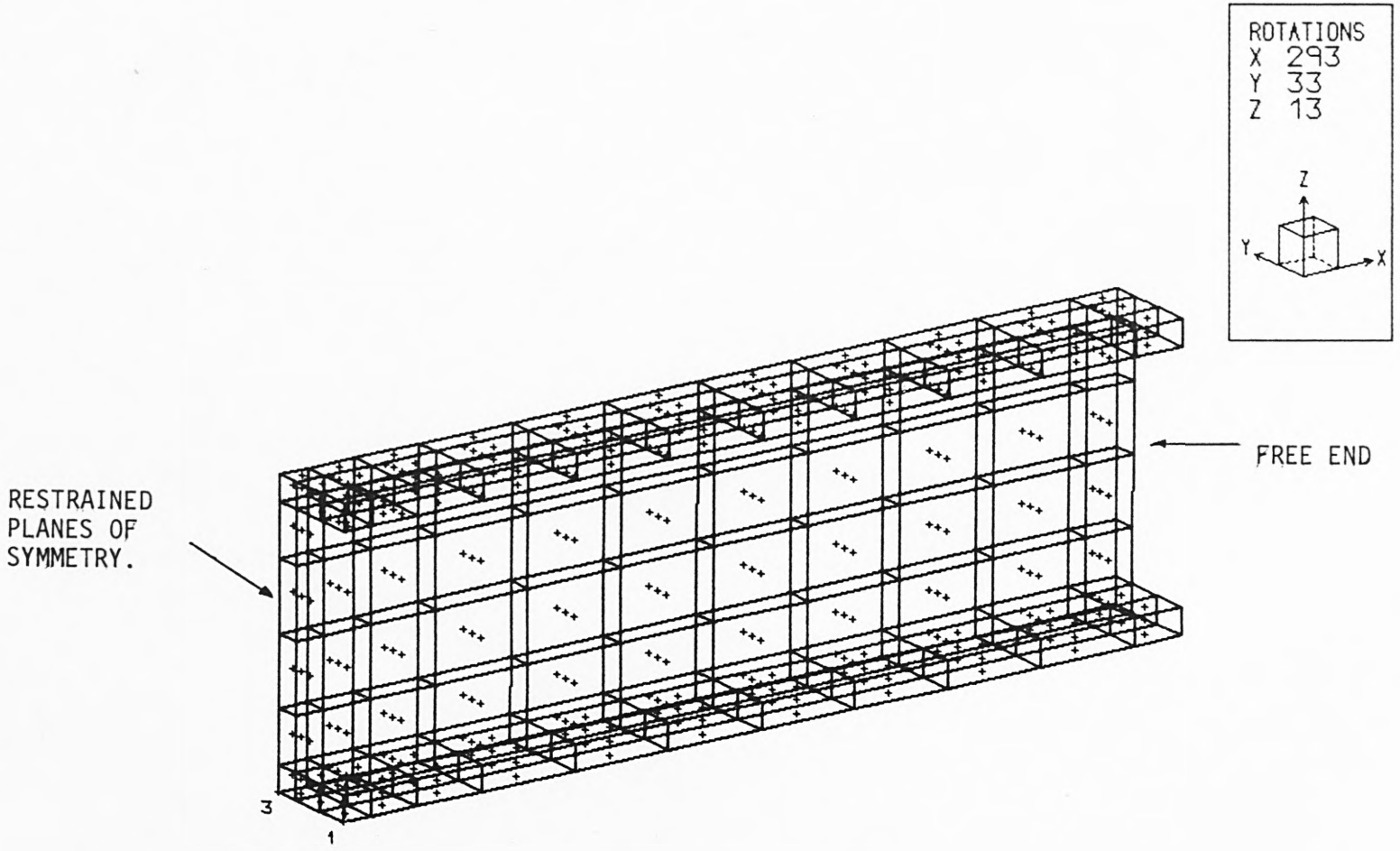

FIG 9.12 THREE-DIMENSIONAL FINITE ELEMENT MESH OF THE BOX BEAM

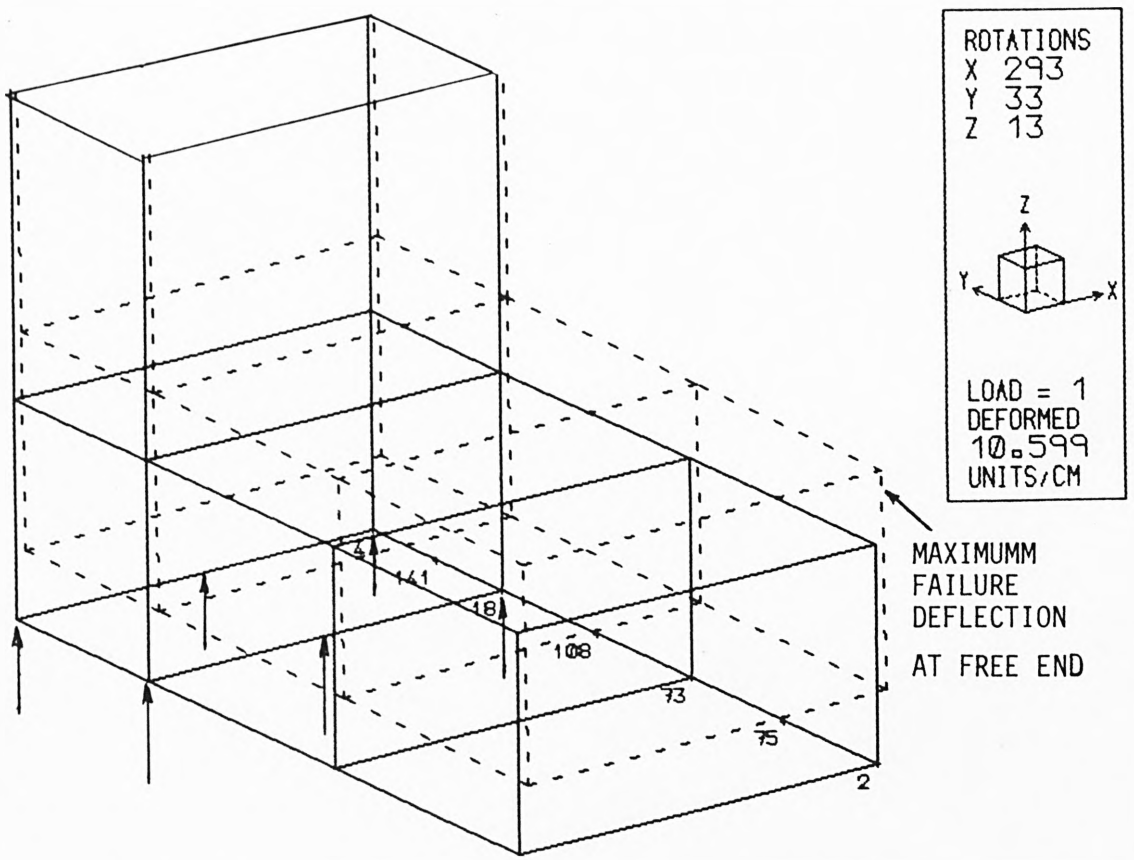

FIG 9.13 UNIFORM DEFLECTION OF THE 3D BOX BEAM FACING LOADING.

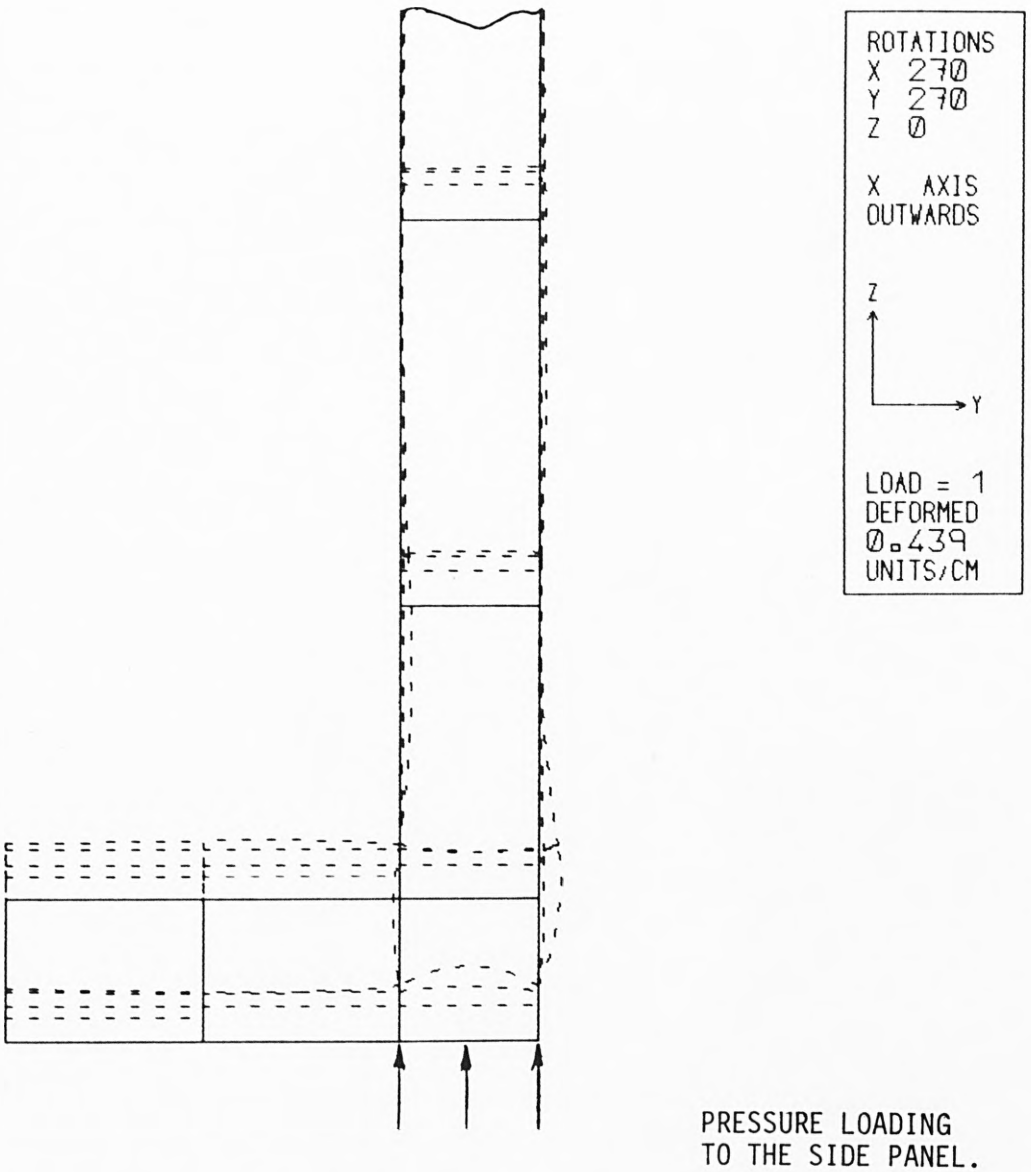

FIG 9.14 LOCAL DEFORMATION DUE TO THE PRESSURE LOADING AT THE FREE END.

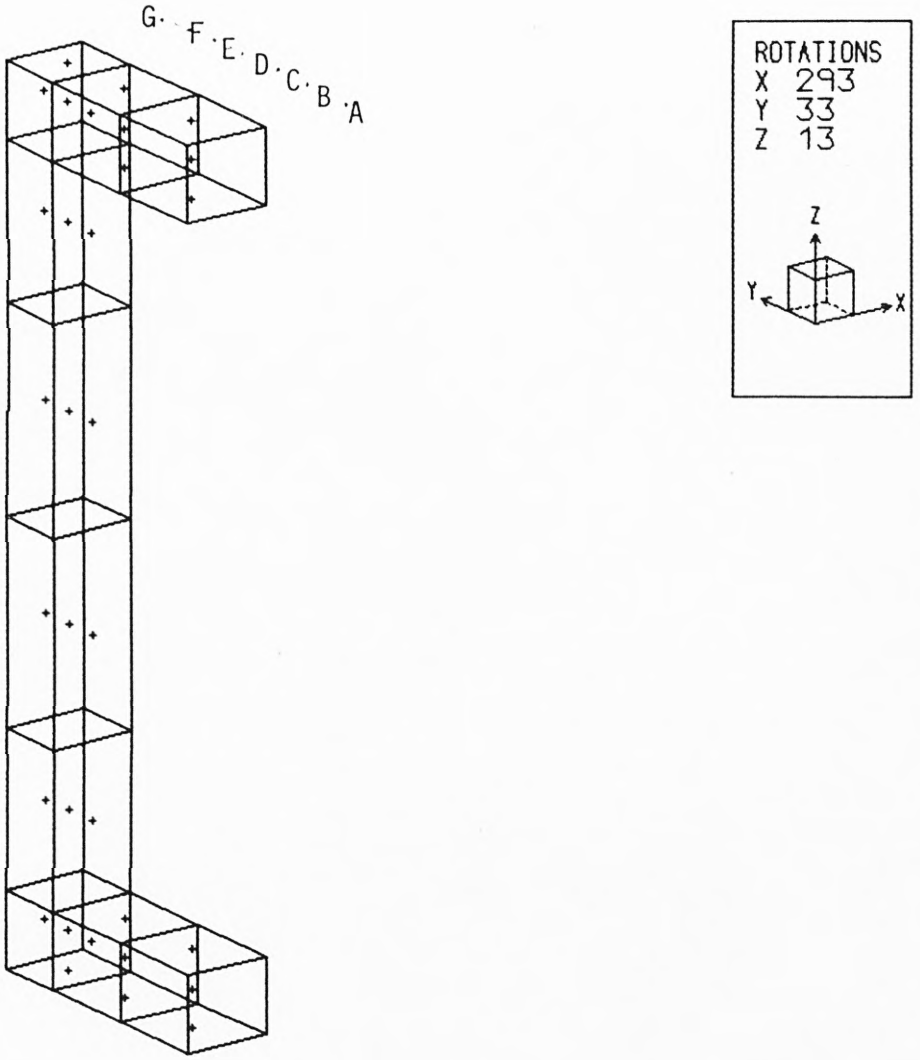

FIG 9.15 VITAL AREA OF THE BOX BEAM AT RESTRAINED END.

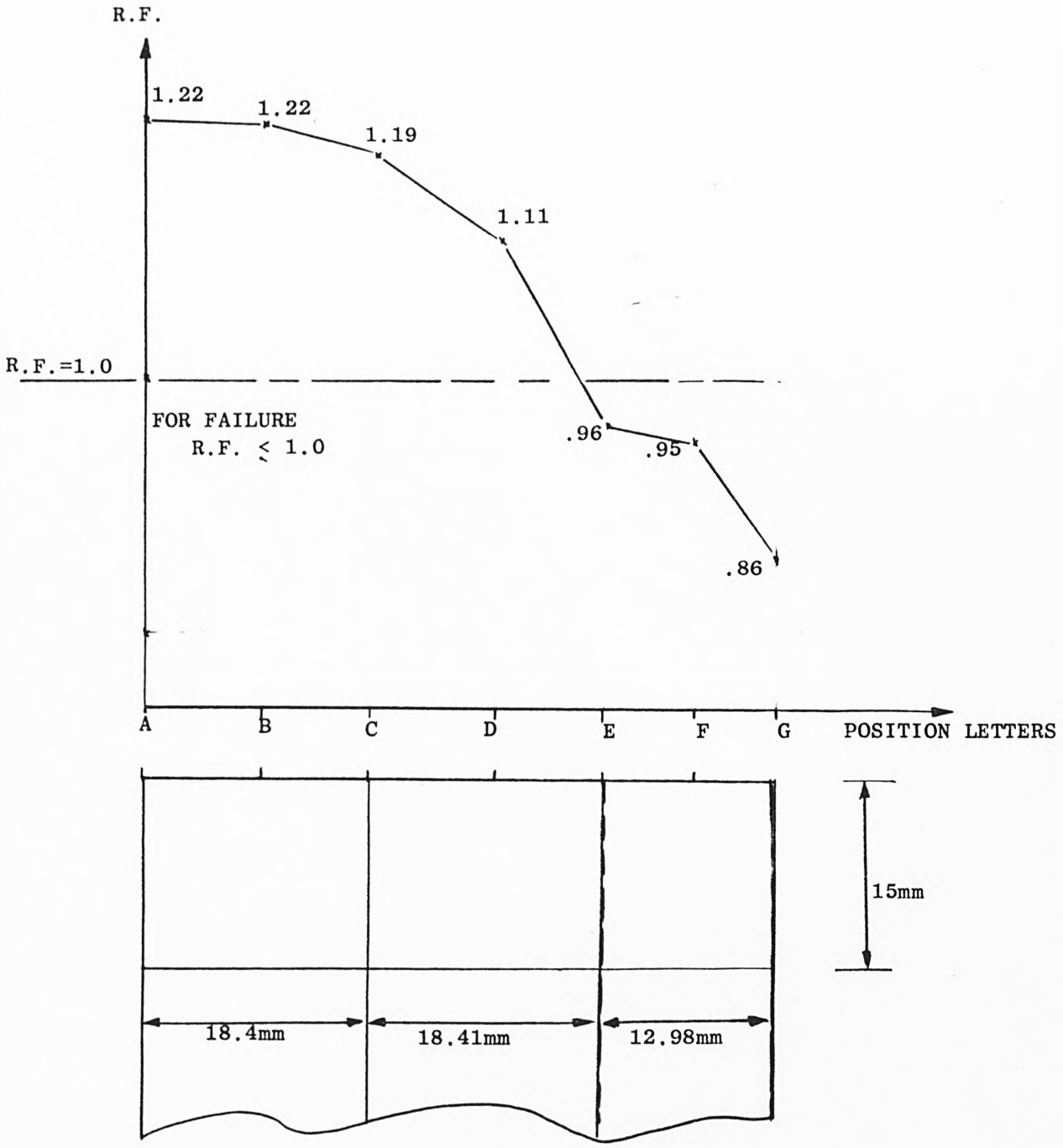

FIG. 9.16 TSAI-HILL FACTOR ACROSS THE WIDTH OF THE BEAM FOR THE 0° PLY OF THE UPPER FACING (TOP PANEL)

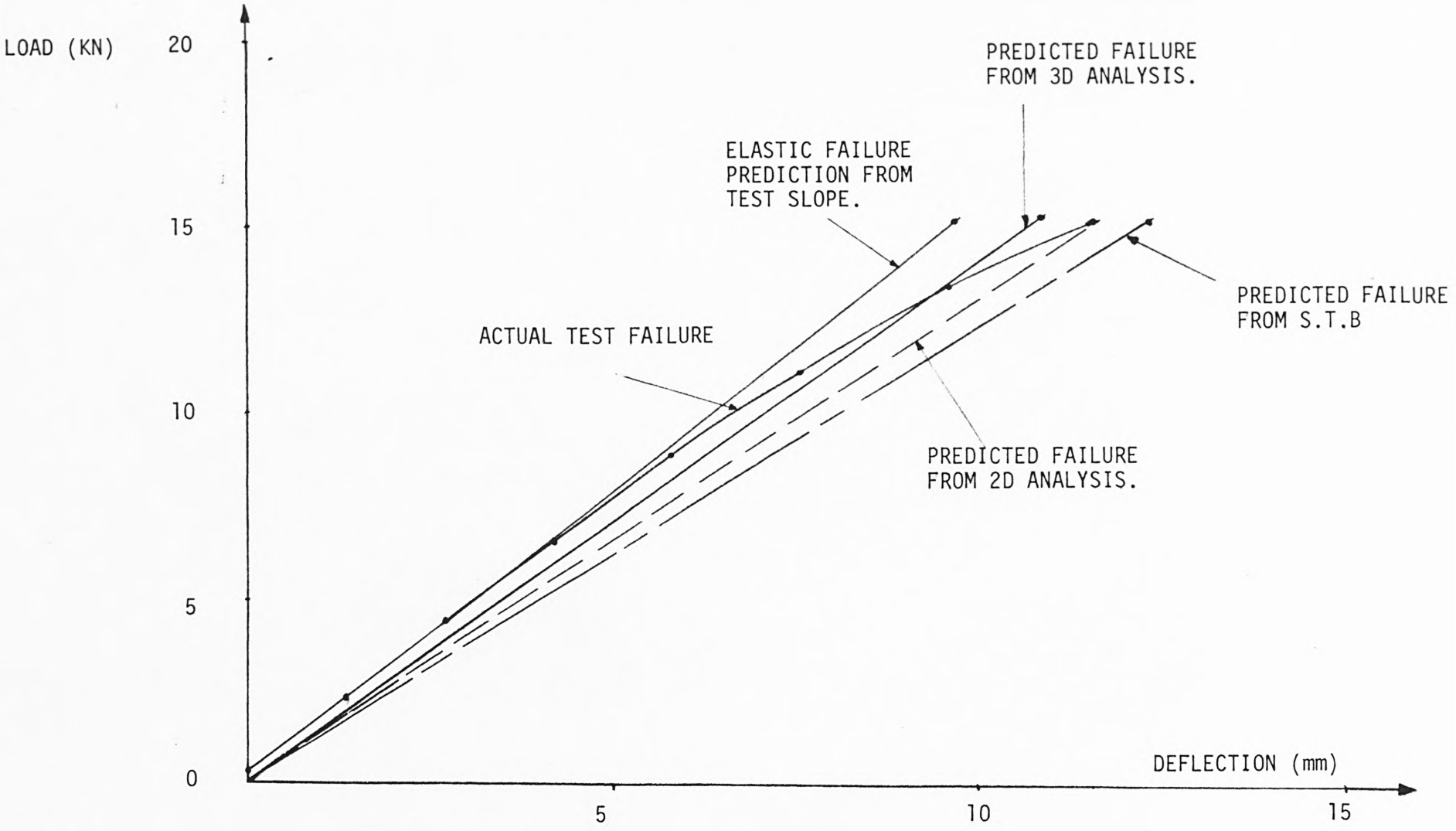

FIG 9.17 COMPARISON OF DEFLECTION BETWEEN TEST AND VARIOUS METHODS OF ANALYSIS.

REFERENCE TEST TABLE	PLY STACKING SEQUENCE	$\frac{h_c}{h_f}$	δ_E mm (ELASTIC) AT P = 150N		$\frac{TH-T}{T}$ x 100 % DIFFERENCE	δ_F (mm (FAILURE) AT P_f		$\frac{TH-T}{TH}$ x 100 % DIFFERENCE
			THEORY	TEST		THEORY	TEST	
6.1(a)	$(\dot{0}/\dot{90}\text{-C}\dot{0})_s$	67.0	1.73	1.62	6.0	20.41	19.24	5.7
6.1(b)	$(\dot{0}/\dot{90}\text{-C}\dot{0})_s$	16.27	21.7	20.4	6.0	63.6	69.5	-9.3
6.1(c)	$(\dot{0}/\dot{90}\text{-C}\dot{0})_s$	33.2	6.02	5.84	3.0	35.6	36.33	-2.0
6.2	$(\dot{90}/\dot{0}/\dot{90}/\dot{0}\text{-HDC90})_s$	11.25	1.66	1.58	4.8	13.26	12.9	2.7
6.2	$(+\dot{45}/-\dot{45}/\dot{0}/\dot{90}\text{-HDC90})_s$	10.03	1.62	1.57	3.08	16.63	15.64	5.9

TABLE 9.1 COMPARISON OF DEFLECTIONS IN TESTS AND F.E.A. (2D)

All failures were compressive failures in the facings, both in tests and predictions

FLEXURAL SANDWICH BEAM TEST STRENGTH = 886.4N

(Compressive Failure of Facing)

POSITION LETTERS (Fig.9.1)	PLY ANGLE	COMPRESSIVE FACING		TENSILE FACING	
		R.F.	PREDICTED STRENGTH (N)	R.F.	PREDICTED STRENGTH (N)
A	0°	.956	847.4	3.18	2818.7
	90°	.994	881.1	.97	859.8
C	0°	.956	847.4	3.1	2747.8
	90°	.996	882.8	.949	841.2
E	0°	.951	843	3.07	2721.2
	90°	.994	881.1	.944	836.7
G	0°	.952	844	3.07	2721.2
	90°	.994	881.1	.945	837.6
I	0°	.956	847.4	3.1	2747.8
	90°	.996	882.8	.949	841.2
AVERAGE VALUE	0°	.954	845.6		
	90°	.995	882.0		

STRENGTH PREDICTION OF $(0^\circ/90^\circ\text{-}C0^\circ)_s$ BEAM $\frac{h_c}{h_f} = 33.2$

REFERENCE TEST TABLE OF 6.1(c)

TABLE 9.2

BEAM SPAN = 508mm MATERIAL STRENGTH FOR COMPRESSIVE FACING
σ_{1UC} = 440 MPa, σ_{2UC} = 116 MPa

PLY STACKING SEQUENCE	REF. TEST TABLE	$\frac{h_c}{h_f}$	PLY ANGLE	TSAI-HILL R.F. VALUE	PREDICTED STRENGTH (N)
$(0/90-C0)_s$	6.1(a)	67	0°	.944	1670.6
			90°	.972	1720.1
	6.1(b)	16.3	0°	.972	426.4
			90°	1.042	458.0
	6.1(c)	33.2	0°	.954	845.6
			90°	.955	882.0

BEAM SPAN = 254 MPa σ_{1UC} = 641 MPa, σ_{2UC} = 161 MPa
$\frac{h_c}{h_f}$ = 11.2

PLY STACKING SEQUENCE	POSITION OF PLY K	PLY ANGLE	TSAI-HILL R.F. VALUE		PREDICTED STRENGTH	
			UPPER	LOWER	UPPER(N)	LOWER(N)
REFERENCE TABLE 6.2	COMPRESSIVE FACING	90°	.922	.958	1102.3	1145.4
		0°	.946	.985	1131.0	1177.6
		90°	.997	1.04	1192	1243.4
$(90/0/90/0-HDC90)_s$		0°	1.03	1.07	1231.4	1279
		HDC90°				
	TENSILE FACING	0°	3.44	3.30	4113	3945
		90°	.99	.95	1183.6	1135.8
		0°	3.16	3.04	3778	3634.6
		90°	.912	.878	1090.4	1049.7
$(+45/-45/0/90-HDC90)_s$	COMPRESSIVE FACING	45°	.958	.996	1472.2	1530.6
		-45°	.996	1.038	1530.6	1595.2
		0°	1.046	1.091	1607.5	1676.6
		90°	1.129	1.179	1735	1811.9
		HDC90°				
REFERENCE TABLE 6.2	TENSILE FACING	90°	.792	.76	1217.1	1167.9
		0°	2.85	2.73	4379.9	4195.4
		-45°	.969	.931	1489.1	1430.7
		45°	.93	.895	1429	1375.4

TABLE 9.3 STRENGTH PREDICTIONS OF MULTIDIRECTIONAL SANDWICH BEAMS

TEST REFERENCE TABLE	PLY STACKING SEQUENCE	$\frac{h_c}{h_f}$	TEST δ_E(mm) AT P=150N	F.E.A. δ(mm) AT P = 150N			
				CENTRALLY UNIFORM	% DIFF.	PRESSURE	% DIFF.
6.1(a)	$(\dot{0}/\dot{90}\text{-}C\dot{0})_s$	67.0	1.62	1.74	6.9	1.68	3.6
6.1(b)	$(\dot{0}/\dot{90}\text{-}C\dot{0})_s$	16.27	20.4	21.27	4.1	21.1	3.3
6.1(c)	$(\dot{0}/\dot{90}\text{-}C\dot{0})_s$	33.2	5.84	5.9	1.0	5.73	-1.9
6.2	$(\dot{90}/\dot{0}/\dot{90}/\dot{0}\text{-}HDC\dot{90})_s$	11.25	1.58	1.79	11.7	1.70	7.0
6.2	$(\dot{45}/\text{-}\dot{45}/\dot{0}/\dot{90}\text{-}HDC\dot{90})_s$	11.07	1.57	2.13	26	1.8	12.7

TABLE 9.4 COMPARISON OF DEFLECTIONS IN TESTS AND F.E.A. (3D)

SPAN = 508mm COMPRESSIVE FACING				σ_{1UC} = 440 MPa σ_{2UC} = 116 MPa
PLY STACKING SEQUENCE	$\frac{h_c}{h_f}$	PLY ANGLE	TSAI-HILL R.F. VALUE	PREDICTED STRENGTH
$(0/90\text{-}C0)_s$	67	0 90	1.01 1.03	1787.4 1822.8
	16.27	0 90	1.01 1.03	444.0 452.8
	33.2	0 90	.99 1.0	877.5 886.4
SPAN = 254mm COMPRESSIVE FACING				σ_{1UC} = 641 MPa σ_{2UC} = 161 MPa
$(90/0/90/0\text{-}HDC90)_s$	11.25	90 0 90 0	1.08 1.07 1.08 1.07	1291.12 1279.3 1291.2 1279.3
$(45/-45/0/90\text{-}HDC90)_s$	11.07	+45 -45 0 90	1.06 1.06 1.05 1.09	1629.0 1629.0 1613.6 1675.1

TABLE 9.5 STRENGTH PREDICTIONS OF VARIOUS SANDWICH BEAMS (3D)

REFERENCE TEST TABLE	PLY STACKING SEQUENCE	TEST FAILURE STRENGTH(N)	2D-PREDICTED FAILURE STRENGTH (N)	% OF DIFF.	3D-PREDICTED FAILURE STRENGTH (N)	% OF DIFF.
6.1(a)	$(0/90\text{-}C0)_s$	1769.7	1670.6	-5.9	1787.4	1.0
6.1(b)		439.6	426.4	-3.0	444	1.0
6.1(c)		886.4	845.6	-4.8	877.5	-1.0
6.2	$(90/0/90/0\text{-}HDC90)_s$	1195.6	1131.0	-5.7	1279.3	6.5
6.2	$(45/-45/0/90\text{-}HDC90)_s$	1536.8	1472.2	-4.4	1613.6	4.7

TABLE 9.6 COMPARISON OF BEAM STRENGTH PREDICTIONS BETWEEN TESTS AND THEORY

BOX-BEAM TEST FAILURE STRENGTH = 15034N, σ_{1UC}= 440 MPa, σ_{2UC}= 116 MPa

σ_{1UT}= 1700MPa, σ_{2UT}= 111 MPa

POSITION LETTERS	PLY ANGLE	TOP PANEL (UPPER FACING)		BOTTOM PANEL (LOWER FACING)	
		R.F.	PREDICTED (N) STRENGTH	R.F.	PREDICTED (N) STRENGTH
A	90°	.82	12328	.79	11877
	0°	.82	12328	2.61	39239
B	90°	.98	14733	.94	14132
	0°	.98		3.01	45252
C	90°	1.09	16387	1.03	15485
	0°	1.09		3.14	47206
D	90°	1.11	16688	1.06	15936
	0°	1.11		3.27	49161
E	90°	1.09	16387	1.03	15485
	0°	1.09		3.14	47206
F	90°	.98	14733	.94	14132
	0°	.98		3.01	45252
G	90°	.82	12328	.79	11877
	0°	.82		2.61	39239
AVERAGE STRENGTH	90°		14798		14132
	0°		14798		

TABLE 9.7 PREDICTED STRENGTH OF BOX-BEAM USING 2-D ELEMENT

σ_{1UC} = 440 MPa σ_{2UC} = 116 MPa

σ_{1UT} = 1700 MPa σ_{2UT} = 111 MPa

BOX-BEAM TEST FAILURE STRENGTH = 15034N

POSITION LETTERS	PLY ANGLE	TOP PANEL (UPPER FACING)		BOTTOM PANEL (LOWER FACING)	
		R.F.	PREDICTED STRENGTH (MPa)	R.F.	PREDICTED STRENGTH (MPa)
A	90°	1.23	18492	1.17	17590
	0°	1.22	18341	3.59	53972
B	90°	1.23	18492	1.17	17590
	0°	1.22	18341	3.61	54273
C	90°	1.20	18041	1.14	17139
	0°	1.19	17890	3.54	53220
D	90°	1.12	16838	1.07	16086
	0°	1.11	16688	3.40	51115
E	90°	.97	14583	.92	13831
	0°	.96	14433	3.01	45252
F	90°	.96	14433	.92	13831
	0°	.95	14282	3.05	45954
G	90°	.87	13079	.83	12478
	0°	.86	12929	2.75	41343
AVERAGE RESULT	90°	1.083	16282	1.0314	15506
	0°	1.0728	16128	3.278	49281

PREDICTED STRENGTH OF BOX-BEAM USING 3-D ELEMENT

TABLE 9.8

10. FINITE ELEMENT ANALYSIS OF THE JOINT

10.1 INTRODUCTION

In the design chapter of this work (Section 2.2) the contributions of the sandwich element to the joint strength were identified and later in Chapter 4 they were investigated further by tests through the process of elimination in so far as the set design strengths were achieved in the three modes of loading. Much emphasis was made in the case of longitudinal shear, being the primary load case, in limiting the failure of the joint to the composite. Nevertheless, as the ratio of thickness in the facings laminate of slot panel to that of the local tongue section $(h_{fm}/h_{ft})_v$ increases for the purpose of future design, the discontinuity in the joint might well be in the adhesive part resulting in areas of high stress concentration which could lead to failure. To obtain the optimum strength of the joint it was considered that the ply angles as well as the core were important in providing stiffnesses and strengths in the directions most needed. All of these parameters were present in the case of longitudinal shear loading hence the subject of this and the next chapter was to investigate the behaviour of the joint by finite element stress analysis and to predict its static strength for the purpose of future design methods.

To understand the behaviour of the joint and to locate the possible areas of stress concentration, the reinforcement type '1b' of Fig. 3.1 and Fig. 3.4 was meshed with PAFEC 2-D six-noded triangular and eight-noded rectangular isoparametric isotropic thick shell elements with sandwich capability. The reason for using this particular type of element was mainly due to the existance of stress contour plotting facilities available within the PAFEC package. One quarter of the tongue

panel with one eighth of the slot panel of the test section Fig. 3.4 were modelled, allowing for division of the planes of symmetry, see Fig. 10.1. The stiffness matrix used for this analysis was based on an effective modulus of elasticity and Poisson's Ratio for the 0/90 facing which were obtained by test for the stress analysis of structures with cross-ply sandwich composites. The finite element mesh was constructed on the assumption that the only connection between the tongue and the slot panel was at the tip of the tongue to the inner facing of the slot panel which was represented by simply joining the elements at right angles through the nodal points. It was done in this way because there were no failures in the adhesive in the actual joint tests. This made the mesh geometrically slightly non-representative but, because this connection was the major load path of the joint system, it should provide some clue to where the stress concentration occurred.

The displaced shape of the tongue panel and the absolute stress contour are given in Figs. 10.2 and 10.3 respectively for the joint failure load. The magnitude of the stress contours were not correct because of the orthotropy effect of the facings and core and the fact that the stress averaging does not take place at the tongue and slot interface elements. However this result did show the presence of high tensile stresses in the tongue radius nearest to the load application and the presence of high compressive stresses in the other end as well as the stress concentrations at both ends of the tongue tip to slot interface. Putting a unit tensile stress on the tongue panel gave non-dimensionalised stresses or stress concentrations, (σ/σ_o). The maximum principal stress concentrations were plotted against the width of the joint at the root of the tongue and at the inner facing of the slot panel, these are shown in Fig. 10.4 and 10.5 respectively. The principal stresses were compressive at the far end of the tongue root where there

was a sudden change of distribution suggesting local buckling. They levelled off at a low tensile stress for much of the width before increasing sharply to a maximum tensile principal stress concentration at the near end. The pattern for the stress distribution in the inner slot facing was somewhat reverse to that of the tongue giving a maximum tensile stress at the far end of the joint and gradually decreasing the concentration to small values at the near end as expected.

This introductory analysis shows the complexity of the stress interaction involved in the joint system. To predict the strength of the joint the magnitude of these stresses should be representative to that of the test where the adhesive surrounds the whole section of the tongue and provides connections to the core and the slot facing therefore reducing the stress concentration at the root of the tongue and at the inner slot facing. It was for these reasons that a 3-D analysis was needed for the strength prediction of this type of joint since all the parameters involved could be represented as accurately as possible both geometrically and in material properties as demonstrated in the analysis of the box beam.

10.2 LONGITUDINAL SHEAR JOINT TYPE '1b' [90/0/90/0-C90].

The use of three dimensional elements discussed in Section 8.4 overcame the difficulties outlined with the 2-D element in the preceding section. The geometrical configuration of the joint including the bulk of adhesive and its importance in relation to the slot and tongue sandwich elements were thought to be a major factor in reducing the stress concentration in the tongue section and in the inner slot facing. The transfer of stresses to the composites of the joint were performed

via the adhesive system which was represented by the 3-D elements hence the absence of singularities in the strength prediction of the composite. The finite element mesh of the same joint (i.e. type 1b) was constructed using the test section of Fig. 4.3 and utilizing all planes of symmetry, see Fig. 10.6. The restriction on the number of elements that can be handled by the PAFEC package on the Hewlett-Packard computer, made it necessary to use longer elements than was really desirable to keep the total number of elements down. The elements at the largest stress concentration areas were set at 4mm long which was appropriate for the two core cell-sizes (4.7 and 3mm). Larger elements were used for areas further away, see Fig. 10.7. Each facing element was of two ply thickness. The thickness was obtained by measuring the 4-ply facing laminate giving t ply = 0.230mm as compared to the nominal ply thickness of 0.1905mm for the standard two ply facing. The small increase was due to the additional adhesive layer. The glue-line at the tongue and slot facing (inner) interface and along the side of the tongue section was 3mm thick and was represented by one 3-D element across the thickness, of the same length as the elements in the composite, to maintain a rectangular mesh in the body of the joint. The elements in the fillets at the tongue radius were 3-D wedge type which were joined to the 2-D triangular composite facing elements and to the core element of the tongue panel.

The transition of small elements in the area of interest to large elements elsewhere was made as smoothly as possible whilst maintaining the acceptable degrees of freedom (number of elements) of the mesh, thus the element aspect ratios were rather larger than desirable for maximum accuracy of the analysis. The mesh was one of 610 elements. The complex nature of the joint made creating and numbering the finite element mesh a difficult and lengthy task. The use of the Pafec

Integrated Graphic System (PIGS) reduced these difficulties considerably whilst limiting to a minimum the front width for the stiffness matrix, see Zienkiewicz (17). The self-equilibrating loads and the constrained mesh for all planes of symmetry are shown in Fig. 10.8.

The overall behaviour of the finite element mesh under ultimate deformation was the same as the test. A peel stress developed in the tip of the tongue at the far end which was due to the moment action of the offset load paths on the joint. The action of each ply both in the tongue and in the slot section under deformation are shown in Fig. 10.9. Note that the sign convention for the respective sections of the joint are given in the global plane. This does confirm the points highlighted in the design section for choosing a suitable adhesive for this type of joint, that is to say that a low tensile modulus adhesive would give rise to peel stresses which may cause the discontinuity in the adhesive. The peel problem is particularly serious for the unidirectional fibre composite at the inner facing of the slot section since they generally have a low transverse strength, even when compared with the adhesive, particularly if the adhesive is of the ductile peel-resistant type. However since the joint failure was tensile in the composite facing at the tongue root, the effect of peel on the adhesive and on the slot facings was not considered further in this section.

Using the output from the orthtropic sandwich element it is possible to find the highest stressed position. This was the root of the tongue radius where the adhesive elements are joined to the slot panel composite and is the main area for inspection. This and other areas of stress concentration are shown in Fig. 10.10. The width of composite at the root of the tongue together with the dimensions are given in Fig. 10.11. All the stresses are obtained from the Gauss points which are 2mm away from the singularity, i.e. the connection to

the outer slot facing, these points give the most accurate results, being the points used specifically for numerical integration in the finite element analysis. Fig. 10.12 show the longitudinal and transverse stress distribution for the 90° ply plotted against the width of the composite at the root of the tongue. The stress distribution of the tongue just inside the slot panel (ω_1) was added to Fig. 10.12. This was done to show the effect of the adhesive filleting in the slot on the stress concentration of the tongue section. The reduction of concentration is more apparent in the transverse direction of the 90° ply at position 'L', where the magnitude is more than halfed from 0.238 to 0.106. Note that the stresses are given in the principal material directions. This pattern was also repeated for the longitudinal and the shear stress distribution for the 0° ply and the 90° ply which are shown in Fig. 10.13 and 10.14 respectively. Note that the shear stress distribution for the 0° ply is the same as for the 90° ply with opposite sign.

The effect of the adhesive thickness on the stress distribution at the inner slot facing, see Fig. 10.15, was investigated by plotting the transverse stress concentration along the width (X wise) and normal (Z wise) to the joint for the 90° ply. This was the ply most likely to fail due to peel and shear stresses at the tip of the tongue. These plots are given in Figs. 10.16 and 10.17. The data for the latter was obtained at position 'B' where the maximum stress concentration occurs. Note that all the distributions were plotted using the Tables 10.1, 10.2 and 10.3 for the static strength predictions of the joint. These plots indicate that the adhesive filleting in the slot does reduce the stress concentration in the tongue and slot composite facings, particularly at the root of the tongue where the peak stresses in both 90° and 0° ply occur at the end of the radius position 'L', σ_2/σ_o = 0.34, σ_1/σ_o = 1.3

respectively, therefore indicating that the width of the tongue would not fail first for any given number of ply reinforcements and orientations. This is one of the advantages of the analysis in providing information for the area of the joint which otherwise could not have been available since the whole section is hidden by adhesive in the slot panel.

The shear stress distribution peaks at the far end of the radius while increasing slightly to a maximum value of ± 0.214 at position 'M' suggesting that, although the joint loading is one of longitudinal shear, it is highly unlikely that the joint with 90°/0° reinforcement will fail in shear mode alone. As for the slot facing (inner) the transverse tensile stress concentration in the 90° ply at the far end is at its maximum at position 'B', Fig. 10.15, before dropping sharply to a small transverse compressive value at the near end. Moreover the thick adhesive line at the tip of the tongue meant that the peel stress effect at position 'B' on the 90° ply was not considerable, see Fig. 10.17. The magnitude of both of which were not giving any problem for this case of reinforcement therefore they are not considered further in this section. It is now known from the plots that the area where the failure initiates is at positions 'M' and 'M' at the end of the radius nearest to the load application points, the values of which are given in Table 10.1.

Also shown in this table is the static strength prediction using these stresses with the two failure criteria discussed in Chapter 7 and the material static strength. The comparison between the two criteria will be given in the next chapter. These values indicate that the analysis is in good agreement with the test failure observed.

10.3 LONGITUDINAL SHEAR JOINT TYPE 2a [90/0/+45/-45/90/0 - HDC 90].

The joint was re-analysed using the mesh shown in Fig. 10.6 but with a few alterations which were necessary in order to represent the reinforcement type 2a of the test section of Fig. 4.3, case 2.0. The alterations consisted of extending the tongue panel in the global 'Y' direction in order to accommodate the change in the test specimen (see Fig. 3.4 and D = 101.6mm) and rearranging the material properties.

The modifications to the tongue section were made mainly due to the increase in the load bearing capacity of the joint, by increasing the tongue length to that for which the tests were carried out. To do this additional elements were added to make up the difference in length as well as modifying the constrained planes of symmetry in the finite element mesh of Fig. 10.8, leaving the elements aspect ratio in the areas of interest the same.

Rearranging the material properties meant that each facing element local to the reinforcement could not be thicker than three plies because the facing was represented by two elements and each ply could be of different orientation with respect to another. Even with the three ply facing elements, the accuracy of the analysis was not affected due to the element aspect ratio which was dependent on the size of the 3-D core element. A better aspect ratio for the core element (20 noded brick and 15 noded wedge elements) would give significant rise to the maximum number of degrees of freedom that can be handled by the computer. Hence an aspect ratio of h/L = 6.49/4 = 1.62 was used for the 3-D core elements at the areas of interest which is an approximation to the standard cell size of 4.7mm and the high density core cell size of 3mm.

Tables 10.4 and 10.5 show the stress concentrations in the root of the tongue section at the position letters in Fig. 10.11. Comparing these tables with Table 10.1 for the reinforcement type 2a and 1b respectively for the common plies such as 90° and 0° certain differences can be seen. The concentrations at both ends of the bond line (end of radius) B, H are smaller for both plies. Moreover the compressive stress concentration parallel to 90° ply extends further from point 'J' to 'K' but generally the pattern of distribution remain the same. These reductions in concentrations occur despite the increase in the magnitude of the applied load and the depth of the tongue panel, both of which give rise to the overall induced moment. The resulting compressive stress concentrations in the far end of tongue radius are not large enough to cause local buckling failure in any of the 6-ply facing. In the tensile region the concentrations for 90° and -45° plies are severe as expected. The stress distributions for the -45° ply are given in Fig. 10.18 and 10.19 along the width of the tongue. The transverse and shear stress concentrations reach their peak at positions 'M' and 'N' respectively. The concentration parallel to the fibre direction is at its highest at position 'B' which is the far end of the tongue. The effect in the +45° ply is opposite to that of the -45° with different concentrations which are not severe. However the effect would be reversed if the loading were in the opposite directcion. Note that the loading direction of the joint in the longitudinal shear mode could be reversed.

The adhesive fillet stresses, particularly the peel stress in the far end of the slot, were checked using the Von-Mises Criterion. The magnitude was not large and did not give any problem and therefore was not considered further.

The size of the reinforcement local to the tongue and the possible stress concentrations in the respective plies were also checked. Although the magnitude of these concentrations did not give any problem, the shape of the reinforcement was not investigated further, as the objective of this thesis was in establishing a method with which these joints could be analysed.

The stress concentrations in the composite at the outer slot facing were also small in comparison to the inner facing where major load transfer occurs. As indicated from the joint reinforcement type 1b, the highest stressed area of the composite facing which is likely to cause failure is the far end of the slot. The position is given in Fig. 10.20. The stress concentrations were obtained from the Gauss Points which are denoted as upper and middle relative to the centreline of the tongue facing laminate. The distribution pattern across the width of the slot remains the same as Fig. 10.17 with lower stress concentration in the composite adjacent to the core fillet adhesive. The highest stressed position was at the intersection of the tongue and inner slot facing laminates. Table 10.6 shows the stress concentration at the upper and middle positions of the slot composite together with the Tsai-Hill R.F. and the predicted strengths. In the 90° ply adjacent to the glue line, the transverse stress concentrations, σ_2/σ_o = 0.3286, are maximum at position 'A' which is to be expected. Shear stresses are low and most of the stress is reacted in the 0° ply with maximum value of σ_1/σ_o = 1.3174. These concentrations are used to give the predicted failure strengths, using the Tsai-Hill Criterion for the composite. The predictions are described in the next chapter.

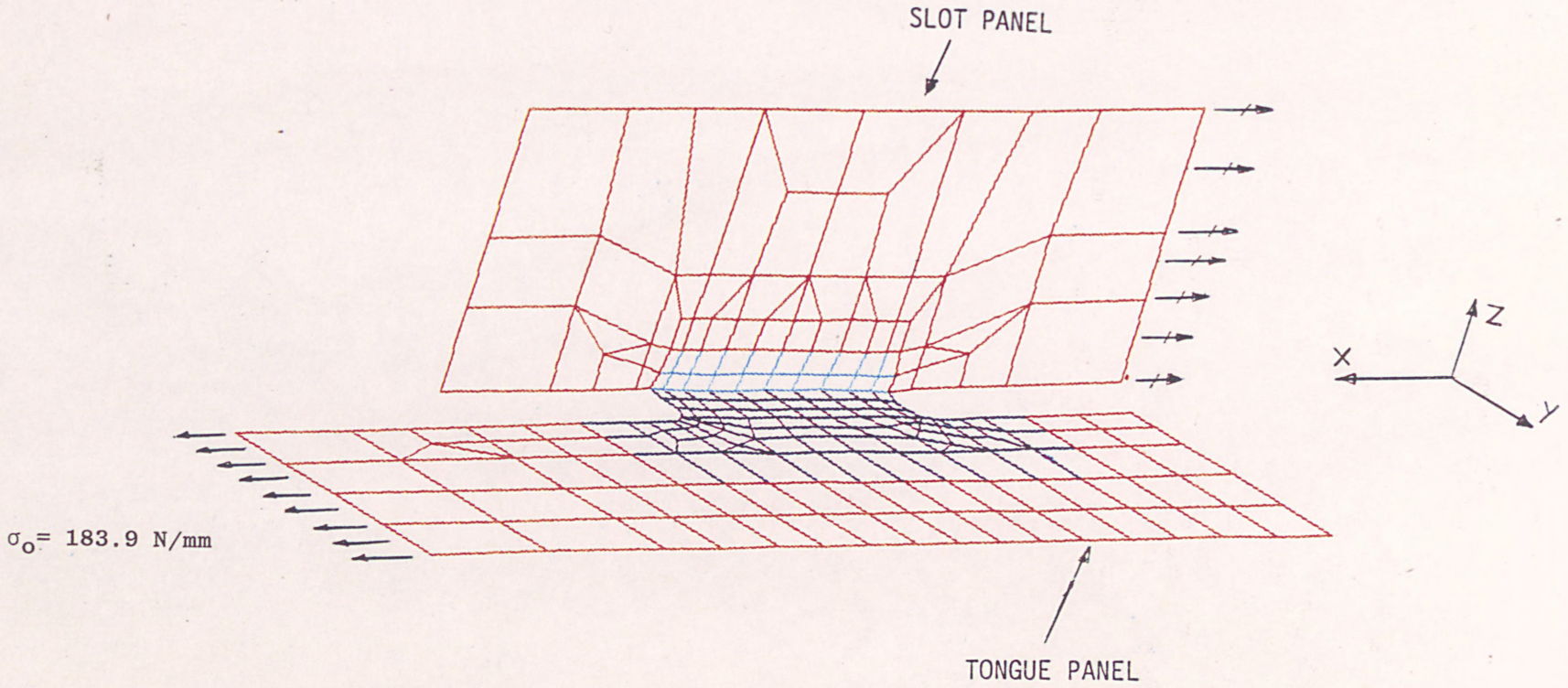

FIG 10.1

TWO DIMENSIONAL FINITE ELEMENT MESH OF TONGUE AND SLOT JOINT

SCALE OF DISPLACEMENT=0.00586 INCHES/CM

MAXIMUM SCREEN DISPLACEMENT=10 CM

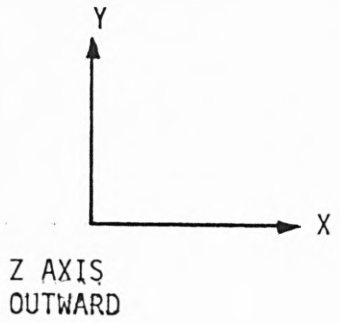

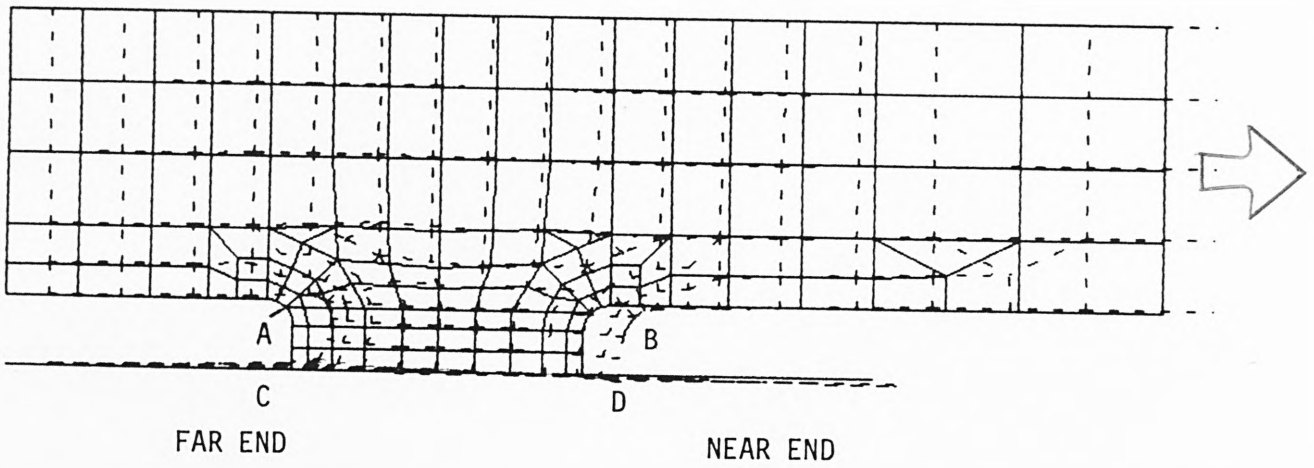

FIG 10.2 DEFLECTED SHAPE OF THE TONGUE AND SLOT JOINT (2D)

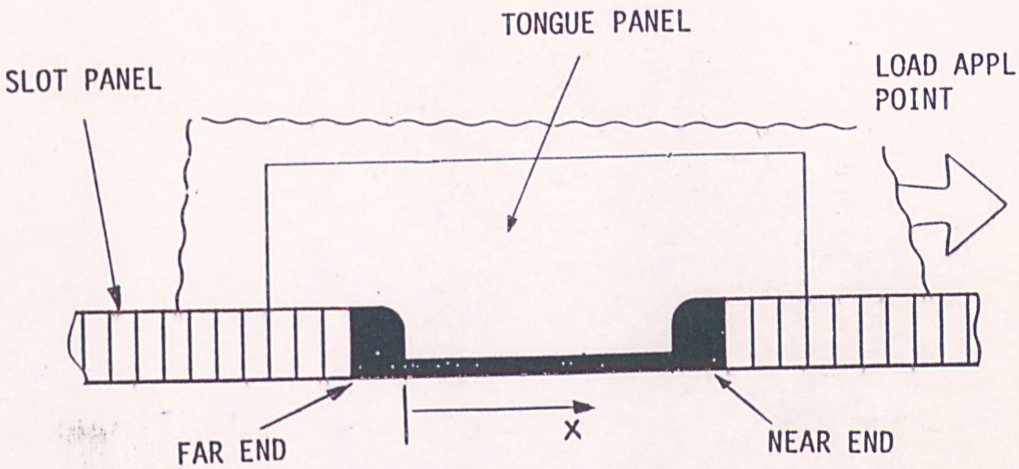

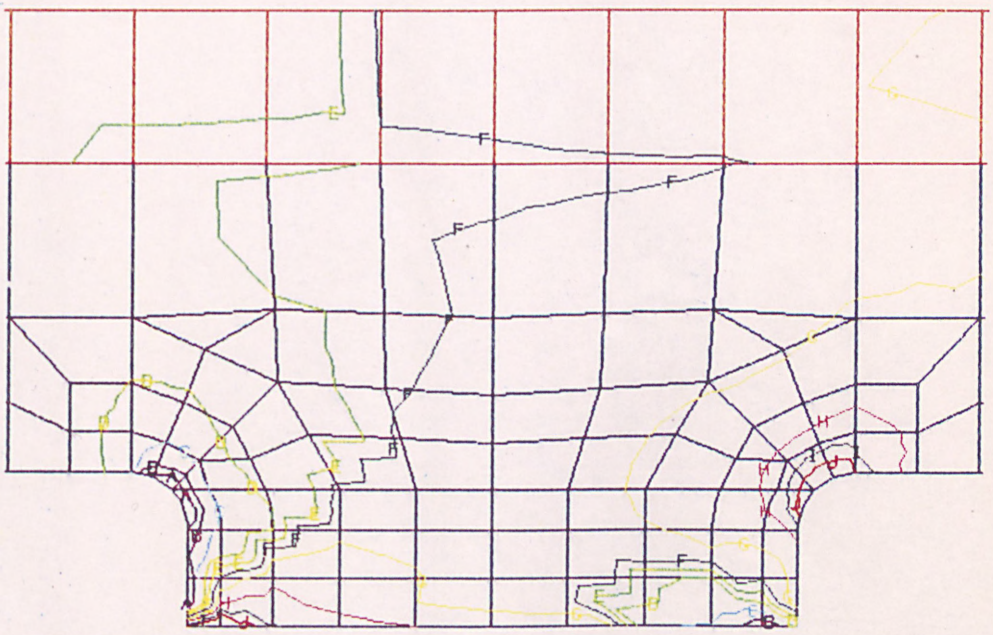

	/ 10⁵
-1.425	A -0.38
-1.087	B -0.29
-0.787	C -0.21
-0.450	D -0.12
-0.112	E -0.03
0.187	F 0.05
	G 0.14
0.862	H 0.23
1.20	I 0.32
1.537	J 0.41

FIG 10.3

ABSOLUTE STRESS CONCENTRATION CONTOUR IN THE TONGUE PANEL

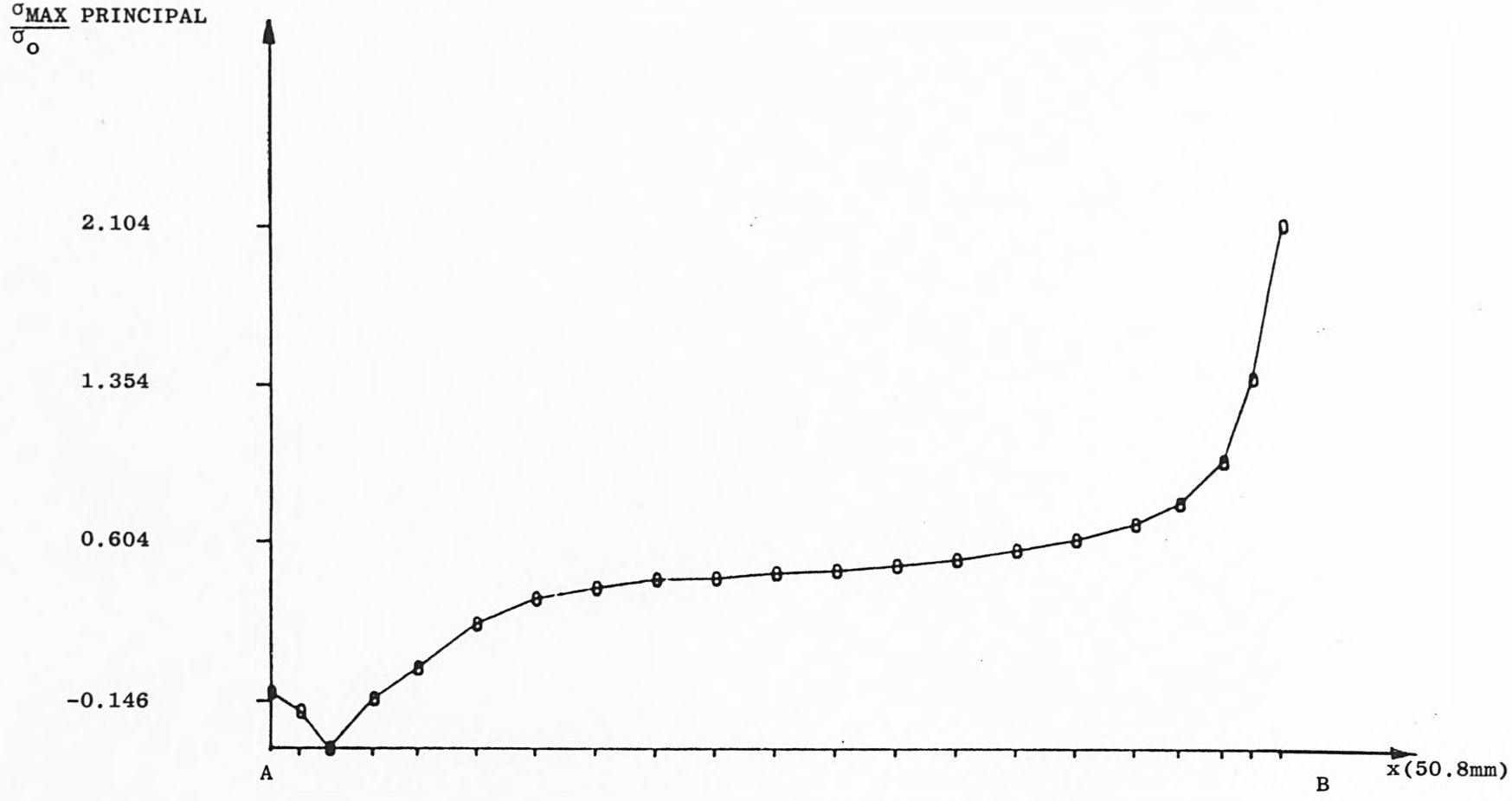

FIG. 10.4
MAXIMUM PRINCIPAL STRESS ACROSS THE ROOT OF THE TONGUE (TOP FACING)

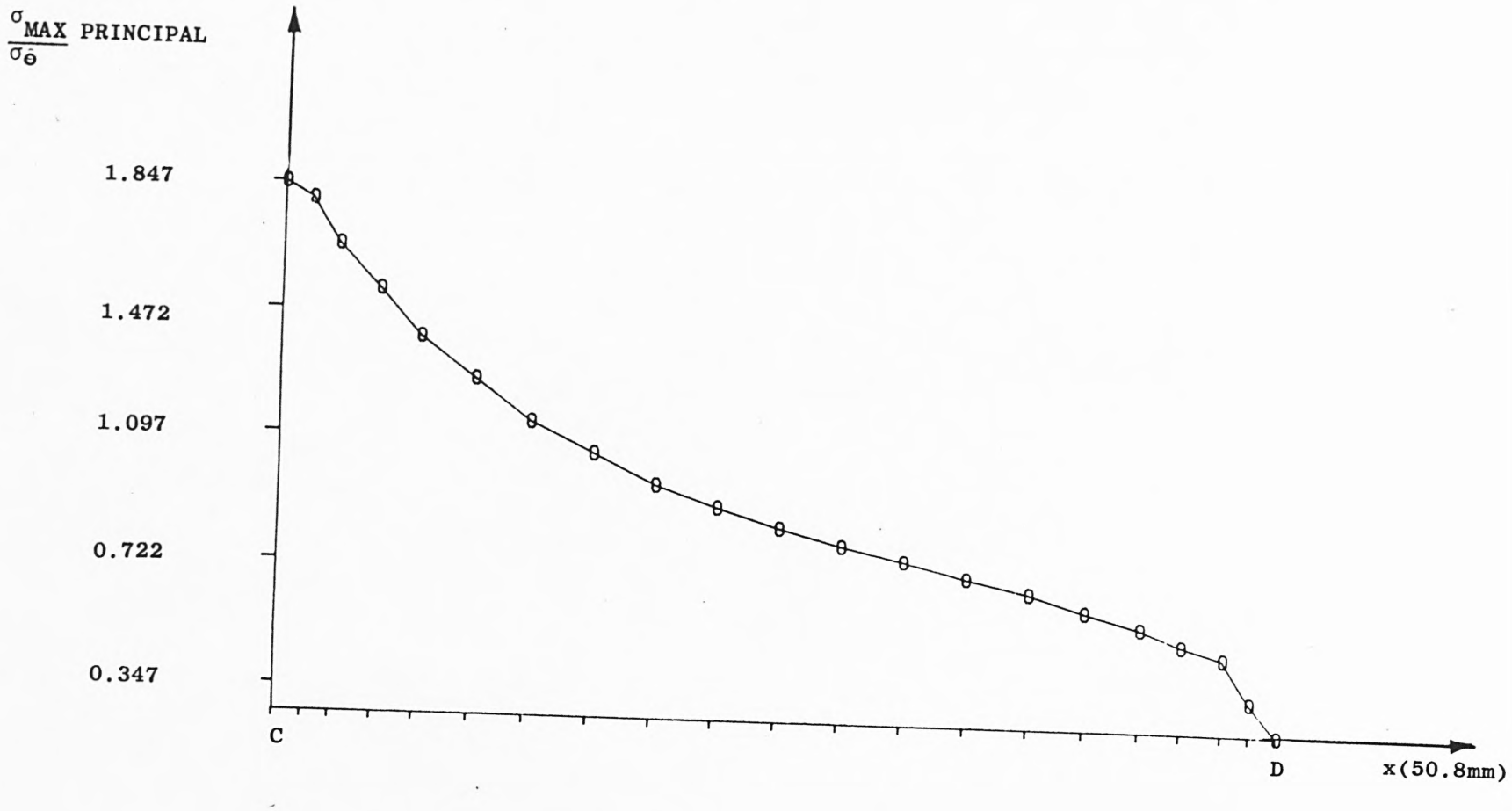

FIG. 10.5

MAXIMUM PRINCIPAL STRESS CONCENTRATION IN SLOT FACING

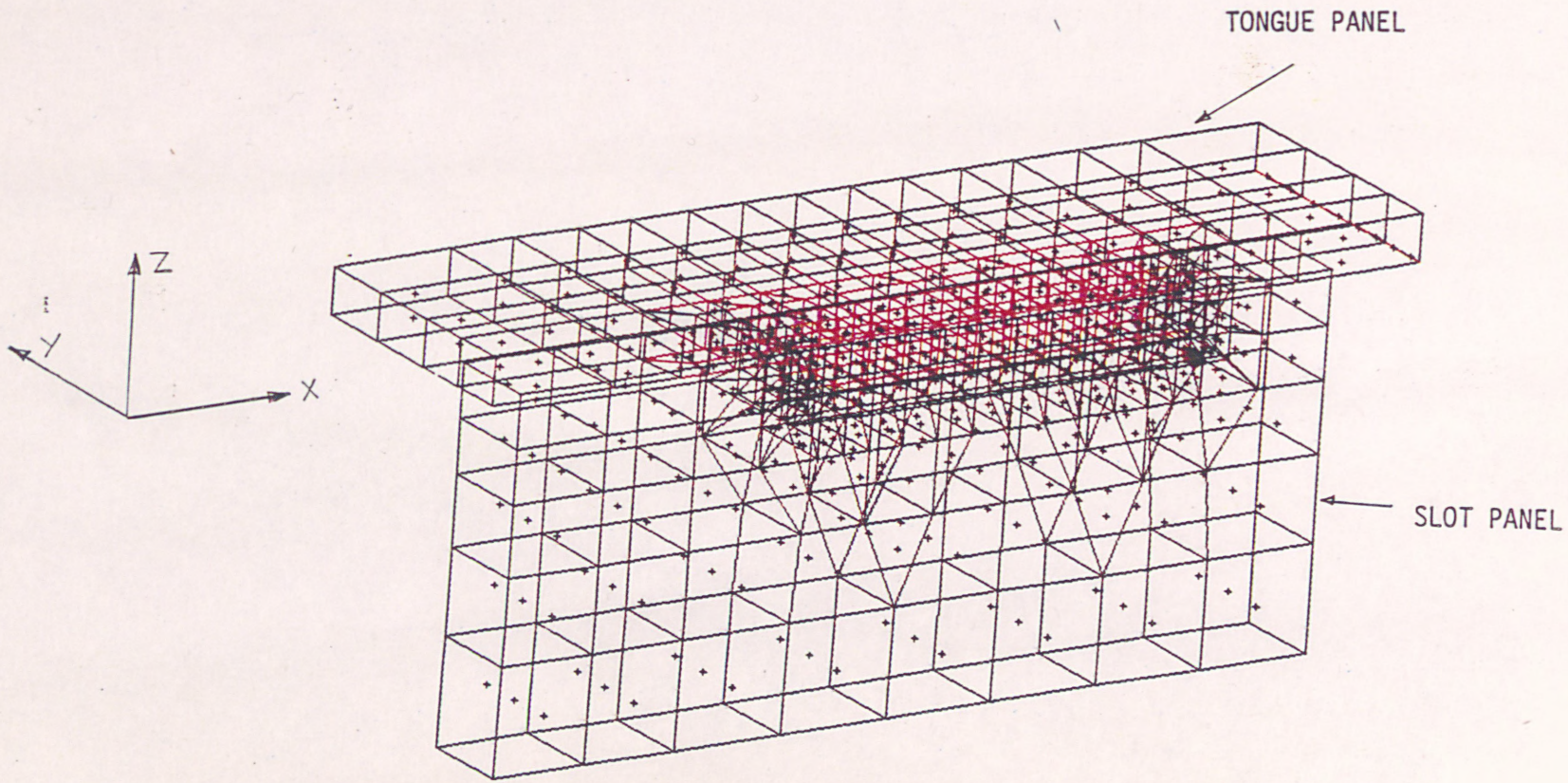

FIG 10.6

THREE DIMENSIONAL FINITE ELEMENT MESH OF TONGUE AND SLOT JOINT

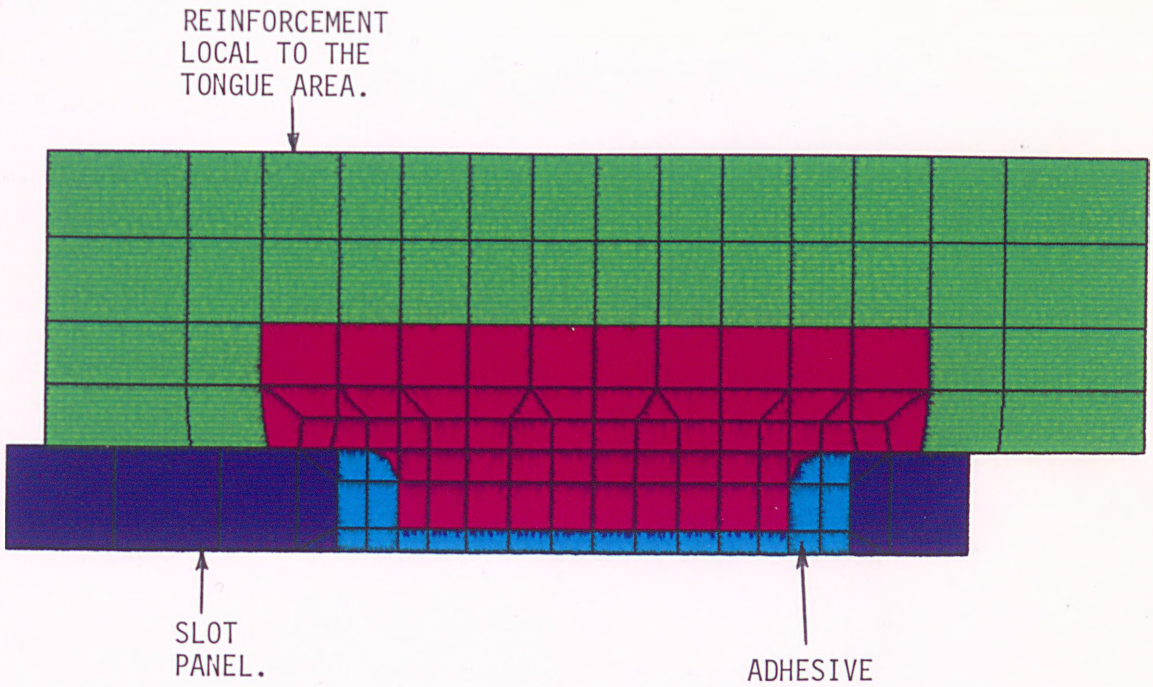

TYPE MENU OPTION V

FIG 10.7 3D BLOCKFILL MESH OF THE TONGUE AND SLOT JOINT

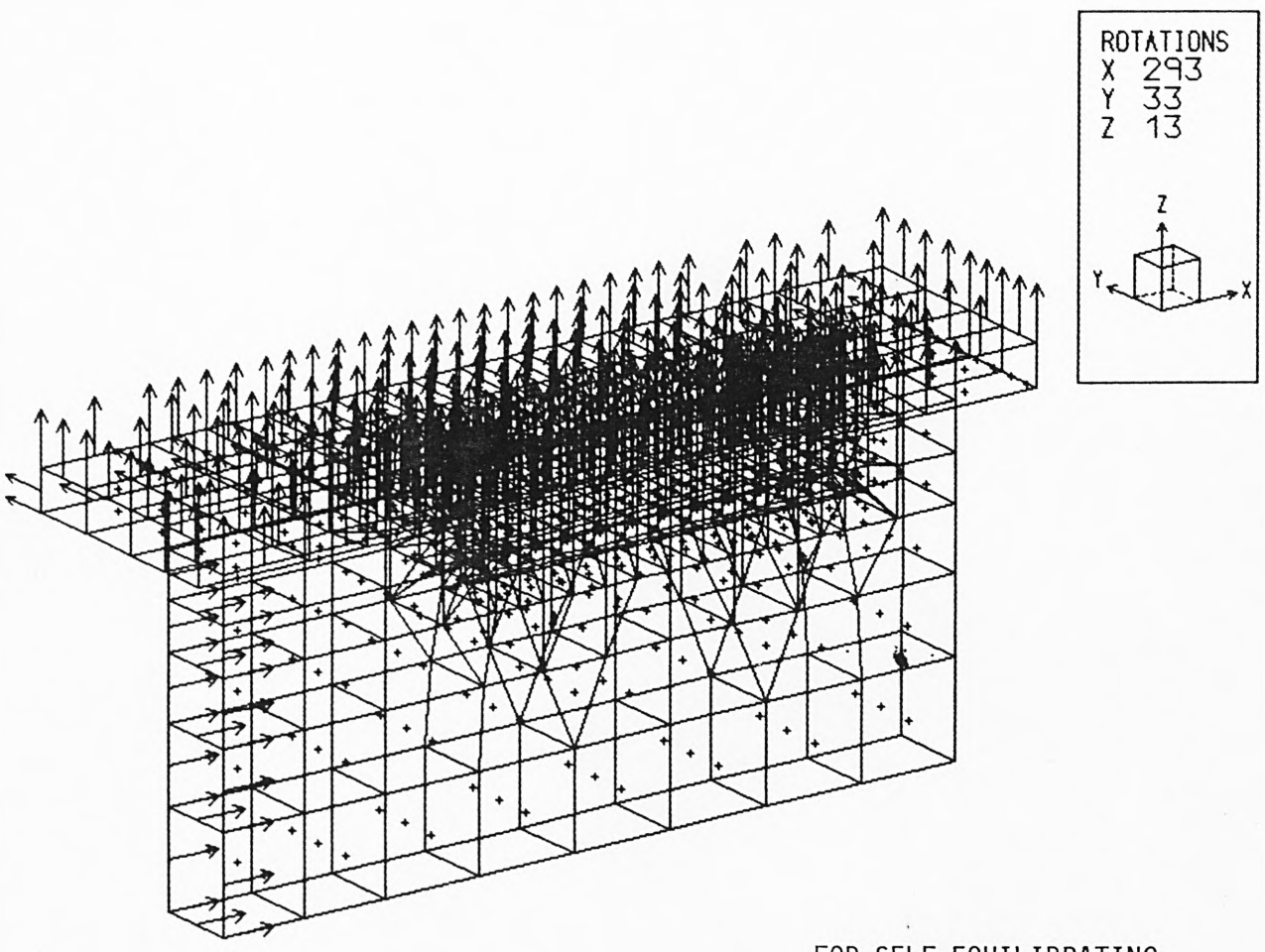

FOR SELF-EQUILIBRATING LOADS, THE SIGN OF THE ARROWS SHOULD BE REVERSED.

FIG 10.8 CONSTRAINED PLANES OF SYMMETRY OF THE TONGUE AND SLOT JOINT.

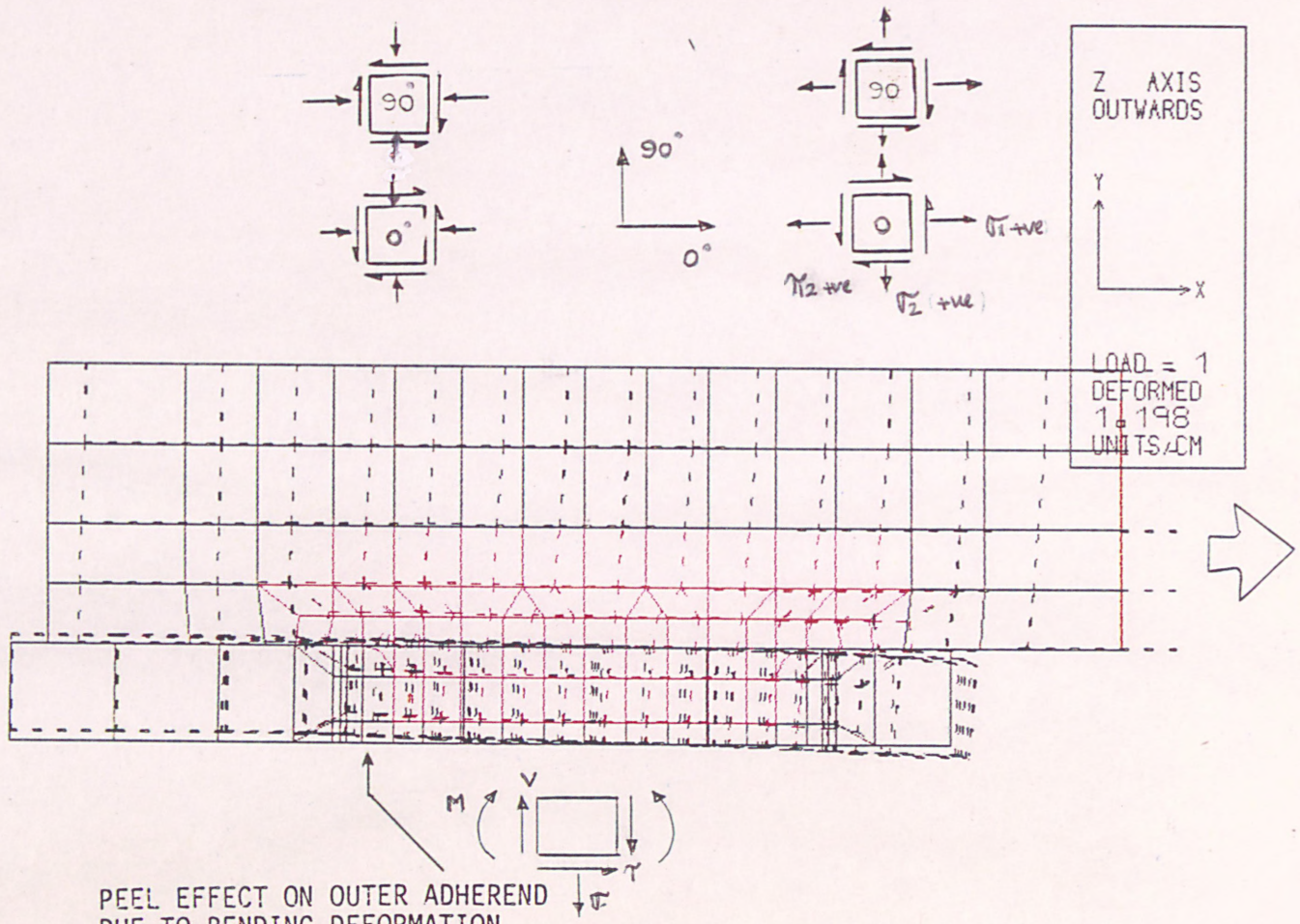

FIG 10.9

DEFORMATION OF THE TONGUE AND SLOT JOINT (TYPE 1B)

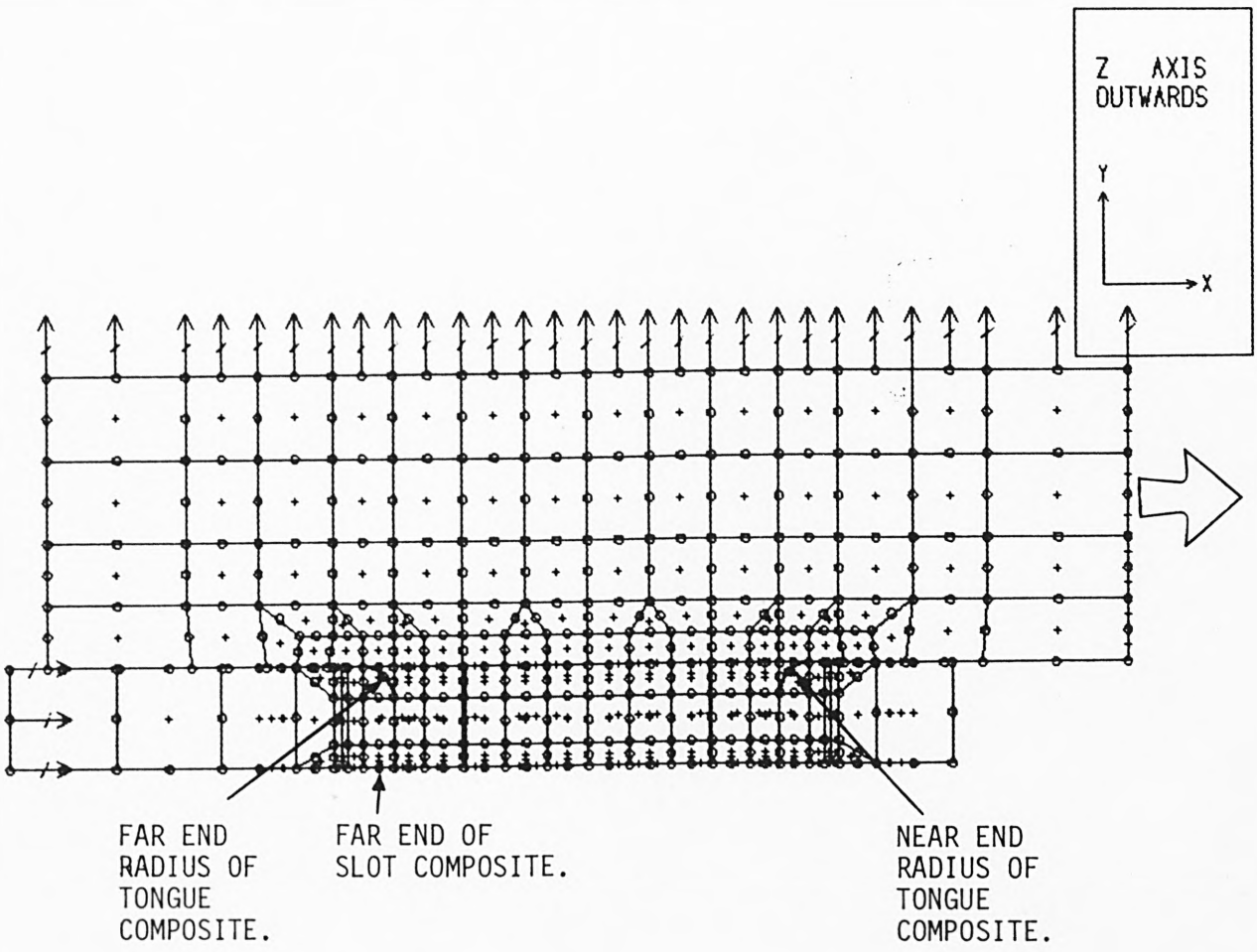

TYPE MENU OPTION

FIG 10.10 DESCRIPTION OF THE IMPORTANT AREAS OF STRESS CONCENTRATION.

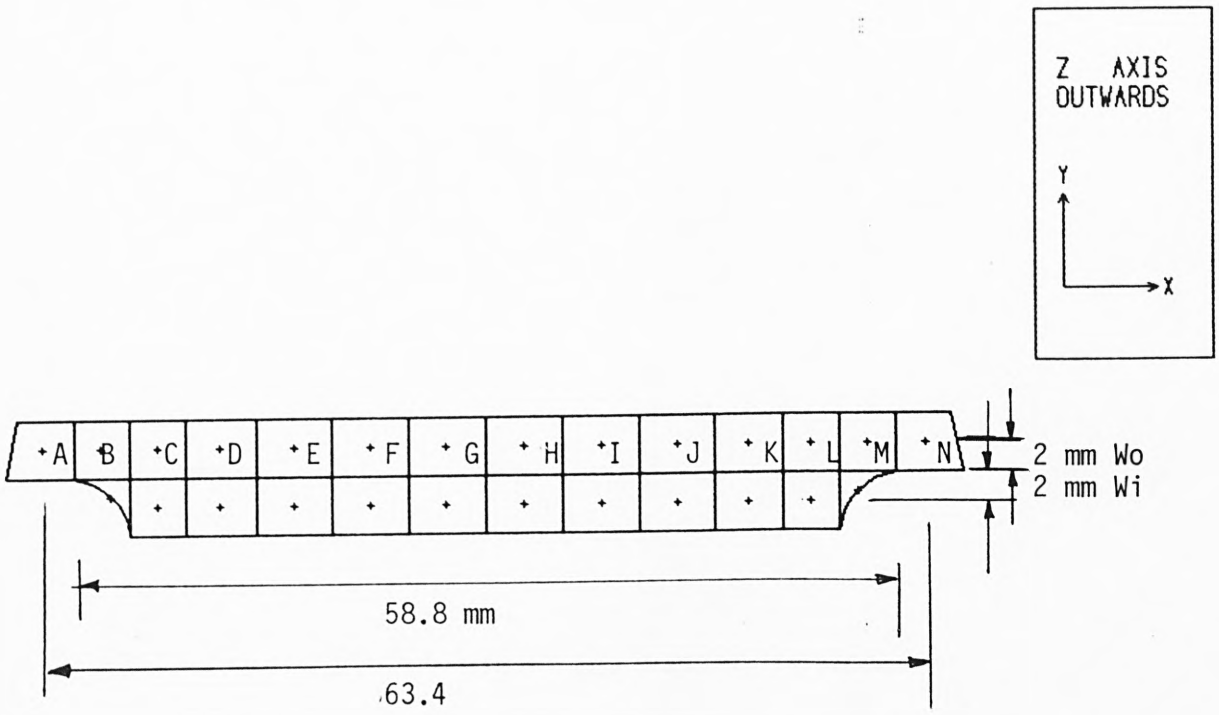

FIG 10.11 WIDTH OF THE COMPOSITE AT THE ROOT OF THE TONGUE.

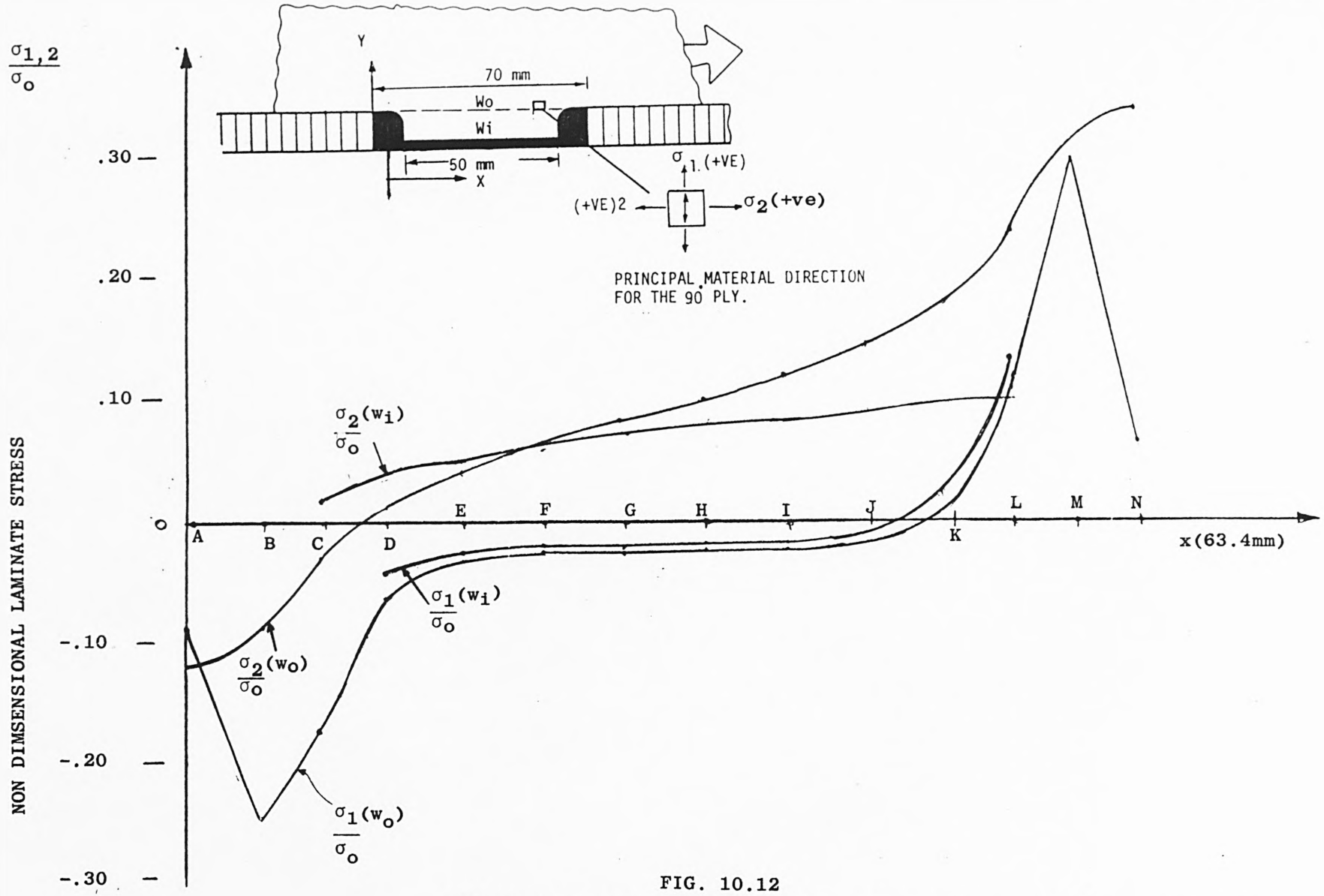

FIG. 10.12

LONGITUDINAL AND TRANSVERSE STRESS DISTRIBUTION OF 90° PLY AT THE ROOT OF TONGUE

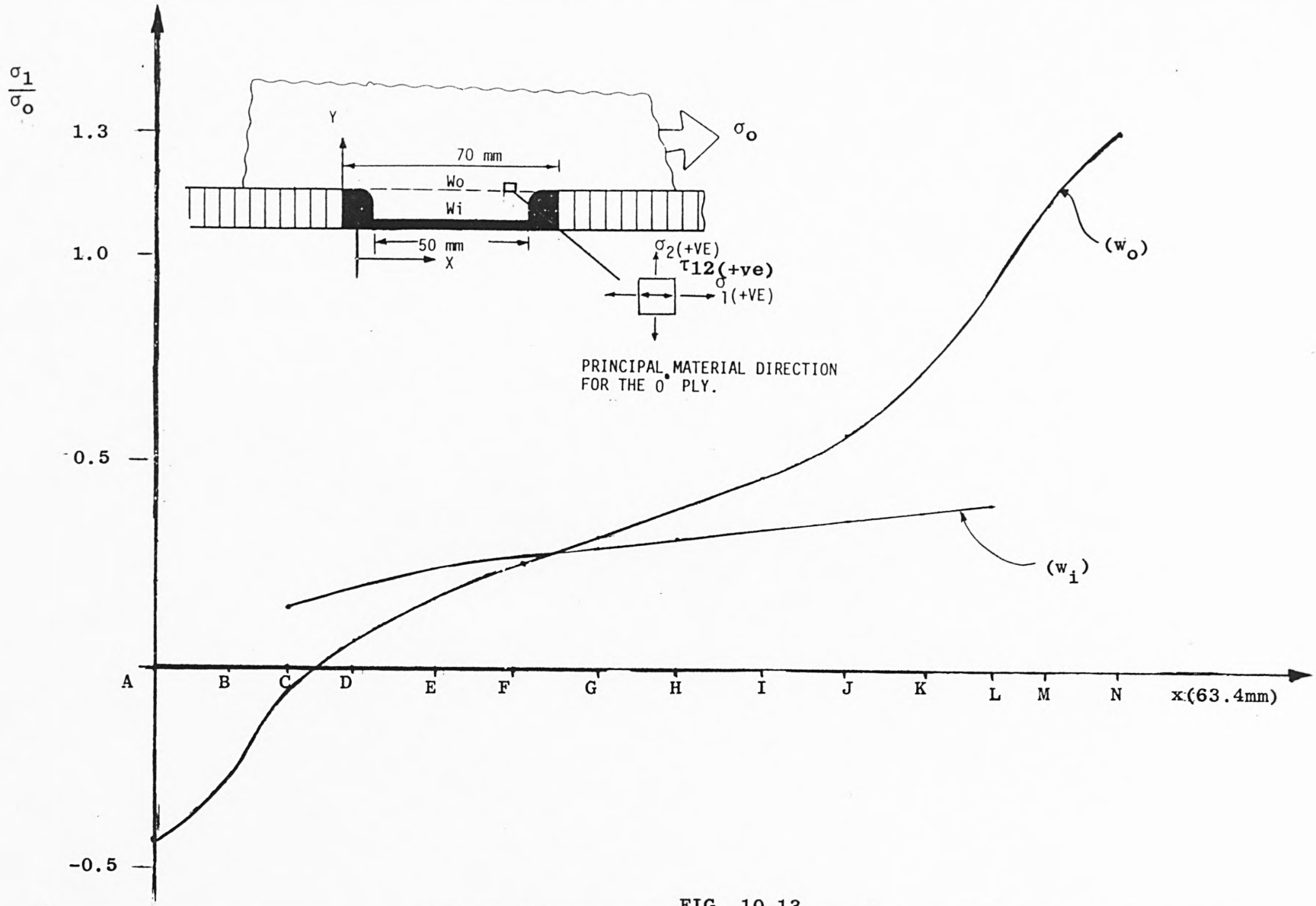

FIG. 10.13
LONGITUDINAL STRESS DISTRIBUTION OF 0° PLY AT THE ROOT OF THE TONGUE

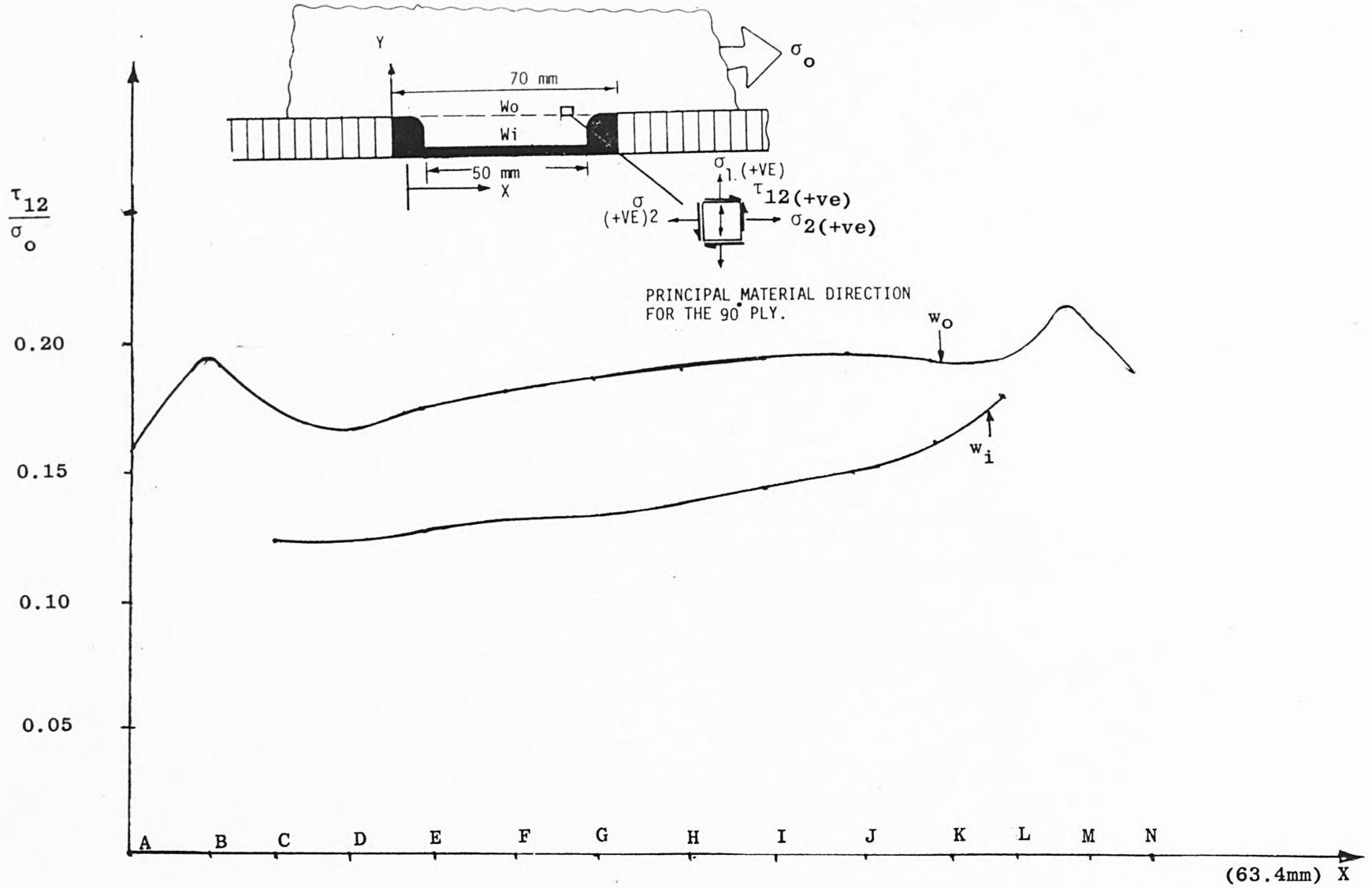

FIG. 10.14

SHEAR STRESS DISTRIBUTION FOR 90° PLY ALONG THE ROOT OF THE TONGUE

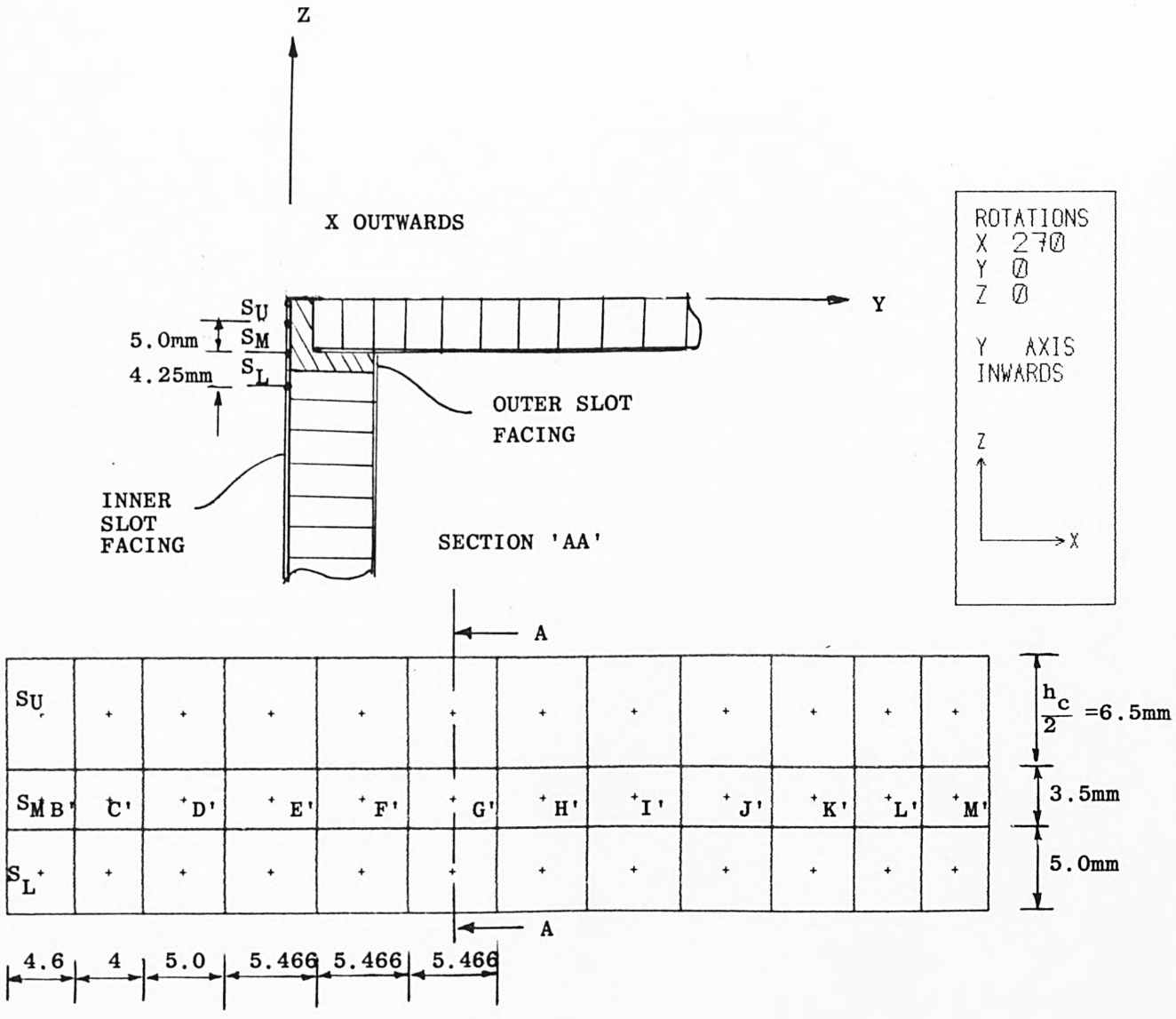

where S_U = SLOT SKIN UPPER
S_M = SLOT SKIN MIDDLE
S_L = SLOT SKIN LOWER

FIG. 10.15

VITAL AREA OF COMPOSITE AT SLOT SKIN (INNER)

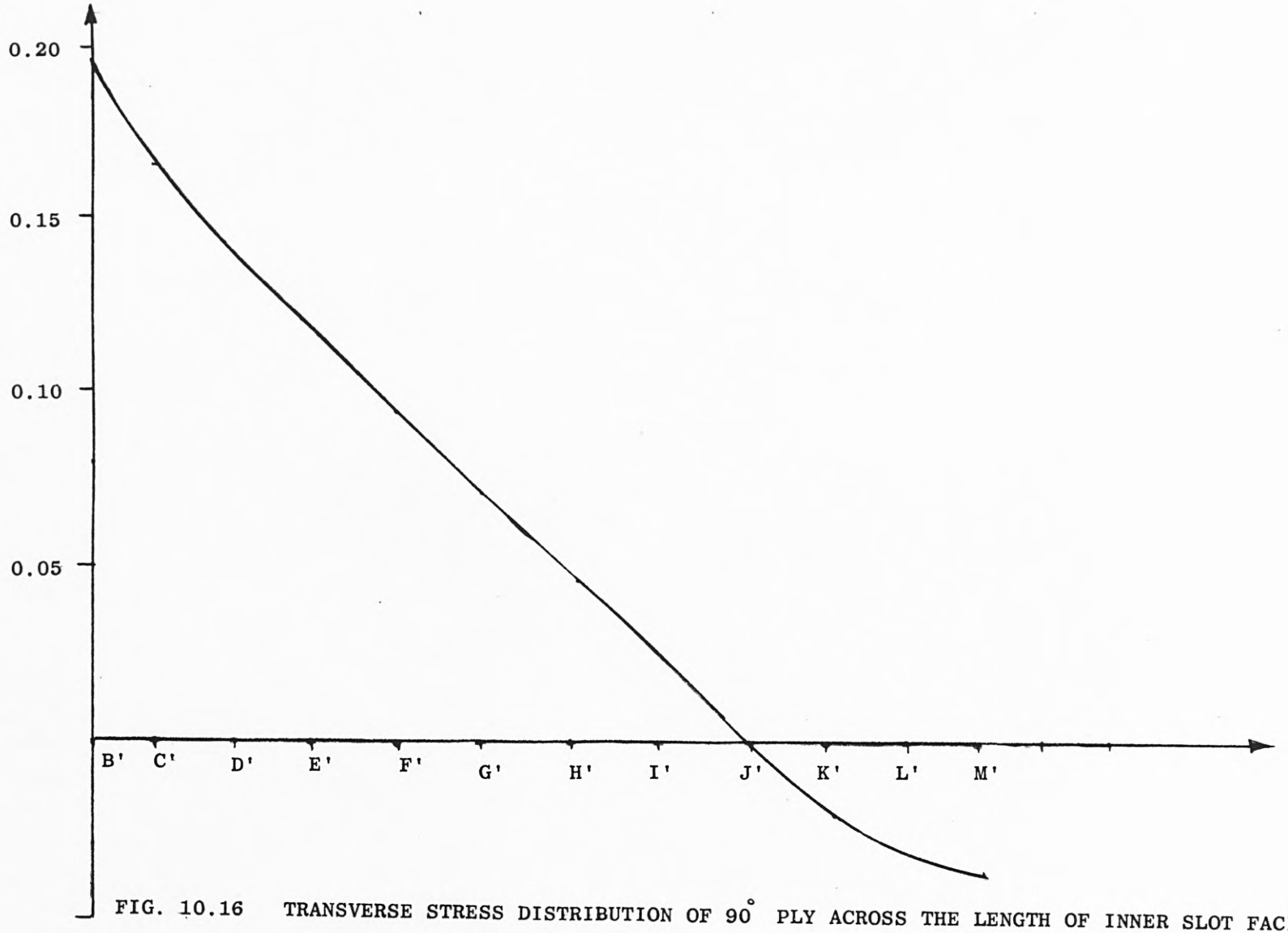

FIG. 10.16 TRANSVERSE STRESS DISTRIBUTION OF 90° PLY ACROSS THE LENGTH OF INNER SLOT FACING

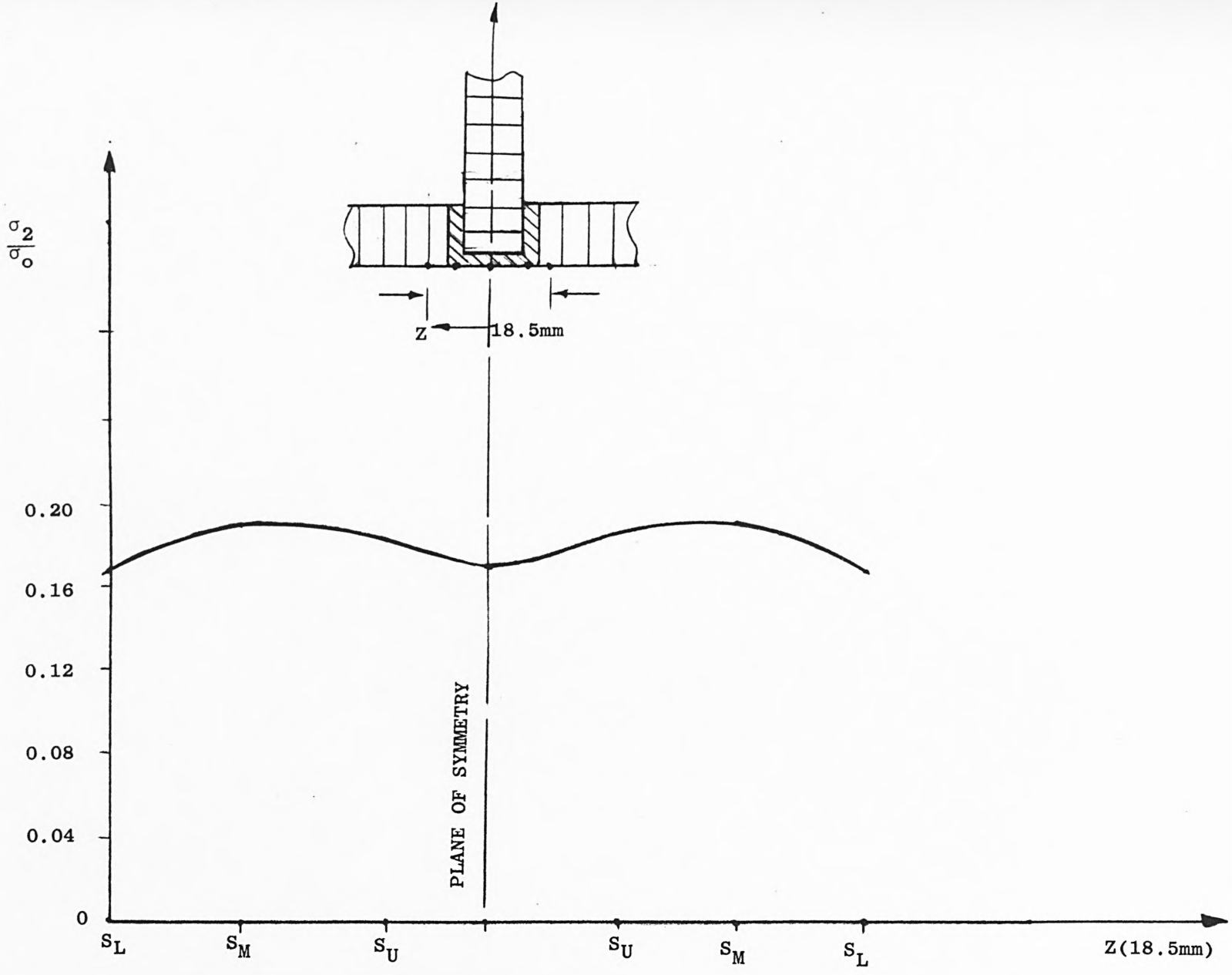

FIG. 10.17 TRANSVERSE STRESS DISTRIBUTION OF 90° PLY ACROSS THE WIDTH OF SLOT

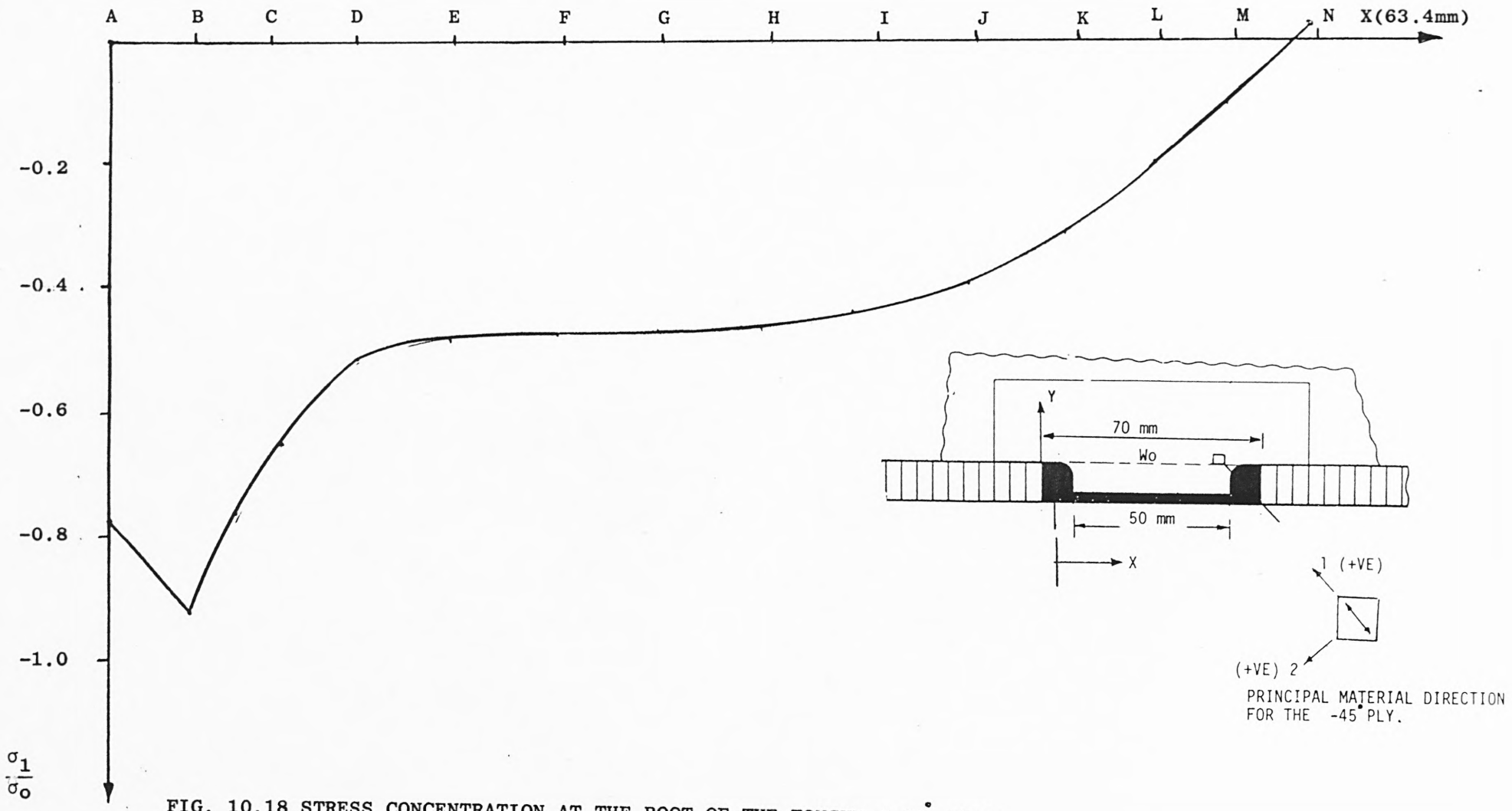

FIG. 10.18 STRESS CONCENTRATION AT THE ROOT OF THE TONGUE (-45° PLY)

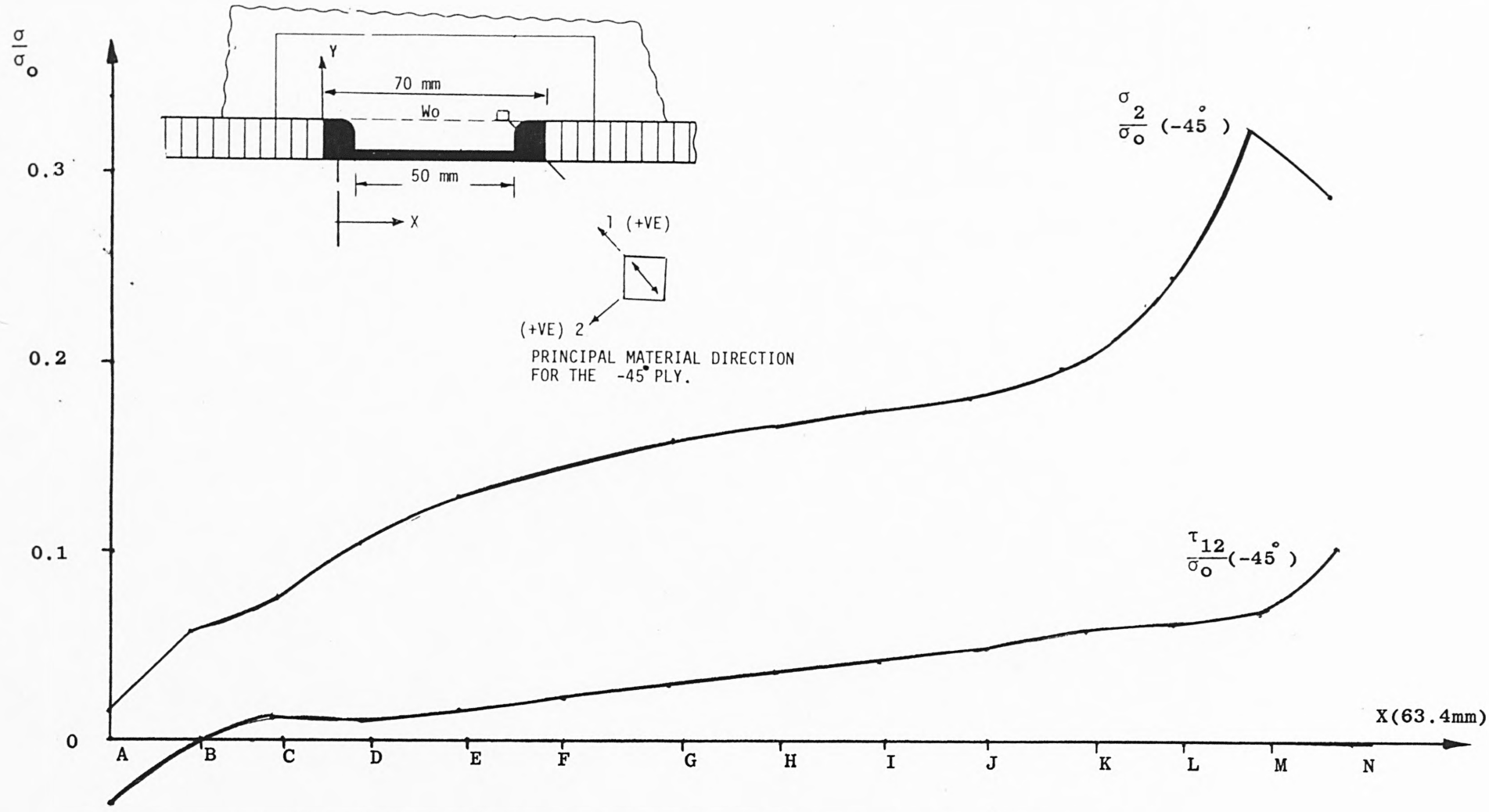

FIG. 10.19 STRESS CONCENTRATION AT THE ROOT OF THE TONGUE (-45° PLY)

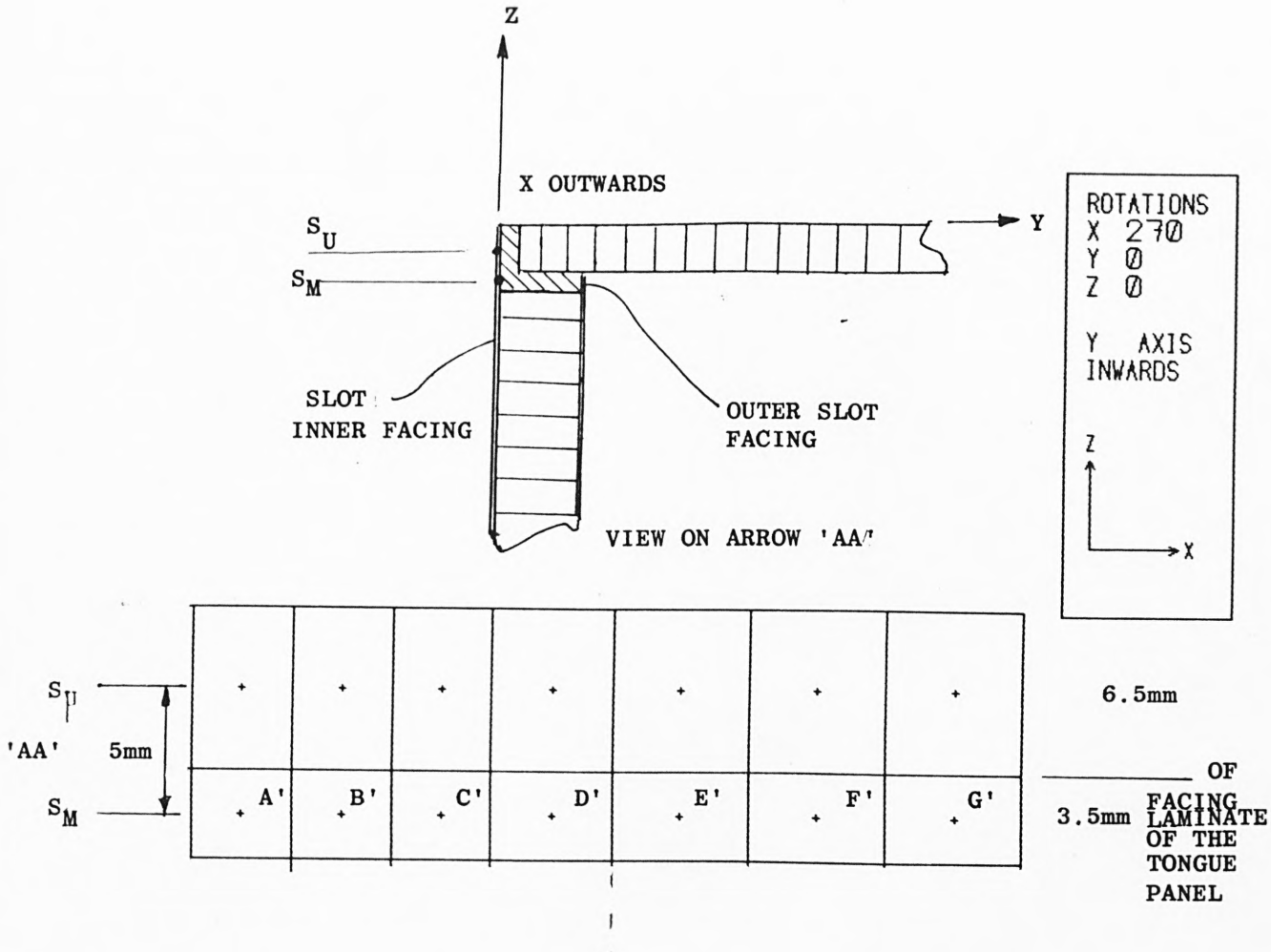

S_U = SLOT FACING UPPER

S_M = SLOT FACING MIDDLE

FIG. 10.20

VITAL AREA OF THE FAR END SLOT COMPOSITE FACING (INNER)

LONGITUDINAL SHEAR TEST STRENGTH OF $(90^\circ/0^\circ)_s$ = $\frac{7833(\text{FAILURE LOAD})}{37.52 \times 3.81 \times 2}$ = $274(\sigma_o)$MPa

POSITION LETTERS	PLY ANGLE	$\frac{\sigma_1}{\sigma_o}$	$\frac{\sigma_2}{\sigma_o}$	$\frac{\tau_{12}}{\sigma_o}$	TSAI-HILL R.F.	TSAI-HILL HOFFMAN R.F.
A	90°	-.092	-.118	-.16	1.57	3.09
	0°	-.434	-.048	+.16	1.57	2.32
B	90°	-.254	-.092	-.194	1.35	1.91
	0°	-.297	-.083	+.194	1.35	1.87
C	90°	-.179	-.03	-.170	1.61	2.5
	0°	-.073	-.052	+.170	1.61	2.77
D	90°	-.065	.009	-.168	1.66	2.59
	0°	.053	-.015	+.168	1.66	2.97
E	90°	-.036	.037	-.176	1.57	2.27
	0°	.154	-.002	+.176	1.59	2.82
F	90°	-.027	.059	-.183	1.49	2.02
	0°	.238	.005	+.183	1.53	2.68
G	90°	-.026	.078	-.188	1.43	1.83
	0°	.311	.009	+.188	1.48	2.60
H	90°	-.024	.097	-.192	1.37	1.68
	0°	.383	.0133	+.192	1.45	2.54
I	90°	-.023	.118	-.195	1.32	1.55
	0°	.463	.018	+.195	1.42	2.52
J	90°	-.0145	.144	-.197	1.26	1.43
	0°	.562	.026	+.197	1.40	2.55
K	90°	.0122	.183	-.196	1.2	1.3
	0°	.704	.0405	+.196	1.39	2.64
L	90°	.121	.238	-.196	1.09	1.13
	0°	.894	.08	+.196	1.35	2.50
M	90°	.299	.312	-.214	.92	.86
	0°	1.14	.139	+.214	1.17	1.76
N	90°	.069	.34	-.190	.92	.84
	0°	1.30	.087	+.190	1.35	2.94
O	90°	-.016	.34	-.096	1.1	1.16
	0°	1.31	.067	+.096	2.31	26.3

TABLE 10.1 STRESS CONCENTRATION IN THE COMPOSITE AT THE ROOT OF THE TONGUE

POSITION LETTERS	PLY ANGLE	$\frac{\sigma_1}{\sigma_o}$	$\frac{\sigma_2}{\sigma_o}$	$\frac{\tau_{12}}{\sigma_o}$	TSAI-HILL R.F.
C	90°	-.176	.0168	-.124	2.17
	0°	.104	-.0409	.124	2.20
D	90°	-.0646	.0420	-.124	2.18
	0°	.177	-.008	.124	2.24
E	90°	-.036	.0536	-.128	2.09
	0°	.217	.0016	.128	2.18
F	90°	-.028	.0635	-.132	2.01
	0°	.253	.0057	.132	2.11
G	90°	-.0256	.0715	-.135	1.94
	0°	.284	.008	.135	2.06
H	90°	-.0234	.078	-.139	1.87
	0°	.309	.009	+.139	2.0
I	90°	-.0195	.084	-.144	1.80
	0°	.333	.012	+.144	1.93
J	90°	-.0082	.091	-.151	1.71
	0°	.356	.0163	+.151	1.84
K	90°	.024	.097	-.162	1.60
	0°	.372	.025	+.162	1.71
L	90°	.135	.106	-.180	1.43
	0°	.387	.055	+.180	1.51

TABLE 10.2 POSITION JUST BELOW THE ROOT OF THE TONGUE

σ_o = 274

POSITION LETTERS	PLY ANGLE	$\frac{\sigma_1}{\sigma_o}$	$\frac{\sigma_2}{\sigma_o}$	$\frac{\tau_{12}}{\sigma_o}$	TSAI-HILL R.F.
B'	90°	-.128	.194	-.058	1.86
	0°	.774	.009	.058	4.13
C'	90°	-.108	.164	-.057	2.15
	0°	.653	.007	.057	4.35
D'	90°	-.088	.144	-.059	2.36
	0°	.573	.008	.059	4.33
E'	90°	-.073	.118	-.06	2.70
	0°	.475	.006	.06	4.39
F'	90°	-.058	.094	-.06	3.11
	0°	.376	.005	.06	4.50
G'	90°	-.045	.07	-.059	3.58
	0°	.282	.003	.059	4.59
H'	90°	-.031	.048	-.059	4.09
	0°	.192	.002	.059	4.68
I'	90°	-.017	.024	-.058	4.59
	0°	.099	0	.058	4.79
J'	90°	.007	0	-.057	4.90
	0°	.003	0	.057	4.90
K'	90°	.022	-.022	-.055	4.89
	0°	-.087	0	.055	4.87
L'	90°	.049	-.035	-.051	4.95
	0°	-.142	.005	.051	4.86
M'	90°	.074	-.038	-.046	5.26
	0°	-.163	.010	.047	5.05
AT POSITION B'	S_L 90°	-.088	.169	-.123	1.63
	0°	.671	.013	.123	2.20
	S_U 90°	-.084	.184	-.001	2.15
	0°	.726	.018	.001	8.08

TABLE 10.3 STRESS CONCENTRATION OF SLOT INNER COMPOSITE SKIN (S_M)

LONGITUDINAL SHEAR STRENGTH OF THE JOINT = 12.37×10^3N "σ_o = 319.56 MPa

POSITION LETTERS	PLY ANGLE	$\frac{\sigma_1}{\sigma_o}$	$\frac{\sigma_2}{\sigma_o}$	$\frac{\tau_{12}}{\sigma_o}$	TSAI-HILL R.F.	PREDICTED STRENGTH kN
A	90°	-.0582	-.1336	-.0795	2.36	29.193
	0°	-.500	-.0429	.0795	2.394	29.614
	-45°	-.7698	.0127	-.0357	2.40	29.688
	+45°	.2112	-.189	.0357	2.45	30.306
B	90°	-.2487	-.0801	-.1085	2.035	25.173
	0°	-.2528	-.0807	.1085	1.99	24.61
	-45°	-.920	.0582	-.0001	1.99	24.61
	+45°	.4162	-.217	-.0001	2.26	27.95
C	90°	-.193	-.022	-.0867	2.65	32.78
	0°	-.0441	-.0532	.0867	2.65	32.78
	-45°	-.654	.0732	.0122	2.47	30.55
	+45°	.4162	-.1477	-.0122	3.21	39.71
D	90°	-.0641	.0088	-.0823	2.88	35.625
	0°	.0494	-.0145	.0823	2.89	35.75
	-45°	-.5163	-.1017	.0094	2.45	30.306
	+45°	.5007	.1017	-.0094	4.163	51.46
E	90°	-.0353	.0363	-.0876	2.62	32.409
	0°	.1496	-.0015	.0876	2.72	33.64
	-45°	-.485	.1289	.0151	2.16	26.72
	+45°	.5977	-.0935	-.0151	4.34	53.68
F	90°	-.0403	.0575	-.092	2.384	29.49
	0°	.232	.0016	.092	2.59	32.038
	-45°	-.4725	.146	.0222	1.97	24.37
	+45°	.6603	-.0867	-.0222	4.238	52.424
G	90°	-.055	.0741	-.0945	2.22	27.46
	0°	.298	.0014	.0945	2.52	31.172
	-45°	-.460	.1574	.0288	1.84	22.76
	+45°	.701	.0817	-.0288	4.08	50.47
H	90°	-.0685	.089	-.0948	2.11	26.10
	0°	.357	.00114	.0948	2.47	30.55
	-45°	-.447	.1665	.0347	1.77	21.89
	+45°	.732	-.076	-.0347	3.93	48.61

TABLE 10.4 STRESS CONCENTRATION IN THE COMPOSITE AT THE ROOT OF THE TONGUE

LONGITUDINAL SHEAR STRENGTH OF THE JOINT = 12.37×10^3N, $\sigma_o = \frac{12.37 \times 10^3}{2 \times 50.8 \times .381} = 319.56$MPa

POSITION LETTERS	PLY ANGLE	$\frac{\sigma_1}{\sigma_o}$	$\frac{\sigma_2}{\sigma_o}$	$\frac{\tau_{12}}{\sigma_o}$	TSAI-HILL R.F.	PREDICTED STRENGTH kN
I	90°	-.0842	.1051	-.09607	1.97	24.369
	0°	.4224	.0006	.09607	2.45	30.30
	-45°	-.4255	.1749	.0413	1.70	21.029
	+45°	.7604	-.0688	-.0413	4.81	59.50
J	90°	-.0935	.1267	-.0954	1.838	22.73
	0°	.510	.0029	.0951	2.45	30.3
	-45°	-.3818	.1859	.0491	1.62	20.04
	+45°	.7948	-.0557	-.0491	3.57	44.16
K	90°	-.0782	.1596	-.0932	1.65	20.41
	0°	.6321	.0136	.0929	2.45	30.30
	-45°	-.2979	.2049	.0579	1.50	18.55
	+45°	.851	-.0122	-.0579	3.43	42.43
L	90°	.0394	.2059	-.0932	1.41	17.44
	0°	.7854	.0526	.0932	2.27	28.08
	-45°	-.1630	.2475	.0607	1.307	16.167
	+45°	.9857	.0115	-.0607	3.18	39.33
M	90°	.2071	.2653	-.1101	1.12	13.85
	0°	.9795	.1067	.1101	1.73	21.4
	-45°	-.0879	.3254	.0625	1.026	12.69
	+45°	1.2517	.0466	-.0626	2.66	32.90
N	90°	-.0563	.3073	-.0867	1.046	12.94
	0°	1.1954	.050	.0863	2.24	27.7
	-45°	.0353	.2885	.1014	1.07	13.23
	+45°	1.1015	.0695	-.1014	1.96	24.24

TABLE 10.5 STRESS CONCENTRATION IN THE COMPOSITE AT THE ROOT OF THE TONGUE

JOINT LONGITUDINAL SHEAR STRENGTH = 12.37×10^3 σ_o = 319.56 MPa

POSITION LETTERS	PLY ANGLE	$\frac{\sigma_1}{\sigma_o}$	$\frac{\sigma_2}{\sigma_o}$	$\frac{\tau_{12}}{\sigma_o}$	TSAI-HILL R.F.	PREDICTED STRENGTH kN
A'_M	90°	-.2412	.3286	-.0826	.975	12.06
	0°	1.3174	.0088	.0823	2.36	29.193
B'_M	90°	-.189	.2613	-.0867	1.18	14.596
	0°	1.0452	.0075	.0860	2.44	30.183
C'_M	90°	-.1605	.2134	-.0842	1.396	17.268
	0°	.8543	.0045	.0838	2.60	32.162
D'_M	90°	-.1305	.1859	-.0864	1.53	18.926
	0°	.7448	.00619	.0860	2.59	32.038
E'_M	90°	-.1604	.15114	-.0876	1.74	21.52
	0°	.6039	.0049	.0873	2.62	32.409
F'_M	90°	-.08199	.1180	-.087	2.0	24.74
	0°	.4725	.0039	.087	2.68	33.151
G'_M	90°	-.0601	.0880	-.0860	2.26	27.956
	0°	.3536	.0031	.0860	2.74	33.894
A'_u	90°	-.1098	.3048	-.0077	1.135	14.04
	0°	1.1922	.0366	.0072	4.05	50.098
B'_U	90°	-.1470	.2484	-.00224	1.38	17.07
	0°	.9857	.0156	.00187	5.28	65.313
C'_U	90°	-.1467	.2112	.00347	1.61	19.916
	0°	.8418	.0079	-.0038	6.25	77.312
D'_U	90°	-.1245	.1821	.0075	1.88	23.255
	0°	.7260	.0074	-.0077	7.08	87.579
E'_u	90°	-.1004	.1502	.00807	2.23	27.585
	0°	.5977	.0066	-.0083	8.43	104.279
F'_u	90°	-.0810	.1183	.0080	2.82	34.883
	0°	.4725	.0047	-.00817	10.47	129.51
G'_U	90°	-.0616	.0892	.0076	3.47	42.924
	0°	.3536	.0034	-.0077	14.43	178.5

STRESS CONCENTRATION IN THE COMPOSITE AT THE INNER SLOT FACING

TABLE 10.6

11. FAILURE STRENGTH PREDICTIONS

11.1 STRENGTH PREDICTIONS OF REINFORCED JOINT TYPE 1b

[90°/0°/90°/0°- C 90°]$_s$

11.1.1 Comparison of Tsai-Hill and Tsai-Hill/Hoffman Failure Criterion

In Table 10.1 the value of both failure criterion were given for the different positions at the root of the tongue composite in the joint. The analysis here is done in plane stress and calculated at a finite point in the structure (Gauss-Point). Hence there are no σ_3 terms and the composite predictions are given in the principal material directions. The material failure strengths are shown in the respective directions thus:

STATIC STRENGTH MPa				
TENSILE		COMPRESSIVE		SHEAR STRENGTH
σ_{1UT}	σ_{2UT}	σ_{1UC}	σ_{2UC}	τ_{12U}
1700	111.4	641	161	76.5

Then both criteria will suit no matter what the ply angle. A summary of lowest R.F. values for the 0° and 90° plies is shown below:

POSITION	PLY ANGLE	TSAI-HILL R.F.	HILL/HOFFMAN R.F.
N	90°	0.92	0.84
M	0°	1.17	1.76

It was found that generally the Hill/Hoffman Criterion gave better R.F. values for the 0° ply at any position in the root of the tongue composite than the Tsai-Hill R.F. values. The largest contributor to the

high R.F. values are the two extra terms, namely $F_1\ \sigma_1$ and $F_2\ \sigma_2$. However with the 90° ply the values of σ_2/σ_o and τ_{12}/σ_o increases as the Hill/Hoffman R.F. value decreases to a lowest reserve factor of 0.84 at position 'N'. This is 9.5% less than the predicted Tsai-Hill R.F. value which indicates the extreme characteristic of the Hill/Hoffman Criterion in the tensile and compressive state of stress. Another contributor to the low R.F. value is due to the fact that the compressive strengths are accounted for even though the stresses are tensile, thus having greater influence on the predicted R.F. values. The Tsai-Hill Failure Criterion was also chosen for the strength prediction of the joint, mainly because of the lack of the sudden change of R.F. value and also because the criterion has been used successfully at the City University for the composite strength prediction by various researchers and hence more confidence can be placed on the criterion.

11.1.2 Strength Predictions

It is important to note that in the remainder of this chapter, attempts at predicting composite failure strength statically have been made where the joint is known to fail in the composite. In support of this the adhesive strengths were checked. These proved to be more than adequate in providing continuity of the joint. This was mainly due to the type and bulk use of the adhesive used in the joint system. Therefore the composite will fail before the adhesive but the initial failure site is so small that it can not be seen by eye and therefore the prediction is needed to show which material fails first.

In the composite at the root of the tongue, Table 10.1, the 90° ply is expected to fail first at the positions 'N' and 'M' at 7.206 kN, both of which are some 2mm away from the singularity. These underestimated

the experimental failure by about 8.7%, which seems reasonably accurate. Although the predicted strength at both positions are the same, it is so for different stress concentrations. None of these individually exceeds the material strengths, indicating the value of the failure criterion for combinations of stresses. Furthermore a combination of loading tensile and shear stresses at the end of the bonded connection at position 'N' might initiate the failure which would then propagate to position 'M'. It can also be added that, although the prediction was lower than the joint strength it was so by only 8.7% which is a small difference, allowing for all the possible errors. The next most highly stressed position was also in the 90° ply at point 'L' at 8.538 kN which was an overestimate of 8.2%. Failure of the 90° plies means that most of the load transfer would take place in the 0° plies at these points which is indicated by the subsequent failure of the 0° ply at position 'M' at about 9.164 kN which is an overestimate of 14.5%. It is interesting to note that the Hill Criterion predicts an equal strength prediction at the far end of the joint where both the 0° and 90° plies have compressive stress concentrations. However the predicted strengths by the Hill/Hoffman Criterion are not equal in the same compressive area, which indicates the characteristics of the Tsai-Hill Criterion. The failure distribution is illustrated graphically in Fig. 11.1.

In the area of the tongue composite within the slot panel, Table 10.2, higher strengths are predicted for the width of the tongue again with the lowest strength situated in the tensile region position 'L', indicating that the joint failure would not be initiated in this area for any given local reinforcement. Here both the 0° and 90° plies have less stress concentration resulting in a higher strength prediction. This is because of the presence of the bulk adhesive which provides an additional load path from the tongue panel to the outer composite facing

of the slot panel. The major load path of the joint system is the connection at the tip of the tongue to the inner slot facing. Table 10.3 shows the predicted values with the 90° layer at far end of slot panel point 'B' proving to be the weakest ply as expected. Furthermore if there is to be any failure in this area of the joint, it will be so mainly due to the transverse tensile stess concentration in the 90° ply, the value of which is not large enough to initiate the joint failure here, see Fig. 11.2. However with the suitable reinforcement local to the tongue such as joint type 2a, the concentration at the far end of the inner slot facing gives the lowest predicted strength which is reported in the last section of this chapter.

It is important to note that the aim of this work is primarily to establish whether the proposed method of stress analysis can be used for the design of this type of joint by predicting the static strength for a given local reinforcement. As a general conclusion to the last two paragraphs it can be stated that the analysis predicted generally lower failure loads for composite failure than occurred experimentally. The predicted failure and the location were in the composite facing at the root at the tongue at position 'M' which coincided with the test results.

11.2 STRENGTH PREDICTIONS OF JOINT REINFORCEMENTS TYPE 2a

There are two likely failure sites for the composite facing, these are at point 'M' and at the area near to 'B', both of which occur in the 90° ply. These locations were obtained from the last column in Tables 10.1 and 10.3 respectively. With the reinforcement type 2a the local tongue facing consists of a total of 6 plies, two of which were

orientated at ±45°. These provide additional strength for the joint not to fail at point 'M' therefore limiting the failure to the far end of the inner slot composite where the two cross ply facings delaminated. This was difficult to observe by the naked eye. It had already been established experimently that this failure mode was mainly due to tranverse tensile cracking of the 90° ply being the first ply adjacent to the adhesive line. In support of this the prediction given in this section will show this as the location of the first ply failure with this case of reinforcement.

In the composite facing at the root of the tongue, Table 10.4, in the compressive region points A to D, the predicted strength for the 0° and 90° plies are approximately the same but different for the ±45° ply at these points, giving further evidence of the characteristics of the Tsai-Hill Criterion. The lowest strength prediction in the composite at the root of the tongue is obtained from Table 10.5 at the tensile stress concentration area in the -45° ply. Here this ply is weaker than the 90° ply, the former at 12.69 kN, point 'M', and the latter at 12.94 kN, at point 'N', which are about 2.5% and 4.4% over the static failure strength. The largest contributor to the magnitude of the predicted strength in the composite both for the -45° and 90° plies, are the tensile strength concentration transverse to the fibre direction at points 'M' and 'N' respectively. These predictions show that the joint failure does not initiate from this area of the composite which coincides with the test result. The failure strength curve for the last four points at the near end of tongue composite are given in Fig. 11.3.

It is important to remember that, although the composite facing of the slot panel remains the same as the joint reinforcement type 1b and also that the analysis is linearly elastic, extrapolating the failure strength from the failure curve of Fig. 11.2 is not valid because of the

change in the joint loading geometry and of the increase in stiffnesses in the local area of the tongue panel, hence Table 10.6. The lowest predicted strength of the joint is now at point 'A_M' which is the nearest Gauss Point to the far end of the bonded connection in the inner slot composite and to the centreline of the tongue facing. As expected the failure is in the 90° ply giving a predicted static strength of 12.06 kN, a 2.5% underestimation of the joint test failure strength. Moreover the dominant concentration is the transverse tensile stress, which is the main contributor to the Tsai-Hill Criterion, arising from the shear and tensile stresses from the far end of the tongue composite. Hence the ultimate failure of the joint depends on the transverse tensile strength of the 90° ply at position 'A_M' which is quite accurate when compared to the experimental result.

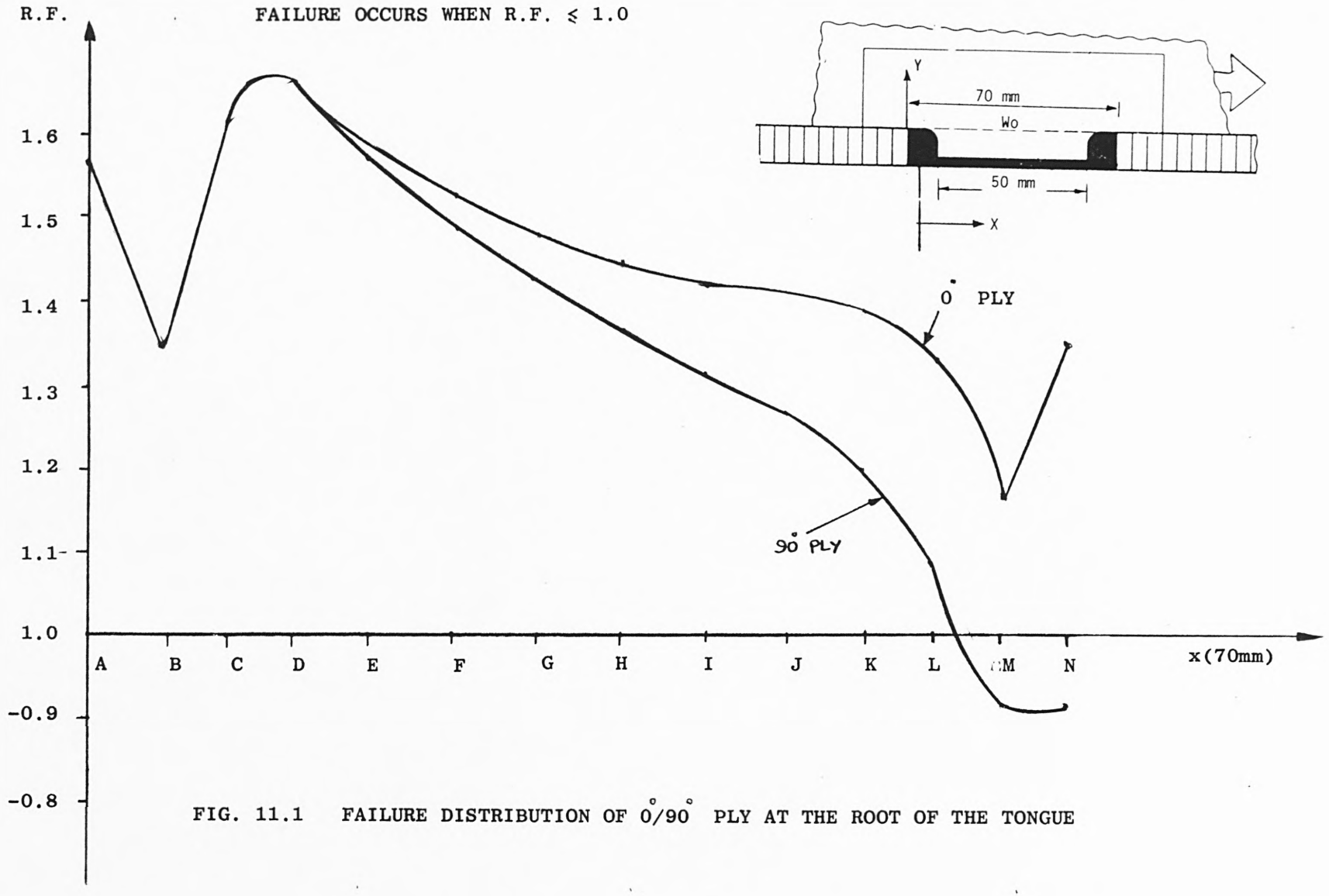

FIG. 11.1 FAILURE DISTRIBUTION OF $0^{\circ}/90^{\circ}$ PLY AT THE ROOT OF THE TONGUE

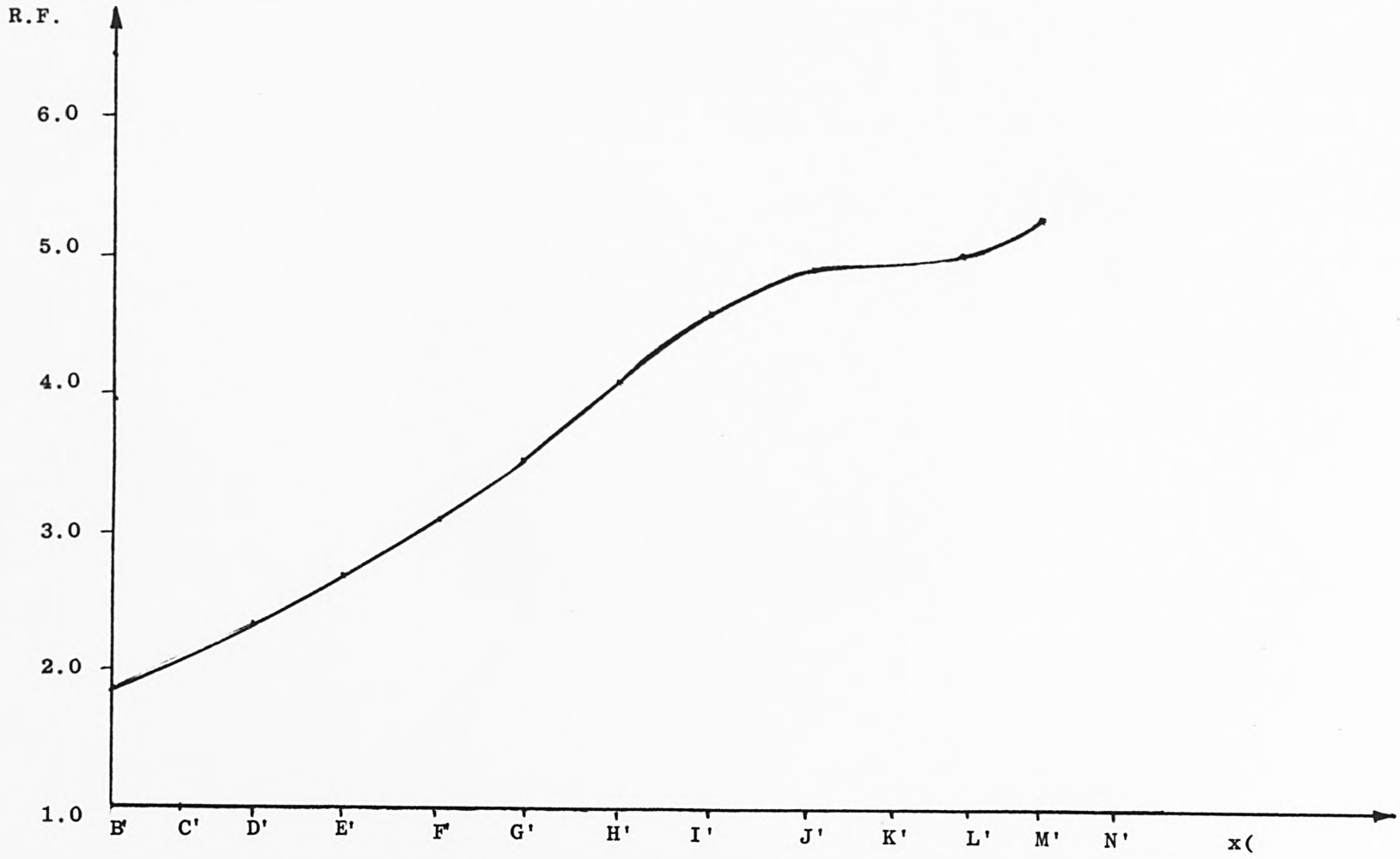

FAILURE DISTRIBUTION OF 90° INNER SLOT FACING

FIG.11.2

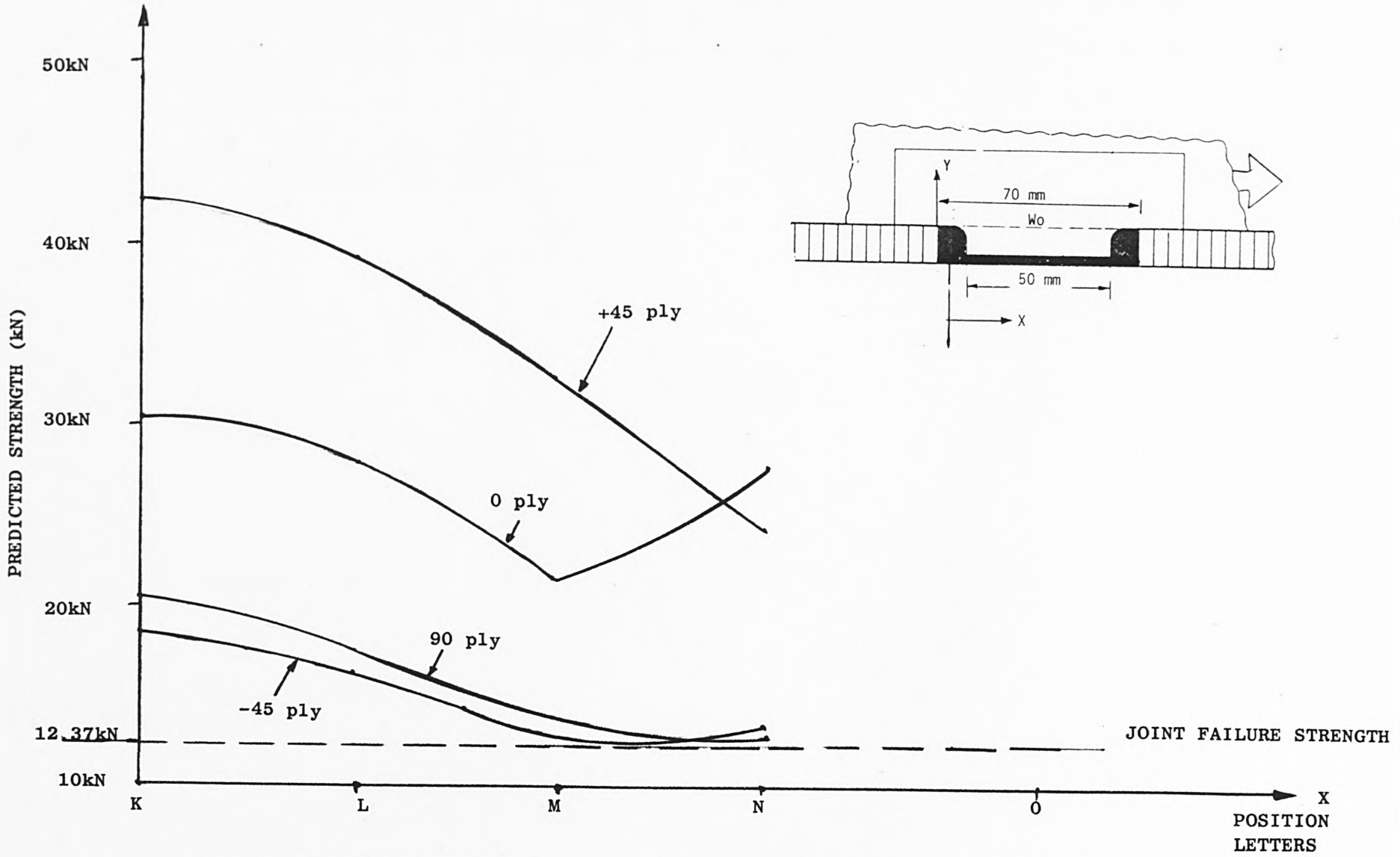

FIG. 11.3 PREDICTION OF FAILURE STRENGTH IN THE TENSILE REGION OF THE TONGUE COMPOSITE

12. DISCUSSION

In the last few chapters a method of predicting the tongue and slot joint failure was attempted. The accuracy of the method hinges on several factors such as the accuracy of the material data and the accuracy of the finite element analysis. In theory any type of structure can be analysed to give the stress concentrations and therefore to predict the failure strength of this component provided that the materials of the structure are the same as that of Chapter 5. If so then the problem is one for the stress analyst to obtain confidently the stress concentrations. The method analyses the facing laminate as plane stress from which the failure strength can be predicted using the Tsai-Hill Criterion with good accuracy. Three dimensional objects such as the core and the adhesive can equally have their strengths predicted. An extension to the Tsai-Hill Criterion to allow for a tri-axial stress situation would be needed if the facing laminates were thick enough so that the stresses in the 'Z' (3) direction cannot be ignored.

If the work described was thought to be sufficiently accurate for use by designers for materials other than reported in this thesis, then a range of stress ratios including compressive ones would be needed for which procedures had been laid in the previous chapters. However in the composite of the joint it is the tensile stresses that cause damage. The longitudinal shear testing of the joints showed the peel stresses in the tongue composite at the far end of the joints to be compressive, but tensile at the near end. The joint with the reinforcement type 1b failed at the site of these tensile stresses. However as the number of plies reinforcing the local tongue area increases, it is the failure site not the failure mode which shifts to the inner slot composite at the far end of the joint. It was the tensile peel stresses in the adhesive at the

far end of the slot which caused failure in the inner slot facing of the joint, i.e. reinforcement type 2a. Should a new adhesive be introduced the 'longitudinal shear loading' specimens and the lap-shear test specimens are quite suitable for checking the compatibility of the adhesive to the joint system. Generally it was found that a very ductile type of adhesive is not suitable particularly if it is dissimilar with the adhesive used for the composite sandwich panel fabrication.

In two dimensional analysis the Tsai-Hill Criterion has been shown to be perfectly adequate for predicting the composite failure. This was also applicable in the three dimensional analysis where the facings composite were analysed as plane stress. The compressive strengths used in the prediction were obtained from the material tests and, although flexural testing of the composite in the fibre direction was intended to give the compressive strength, inter-cell buckling developed in the thin facing giving a low strength in compression.

For the prediction of joint strength, a different approach was necessary to obtain a compression strength of a unidirectional ply in a thick laminate. Short column compression testing of an 8-ply laminate proved to be adequate for obtaining the higher strength which was necessary to represent the condition in the joint and hence give a more accurate strength prediction. The analysis used was linear as the work is primarily on the prediction of strength where the stresses in the adhesive are much lower than the yield strength of the adhesive. This would not be entirely correct for joints with sufficient reinforcement both in the local tongue area and in the slot facing. Static predictions for these joints cannot be accurately attempted without the use of an elastoplastic analysis. The effect of adhesive plastic yielding reduces the concentrations at the far end of the joints so that a redistribution of the adhesive stresses takes place, thus more load is transferred by

the parts of the adhesive that are not as highly stressed. This situation did not arise in any of the reinforced joints since the adhesive stresses were very low and therefore the failure was limited to the composite facing.

In Chapter 9 both 2-D and 3-D analysis as well as the prediction technique were attempted on both flexural simple beam and box type beam, so that the possible errors from the finite element analysis were eliminated. The static strength predictions using the Tsai-Hill Criterion gave generally accurate results with sandwich beams of different core thicknesses. However with the beams having more than two plies in the facings, the prediction becomes less accurate mainly due to the fact that as the facing thickness increases, the possibility of inter-cell buckling diminishes therefore using the flexural compressive strength data in the failure criterion is not entirely correct. The compressive data obtained from the 8-ply laminate was found to be more appropriate in predicting the failure strength. The box beam which was more of a structure than a simple beam test, was analysed by both the 2-D and 3-D methods, under-predicting by 1.6% and overestimating by 6.8% respectively. Thus confidence can be placed in predicting composite failure of the joint.

Two dimensional analysis of the joints was attempted in Chapter 10 mainly as a guide to the highest stressed positions. There was geometrical misrepresentation, unavoidable in modelling a 3-D structure into a 2-D one. Nevertheless it did show the complexity of the analysis which was needed for accurate strength prediction since the joint has a number of areas of high stress concentrations and hence the three dimensional analysis was needed.

Static prediction in the joints was attempted in Chapter 11, the accuracy of which was considered to be dependent on the accurate

representation of the joint for both the reinforced joints types 1b and 2a. The composite facings gave the lowest predicted strengths, with the failure site in the near end of the tongue radius, which is the end of the bonded connection of outer slot facing to the tongue facing and at the far end of the inner slot facing composite respectively. The comparison of predicted strengths with the experimental results are summarised as below.

PLY STACKING SEQUENCE	REINFORCE-MENT TYPE	PREDICTED HIGH STRESSED PLIES	FAILURE STRENGTH		% OF DIFF.
			THEORY(N)	TEST(N)	
$(\dot{9}\dot{0}/\dot{0}/\dot{9}\dot{0}/\dot{0}\text{-}C\dot{9}\dot{0})_s$	1b	$\dot{9}\dot{0}$ M	7206	7833	-8.7
$(\dot{9}\dot{0}/\dot{0}/+\dot{4}\dot{5}/-\dot{4}\dot{5}/\dot{9}\dot{0}/\dot{0}\text{-}HDC\dot{9}\dot{0})_s$	2a	$\dot{9}\dot{0}$ A'_M	12061	12370	-2.5

These percentages agree with the failure paths and are the actual strengths because the initial 90° ply failure in the joint type 1b will alter the stress distributions therefore putting more stress concentration in the already highly stressed 0° ply and, since the reinforcement is a combination of 0° and 90° plies, failure of either ply constitutes the total failure of the joint. Similarly for the joint type 2a, initial failure of 90° ply at the inner slot composite was due to both interlaminar normal and shear stresses arising from the large stress concentration at the far end of the joint. Because of this high stress concentration in the adhesive (at the tongue and slot interface) layer, high stresses (transverse tensile) are produced in the adjacent ply of the adherend laminate (90° ply) therefore causing failure of the joint. This failure in the actual joint test was observed to be the delamination of the 90° ply from the outer 0° ply with the 0° ply being intact as predicted in the analysis. An effective way of reducing the local high stresses in the plies adjacent to this adhesive layer is to

use woven plies in the adherend laminate so that the adhesion takes place in many layers and, consequently, stresses are distributed in many plies. Interleaving is particularly desirable when the number of plies in the laminate is large.

13. CONCLUSIONS

It was shown both experimentally and theoretically that the reinforced tongue and slot joint can be used effectively as a method of joining a composite sandwich panel together with an adhesive bond. Generally to prevent premature joint failure (i.e. adhesive/core rupture), ductile epoxy adhesives are not to be used for this type of joint configuration. Furthermore excellent adhesion is obtained when the matrix material of the composite is also used as the adhesive in the joint. The lap shear test specimen portrays adequately the compatibility between the matrix of the laminates and the adhesive in the joint.

In obtaining the flexural compressive strengths of the unidirectional composite along and transverse to the fibre direction, the cross ply $[(90°/0° - C90°)_s]$ sandwich beam specimen portrayed the compressive strengths better than the unidirectional $[(0°/0° - C90°)_s]$ sandwich beam specimens. Similarly for the buckling compressive strengths, the 8-ply laminate short column compression test portrayed the compressive strengths better than the unidirectional sandwich short column tests.

The two dimensional orthotropic sandwich element coupled with Tsai-Hill failure criterion can be used effectively for the static analysis and strength prediction of a large composite sandwich structure. For the areas of high stress concentration such as joints, the three dimensional orthotropic sandwich element can be used adequately for static analysis and strength prediction provided that very large plastic deformations do not occur. The most important point arising from the predictions was that the tensile stresses in the composite at the neck of the tongue and at the far end of the inner slot facing caused the damage and hence failure.

The strength predictions in all the joints were just below those determined in the joint test.

REFERENCES

1. Benson, N.K. "The Mechanics of Adhesive Bonding", Applied Mechanics Review, Volume 14, Number 2, Feb.1961, p.83.

2. Perry, H.A. "Adhesive Bonding of Reinforced Plastics", McGraw Hill, New York, 1959.

3. Grinius, V.G. "Efficient Joint Design for Reinforced Plastic Structure", National Symposium on Joining of Materials for Aerospace Systems, 1965.

4. Dastin, S.J. "Bonded Berylium Structures", National Symposium on Joining of Materials for Aerospace Systems, 1965.

5. Doyle, A.C. "A Scandal in Bohemia" (The Works of A. Conan Doyle). New York, P.F. Collier and Sons, pp.3-18.

6. Structural Sandwich Composites, MIL-HDBK-23A.

7. Benson, A.S. and Mayers, J. "General Instability and Face Wrinkling of Sandwich Plates - Unified Theory and Applications", Stanford University, Stanford, California, AIAA Paper No.66-138.

8. Hull, D. "An Introduction to Composite Materials", Cambridge University Press, 1981.

9. Broutman, L.J. and Krock, R.H. (eds) 'Composite Materials'. Vols.7 and 8, ("Structural Design and Analysis", Pts.I and II edited by C.C. Chamis) Academic Press, New York, 1975.

10. Vicaris, A.A. and Toland, R.H. "Failure Criteria and Failure Analysis of Composite Structural Components", Composite Materials, Vol.7, pp.51-97 ("Structural Design and Analysis", Pts.I and II edited by C.C. Chamis), Academic Press, New York, 1975.

11. Wu, E.M. "Phenomenological Anisotropic Failure Criterion", Composite Materials, Vol.2, pp.353-431 ("Structural Design and Analysis", Pts.I and II edited by C.C. Chamis), Academic Press, New York, 1975.

12. Hill, R. "The Mathematical Theory of Plasticity", Oxford University Press, London, 1950.

13. Jones, R.M. "Mechanics of Composite Materials",

14. Hoffman, O. "The Brittle Strength of Orthotropic Materials", Journal of Composite Materials, Vol.1, 1967, p.200.

15. Tsai, S.W. and Wu, E.M. "A General Theory of Strength for Anisotropic Materials", Journal of Composite Materials, Vol.1.12, 1978, p.275.

16. Henshall, R.D. "PAFEC-75" Manual.

17. Zienkiewicz, O.C. "The Finite Element Method in Engineering Science", published by McGraw-Hill, 1971.

18. Berar, C. "Thick Faces Theory of Orthotropic Flat Sandwich Plates", Rev.Roum.Sci.Tech.Ser.Mec.A. 1984, pp.173-186, Vol.29, Part 2.

19. Schmit, J.R. and Monforton, G.R. "Finite Deflection Discrete Element Analysis of Sandwich Plates and Cylindrical Shells with Laminated Faces", in AIAA/ASME 10th Structures, Structural Dynamics and Materials Conf., New Orleans, 1969

20. Whitney, J.M. "Stress Analysis of Thick Laminated Composite and Sandwich Plates", Air Force Materials Laboratory, Wright-Patterson Air Force Base, Ohio 45433, 26 July 1972.

21. "A Finite Element Analysis Including Transverse Shear Effect for Applications to Laminated Plates", AIAA Journal, Vol.9.
C.W. Pryor Jr. Macdonald Douglas Corporation, St. Louis, M and
R.M. Barker, Virginia Polytechnic Institute, Blocksburg VA

22. Reissner, E. "The Effect of Transverse Shear Deformation on the Bending of Elastic Plates", Journal of Applied Mechanics, V01.12, 1945, pp.69-77.

23. Yen, K.Y., Gunturkun, S. and Pohle, F.V. "Deflection of a Simply Supported Sandwich Plate Subjected to Transverse Loads", NACA-TN 2581.

24. Pag ano N.J. "Exact Solutions for Rectangular Bidirectional Composites and Sandwich Plates", June 1970, Wright-Patterson Air Force Base, Ohio.

25. PAFEC '75' Systems Manual.

Modified computer routines (Appendices I and II) have been removed for copyright reasons

APPENDIX I

APPENDIX II